STUDY OF PHYSICAL PROPERTIES OF SOME LIQUID CRYSTALS HAVING NEMATIC AND SMECTIC PHASES

THESIS SUBMITED FOR THE DEGREE OF DOCTOR OF PHILOSOPHY
(SCIENCE) OF THE UNIVERSITY OF NORTH BENGAL
NOVEMBER, 1995

BY
BANANI ADHIKARI

Liquid Crystal Research Laboratory
Department of Physics, North Bengal University
Raja Rammohanpur, Darjeeling, West Bengal
734 430 - INDIA

❑ *Dedicated to my Late Grandmother* ❑

❖

DEPARTMENT OF PHYSICS
UNIVERSITY OF NORTH BENGAL
P.O. North Bengal University
Dist. Darjeeling (W.B.)
Pin - 734430 INDIA.

Phone : Office - (03556) 414
From Siliguri dial 92-414
Railway Station : New Jalpaiguri (NFR)
Airport - Bagdogra

(TO WHOM IT MAY CONCERN)

This is to certify that the work reported in this thesis entitled "Study of Physical Properties of some Liquid Crystals having Nematic and Smectic Phases" by Miss Banani Adhikari has been carried out by the candidate herself under my direct supervision and guidance. Miss Banani Adhikari has fulfilled all the requirements for the submission of the thesis for Ph.D degree of the University of North Bengal. Some part of the research work presented in this dissertation has been performed in collaboration with others. However, even in those works her contribution is very substantial. In character and disposition Miss Banani Adhikari is fit to submit the thesis for the Ph.D. degree.

Ranjit Paul

Date: 30th Nov, 1995

(Ranjit Paul)
Professor of Physics and Supervisor.

ACKNOWLEDGEMENTS

At the outset, I would like to express my profound gratitude to Prof. Ranjit Paul, Department of Physics, University of North Bengal for his active help and supervision throughout the length of my research work. I would also like to extend my gratitude to Dr. Sukla Paul, Reader, Department of Physics, North Bengal University for her help and inspiration.

I would like to thank Hoffmann-La-Roche Co., Basel, Switzerland and E. Merck, U.K., for the gift of the liquid crystal samples used in my research work. I am grateful to Prof. H. Schenk, Laboratory for Crystallography, University of Amsterdam for kindly donating the liquid crystalline compound HAB. I am also thankful to Prof. R. A. Vora, M. S. University of Baroda, India for synthesis and DSC of a liquid crystalline sample HBAAB.

I am sincerely thankful to all members of the Department of Physics, North Bengal University. My special thanks go to Dr. P. K. Mandal, Dr. S. Gupta, Dr. M. K. Das, Mrs. A. Nath, Mr. G. Chaudhuri, Mr. S. K. Giri, Mr. N. K. Pradhan and Mr. P. Sarkar for their continuous assistance and co-operation to me in carrying out my work successfully. The staff members of the University Science Instrumentation Centre are also gratefully acknowledged for their help.

I would dearly like to thank Mr. S. K. Sarkar, Department of Physics, North Bengal University for his constant help in the various designs and technical aspects of the different equipment used by me throughout this work.

Due thanks are recorded to the University of North Bengal and the Council of Scientific and Industrial Research, New Delhi for providing me with a research fellowship. The University Grants Commission, New Delhi and Inter University Consortium for DAE Facilities, Indore are duly acknowledged for their financial assistance in procuring different instruments used in this research work.

I end by expressing my warmest appreciation to my family, especially my parents, whose support went a long way in enabling me to complete this work.

Banani Adhikari

Date : 30. 11. '95 *(Banani Adhikari)*

North Bengal University

CONTENTS

CHAPTER - 1

INTRODUCTION

Liquid crystalline materials are organic compounds with a state of order intermediate between those of solid crystals and isotropic liquids. The discovery of liquid crystals is dated back to the year 1888 when the botanist F. Reinitzer [1] observed the cloudy melting of cholesteryl benzoate and cholesteryl acetate. He donated these compounds to the physicist O. Lehmann [2] who described liquid crystals as a novel state of matter possessing anisotropic viscous, electrical, optical and mechanical properties. Friedel [3,4] suggested the term "mesomorphic phase" or "mesophase" to this state of matter. There are thousands of organic chemicals which are known to form mesophases [5,6]. In addition to this, few organo-metallic [7,8] and inorganic chemicals [9] also show liquid crystalline properties as well.

One of the most important properties of liquid crystals is the combination of long-range orientational ordering of the particles constituting the substance with a total or partial absence of long-range order in the positioning of their centres. The former is the characteristic of solids while the later is the characteristic behaviour of liquids where the short-range order is observed in the positioning of molecules, but long-range order is absent. The molecules of the compounds showing mesophases are generally non-spherical in shape —— rod like (in the form of spherocylinders or ellipsoid of revolution) or disc like. Anisotropic dispersive forces between the molecules play a major role in the stabilization of the liquid crystal phases. There are many books and review articles on liquid crystals which give details regarding molecular structure and physical properties of the compounds exhibiting mesophases, of which a few [5,6,8,13-21] are listed here. Recent developments in the field of liquid crystals and applications

are also available [22-26].

1. Classification of Liquid Crystals

On a broad basis, liquid crystals are classified into two types, viz. 'lyotropic' and 'thermotropic'.

1.1 Lyotropic mesophase

Lyotropic liquid crystals are solutions of anisotropic molecules in an isotropic solvent [27-30]. The amount of solvent is the controlling parameter for forming such mesophases. Solutions of soap and water are typical examples of lyotropics and their mesomorphic properties appear both as functions of concentration and temperature. Lyotropic liquid crystals play an important role in living systems and are particularly important for the present day understanding of the structure and properties of biomembranes [23]. Since this dissertation is not concerned with lyotropic liquid crystals it will not be discussed any further.

1.2 Thermotropic mesophase

In thermotropic liquid crystals mesomorphic behaviour is induced due to changes in temperature. Thermotropic liquid crystals which show reversibility of phase transitions are called enantiotropic. In certaion cases, mesomorphism is depicted only during cooling of the compound and phases of this kind are called monotropic. Friedel [31a] from his detailed optical and x-ray studies have classified thermotropic liquid crystals into three types: nematic, cholesteric and smectic.

Classification of smectic liquid crystals are based mainly on the optical and miscibility studies of Sackmann and Demus [31b]. A brief description of different thermotropic mesophases are given below.

1.2.1 Nematic mesophase

The term "nematic" coined by Friedel from a Greek word thread, describes the thread like lines seen in nematic liquid crystals under a polarising microscope. In nematics, there is no correlation between the molecular centres of gravity, but the direction of molecular long axes do statistically have a preferred direction called "director", denoted by $\hat{n}$. Since there is no restriction regarding the positions of the centre of mass, the molecules in the phase have a high degree of mobility and the nematic phase is markedly affected by external fields. In addition, the preferential orientations $\hat{n}$ and $-\hat{n}$ are not distinguishable (all orientations of the ends of the molecules are equally probable). The nematic phase is an optically uniaxial medium. Another characteristic property of this phase is that the right-and left-handed forms are indistinguishable (achirality), indicating the system to be a racemic mixture of right and left-handed molecules. X-ray studies indicate that fluctuations of smectic like order parameter manifests itself in certain nematic phases, the so-called "cybotactic nematic" phases, first observed and classified by de Vries [32]. In nematics of this kind there exist domains wherein the centres of molecules lie in a well defined plane, the molecules itself being either perpendicular to the plane (normal cybotactic nematic phase) or tilted with respect to the plane (skewed cybotactic nematic phase). Generally, these domains extend only

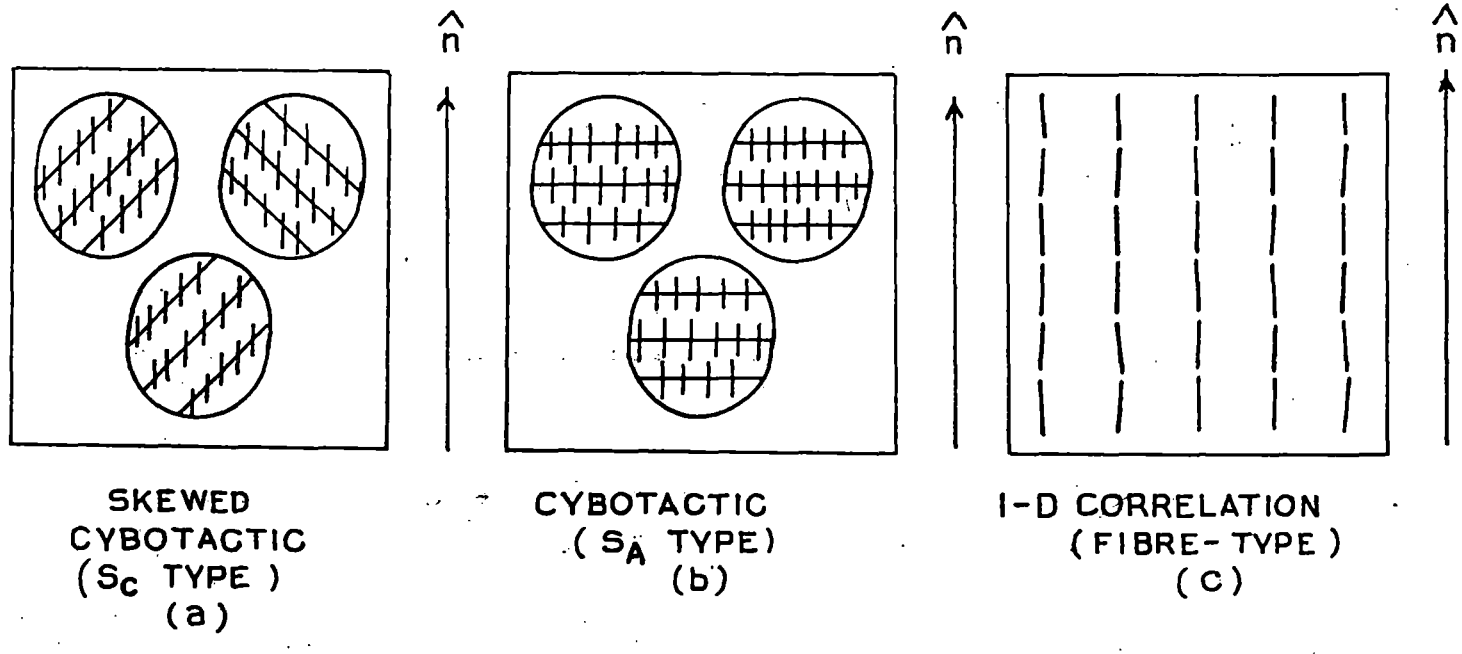

Figure 1.1. Schematic diagram showing molecular arrangements in nematics having three types of short range order.

upto limited distances. Another type of nematic phase is encountered in certain liquid crystalline compounds [33] which possesses one dimensional correlation of molecules along the director, $\hat{n}$, thus leading to the existence of strings of molecules or fibres in the nematics. This type of nematic is called fibre-type nematic. Figure 1.1 shows the schematic diagram of molecular arrangement in nematics having three different types of short range order. In addition to this, biaxial nematic liquid crystals have also been reported in certain polymeric liquid crystals [34a] and lyotropic systems [34b].

1.2.1a Cholesteric or chiral nematic phase

Cholesteric liquid crystals have a two dimensional nematic structure comprising of optically active molecules. There is no long range order in the centre of mass of the molecules and the molecules are parallel to a preferred direction $\hat{n}$, which has a helical symmetry. The pitch of the helix is temperature and concentration dependent. No substance has been found to exhibit both nematic and cholesteric phases, though cholesteric can undergo transition to nematic phase under the action of external electric and magnetic fields. Addition of a small amount of cholesteric compound to a nematic substance causes it to exhibit cholesteric phase. The cholesteric phase is thus a variation of the nematic phase and may be called chiral nematic (N^*) phase [35-37].

1.2.2 Smectic mesophases

Smectic liquid crystals characteristically exhibit the

presence of equidistant molecular layers. Within the layers the molecular centres lie in a single plane, while their long axes are either perpendicular or tilted relative to this plane. In both cases the arrangement of the centres of the molecules within each layer correspond to a two dimensional liquid (the presence of short range order and absence of long range order). The smectic liquid crystals are generally more viscous than nematics. The interlayer attractions are weaker than the lateral forces between the molecules and the layers can slide over each other, thus showing fluid behaviour. In some smectic phases, a periodicity characteristic of a two - dimensional solid is observed in the positioning of the centres of the molecules within each layer, while the molecular long axes remain either perpendicular or inclined to the plane of the layer. Different types of thermotropic smectic phases have been identified [38-47], which are designated as follows [48]

$$S_A,\ S_B,\ S_C,\ S_F,\ S_G,\ S_H,\ S_I,\ S_J,\ S_L,\ldots\ldots$$

In addition to orientational and translational order, smectic liquid crystals also exhibit another type of order known as "bond orientational order" which can be seen in the following way. Let there be a fictitious bond between a molecule and its nearest neighbour. Then, if the orientation of this bond (i.e. the bond angle θ_b, as shown in Figure 1.2) with respect to some axis, X, chosen within the smectic layer, remains constant over distances, r, very much greater than the inter moleculer distance, a, as well as the in-plane positional correlation length ξ, then the phase is said to posses long range bond orientational order (BOO). Smectic liquid crystals having long range BOO in addition to long range moleculer orientational

Figure 1·2 BOND ORIENTATIONAL ORDER

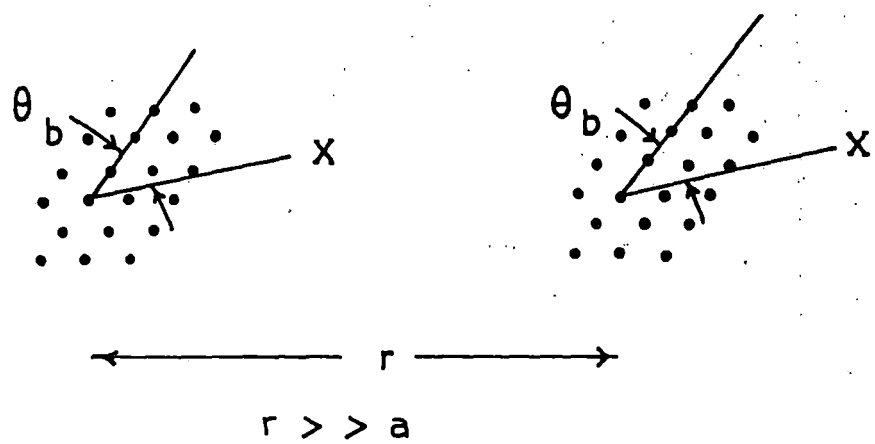

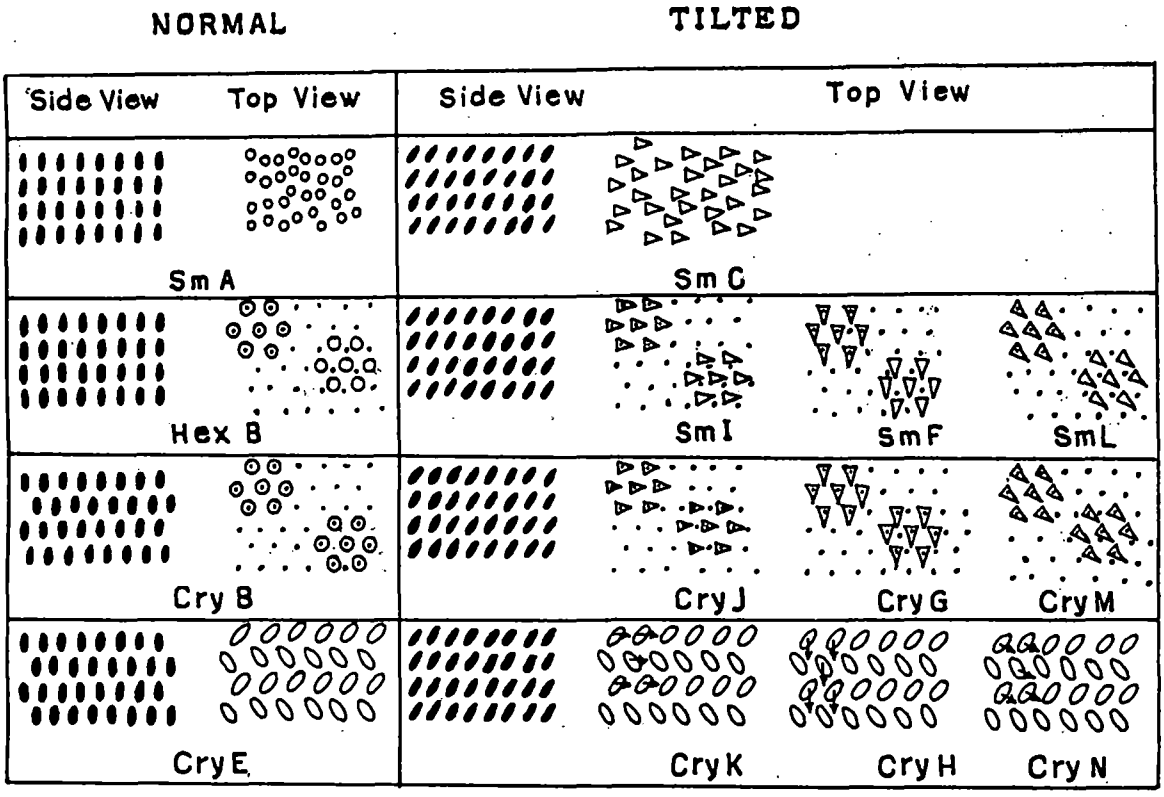

Figure 1.3. Schematic illustration of the moleculer order in various liquid crystal phases with a layer structure. The triangles represent molecular tilt direction and small dots represent two dimensional hexagonal lattices.

order within the layer, and long range positional order within as well as normal to the layer are reclassified as the so called "crystal" phases viz. Cry B, Cry G, Cry J, Cry E, Cry H etc. [19]. The so called "true" smectics on the other hand are charectarised by different degrees of ordering ranging from short range order (SRO), quasi long range order (QLRO) to long range order (LRO). A schematic illustration of molecular order in various smectic liquid crystals is shown in Figure 1.3 [48a]. Since the present work is mostly concerned with S_A, S_B and S_C phases only these phases will be discussed in more detail.

1.2.2a Smectic A phase

In smectic A phase, the preferred direction of the long molecular axes is perpendicular to the plane in which the centres of mass of the molecules are principally situated. There is a long-range translational order in the positioning of the smectic layers, but within each layer the distribution of the molecular centres is random [41,49,50], with only a short range order typical of liquids. The smectic A molecules can rotate about the long axis sweeping out a volume which is cylindrical in shape. Due to this infinite fold rotational symmetry about an axis parallel to the direction normal to the layer, smectic A liquid crystals at thermal equilibrium are uniaxial systems [51] with the optic axis perpendicular to the plane of the layer. Recent studies [52-58] have shown that the smectic A phase can be further subdivided into several distinct phases such as monolayer smectic A_1, bilayer smectic A_2, partially bilayer smectic A_d, and smectic antiphase $\tilde{A}$. Details regarding this polymorphism can be found in many recent publications [59-67].

1.2.2b Smectic C phase

The smectic C phase is very similar to the smectic A phase with one dimentional density wave of orientationally ordered molecules. However, the average orientation direction, $\hat{n}$, of the molecules which form the liquid crystal is tilted at an angle θ_t(say), with respect to the layer normal (Figure 1.4a). The layer spacing of the smectic C phase is less than that of the corresponding A phase due to this tilt. The tilt angle in the smectic C phase may be constant or temperature dependent [59]. The medium is biaxial since the director fluctuations in the n-z plane are different in magnitude from those in an orthogonal plane containing $\hat{n}$. A quadrupolar charge distribution in the molecules helps in formation of smectic C phase. A two dimensional model to demonstrate this effect is shown in Figure 1.4b where it is seen that the intermolecular electrostatic interaction is repulsive when the molecules are oriented in the direction of the layer normal (lower part of Figure 1.4b) and can be reduced by a tilted arrangement (upper part of Figure 1.4b). Again, packing considerations of the hydrocarbon chains of the molecules exhibiting this mesophase is such that, a tilted arrangement of the molecules within the layer is energetically more favourable.

1.2.2c Smectic B phase

Smectic B liquid crystals also have layered structure with the molecular long axes arranged perpendicular to the layer normal. However, the constituent molecules of the phase are packed in a hexagonal array in the plane of the layers, representing two - dimensional crystals. On the basis of x-ray

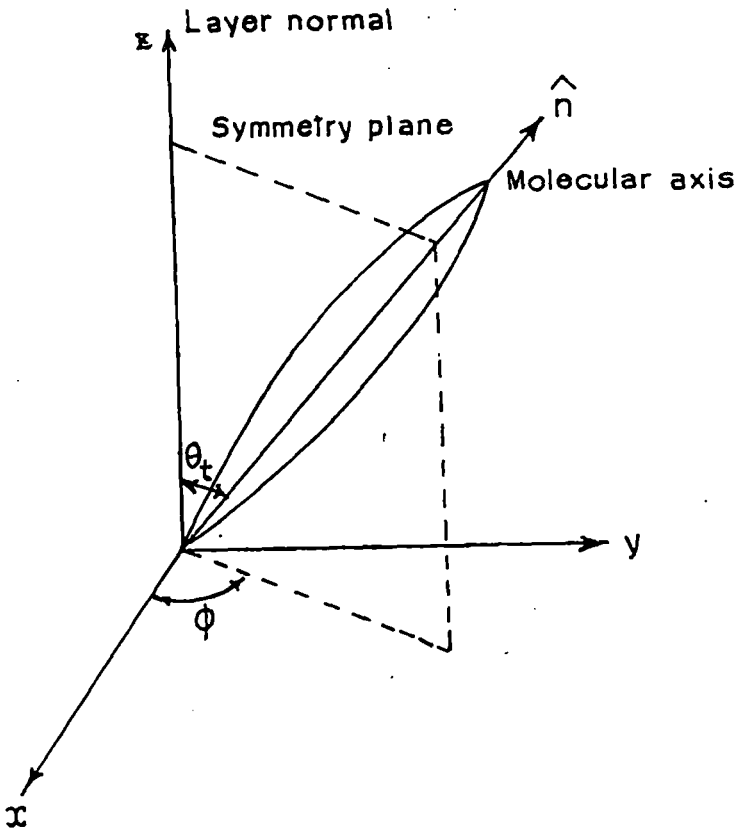

Figure 1.4a. Orientation of a molecule within the smectic C layer, showing the tilt angle θ_t with respect to the layer normal.

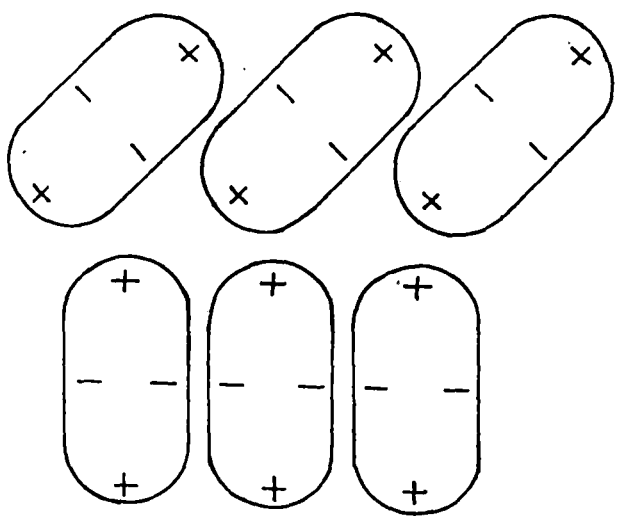

Figure 1.4b. A two dimensional model to demonstrate the quadrupolar origin of tilt in the smectic C phase[23].

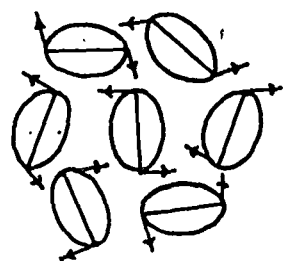

Figure 1.5. Schematic diagram of a cluster of smectic B molecules leading to a co-ordinated rotational motion within the hexagonal net.

[60] and electron diffraction [61] experiments done on bulk aligned samples as well as on thin films, the traditional smectic B phase has been further reclassified into crystal B phase and hexatic B phase [48b]. The hexatic B phase has also a layer structure with the long axis of molecule (molecular director) parallel to the layer normal. The centre of mass of the molecules exhibit a three - dimensional long range bond orientational order but only a short-range translational order. The crystal B phase, however, has long range inter- and intra layer translational order and long range bond orientational order as well. The Crystal B phase is still considered liquid crystal because of the weak coupling between the smectic layers. Hence, they exhibit shear and flow properties under stress. The Mössbauer spectra of this phase is also inconsistent with that of solid.

Due to the hexagonal arrangement of the molecules within the layers of the smectic B phase, a highly co-ordinated or synchronised rotational motion of the molecules exists [62-64], such that the edge of one molecule is presented to the side of a neighbouring molecule (Figure 1.5). Due to this hindered rotation, the smectic B phase may show optical biaxiality. In the present dissertation an attempt has been made to study the effect of this biaxiality in the smectic B phase of a liquid crystalline compound [65].

The layers of the hexagonal smectic B phase are so stacked so as to give a number of possible variations in packing arrangement between correlated layers, e.g., bilayer (ABAB.... packing), trilayer (ABCABC.... packing), random (ABCBCA....) or (rarely) correlated monolayer (AA....) structures. The stacking may change with temperature in the smectic B phase for the same compound. No change in enthalpy or texture accompany the changes

in the staking type.

1.3 New liquid crystalline phases

1.3a Discotic phases

A fundamentally new mesophase, unlike the previously mentioned ones was reported in 1977 by Chandrasekhar et al [66]. The molecules of the phase are disc-like in appearance and are stacked like coins to form a new class of liquid crystals, known as discotic liquid crystals. The structure of the mesophase may be classified broadly into three types, the columnar (of which several variants have been identified) the nematic and the lamellar. Previously, very similar disc-like mesogens have been identified in petrolium and coal tar [67,68]. In recent years, significant amount of research have been performed with discotic liquid crystals [69-73].

1.3b Blue phase

The existence of this phase has been observed in a very small temperature range ($\approx 0.1^{\circ}C$) between the cholesteric and isotropic phase. Compounds exhibiting "blue" phase have a short pitch (< 7000 Å) and can display upto the 3 different variety of blue phases [74]. The structures of these blue phases are not very clear, they exhibit cubic symmetry and have a structure closely related to the cholesteric phase. The structures are explained in terms of defects in the cubic array. Blue phases do not possess double refraction, but show optical activity and selective reflection of circularly polarised light.

1.3c Chiral tilted smectic phases

Chiral smectic liquid crystals represent a class of materials which exhibit phases with a dipolar ordering i.e. they can form ferroelectric (FE), ferrielectric (FI) and antiferroelectric (AF) phases [75]. In these phases the molecules are tilted from the smectic layer normal. Due to the tilt the rotation of molecules about their long axes is not isotropic, resulting in a non-compensated macroscopic component of the molecular dipole-moment. This component lies in the smectic layer oriented perpendicularly to the tilt direction, parallel to a local polar two fold axes [76]. The ferroelectric smectic C^* phase is analogous in structure to the smectic C phase except that the molecules possesses chirality, resulting in a spontaneous "ferroelectric polarization". The chiral interactions lead to a twisted structure and consequently the polarization also has a helical arrangement too. In fact, all tilted smectic phases have equivalent ferroelectric smectic phases (smectic F^*, smectic I^*, smectic J^*, smectic G^*, smectic K^*, smectic H^*) where the constituent molecules are chiral. While the FI phase has the local dipole moments partially compensated, it is supposed that in AF phase the molecules in the neighbouring smectic layers are tilted to the opposite direction, as a result of which the opposite dipole-moments in the next layers cancels to zero. Recently, both antiferroelectric [75a] and ferrielectric [75b] smectic phases have been observed in a substance MHPOBC. Ferroelectric liquid crystals are very important for fast switching electrooptical display devices.

1.3d Polymer dispersed liquid crystals

This new class of liquid crystals generally consists of micron size droplets of low molecular weight nematic liquid crystals dispersed in a polymer binder. The nematic droplets scatter light causing a white opaque appearence in PDLC films. Application of appropriate voltage causes the nematic droplets to align in such a way that their refractive indices nearly matches that of the polymer causing transparency. They are widely used in displays, switchable windows and other light shutter devices [77-79].

1.3e Injected smectic phase

Injected smectic phases are formed in binary mixtures whose components show only nematic phases in their pure states [80-81]. One of components of the mixture characteristically have a strong terminal polar group while the other have non-polar terminal group [82-97]. Dipole-induced dipole interactions evidently play a major part in this phase stabilization. Injected smectic phase has also been observed in mixtures of other types of molecules [98-100]. Quantitative understanding of the formation of this phase is difficult as it would require potential dependent attractive and repulsive interactions for both the components. However, a model for the induced smectic phase has been discussed by de Jeu et al [101].

1.3f Re-entrant phase

Normally liquid crystals on heating give rise to a series of mesophases charecterised by increasing disorder with respect to

orientational, positional and translational ordering. However, in contrary to this, in certain cases the less ordered phase reappears at a lower temperature than the more ordered phase. This phenomenon is known as re - entrant polymorphism, first discovered by Cladis etal [102] in 1975. This phase has been observed in mixtures [102-103] as well as in single compounds at high pressure [104-105] or at atmospheric pressure [106-113]. Re-entrant smectic phase have also been reported in terminal polar compounds. The mechanism of the formation of the re-entrant nematic phase at lower temperature has been explained by Cladis [114-116]. Based on the molecular point of view, Chandrasekhar [117] has reviewed and discussed qualitatively the re-entrant phenomenon.

REFERENCES

[1]. F. Reinitzer, Monatsch. Chem., 9, 421 (1888), Liq. Cryst., 5, 7 (1989).

[2]. O. Lehmann, Z. Physik. Chem., 4, 462 (1889).

[3]. G. Friedel : In Colloid Chemistry, ed. J. Alexander, Vol.1, p-102ff. The Chemical Catalogue Company, Inc., N.Y. (1926).

[4]. G. Friedel and E. Friedel, Z. Krist., 79, 1 (1931).

[5]. W. Kast, Landelt-Bornstein Tables, vol.2, 6th edition, p-266, Springer-Verlag (1969).

[6]. D. Demus and H. Demus, Flüssige Kristalle in Tabellen, VEB Deutscher Verlag fur Grundstoffindustrie, Leipzig (1973).

[7]. G. H. Brown, J. Electronic Materials, 2, 402 (1973).

[8]. H. Kelker and R. Hartz, Hand book of Liquid Crystals, Verlag Chemie, Weinheim, p. 67 (1980).

[9]. H. Zocher, Liquid Crystals (2), part 1, ed. G. H. Brown, G & B Science Publisher, Inc. N.Y., 115 (1969).

[10]. I.G. Chistyakov, Zhidkie Kristally (Liquid Crystals), Nauka, Moscow (1966).

[11]. P. G. de Gennes, The Physics of Liquid Crystal, Clarendon Press, Oxford,(1974).

[12]. L.M. Blinov, Usp. Fiz. Nauk, 114, 67 (1974) [Sov. Phys. Usp., 17, 658 (1975).

[13]. G. W. Gray, Molecular structure and the properties of Liquid Crystals, Academic Press (1962).

[15]. E.B. Priestley, P.J.Wojtowicz and P. Sheng, eds., Introduction to Liquid Crystals, Plenum, New York, 1974.

[16]. S. Chandrasekhar, Liquid Crystals, Cambridge University Press, Cambridge, (1977).

[17]. G.W. Gray and P.A.Winsor (Editor) Liquid crystals, Vol 1 and

2, Ellis Horwood Limited, (1974).

[18]. G. Vertogen and W.H. de Jeu, Thermotropic Liquid Crystals, Fundamentals, Springer-Verlag (1988).

[19]. P.S. Pershan, Structure of Liquid Crystal Phases, World Scientific, (1988).

[20]. G.W. Gray and J.W. Goodby (Editors), Smectic Liquid Crystals, Leonard-Hill (1984).

[21]. G.R. Luckhurst and G.W. Gray, (Editors) The Molecular Physics of Liquid Crysals, Academic Press (1979).

[22]. Advances in Liquid Crystals ed. G. W. Brown, vol 1-6 Academic Press, (1975 - 1983).

[23]. Liquid Crystals, Applications and Uses, (Ed. B. Bahadur, World Scientific (1991). Vol. 1,2 and 3.

[24]. Thermophysical properties of liquid crystals, A.L. Tsykalo, Gordon and Breach Science Publishers.

[25]. Modern topics in Liquid Crystals, (Ed. A. Buka). World Scientific (1993).

[26]. Physics of Liquid Crystalline Materials, (Ed. I.C. Khoo and K. Simoni), Gordon and Breach Science Publishers.

[27]. A.S.C. Lawrence, "Lyotropic Mesomorphism in Lipid-Water Systems, Mol. Cryst. Liq. Cryst. 7, 1 (1969).

[28]. P.A. Winsor, Chem. Rev. 68, 1 (1968).

[29]. P. Ekwall, L.Mandell and K. Fontell, Mol. Cryst. Liq. Cryst. 8, 157 (1969).

[30]. V. Luzzati and F. Reiss-Husson, Nature, 210, 1351 (1966).

[31a]. G. Friedel, Ann Physique, 18, 273 (1922).

[31b]. H. Sachmann and D. Demus, Mol. Cryst. Liq. Cryst., 21 239 (1973).

[32]. A.de Vries, Mol. Cryst. Liq. Cryst. 10, 31 (1970); ibid 10, 219 (1970); ibid 11, 36 (1970).

[33]. K. Usha Deniz, A.S. Paranjpe, V. Amirthalingam and K.V.

Muralidharan, Mol. Cryst. Liq. Cryst. (Letters),49, 265 (1979).

[34a]. K. Praefcke, B. Kohne, B. Gundogan, D. Singer, D. Demus, S. Diele, G. Pelzl and U. Bakowsky, Mol. Cryst. Liq. Cryst. 198, 393 (1991).

[34b]. L.Y. Lu and A. Saupe, Phys. Rev. Lett. 45, 1000 (1980).

[35]. G.H. Brown, Amer. Scientist, 60, 64 (1972).

[36]. T. Nakagiri, H. Kodama and K.K. Kobayashi, Phys. Rev. Lett., 27, 564 (1971).

[37]. I.G. Chistyakov, Sov. Phys. Ups., 9, 551 ((1967)

[38]. K. Herrmann and A.H.Krummacher, Z. Kristallogr. Mineral. Petrogr., A81, 317 (1932).

[39]. G. Friedel, C.R. Acad. Sci., Paris, Ser. A.B., 180, 269 (1925).

[40]. H. Sackmann and D. Demus, Mol. Cryst. Liq. Cryst., 21, 171 (1973).

[41].S. Diele, P. Brand and H. Sackmann, Mol. Cryst. Liq. Cryst., 16, 105 (1972).

[42]. D. Demus, G. Kunicke, J. Neelson and H. Sackmann, Z. Naturforsch., 23a, 84 (1968).

[43]. D. Demus, S. Diele, M. Klapperstuck, V. Link and H. Zaschke, Mol. Cryst. Liq. Cryst., 15, 161 (1971).

[44. A.de Vries, Mol. Cryst. Liq. Cryst., 24, 337 (1974).

[45]. J. Falgueirettes and P. Delord, in Liquid Crystals and Plastic Crystals, Vol 2, (Eds. G.W. Gray and P.A. Winsor), Halstead, New York, 1974, p. 62.

[46]. A.de Vries and D.L. Fishel, Mol. Cryst. Liq. Cryst., 16, 311 (1972).

[47]. A.de Vries, in proceedings of the International Liquid Crystal Conference, Bangalore, December, 1973, Pramana Supplement I, p. 93.

[48]. H. Kelkar and R. Hatz, Handbook of Liquid Crystals, Verlag Chemie, Chapter 1, p. 6 (1980).

[48a].C.C. Huang in Bond Orientational Order in Condensed Matter Systems, (Ed. K.J. Strandburg) Springer - Verlag, Berlin - New York, p.78-136, 1992.

[49]. G.C. Fryberg, E. Gelerinter and D.L. Fisher, Mol. Cryst. Liq. Cryst., 16, 39 (1972).

[50]. G.R. Luckhurst and A. Sanson, Mol. Cryst. Liq. Cryst., 16, 179 (1972).

[51]. P.G. de Gennes, The Physics of Liquid Crystals, Clarendon, Oxford, 1974.

[52]. A.M. Levelut, R.J. Tarento, F. Hardouin, M.F. Achard and G. Sigaud, Phys. Rev., A24, 2180 (1981).

[53]. G. Sigaud, F. Hardouin, M.F. Achard and A.M. Levelut, J. Physique, 42, 107 (1981).

[54]. F. Hardouin, N.H. Tinh, M.F. Achard and A.M. Levelut, J. Physique, 43, L.327 (1982).

[55]. C. Druon and J.M. Wacrenier, Mol. Cryst. Liq. Cryst., 98, 201 (1983).

[56]. I. Hatta, Y. Nagai, T. Nakayama and S. Imaizumi, J. Phys. Soc. Jpn., 52, Suppl. 47 (1983).

[57]. C. Chiang and C.W. Garland, Proc. of Tenth International Liquid Crystal Conference, York, July, 1984, abstract no. E20.

[58]. F. Hardouin, A.M. Levelut, M.F. Achard and G. Sigaud, J. de Chemie Physique, 80, 53 (1983).

[59]. T.R. Taylor, J.L. Fergason and S. L. Arora, Phys. Rev. Lett. 24, 359 (1970).

[60]. R. Pindak, D.E. Moncton, S.C. Davey and J.W. Goodby, Phys. Rev. Lett., 46, 1135 (1981).

[61]. M. Cheng, J.H. Ho, S.W. Hui and R. Pindak, Phys. Rev. Letts., 59, 1112 (1987).

[62]. M. Lambert and A.M. Levelut in Anharmonic Lattices, Structural Transitions and Melting (Ed. T. Riste), Noordhoff, Leiden, 1974, p. 375.

[63]. H.M. Richardson, A.J. Leadbetter and J.C. Frost., Ann. Phys., 3, 177 (1978).

[64]. A.J. Leadbetter, M.A. Mazid and R.M. Richardson, Liquid Crystals, (Ed. S. Chandrasekhar), Heyden, London, p. 65 (1980).

[65]. Chapter 5.

[66]. S. Chandrasekhar, B.K. Sadashiva and A.K. Suresh, Pramana, 9, 471 (1977).

[67]. J.E. Zimmer and J.L. White, Mol. Cryst. Liq. Cryst., 38, 177 (1977).

[68]. J.D. Brooks and G.H. Taylor, Carbon, 3, 185 (1965).

[69]. D. Guillon, A. Skoulios, C. Piechocki, J. Simon and P. Weber, Mol. Cryst. Liq. Cryst., 100, 275 (1983).

[70]. J. Luz, Tenth Int. Conf. on Liquid Crystals, York, July 1984, abstract no H2.

[71]. P.G. de Gennes, J. de Phys., Lett., 44, 657 (1983).

[72]. A.C. Ribeiro and A.F. Martins, Tenth Int. Conf. on Liquid Crystals, York, July, 1984, abstarct no. H6.

[73]. C. Destrade, H. Gasparoux, P.Foucher, N.H. Tinh, J. Malthete and J. Jacques, J. Chem. Phys., 80, 137 (1983).

[74]. S. Meiboom, M. Sammon, Phys. Rev. Lett., 44, 882 (1980).

[75]. M. Glogarova in Modern Topics in Liquid Crystals (Ed. A. Buka), World Scientific, p. 271 (1993).

[75a].A.D.L. Chandani, Y.Ouchi, H.Takezoe, A. Fukada, K. Terashima, K. Furukawa and A. Kishi, Jpn. J. Appl. Phys., 28, L 1261 (1989).

[75b]. E. Gorecka, A.D.L. Chandani, Y. Ouchi, H.Takezoe, A. Fukada, Jpn. J. Appl. Phys. 29, L 111 (1990).

[76]. R.B. Meyer, L. Libert, L. Strzelecki and P. Keller, J.

Physique Lett. 36, L69 (1975).

[77]. J.W. Doane, A. Golemme, J.L. West, J.B. Whitehead, Jr., and B.G. Wu, Mol. Cryst. Liq. Cryst. 165, 511 (1988).

[78]. P.S. Drzaic, J. Appl. Phys. 60, 2142 (1986).

[79]. G.P. Montgomery, Jr. in Large-Area Chromogenics: Materials and Devices for Transmittance Control, C.M. Lampert and G.G. Granqvist (Ed. SPIE).

[80]. J.S.Dave, P.R.Patel and K.L.Vasant, Mol. Cryst. Liq. Cryst., 8,93 (1969).

[81]. C. S. Oh, Mol. Cryst. Liq. Cryst., 42, 1 (1977).

[82]. J.W. Park, C.S. Bak and M.M. Labes, J. Amer. Chem. Soc., 97, 4398 (1975).

[83]. C.S. Oh, Mol. Cryst. Liq. Cryst. 42, 1 (1977).

[84]. A.C. Griffin, T.R. Britt, N.W. Buckley, R.F. Fisher, S.J. Havens and D.W. Goodman, Liquid Crystals and Ordered Fluids, Vol.3, Eds. J.F. Johnson and R.S. Porter (Plenum Press, New York, 1978) p 61.

[85]. B. Engelen and F. Schneider, Z. Naturforsch., 33A, 1077 (1978).

[86]. B. Engelen, G. Heppke, R. Hopf and F. Schneider, Ann. Phys., 3, 403 (1978).

[87]. L.J. Yu and M.M. Labes, Mol. Cryst. Liq. Cryst. 54, 1 (1979).

[88]. M. Domon and J. Billard, J. Phys. (Paris), 40, C3-413 (1979).

[89]. K.P.L. Moodithaya and N.V. Madhusudana in "Liquid Crystals", Proc. Int. Liq. Cryst. Conf., Bangalore, Dec. 8, 1979, Ed. S. Chandrasekhar (Heyden, London 1980) p. 297.

[90]. F.Schneider and N.K. Sharma, Z. Naturforsch., 36a, 62 (1981).

[91]. F.Schneider and N.K. Sharma, Z. Naturforsch., 36a, 1086

(1981).

[92]. K. Araya and Y. Matsunaga Mol. Cryst. Liq. Cryst. 67, 153 (1981).

[93]. G. Derfel, Mol. Cryst. Liq. Cryst. 82, 277 (1982).

[94]. J. Szabon and S. Diele, Crystal Res. Tech.,17, 1325 (1982).

[95]. K.W. Sadowska, A. Zywocinski, J. Stecki and R. Dabrowski, J. Phys. (Paris), 43, 1673 (1982); W. Waclawek, R. Dabrowski and A. Domagala, Mol. Cryst. Liq. Cryst. 84, 255 (1982).

[96]. A. Boij and P. Adomenas, Mol. Cryst. Liq. Cryst. 95, 59 (1983).

[97]. E. Chino and Y. Matsunaga, Bull. Chem. Soc. Japan, 56, 3230 (1983).

[98]. N.K. Sharma, G. Pelzl, D. Demus and W. Weissflog, Z. Phys. Chem. (Leipzig), 261, 579 (1980).

[99]. J.W. Goodby, T. M. Leslie, P.E. Cladis and P.L. Finn. Proc. ACS Symposium on Liquid Crystals and Ordered Fluids, Las Vegas, 1982, Ed. A.C. Griffin And J.F. Johnson (Plenum, New York, 1984) p. 89.

[100]. N.V. Madhusudana, V.A. Raghunathan and M. Subramanya Raj Urs, Mol. Cryst. Liq. Cryst. 106, 161 (1984).

[101]. W.H. de Jeu, L Longa and D. Demus, J. Chem. Phys., 84, 6140 (1986).

[102]. P.E. Cladis, Phys. Rev. Lett. 35, 48 (1975).

[103]. D.Guillon, P.E.Cladis and J. Stamatoff, Phys. Rev. Lett. 41, 1598 (1978).

[104]. P.E.Cladis, R.K. Bogardus, W.B Daniels and G.N.Taylor, Phys. Rev. Letters, 39, 720 (1977).

[105]. P.E.Cladis, R.K. Bogardus, and D.Aadsen, Phys. Rev. A18 2292 (1978).

[106]. F.Hardouin, G.Sigaud, M.F.Achard and H.Gasparoux, Solid St. Commun. 30, 265 (1979), Phys.Lett. 71A, 347 (1979).

[107]. N.V. Madhusudhana, B.K.Sadashiva and K.P.L.Moodithaya, Curr. Sci. 48, 613 (1969).

[108]. F. Hardouin, G. Sigaud, M.F.Achard and H.Gasparoux, Phys. Lett. 3, 71A, 347 (1979).

[109]. 15. N.H. Tinh and H. Gasparoux, Mol. Cryst. Liq. Cryst. Lett., 49, 287 (1979).

[110]. K. P. L. Moodithaya, and N.V. Madhusudhana, Proc. Int. Liq. Cryst. Conf., Bangalore, Dec. 8, 1979, Ed. S. Chandrasekhar.

[111] J.C.Dubois, N.H.Tinh, A. Zann and J. Billard, Nouv. J. Chimie, 2, 647 (1978).

[112]. B. K. Sadashiva, Proc. Int. Liq. Cryst. Conf. ,Bangalore, Dec.8, 1979, ed. S. Chandrasekhar, P-165, Heyden (19880).

[113]. C. Legrand, J. P. Parneix and A. Chapton, Tenth Int. Conf. on Liquid Crysts.,York, 1984, Abstract no -E 18.

[114]. P. E. Cladis in "Liq. Crystals ", Proc. Int. Conf. Bangalore, 1979, Ed. S. Chandrasekhar (Heyden, London , 1980) p-105.

[115] P. E. Cladis , Mol. Cryst. Liq. Cryst., 67, 177 (1981).

[116]. P. E. Cladis , D. Guillon, F. R. Bouchet and P. L. Finn, Phys. Rev., 23A, 2594 (1981).

[117]. S. Chandrasekhar, Mol. Cryst. Liq. Cryst.,124, 1 (1985).

CHAPTER - 2

THEORETICAL BACKGROUND

2.1 Theories of liquid crystalline phases

The theories of liquid crystalline phases have been described in detail in several books [1-5]. I am giving below, the salient features of the mean-field theories of nematic and smectic A phases as developed by Maier-Saupe [6] and McMillan [7,8] respectively.

2.1.1 Maier-Saupe mean field theory of nematic phase of rod like molecules

In Chapter 1 it has been mentioned that the rod like molecules of a liquid crystalline substance tend to align their long axes along a preferred direction, called the director $\vec{n}$, below a certain temperature. The problem of the nematic phase (N) and the Nematic-Isotropic (N-I) transition has been successfully solved in 1959 by Maier and Saupe. They assumed that the molecular force of the induced dipole-induced dipole type (i.e anisotropic dispersive force) between two neighbouring molecules is primarily responsible for this phase. The distribution of the molecular long axes about the director is given by an orientational distribution function $f(\cos\theta)$, assuming cylindrical symmetry of the mesophase, where θ is the angle between the director and the molecular long axis. Since the molecules within the system have no head to tail asymmetry, then $\vec{n} = -\vec{n}$, and $f(\cos\theta)$ is an even function of $\cos\theta$. The distribution function can also be written as [9]:

$$f(\cos\theta) = \sum_{L \text{ even}} (2L+1)/2 \, \langle P_L(\cos\theta) \rangle \, P_L(\cos\theta) \qquad 2.1$$

where $P_L(\cos\theta)$ are the L^{th} even order Legendre polynomials, and

$\langle P_L(\cos\theta)\rangle$ are the statistical average given by

$$\langle P_L(\cos\theta)\rangle = \int_0^1 P_L(\cos\theta)\, f(\cos\theta)\, d(\cos\theta) \Big/ \int_0^1 f(\cos\theta)\, d(\cos\theta) \qquad 2.2$$

$\langle P_L\rangle$ are called the orientational order parameters, of which the first member, i.e, $\langle P_2\rangle$ is commonly called the order parameter. This order parameter gives the measure of how well aligned the molecules are in a nematic phase. $\langle P_2\rangle$ is equal to one for perfectly oriented sample and is equal to zero for randomly oriented, i.e, isotropic liquid.

A phenomenological expression for the mean field can be written as follows. The average field should be such that the potential of the molecule under study should be minimum when it makes θ =0 with $\hat{n}$ i.e., the mean field would tend to rotate the molecules towards $\hat{n}$. Secondly the torque of the mean field should be more, more aligned are the molecules in the system. On these two considerations the potential energy of a molecule making an angle θ with the director $\hat{n}$ is [6]

$$V(\cos\theta) = v\langle P_2\rangle\, P_2(\cos\theta) \qquad 2.3$$

where v is the coupling constant.
Hence, the orientational distribution function $f(\cos\theta)$ and the partition function Z are given by,

$$f(\cos\theta) = Z^{-1} \exp\left[-V(\cos\theta)/kT\right] \qquad 2.4$$

$$Z = \int_0^1 \exp\left[-V(\cos\theta)/kT \right] d(\cos\theta) \qquad 2.5$$

k being the Boltzmann constant.
Substituting the value of $f(\cos\theta)$ as in equation (2.4) to

equation (2.2), we get for L = 2

$$\langle P_2 \rangle = Z^{-1} \int_0^1 P_2(\cos\theta) \exp [\langle P_2 \rangle P_2(\cos\theta)/T^*] \, d(\cos\theta) \qquad 2.6$$

where $T^* = v/kT$

From the principle of ergodicity it is seen from equation (2.6) that the time average, (i.e. order of a particular molecule averaged over sufficiently long time) is equal to the ensemble average (i.e. the average over all other molecules) and a self consistent solution of it is sought. For all values of T^* (or T) $\langle P_2 \rangle = 0$ is a solution, while for $T^* < .22284$,two other solutions of $\langle P_2 \rangle$ appear. Obviously, the state with minimum free energy is the stable one. It can be shown that for $T^* < .22019$, a state with $\langle P_2 \rangle > 0$ is stable one, which can be identified with nematic phase, whereas for $T^* > .22019$, $\langle P_2 \rangle = 0$, gives the equilibrium state, which is the isotropic liquid.

The nematic-isotropic liquid transition occurs at $T_c^* = 0.22019$ and $\langle P_2 \rangle_c = 0.4289$, according to the Maier Saupe theory. Thus, this transition is always of the first order. However, the N-I transition energy has been calculated to be around 0.83 cal/mole ^{o}K which pretty small compared to usual solid to liquid transition which is around 25 cal/mole^{o}K . This transition is therefore often called weakly first order transition. Values of $\langle P_2 \rangle$ as a function of T^* can be calculated easily by solving equation (2.6) iteratively. For many liquid crystals the Maier-Saupe $\langle P_2 \rangle$ values agree quite well with those found experimentally.

2.1.2. McMillan's theory for smectic A phase

In smectic A phase, there is a periodic density variation along the layer normal (z direction) in addition to the

orientational ordering of the molecular axes. Hence, the nomalised distribution function can be written, in this case, as

$$f(\cos\theta),z) = \sum_{L,\text{even}} \sum_{n} A_{L,n}\, P_L(\cos\theta)\, \cos\,(2\pi nz/d) \qquad 2.7$$

$$\text{with} \int_{-1}^{1} \int_{0}^{d} f(\cos\theta,z)\, dz\, d(\cos\theta) = 1 \qquad 2.8$$

as normalising condition, d being the layer thickness.

McMillan [7,8], following Kobayashi [10,11], assumed a model potential of the following form

$$V_M(\cos\theta,z)=-v[\, \delta\alpha\tau\, \cos(2\pi z/d) + \{\eta + \alpha\sigma\, \cos\,(2\pi z/d)\}\, P_2(\cos\theta)] \qquad 2.9$$

where α and δ are two parameters of the potential. $\eta=\langle P_2(\cos\theta)\rangle$, $\tau=\langle\cos(2\pi z/d)\rangle$ and $\sigma=\langle P_2(\cos\theta)\ \cos(2\pi z/d)\rangle$ are the orientational, translational and mixed order parameters respectively, and $\langle..\rangle$ denotes statistical average of the quantities inside.

The distribution function can be written as

$$f_M(\cos\theta,z) = Z^{-1}\, \exp\,[\, -V_M(\cos\theta,z)/kT\,] \qquad 2.10$$

where the partition function

$$Z = \int_0^1 \int_0^d \exp\,[\, -V_M\,(\,\cos\theta,z)/kT]\, d(\cos\theta)\, dz \qquad 2.11$$

Once again, three self consistency equations containing η,τ and σ can be written and solved iteratively.

Out of several solutions, the equilibrium state is identified by the minimum value of free energy.

In general, we get the following three cases:

Case I: $\eta = 0$, $\tau = 0$, $\sigma = 0$, isotropic liquid.
Case II: $\eta \neq 0$, $\tau = 0$, $\sigma = 0$, nematic liquid crystal.
Case III: $\eta \neq 0$, $\tau \neq 0$, $\sigma \neq 0$, smectic liquid crystal.

While nematic-isotropic transition is always first order, the smectic A - nematic transition can be either first order ($T_{AN}/T_{NI} > 0.88$) or second order ($T_{AN}/T_{NI} < 0.88$), where T_{AN} and T_{NI} are the smectic A- nematic and nematic-isotropic transition temperatures respectively.

2.2 Identification of phases

2.2.1 Texture studies

The most striking feature of liquid crystals is the wide variety of visual patterns they display under polarised light. These patterns called textures are due almost entirely to the defect structure that occurs in the long-range molecular order of the liquid crystalline materials. Appearing under the polarizing microscope as ell ipses, parabolas, hyperbolas, lines and points, colourful structural singularities are understood through topological and geometrical arguments. For the determination of transition temperatures and the identification of liquid crystalline phases, observation of textures is an important technique for the liquid crystal physicist. They are observed in thin layers ($\approx$ 10-20 micrometer) between two glass slides. Change in texture at a particular temperature indicates the occurrence of phase transition. For a given structure, different textures can exist, depending on the special conditions in preparations of the sample.

Homeotropic textures are occasionally observed in phases of nematic, smectic A, smectic B and other orthogonal smectic phases. In smectic C, smectic F and smectic I phases (all tilted smectic phases) broken focal conic texture are generally observed [12]. The in-layer ordered smectic phases often show mosaic texture. Classification of different liquid crystalline phases by the observation of textures alone is often ambiguous, and other methods are needed to support it. Detailed description of various textures, with photographs, is given by Demus and Richter [12].

2.3. X-ray diffraction from mesophases

Studies of the properties of liquid crystals and further developments in the theory of the liquid-crystalline state are based, first and foremost, on the results of structural investigations, and, in particular x-ray structure analysis. From x-ray experiment, the fourier image of the correlation density function can be determined, the reconstruction of which from the scattering data yields information both on the mutual arrangement of molecules in a liquid crystal and the specific features of the orientational and translational long range order. Different liquid-crystalline phases give different x-ray patterns. X-ray data enable the statistical functions characterizing various distortions of the initial crystal lattice to be determined [13,14], and give the parameters of the orientational order in a liquid crystal, the tilt of the molecules, and the electron density distribution in smectic layers [13-19].

Unoriented nematic phase shows x-ray diffraction pattern which is a uniform halo just like that of an isotropic liquid. This is due to the fact that, generally a liquid crystal sample

consists of a large number of domains, the molecules being aligned within each domain in a preferred direction, i.e., the director, but there is no preferred direction for the sample as a whole and naturally, x-ray diffraction pattern has a symmetry of revolution around the direction of x-ray beam.

The principal features of the x-ray pattern of a nematic sample, which is oriented perpendicular to the incident x-ray beam, is shown in the Figures 2.1 (a) and (b). The main halo has split into two crescents for each of which the intensity is maximum in the equatorial direction, i.e., perpendicular to the director (optic axis). These crescents are formed mainly due to the nearest neighbour intermolecular scattering and the corresponding Bragg angle is a measure of lateral intermolecular distance. The angular distribution of the x-ray intensity (Figure 2.1(a)), $I(\psi)$ vs. ψ, also gives the orientational distribution function $f(\cos\theta)$ and order parameters $\langle P_L \rangle$, (L =2,4).

In the meridional direction, at a much smaller Bragg angle, a pair of crescents are also seen. They are connected with apparent molecular length. Sometimes, the inner difuse crescents are replaced by sharp spots and the phase is called " cybotactic nematic phase". In Figure 2.1(b), the four sharp spots arise due to the molecular arrangement within each cybotactic group [20], such that the ends of the molecules constitute well-defined boundary planes which are non orthogonal to the direction of the molecules in the group. This is an example of "skewed cybotactic nematic". In "normal cybotactic nematic" the boundary planes are orthogonal to the director. The tilt angle τ, which is the angle between the molecular long axis and the normal to the plane can be determined from $\tau = (90^{\circ} - \phi/2)$ (Figure 2.1(b)).

The x-ray diffraction pattern from smectic A phase is shown in Figure 2.1(c). The meridional spots are formed due to Bragg

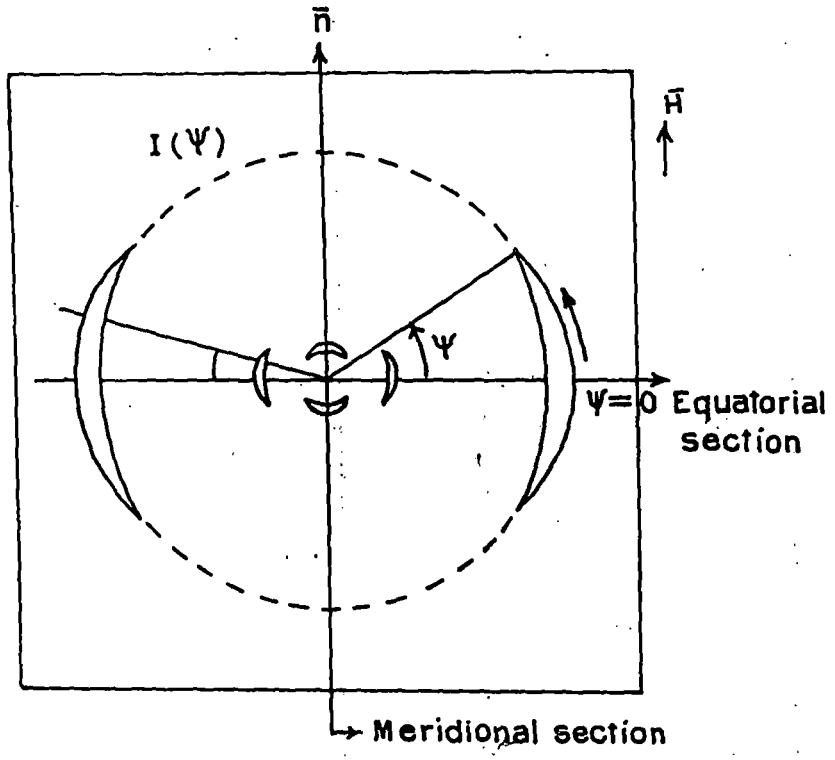

Figure 2.1(a) Schematic representation of the x-ray diffraction pattern of an oriented nematic liquid crystal.

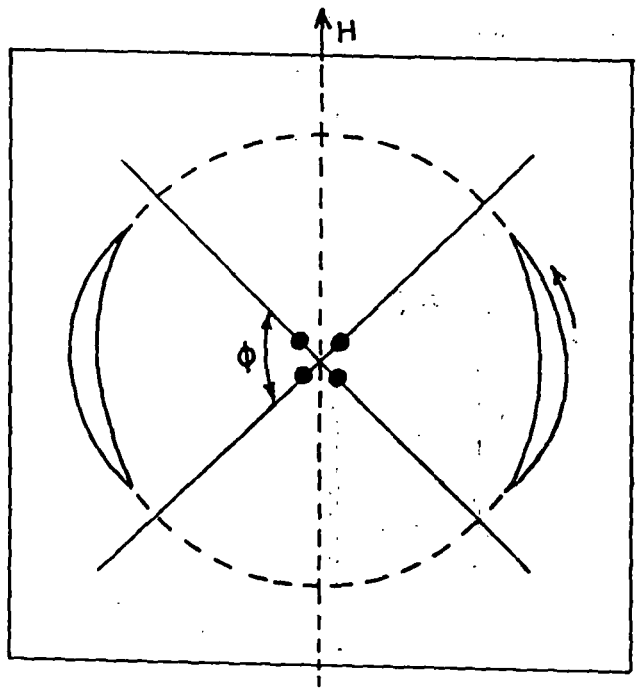

Figure 2.1(b) Schematic representation of the x-ray diffraction pattern of an oriented "skewed cybotactic" nematic liquid crystal.

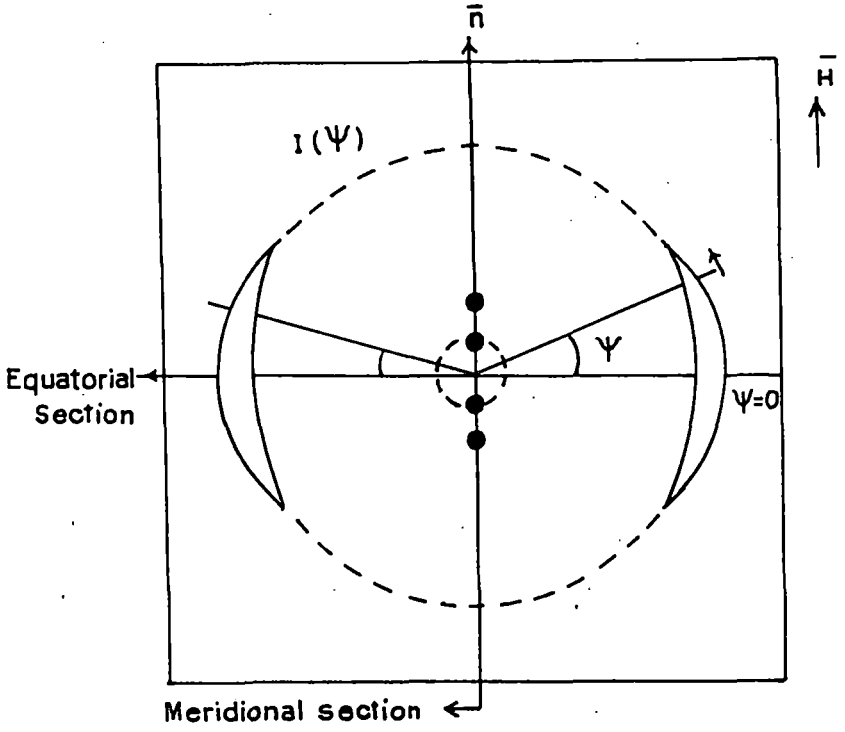

Figure 2.1(c) Schematic representation of the x-ray diffraction pattern of an oriented smectic A liquid crystal.

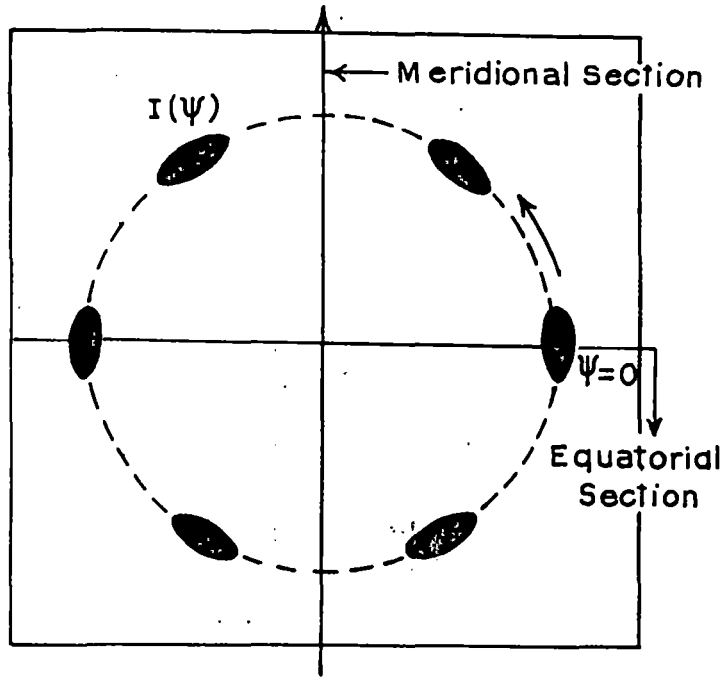

Figure 2.1(d) Schematic x-ray scattering profile for the smectic B phase with the incident x-ray beam parallel to the layer normal.

reflection from the layers and provide the value of the layer thickness. Since the smectic A phase can have only quasi-long range order (QLRO) along its layer normal [3,21], the second order Bragg reflections in the meridional direction are generally very weak and are often absent in the x-ray photographs. When present, these second order reflections provide a method for calculating τ, the translational order parameter.

Figure 2.1 (d) represents the schematic scattering profile for a three-dimentionally ordered system with hexagonal symmetry as in the smectic B phase, with the incident x-ray beam parallel to the layer normal. The outer diffraction ring is split up into six spots of strong intensity. The angular distribution of the x-ray intensity $I(\psi)$ versus ψ gives the measure of the bond orientational order (BOO) within the smectic B phase.

We, also get some faint diffuse rings (crescents) in our x-ray photographs, which may be due to (a) intra molecular atomic scattering, (b) next nearest neighbour intermolecular scattering and (c) effect of white radiation contained in Ni filtered Cu radiation. We are generally not concerned with those diffraction patterns.

2.3.1 Experimental technique and data analysis: x-ray diffraction studies.

X-ray diffraction photographs were obtained with the apparatus described below (Figure 2.2) using nickel filtered CuK_{α} radiation in the transmission geometry on a film [22], using a flat plate camera designed in our laboratory by Jha et al [21]. X- ray diffraction photographs were taken at different temperatures in the presence of a magnetic field. The camera has the provisions to change the collimator (2), spacer (15) and

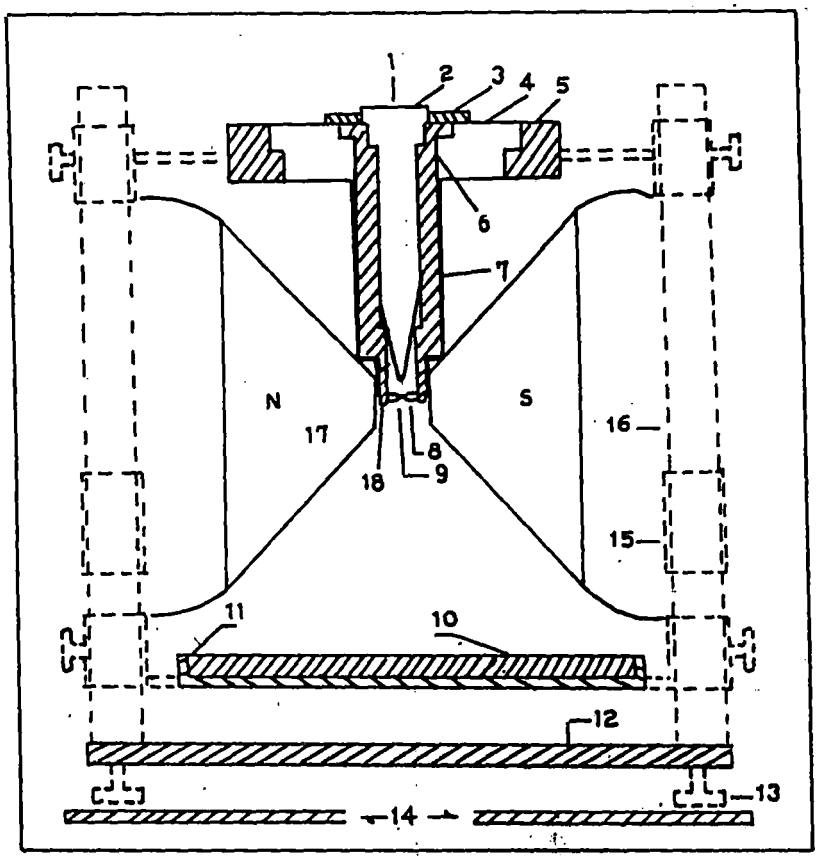

Figure 2.2 Sectional diagram of the x-ray diffraction camera. 1. X-ray 2. Collimator 3. Brass ring 4. Ring of syndanyo board 5. Brass ring 6.Cylindrical brass chamber 7. Asbestos insulation and heater winding 8. Specimen holder and thermocouple 9. Sample 10. Film cassette 11. Film cassette holder 12. Base plate 13. Levelling screw 14. Brass plates over the coils of the electromagnet 15. Removable spacer 16. Supporting brass stand 17. Pole peices 18. Asbestos insulation

sample container (8). The sample was taken in a thin-walled lithium glass capillary of 1 mm diameter. The capillary containing sample was placed inside a brass block. The temperature of the block was controlled within $\pm$ 0.5^{o}C by a temperature controller (Indotherm MD 401). The sample was first heated to the isotropic phase and magnetic field (3 to 6 Kilogauss) was applied parallel to the capillary axis. The substance was allowed to cool to the desired temperature in the presence of the magnetic field. The magnetic field was kept on during the x-ray diffraction experiment. The strength of the magnetic field was measured previously by a gaussmeter (ECIL model GH 867). X- ray beam was collimated by a collimeter of aperture 1 mm. A Ni filter of thickness 0.009 mm was used to obtain predominent CuK_{α} radiation of wavelength 1.5418$\mathring{A}$. When the temperature reached equlibrium then the x-ray tube was switched on. Photographs were taken at various constant temperatures. In case of the determination of orientational order parameters the sample to film distance was maintained at about 5 cm. To obtain better accuracy in the layer thickness measurement, x-ray diffraction photographs of inner spots were taken with sample to film distance increased to about 9 cm.

For the determination of the exact distance between the sample and film I took aluminium-powder photograph. The Bragg angle corresponding to the (hkl) reflecting plane for aluminium can be determined by [23]

$$\sin \theta' = \lambda/2a(h^2 + k^2 + l^2) \qquad 2.12$$

Thus measuring the diameter of the diffraction rings corresponding to (111) and (200) reflections [22] and values of Bragg angles from 2.12, the actual distance between sample and the film can be found out from the relation

$$\tan 2\theta' = \frac{\text{Radius of the ring}}{\text{Sample to film distance}} \qquad 2.13$$

The correction term was then calculated and used to measure the actual sample to film distance, from the apparent distance due to the spacers.

(a). Conversion of optical density to x-ray intensity

The optical density of the x- ray photographs was measured by a microdensitometer (Carl Zeiss MD 100) which has a potentiometric recording (K200) facility for linear scanning. The optical density values obtained from the densitometric scan were converted to relative intensity values by a method explained by Klug and Alexander [24]. An intensity scale was prepared by exposing different portions of a film for different times to x-rays coming through a small rectangular aperture. Multiple film technique was used for smoothening of the calibrated graph. Optical density values of these spots were then measured with the help of microdensitometer. With the front film (first film), an optical density - time in seconds (corresponds to x-ray intensity) graph was drawn. Corresponding to the measured optical densities of the second film, x-ray intensities were recorded from this graph. The average of the ratio's of these intensities corresponding to all the exposures gives the film factor. The intensities of the second film divided by the film factor converts the readings to those of the front film. As the densitometer zeroing was made on unexposed x-ray films, no subtraction for unexposed film optical density was required. The measured O.D. values and corresponding intensities give the film calibration curve as shown in Figure 2.3.

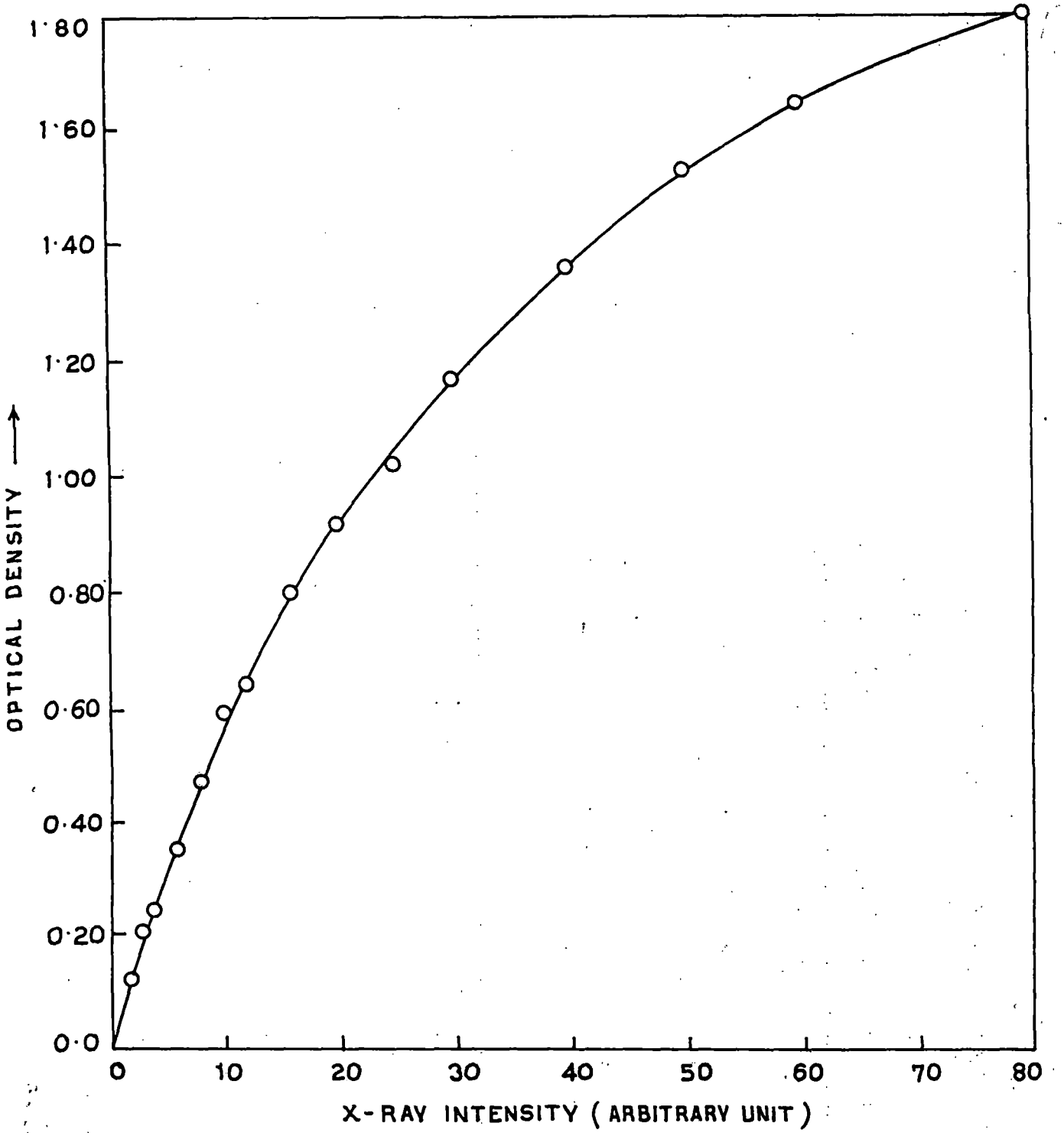

Figure 2.3 Optical density versus x-ray intensity curve used for calibration.

(b). Circular scaning of x-ray photographs

A rotating stage was fabricated by us to facilitate full 360° scanning of the photographs. Photographs were scanned to measure angular intensity distribution $I(\psi)$ which was used to calculate the orientational distribution function $f(\beta)$ and order parameters $\langle P_2 \rangle$ and $\langle P_4 \rangle$. The circular scans of the outer diffraction arc were taken from $\psi = 0$ to $\psi = 360^{\circ}$ at about 1° intervals near the peak and at larger intervals elsewhere. The optical density values obtained from the densitometric circular scan were converted to x-ray intensity with the help of calibration curve. The experimental intensity values were then corrected for background intensity values arising due to the air scattering. The peak intensity position which corresponds to $\psi = 0$ was determined from angle vs. intensity curve (Figure 2.4). Taking nineteen $I(\psi)$ values from $\psi = 0$ to $\psi = 90^{\circ}$ at 5° intervals from the smoothed $I(\psi)$ vs. ψ curve, $f(\beta)$, $\langle P_2 \rangle$ and $\langle P_4 \rangle$ were calculated by using Leadbetter's expression mentioned in later part of this chapter. A computer program has been developed for these calculations.

(c). Linear scaning of x-ray photographs

The diameter of the diffraction rings can be measured from the linear scan of the photographs using the potentiometric recorder and the corresponding optical density vs. linear distance can be plotted.

(d) Deconvolution of x-ray intensities

The experimental x-ray intensity profile were corrected for the finite width of the collimator. Extraction of the pure

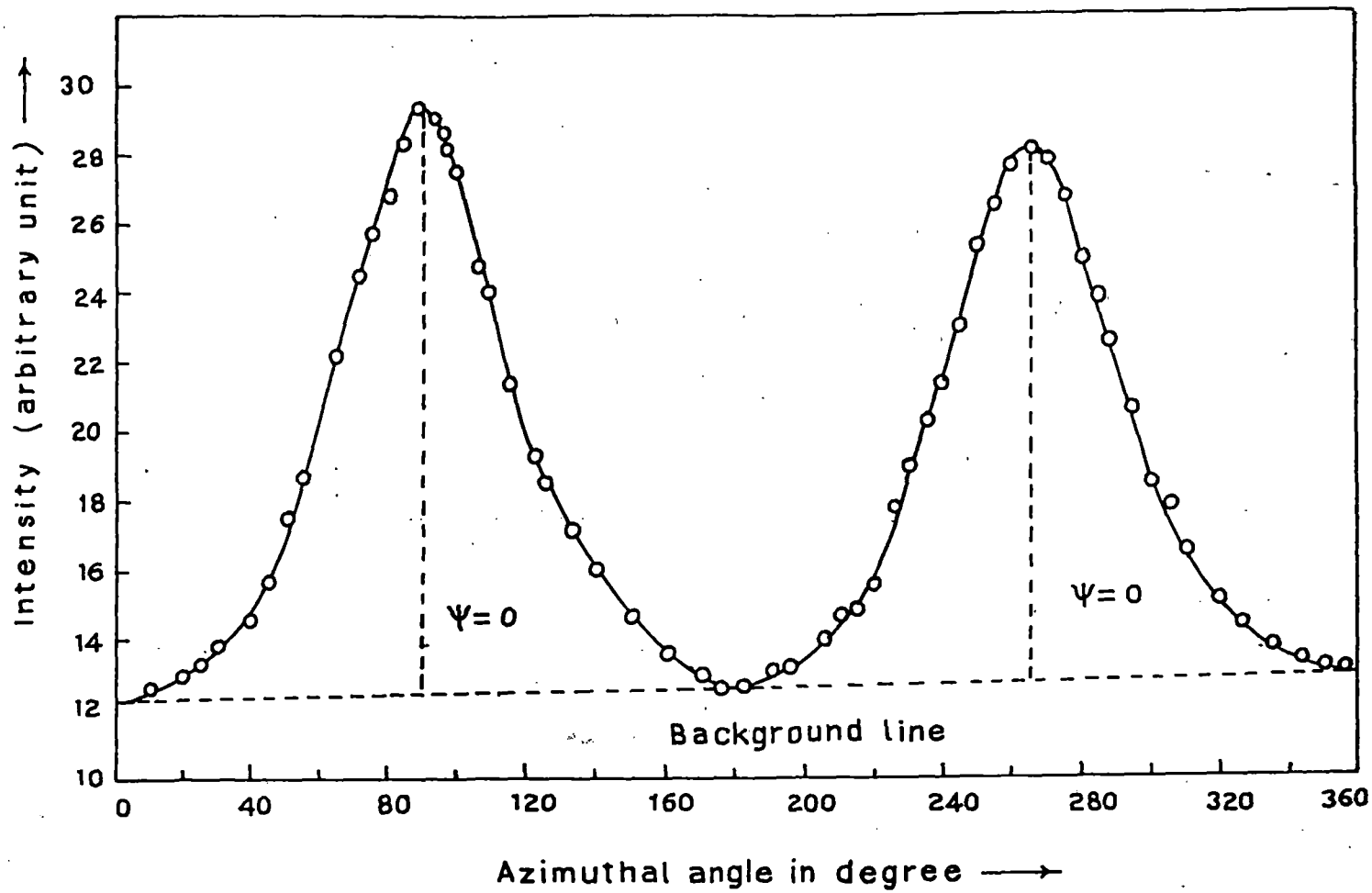

Figure 2.4 Average intensity I(Ψ) versus azimuthal angle (Ψ) curve.

diffraction profile is required for accurate determination of parameters which are affected by the spread of the x-ray diffraction pattern. In this thesis, I have used deconvoluted profiles for the determination of the correlation length ξ and Bond Orientational Order (BOO). For this, I have followed the method of Ergun [25], based on substitution of successive foldings.

The convolution of two integrable functions is defined by,

$$F(s) = \int f(s - u)g(u)du = \int f(u)g(s-u)du \qquad 2.14a$$

where it is assumed that the base domain of integration is the whole s- space. If s is a one dimensional variable, equation 2.14a is termed folding and F(s) is called the fold or convolution of f(s) with g(s). The functions F and g are generally known, the problem is to determine f; this determination is called unfolding or deconvolution. In this case F(s) is the experimentally observed x-ray intensity distribution and g(s) is the intensity distribution of the x-ray beam coming through the collimator. Deconvoluted intensity f(s) is required. As suggested by Ergun [25], the first approximation of the influence of folding is obtained by folding F with g according to equation 2.14a and subtracting the fold of F from F. This difference when added to F yields the first approximation to f and is called the first unfold. The second approximation is obtained by folding the first approximation and adding the difference between F and this second fold to the first approximation. This procedure has been continued until the sum of the absolute values of the difference between F and the fold of n^{th} approximation is minimised. The function g (the intensity distribution of the primary beam), has a bounded support as well as has been normalised i.,e

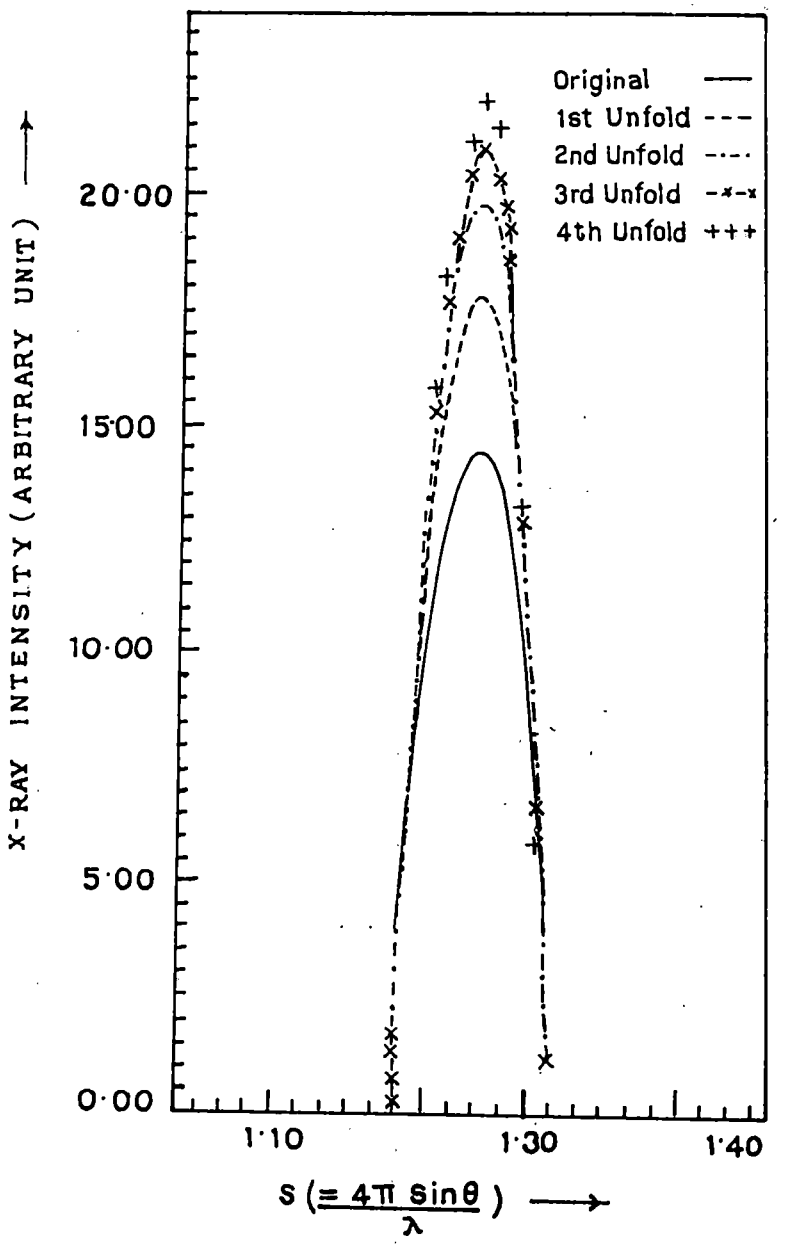

Figure 2.5 The original, first, second, third and fourth unfolded experimental x-ray intensity profile.

$$\int_{-a}^{b} g(u)du = 1 \qquad 2.14b$$

where g(0) corresponds to the value of g at about the midpoint of the primary x-ray beam corresponding to a bragg angle equal to zero. Also, after each iteration the domain of f(s) is reduced by a+b where -a to + b are the limits of the domain of g(u). It has been seen from the width of the primary x-ray beam 3-4 successive foldings are possible. However, as can be seen from Figure 2.5 that the procedure is quite convergent within 3-4 cycles of iteration. A computer programme has been developed for successive foldings and unfoldings where the integrations have been performed numerically by Simpson's Method. The experimental diffraction profile has been often fitted to an analytical form for faster and more convenient numerical integration.

2.3.2 Orientational distribution functions and order parameters

Liquid crystals are characterized by an orientational order of their constituent rod like molecules. The examination of the optical properties of nematic and smectic phases show that they have uniaxial symmetry and the axis of uniaxial (cylindrical) symmetry is parallel to a unit vector $\hat{n}$ called the director. A full description of the orientation of such molecules presupposes a knowledge of the distribution functions. The x-ray pattern of oriented samples consist of equatorial arcs. The distribution of intensity along the diffuse equatorial arcs of x-ray pattern (Figure 2.1a) is related to the distribution function [17].

$$I(\psi) = c \int_{\beta=\psi}^{\pi/2} [\, f_d(\beta)\, \sec^2\psi\, [\, \tan^2\beta - \tan^2\psi\,]^{-1/2} \sin\beta\, d\beta \qquad 2.15$$

where $f_d(\beta)$ is the distribution function for the orientation β for a local cluster of molecules relative to the director $\bar{n}$ (β = 0). The equation (2.15) can be numerically inverted to give $f_d(\beta)$ and are assumed to be close to the singlet distribution function [17].

The orientational order parameters $\langle P_2 \rangle$ and $\langle P_4 \rangle$ were calculated using the relationship

$$\langle P_L \rangle = \int_0^1 P_L(\cos \beta) f_d(\beta) \, d \cos(\beta) \; / \int_0^1 f_d(\beta) \, d \cos(\beta) \qquad 2.16$$

with L = 2, 4

In section 2.3.1a the process of measuring the intensity values $I(\psi)$ from the measured optical densities are discussed. I have calculated the intensity values by angular scanning of the x-ray diffraction photograph for $\psi = 0$ to $\psi = 2\pi$. To calculate $f_d(\beta)$ and order parameter only one quadrant is sufficient. However, I have measured $I(\psi)$ in all the four quadrants separately to calculate $\langle P_2 \rangle$ and $\langle P_4 \rangle$ and obtained almost the same value in each quadrant. Hence, I have used mean $I(\psi)$ (average of four quadrants) values for all calculations reported in this thesis. Errors in order parameter values in this manner are estimated to be $\pm$ 0.02 for both $\langle P_2 \rangle$ and $\langle P_4 \rangle$.

2.3.3 Determination of Bond Orientational Order

The order parameter associated with a system having six-fold symmetry, as in the case of smectic B liquid crystals is the Bond Orientatioanal Order (BOO) [26-29], defined to be the thermal avarage of the quantity

$$\Psi(\vec{r}) = \langle \exp\ (i6\theta(\vec{r}) \rangle \qquad 2.17$$

where the bond angle $\theta(\vec{r})$ is the orientation, relative to any fixed laboratory axis, of a bond between two nearest neighbour molecules. The bond orientational order has been calculated by evaluating the expression,

$$\langle \cos(6\theta) \rangle = \int_0^{\pi/6} \cos(6\theta) f(\theta) d\theta \Big/ \int_0^{\pi/6} f(\theta) d\theta \qquad 2.18$$

where $f(\theta)$ is the angular distribution function of centre of mass of the neighbouring molecules with respect to a central molecule and the angular distribution function has a maximum at $\theta = 0$. Equation 2.18 can be approximated by the following expression,

$$\langle \cos(6\theta) \rangle \approx \int_0^{\pi/6} \cos(6\theta) I(\theta) d\theta \Big/ \int_0^{\pi/6} I(\theta) d\theta \qquad 2.19$$

where $I(\theta)$ is the azimuthal distribution of the x-ray diffraction intensity. Following Vainstein [30] it has been assumed that $I(\theta)$, the intensity distribution, is proportional to $f(\theta)$ the distribution function and consequently has its maximum at $\theta = 0$ also. BOO was calculated for each peak and finally the average over six peaks was taken. The experimental x-ray intensity profile for each peak has been corrected for broadening due to the width of the primary x-ray beam, using a method of deconvolution based on substitution of successive foldings as descibed in section 2.3.1d. The circular scans of the outer diffraction spots (Figure 2.1(d)) was taken from $\psi = 0^{\circ}$ to $\psi = 360^{\circ}$ at 0.5 degree intervals near the peak and at larger intervals elsewhere. The resultant x-ray intensity profile is shown in Figure 2.6 and the peak intensity position

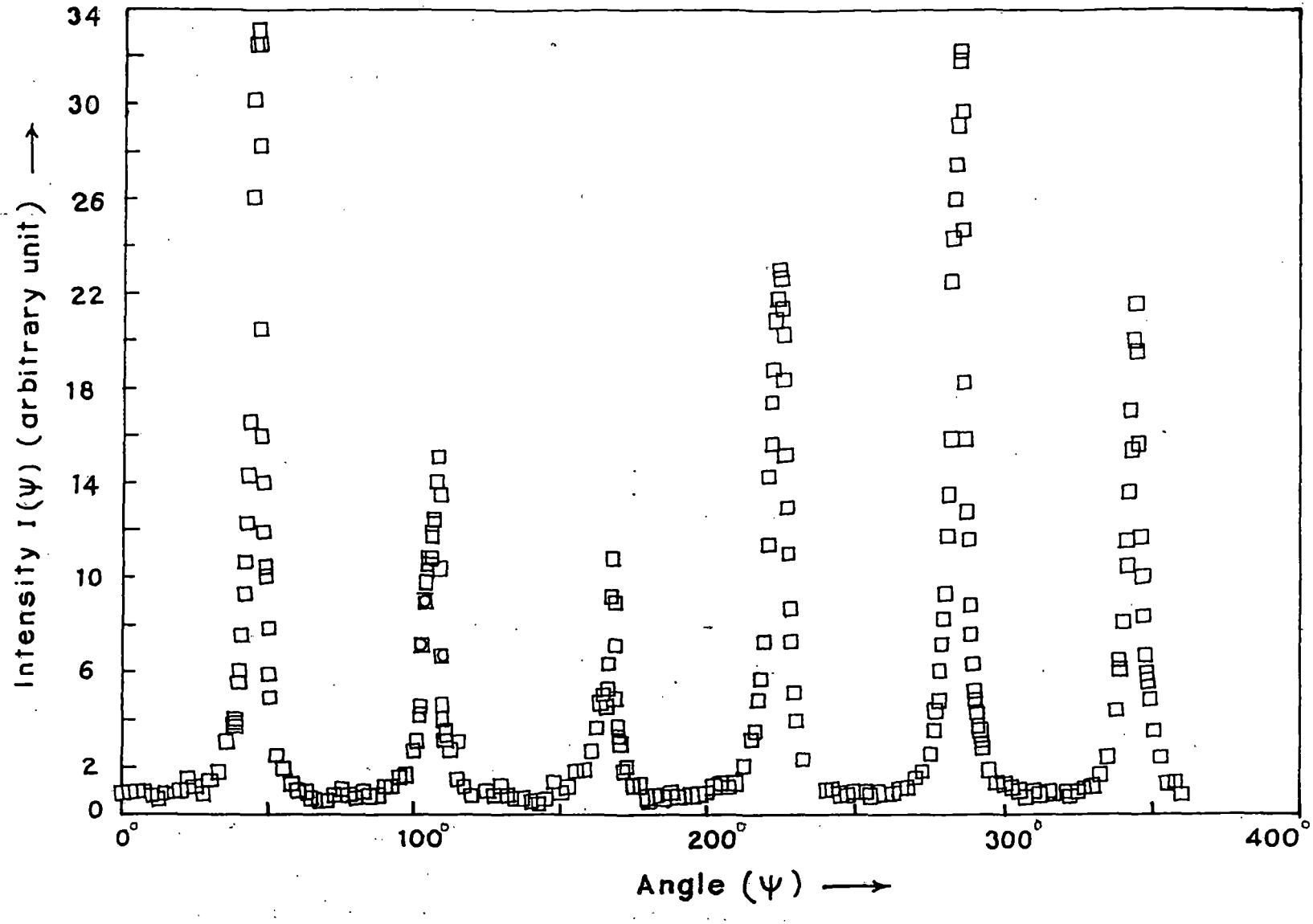

Figure 2.6 X-ray intensity I(ψ) versus azimuthal angle (ψ) curve for the smectic B phase.

corresponding to $\psi = 0$ was determined from this curve following a procedure similar to that followed in the determination of orientational order parameters $\langle P_2 \rangle$ and $\langle P_4 \rangle$. The corrected intensity values plotted against azimuthal angular positions have also been corrected for the background (scattered) intensity values.

2.3.4. Molecular parameters from x-ray studies

(a) Intermolecular distance

The average lateral distance between the neighbouring molecules (D) was calculated from the x-ray diffraction photographs by a formula given by [20]

$$2D \sin \theta = k\lambda \qquad 2.20$$

where 2θ is the Bragg angle for the equatorial diffraction, λ is the wave length of the x- ray and k is a constant which comes from the cylindrical symmetry of the system. Recent calculations [31] have shown that the value of k depends on the order parameter of the sample under consideration. For perfectly ordered state k = 1.117 as given by de Vries [20]. However, since the variation of k with $\langle P_2 \rangle$ is small, I have used the value k = 1.117 for all the calculations.

(b) Apparent molecular length or layer thickness

For apparent molecular length or layer thickness, d, the Bragg equation was used ($2d \sin \theta = \lambda$), where θ is the Bragg angle for the meridional diffraction crescent for an aligned sample or for the inner halo in the case of unaligned samples.

The first order meridional diffraction peaks were used for layer thickness calculation since second order diffraction peaks were either very weak and diffuse or absent.

(c) Transverse correlation length

The transverse (i.e., perpendicular to the director) correlation lengths in both nematic and smectic phases have been determined from the linear scan of outer x-ray diffraction peaks along the equatorial direction. The x-ray intensity profile was first corrected for the use of a flat plate camera following the inverse square law relation. The intensity profile was then deconvoluted for finite width of the collimator. The corrected x-ray intensity profile I(q) in the transverse q(wave vector) direction was fitted using a least-squares method to the Lorentzian form with a quadratic background:

$$I(q) = \frac{a}{b + (q - q_o)^2} + cq^2 + dq + e \qquad 2.21$$

where a, b, q_o, c, d and e are adjusted to obtain the best fit. A computer programme using Lavenberg - Marquardt method [32a] was written for this non-linear least squares fitting, initial values of the parameters being estimated graphically. Convergence was found to be good for all the experimental intensity profiles. The value of q_o gives the position of the x-ray diffraction peak and correlation length ξ is equal to $2\pi(b)^{-1/2}$. As mentioned in section 2.3.1d, in the deconvolution procedure an analytical form for the experimental intensity profile is helpful in the numerical integration process. Thus, I have first fitted the experimental data to a lorentzian form with a quadratic background, as shown in Figure 2.7(a). Figure

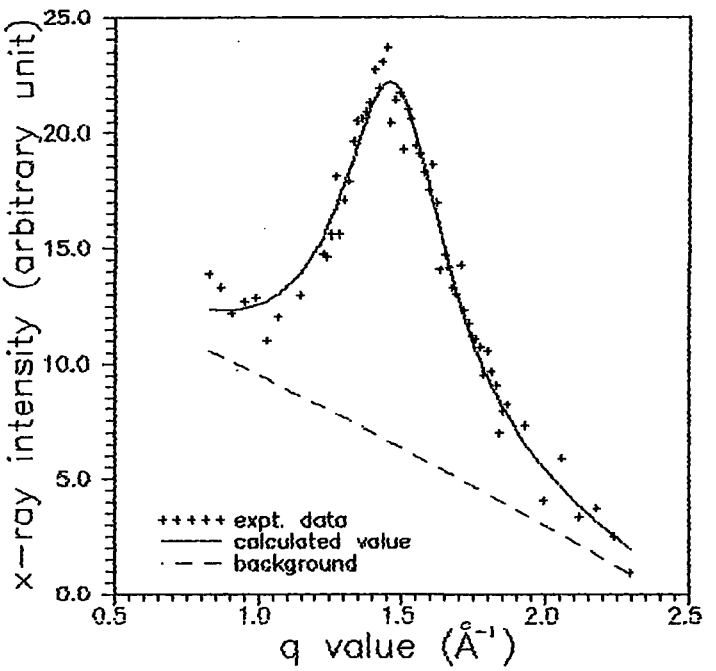

Fig.2.7a Comparison of experimental x-ray intensity data with the calculated value; HAB at 85 deg C.

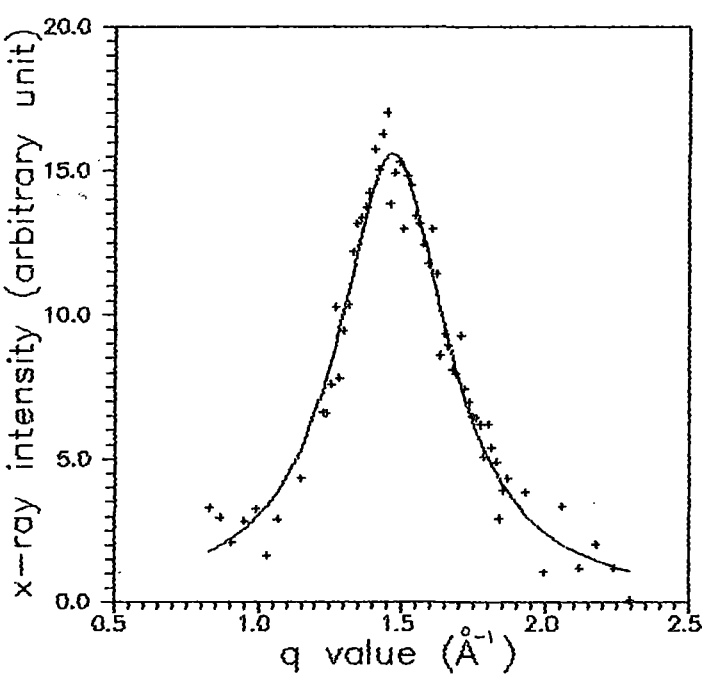

Fig.2.7b Comparison of x-ray intensity obtained from calculated peak value with experimental peak value after substracting the background;HAB at 85 deg C;solid line calculated peak; + expt. intensity minus calculated background.

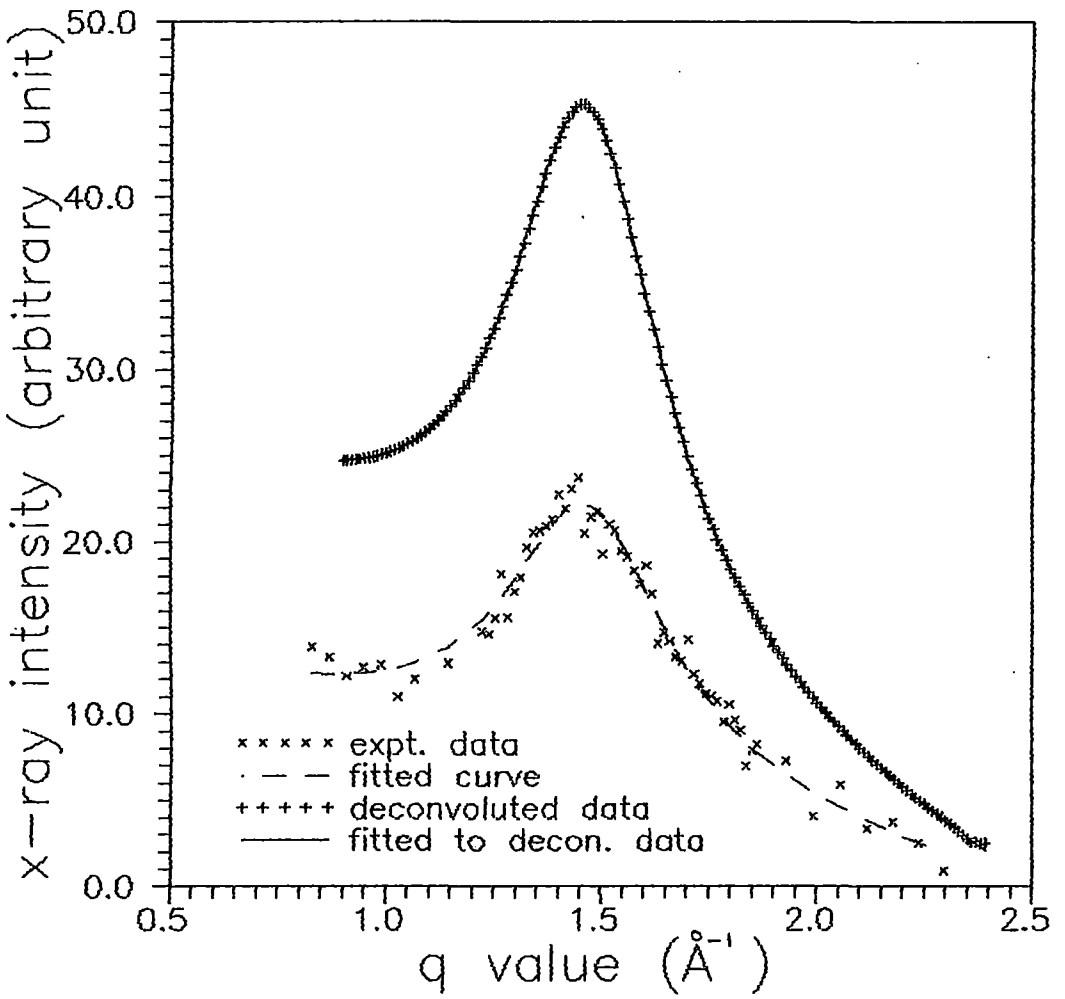

Fig.2.7c Comparison of experimental x-ray intensity data before and after deconvolution; HAB at 85 deg C.

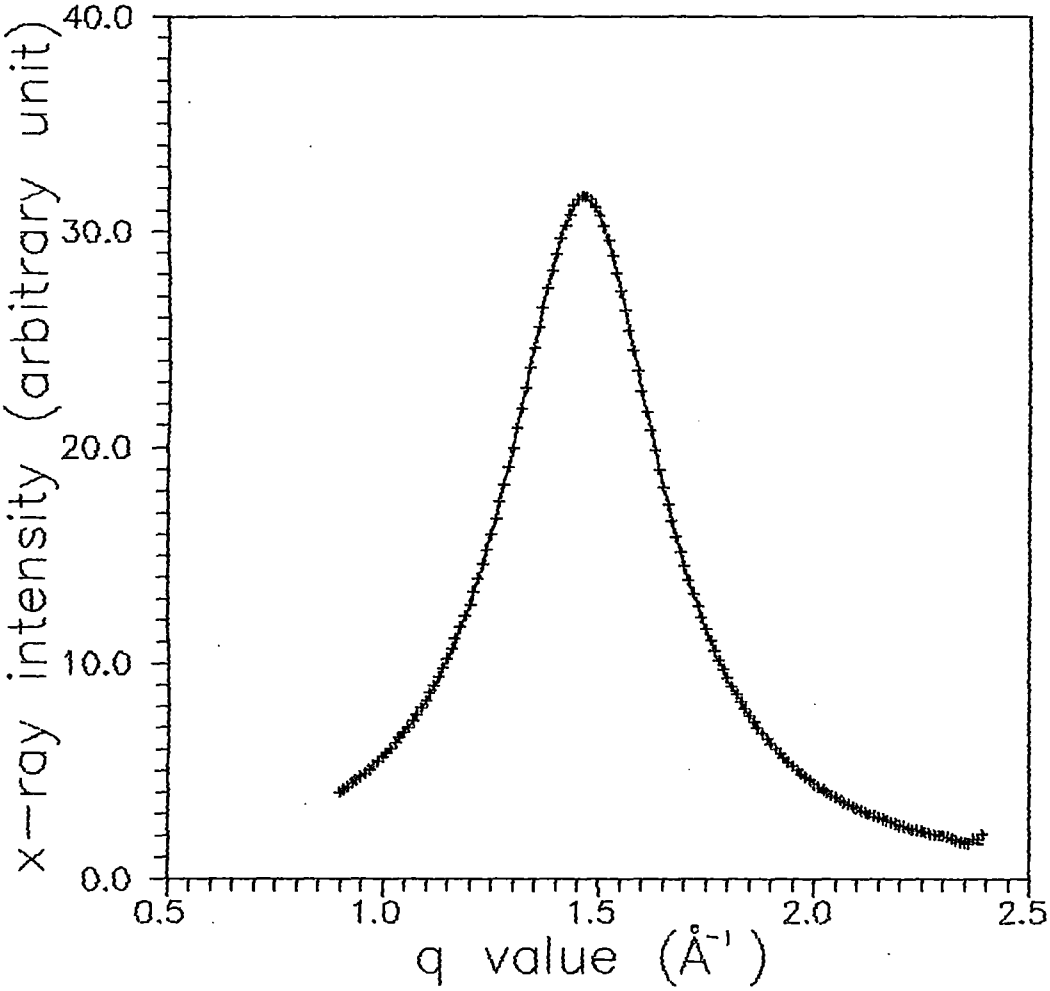

Fig. 2.7d Comparison of x-ray intensity obtained from calculated peak value with experimental peak value after substracting the background; HAB at 85 deg C; solid line calculated peak;+ expt. intensity minus calculated background.

2.7b shows the calculated profile as obtained from this fitting to the experimental data after substracting the background. Figure 2.7c shows the deconvoluted peak (after 3 to 4 iterations) fitted to the form given in eqaution 2.21 together with the experimental x-ray intensity data prior to deconvolution. The calculated peak after substraction from the background is shown in Figure 2.7(d). It can be seen from Figure 2.7c that the deconvoluted intensity data fit extremely well with the Lorentzian form.

2.4 Refractive index of mesophases

Anisotropic crystals (and also aligned liquid crystals) produce double refraction and the ability of a crystal to separate the two refracted rays is measured by its birefringence. In liquid crystalline phases refractive indices are important parameters for technical application. The first birefringence measurements were made by E. Dorn [32], the theoretical explanation of which have given by O. Weiner [33]. and H. Zocher [34,35]. The refractive indices of large number of nematic liquid crystals have been investigated, I refer here some of the earlier works [36-42]. Refractive indices have also been investigated in smectic phases [43-45]. In liquid crystals, due to the anisotropic molecular arrangement, it is necessary to take into account the effect of the anisotropic internal field in evaluating the polarizabilities. Hence, in case of liquid crystals the well known Lorentz - Lorentz formula for isotropic media is generally replaced by Neugebauer's [46] relations or Vuk's formula [47]. Saupe and Maier [48] also applied a more elaborate form of internal field suggested by Neugebauer.

In this study, I have measured the ordinary and extraordinary refractive indices n_o and n_e for different liquid crystal samples

and have calculated the effective polarizabilities α_o and α_e of anisotropic liquid crystals by using the two different internal field models [46,47]. Finally orientational order parameter $\langle P_2 \rangle$ was calculated.

(a) Neugebauer's method

Neugebauer [46] extended Lorentz - Lorentz equations for an isotropic system to an anisotropic system. In this model, Neugebauer calculated the anisotropy of internal field by considering an arbitrary lattice in which the molecules are represented by anisotropic point polarizabilities with parallel principal axes. The effective polarizabilities α_e and α_o of the liquid crystals are given by,

$$n_e^2 - 1 = 4\pi N\alpha_e \left(1-N\alpha_e\gamma_e\right)^{-1} \qquad 2.22$$

$$n_o^2 - 1 = 4\pi N\alpha_o \left(1- N\alpha_o\gamma_o\right)^{-1} \qquad 2.23$$

where γ_i's are the respective internal field constants for ordinary and extraordinary rays, N is the number of molecules per c.c and n_e and n_o are the extraordinary and ordinary refractive indices respectively. The equations for calculating the α_o and α_e obtained from equations (2.22) and (2.23) are

$$\frac{1}{\alpha_e} + \frac{2}{\alpha_o} = \frac{4\pi N}{3}\left[\frac{n_e^2 + 2}{n_e^2 - 1}\right] + \left[\frac{2(n_o^2 + 2)}{n_o^2 - 1}\right] \qquad 2.24$$

and

$$\alpha_e + 2\alpha_o = \frac{9}{4\pi N}\left[\frac{n^2 - 1}{n^2 + 2}\right], \qquad 2.25$$

where $n^2 = 1/3\ (n_e^2 + 2n_o^2)$.
Solving equations 2.24 and 2.25 α_o and α_e values can be obtained.

(b) Vuks Method

Vuks has derived another formula for polarizabilities associated with anisotropic organic molecules, by assuming that the internal field is independent of orientation i.e. an isotropic system with different polarizabilities. The principal polarizabilities and refractive indices can be expresssed as

$$\frac{n_e^2 - 1}{\bar{n}^2 + 2} = \frac{4\pi N}{3}\alpha_e \qquad 2.26$$

$$\frac{n_o^2 - 1}{\bar{n}^2 + 2} = \frac{4\pi N}{3}\alpha_o \qquad 2.27$$

where $\bar{n}^2 = \frac{1}{3}\ (n_e^2 + 2n_o^2)$ is the mean refractive index and α_e and α_o can be calculated directly from the refractive index values.

2.4.1. Calculation of order parameters from polarizabilities

The principal polarizabilities (α_o,α_e) have been calculated by using Vuks' isotropic model and Neugebauer's relations (anisotropic model). The relation between the order parameter, $\langle P_2 \rangle$ and the polarizabilities (α_o,α_e) is given by de Gennes [49],

$$\alpha_e = \bar{\alpha} + \frac{2}{3}\alpha_a \langle P_2 \rangle \qquad 2.28$$

$$\alpha_o = \bar{\alpha} - \frac{1}{3}\alpha_a \langle P_2 \rangle \qquad 2.29$$

and

$$\langle P_2 \rangle = \frac{\alpha_e - \alpha_o}{\alpha_{\parallel} - \alpha_{\perp}} \qquad 2.30$$

where $\bar{\alpha} = (2\alpha_o + \alpha_e)/3$ is the mean polarizability. $\alpha_a = (\alpha_{\parallel} - \alpha_{\perp})$ is the molecular polarizability anisotropy where $\alpha_{\parallel}$ and $\alpha_{\perp}$ are the principal polarizabilities, parallel and perpendicular to the long axes of the molecules in the crystalline state, which are not however available experimentally. To get the values of $(\alpha_{\parallel} - \alpha_{\perp})$ the widely used method of Haller et al [50] was adopted. A graph was plotted with $\log(\alpha_e - \alpha_o)$ versus $\log(T_c - T)$, where T_c corresponded to the nematic isotropic transition temperature. The plot which is found to be a straight line is extrapolated to T = 0, giving $(\alpha_e - \alpha_o)_{T=0} = (\alpha_{\parallel} - \alpha_{\perp})$. For each case a set of values of α_e, α_o and $(\alpha_{\parallel} - \alpha_{\perp})$ were obtained and then from equation 2.30 order parameter $\langle P_2 \rangle$ was calculated.

2.4.2 Measurement of refractive indices

The refractive indices n_e and n_o for extraordinary and ordinary ray were measured by a thin prism technique. The refracting angle of the prism was less than 2^o. The details of the preparation of the prism and the experimental procedure have already been reported by Zemindar et al [51]. For the preparation of a prism two clean optically plane glass plates were used, one surface each of the glass plates was rubbed parallel to the direction of one of their edges. The plates were then treated with a dilute solution of polyvinyl alcohol and

then dried. The preferred direction on the substrate can be obtained by rubbing the same surface in the same direction again by a tissue paper. The prism was then formed by placing the treated surfaces inside with the rubbing direction parallel to the refracting edge of the prism. A thin spacer was placed at the thick edge of the prism for getting the desired refracting angle of the prism. The sides of the prism were sealed with a high temperature adhesive. Liquid crystal sample was placed inside through open top side of the prism and heated to the isotropic state and then cooled down very slowly and the process was repeated several times. No magnetic field was applied. Repeated heating and cooling produced a homogeneous sample with optic axis parallel to the refracting edge of the prism. The prism was then placed in a brass chamber, with transparent windows, whose temperature could be maintained by a temperature controller (Indotherm model 401) at any desired value to an accuracy of $\pm$ 0.5^{o}C by means of an electric oven. The refractive indices were measured for three wavelengths (λ = 6907$\mathring{A}$, 5890$\mathring{A}$, 5461$\mathring{A}$) from a mercury lamp by means of a precision spectrometer, a wavelength selector and a nicol prism.

2.5 Measurement of Densities

The densities of the liquid crystals were measured with the help of a dilatometer of the capillary type. A weighed sample of the liquid crystal was introduced inside the capillary tube of the dilatometer and it was placed in a thermostated water bath. Sufficient time was allowed for equilibrium at any desired temperature before taking each readings. The length of the liquid crystal column was measured at different temperatures with a travelling microscope. The densities were calculated after correction for the expansion of the glass. The accuracy of

the measurement of the densities was within 0.1%.

2.6 Elastic Constant and deformation free energy of nematic liquid crystal

Many of the important physical properties involving the response of the bulk liquid crystal samples can be described by regarding the liquid crystal as a continuous medium. Based on this point of view , Zocher [52], Oseen [53] and Frank [54] developed a phenomenological continuum theory which can explain various field induced effect of liquid crystals.

The elastic constants of a liquid crystal are restoring torques which become apparent when the system is perturbed from its equilibrium configuration. As shown by Zocher [52], Osceen [53] Frank [54] the elastic part of the internal energy density of a pertubed liquid crystal is given by the equation :

$$F_{def} = (1/2)\ [K_1(\mathrm{div}\hat{n})^2 + K_2(\hat{n}.\mathrm{curl}\hat{n})^2 + K_3(\hat{n}\times\mathrm{curl}\hat{n})^2] \qquad 2.31$$

where K_1, K_2, K_3 refers to the splay, twist and bend elastic constants respectively and $\hat{n}$ is the director (Figure 2.8).

2.6.1 Freedericksz transition

Various methods have been used to measure the elastic constants of nematic liquid crystals. One of the most simple and convenient method is Freedericksz transition, where an external electric [55-58] or magnetic [59-66] field is applied to deform a thin layer of surface aligned nematogenic sample having uniform director pattern. Below a critical field the sample remains surface aligned, but above it starts to align itself along the external field for nematogens having positive

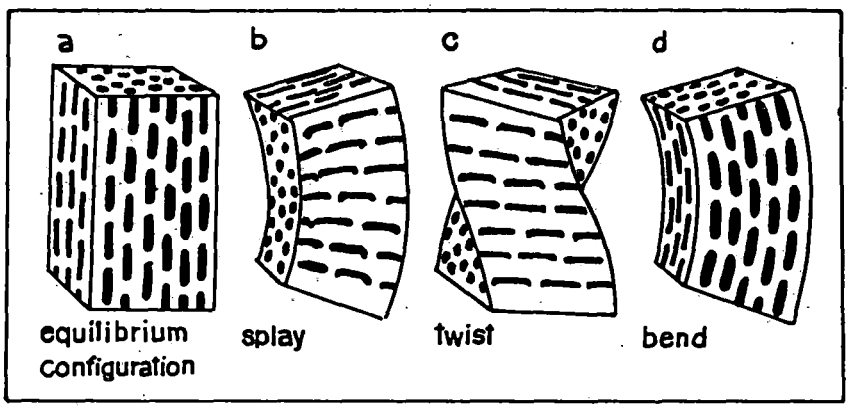

Figure 2.8. (a) An ordered liquid crystal in equilibrium configuration. The deformation states —— splay (b), twist (c) and bend (c) [67].

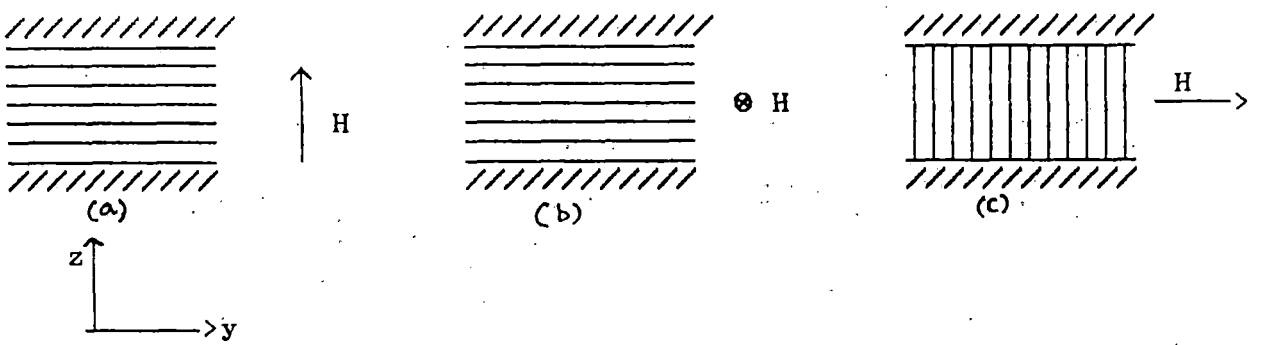

Figure 2.9 Schematic experimental set-up for the determination of elastic constants from Freedericksz transition: (a) splay, (b) twist, (c) bend.

anisotropy ($\Delta\chi > 0$ or $\Delta\varepsilon > 0$). This phenomenon is known as Freedericksz's transition. Depending on the geometry of the arrangement, splay, twist or bend elastic constant can be determined from Freedericksz transition in a magnetic field as shown in Figure 2.9. The threshold magnetic field for all the three geometries can be obtained in a generalised form as

$$(H_C)_i = (K_i/\Delta\chi)^{1/2} \frac{\pi}{d} \qquad 2.32$$

i = 1,2,3 refer to the splay, twist and bend deformations respectively, d is the thickness of the liquid crystal layer, $\Delta\chi$ is the diamagnetic anisotropy. and $(H_c)_i$ is the respective critical magnetic field.

2.6.2 Description of experimental setup for determination of K_1 and K_3.

A block diagram of the experimental setup for studying elastic constants by Freedericksz transition method is shown in Figure 2.10.The monochromatic light beam (sodium D light) is incident on the sample, which is mounted in a brass oven (o), after passing through a lens (L), polarizer (P) and collimating circular slits (C_1, C_2). The temperatures are measured and regulated with an accuracy $\pm$ 0.5^{o}C with the help of a thermocouple inserted in the block containing the sample and a temperature regulator (Indotherm model 457). The transmitted light intensity is detected by a photomultipier tube (M) for photon counting. An analyser is placed in front of the P.M. tube. The polariser and analyser are placed in crossed position. The magnetic field H is applied perpendicular to the direction of the preferred orientation of the liquid crystal sample. The

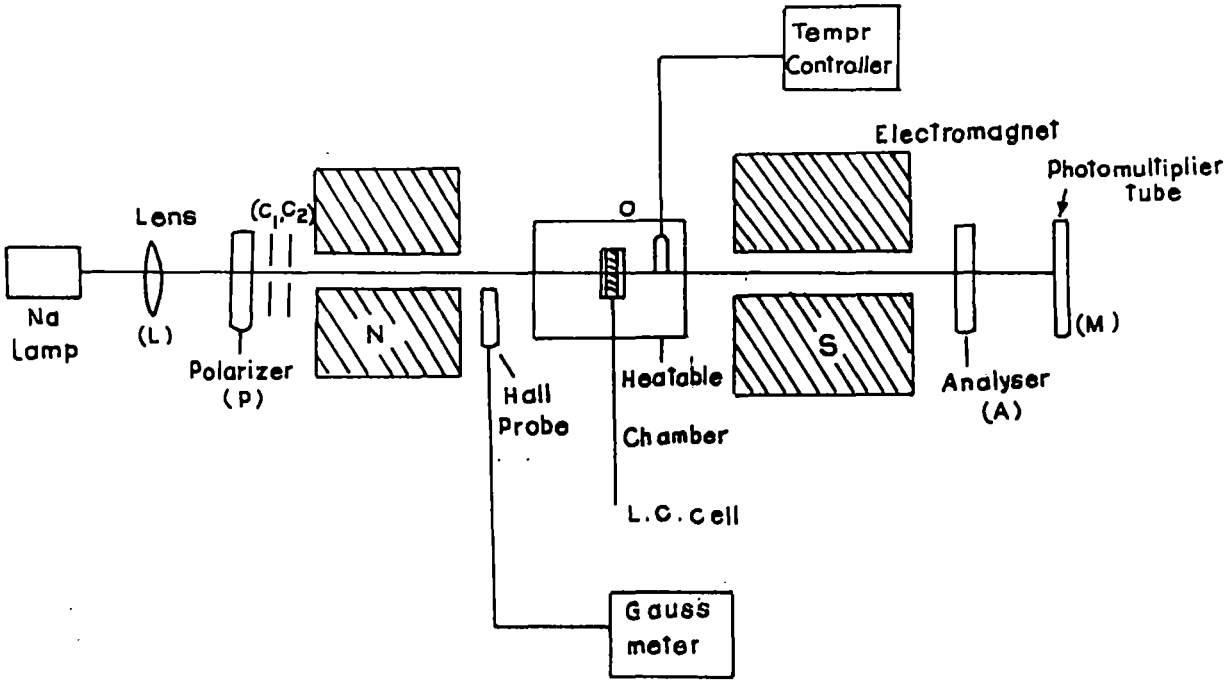

Figure 2.10. Block diagram of the experimental set - up for measuring elastic constants by Freedericksz transition.

field is changed slowly so that the nematic orientation remain in equlibrium with the applied magnetic field. The intensity of the transmitted light is measured as a function of the applied magnetic field for any desired temperature. It is observed that when the field H reaches a critical value H_c the optical properties of the sample change drastically and thus value H_c can be measured from field versus intensity curve within an accuracy of ± 10 gauss. The magnetic field is measured by a sensitive Gaussmeter(Model DGM-102). For the determination of actual threshold it is necessary to maintain the direction of the director exactly normal to the applied magnetic field.

The sample is taken between two plane parallel glass plate separated by a teflon spacer of thickness 50μm. The glass plates are cleaned by different cleaning agent and subsequently dried and treated for homeotropic or homogeneous alignment as required (details of the technique has been given by de Jeu [52]). The splay elastic constant (K_1) is measured using cells with homogeneous planar alignment where inside surface of the glass plates are treated with 1.0% aquous solution of polyvinyl alcohol, dried and then rubbed unidirectionally with tissue paper. In case of bend elastic (K_3) constant measurement it is necessary to treat the glass plates with dilute solution of cetyl trimethyl ammonium bromide in acetone to get homeotropic alignment and using the geometrical arrangement shown in Figure 2.9(c).

Actually, the experiment for the determination of K_1 and K_3 consists of measuring the variation of birefringence of light incident normal to the liquid crystal film. A linealy polarized light incident on the film and the suitable analyser C (i.e., a combination of quater wave ($\lambda/4$) plate and a linear polariser) is used to detect the transmitted light intensity. When the fields exceeds a critical value H_C the transmitted intensity

shows a sudden change. If the field is gradually increased further, the intensity exhibits oscillations because of the change of the phase retardation.

The threshold field for twist deformation cannot be detected optically when viewed along the twist axis. The large birefringence of the medium for this direction of propagation, the state of polarization of the transmitted beam is indistinguishable from that of the emerging beam from the untwist nematic. A total internal reflection technique can be used to measure the K_2 values of the twist deformation. However, I have measured only K_1 and K_3 values at different compositions of a binary liquid crystalline mixture.

REFERENCES

[1]. E.B. Priestley, P.J.Wojtowicz and P. Sheng, eds. Introduction to Liquid Crystals, Plenum, New York, (1974).

[2]. S. Chandrasekhar, Liquid Crystals, Cambridge University Press, Cambridge,(1977).

[3]. G. Vertogen and W.H. de Jeu, Thermotropic Liquid Crystals, Fundamentals, Springer-Verlag (1988).

[4]. G.R. Luckhurst and G.W. Gray, (Editors) The Molecular Physics of Liquid Crysals, Academic Press (1979).

[5]. P. G. de Gennes, The Physics of Liquid Crystal, Clarendon Press, Oxford,(1974).

[6]. A. Saupe and W. Maier Z. Natureforsch, 14a, 882 (1959) and 15a, 287 (1960).

[7]. W.L. McMillan, Phys. Rev., A4, 1238 (1971).

[8]. W.L. McMillan, Phys. Rev., A6, 936 (1972).

[9]. E.B. Priestley, P.S. Pershan, R.B. Meyer and D.H. Dolphin, Vijnana Parishad Anusandhan Patrika 14, 93 (1971).

[10]. K.K. Kobayashi, J. Phys., Soc. (Japan), 29, 101 (1970).

[11]. K.K. Kobayashi, Mol. Cryst. Liq. Cryst., 13, 137 (1971).

[12]. D. Demus and L. Richter, Textures of Liquid Crystals, Verlag Chemie, New York (1978).

[13]. Advances in Liquid Crystals, Vol 6, Ed. G.H. Brown Academic Press (1983), Chapter 1.

[14]. B.K. Vainstein and I.G. Chistyakov, Problems of Modern Crystallography, Nauka, Moscow (1975).

[15]. A.J. Leadbetter, The Molecular Physics of Liquid Crystals, Eds. G. R. Luckhurst & G.W. Gray, Chapter 13, Academic Press (1979).

[16]. A. de Vries, Liquid Crystals, Ed. F.D. SAeva, M. Dekker Inc., New York.

[17]. A.J. Leadbetter and E.K. Norris, Mol. Phys.,38, 669

(1979).

[18]. A. de Vries J. Chem. Phys., 56, 4489 (1972).

[19]. H. Kohli et al Z. Physik, B24, 147 (1976).

[20]. A.de Vries, Mol. Cryst. Liq. Cryst, 10, 219 (1970).

[21]. P.S. Pershan, Structure of Liquid Crystal Phases, World Scientific (1988).

[22]. B. Jha and R. Paul, Proc. Nucl. Phys. Solid State Phys. Symp., India, 19c, 491 (1970).

[23]. C. Kittle, Int. to Solid State Phys, Wiley Eastman, Ch.2 (1976).

[24]. H.P. Klug and L.E. Alexander, X-ray diffraction procedures, John Wiley and Sons, N Y, Page 114 and 473 (1974).

[25]. S. Ergun, J. Appl. Cryst. 1, 19 (1968).

[26]. C.C. Huang in K.J. Standburg (Ed.) Bond Orientational Order in Condensed Matter Systems, Springer - Verlag.

[27]. R. Bruinsma and D.R. Nelson, Phys. Rev. B., 23, 1, 402 (1981).

[28]. E. Gorecka, Li Chen, O. Lavrentovich and W. Pyzuk, Europhysics Letters, 27(7), 507, 1994.

[29]. R.J. Birgeneau and J.D. Litster, J.Phys. Letts. 39, L399, (1978).

[30]. B.K. Vainstein, Diffraction of X- rays by Chain Molecules, Elsevier, Pub. Co. (1966).

[31]. R. Paul. and G. Chaudhuri, Abstract in the 14th International Liquid Crystal Conference, Pisa, 1992, Abs-no-H- P23.

[32]. E. Dorn, Z. Physik, 11, 111 (1910).

[32a].W.H. Pness, S.A. Teukolsky, W.T. Vellering and B.P. Flannery, Cambridge University Press, 1986, Chapter 15.

[33]. O. Weiner, S. Ber. Sächs. Ges. Wissensch., 61, 113 (1909).

[34]. H. Zocher, Naturwiss., 13, 1015 (1925).

[35]. H. Zocher, Z. Krist.,79, 122 (1931).

[36]. F. Grandjean, Compt. rend., 168, 408 (1919).

[37]. N.V. Madhusudana, R. Sashidhar and S. Chandrasekhar, Mol. Cryst. Liq. Cryst., 13, 61 91971).

[38]. Y.Poggi, J. Robert and J. Borel, Mol. Cryst. Liq. Cryst. 29, 31 (1975).

[39]. R Chang, Mol. Cryst. Liq. Cryst., 30, 155 (1975).

[40]. C.C. Huang, R.S. Pindak and J.J. Ho, J. Phys. Lett (Paris), 35, 185 (1974).

[41]. W. Kuczynski and B. Stryla, Mol. Cryst. Liq. Cryst., 31, 267 (1975).

[42]. M. Laurent and R. Journeaux, Mol. Cryst. Liq. Cryst., 36, 171 (1976).

[43]. G. Pelzl and H. Sackmann, Mol. Cryst. Liq. Cryst., 15, 75 (1971).

[44]. G. Pelzl and H. Sackmann, Symp. Faraday Soc., No. 5, 68, (1971).

[45]. Y. Galerne, S.T. Lagerwall and I.W. Smith, Opt. Commun., 19, 147 (1976).

[46]. H. E. Neugebauer, Canad. J. Phys., 32, 1 (1954).

[47]. M. F. Vuks, Optics and Spectroscopy, 20, 361 (1966).

[48]. A. Saupe and W. Maier Z. Natureforsch, 16a, 816 (1961).

[49]. P.G. de Gennes,. Mol. Cryst. liq. Cryst, 12, 193 (1971).

[50]. I. Haller, H.A. Huggins, H.R. Lilienthal and T.R. McGuire, J. Phys. Chem.,77, 950 (1973).

[51]. A.K. Zeminder, S. Paul and R. Paul, Mol. Cryst. Liq. Cryst., 61, 191 (1980).

[52]. H. Zocher, Trans Faraday Soc., 29, 945 (1933).

[53]. C.W. Oseen, Trans Faraday Soc., 29, 883 (1933).

[54]. F.C. Frank, Faraday, Soc. Discussion 25, 19 (1958).

[55]. H. Gruler, T.J. Schiffer and G. Meier, Z. Natureforsh, 27a, 966 (1972).

[56]. H. Gruler and L. Cheung, J. Appl. Phys. 46, 5097 (1975).

[57]. H. Deuling in Liquid Crystals, Solid State Physics Suppl. no. 14, ed. L. Liebert p.77, Academic Press (New York).

[58]. M.J. Bradshaw and E.P. Raynes, Mol. Cryst. Liq. Cryst., 72, 35 (1980).

[59]. V. Freedericksz and V. Tsvetkov, Phy. Z. Soviet Union, 6, 490 (1934).

[60]. V. Freedericksz and V. Zolina, Trans. Faraday Soc. 29, 919 (1933).

[61]. P.P. Karat and N.V. Madhusudana, Mol. Cryst. Liq. Cryst., 40, 239 (1977).

[62]. H.P. Schad and M.A. Osman, J. Chem. Phys. 75 (2) 880 (1981).

[63]. F. Leenhouts, H.J. Boeber, A.J. Dekker and J.J. Jonker, J. Phys. (Paris) Colloque 40, C3-291 (1979).

[64]. H.P. Schad, G. Bauer and G. Maier, J. Chem. Phys. 67, 3705 (1977).

[65]. F. Leenhouts and A. J. Dekker, J. Chem Phys, 74, 1956 (1981).

[66]. H.P. Schad and M.A. Osman, J. Chem. Phys. 75 (2) 880 (1978).

[67]. L. Pohl and U. Finkenzeller in B. Bahadur (Ed.) Liquid Crystals, Applications and Uses, Vol 1. World Scientific p. 166, (1990).

CHAPTER - 3

ORIENTATIONAL ORDER PARAMETERS IN THE SMECTIC C AND NEMATIC PHASE OF HEPTYLOXYAZOXYBENZENE (HAB)

3.1 Introduction

Quantitative knowledge of orientational order parameters (OOP) is necessary to test either the different theories of liquid crystalline mesophases or the applicability of the liquid crystal in a display device. The compound heptyloxyazoxybenzene (HAB), which has a smectic C and a nematic phase, has been a subject of much interest and has been widely studied by different workers [1-6]. OOP of HAB in the nematic phase were determined by Leadbetter et al from x-ray measurements [1]. Chistyakov et al has estimated the tilt angle in the smectic C and nematic phase [2]. A.de Vries had earlier reported the presence of skewed cybotactic nematic phase in this compound [3]. McMillan has measured the anisotropic liquid structure factor in the nematic phase [4]. From x-ray critical scattering Terauchi et al has investigated the nature of the smectic C to nematic phase transition [5]. The ordinary refractive index and birefringence of HAB in the nematic phase have been reported by others [6,7]. In the present work, the density, refractive indices (n_o,n_e), birefringence and OOP values of this compound have been measured both in the smectic C and nematic phases from x-ray diffraction and optical studies. Anomalous temperature variation of the experimental orientational order parameter values in the smectic C phase, as obtained from x-ray scattering intensities, have been explained using a model of random tilt. This model has been succesfully applied to the smectic C phase of a commercial liquid crystal mixture having smectic A phase as well [8], but no such attempt has been made so far on compounds having smectic C phase without smectic A phase. OOP's determined from x-ray diffraction and refractive index studies are found to differ significantly in the smectic C phase, reason for which has been discussed. Experimental data have been analysed to

obtain the temperature variations of intermolecular distance and correlation length. The experimental results have also been compared with those of other workers.

3.2 Experimental

Transition temperatures of this compound as observed under a polarising microscope equipped with a Mettler FP82 Thermo system, were found to agree with literature values. The structural formula and the transition temperatures of HAB are the following:

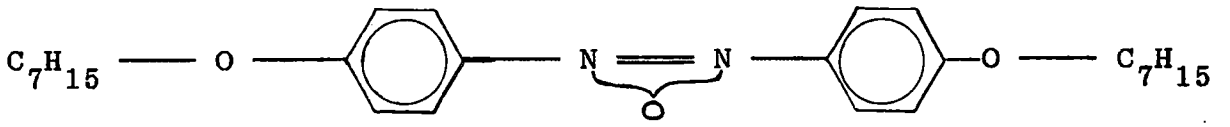

Crystal $\xleftrightarrow{74^{\circ}C}$ Smectic C $\xleftrightarrow{93^{\circ}C}$ Nematic $\xleftrightarrow{124^{\circ}C}$ Isotropic

3.2.1 X-ray diffraction studies

X-ray diffraction photographs were taken in presence of magnetic field, using nickel filtered CuK_{α} radiation of wavelength λ=1.5418 Å. The temperature during the experiment was controlled to $\pm 0.5^{\circ}C$ by a temperature controller (Indotherm 401). The experimental set-up and the procedure for order parameter determination from x-ray diffraction study [9] have been described in detail in Chapter 2. The sample was heated to the isotropic phase and allowed to cool down slowly to the desired temperature in the presence of a magnetic field (6 kilogauss). The x-ray diffraction photographs of oriented samples have been scanned both linearly and circularly by an optical microdensitometer (Carl Zeiss Model MD 100). The optical densities were converted to x-ray intensities as discussed in chapter 2. From the circular scan of the x-ray diffraction

photographs the mean intensity values of the four quadrants were obtained which is given in table 3.1 for the compound. The procedure for the determination of normalised orientational distribution function $f(\beta)$ values using Leadbetter [1] formula, and order parameter are described in chapter 2. The normalised distribution function $f(\beta)$ values at 5^{o} angle intervals, calculated by an even power series of $\cos\beta$ for HAB is given in table 3.2. The $\langle P_2 \rangle$ and $\langle P_4 \rangle$ values for the compound were calculated from the distribution function. Table 3.3 contain $\langle P_2 \rangle$ and $\langle P_4 \rangle$ values at different temperatures for HAB.

The transverse correlation length, ξ, and the intermolecular distance, D, were determined from the linear scan of the x-ray diffraction photographs along the equatorial direction. The values of ξ at different temperatures is given in table 3.6. The intermolecular distance, D, have been calculated using the relation $D=1.117(2\pi/q_o)$, where q_o is the magnitude of the peak scattering vector. The factor of 1.117 has been used for reasons as described in chapter 2. Table 3.7 includes the values of D at different temperatures for HAB, together with the corresponding q_o values.

3.2.2 Refractive index and density studies

The ordinary and extra-ordinary refractive indices (n_o, n_e) and density measurements have been described [10] in detail in chapter 2. The refractive indices (n_o, n_e) and density of HAB at different temperatures for two wavelengths is arranged in table 3.8. Due to absorption of the red light by the sample it was not possible to determine the refractive indices (n_o, n_e) at this wavelength. The experimental uncertainity of refractive index measurements are $\pm$ 0.001. The principal polarizabilities (α_o, α_e) of the compound have been calculated using Vuks [11] and

Figure 3.1 X-ray diffraction photograph of the oriented sample in the nematic phase of HAB at 97°C.

Figure 3.2 X-ray diffraction photograph of the sample in the smectic C phase (HAB at 81°C).

Neugebauer's method [12]. Using the relation given in chapter 2 orientational order parameter $\langle P_2 \rangle$ was calculated. The molecular polarizability anisotropy $\Delta\alpha$ were obtained by an extrapolation procedure, as suggested by Haller et al [13]. The values of the effective polarizabilities α_o and α_e obtained from Vuk's and Neugebauer's method are given in tables 3.9 and 3.10 respectively. The values of order parameters $\langle P_2 \rangle$ at different temperatures obtained from the two different wavelengths and their average value have been included in table 3.11 and table 3.12.

3.3 Discussions

The x-ray diffraction photographs of the oriented sample in the nematic phase shows the presence of skewed cybotactic groups, with the inner ring split up into four spots of strong intensity as shown in Figure 3.1. Tilt angle in the nematic phase has been measured to be 29.5 degree at 97^{o}C, the value changing to 29.2 degree at 93^{o}C (the nematic to smectic C transition point), which are in agreement with those reported by Leadbetter et al [1] but deviate from those given by Chistyakov and Chaikowsky by 3-4 degree [2].

The x-ray diffraction photographs of the smectic C phase of HAB were similar to those obtained from monodomain smectic A samples, indicating that in this sample the director is randomly oriented in a cone about the layer normal of the smectic C phase, which is the laboratory fixed magnetic field direction. Figure 3.2 shows the x-ray diffraction photograph of the oriented sample at 81^{o} C, the possible smectic C configuration in this case is of azimuthal disorder (Figure 2b in Reference 1). Tilt angle, θ_t, in this phase has thus been determined indirectly from the layer thickness, l, using the relation $\theta_t =$

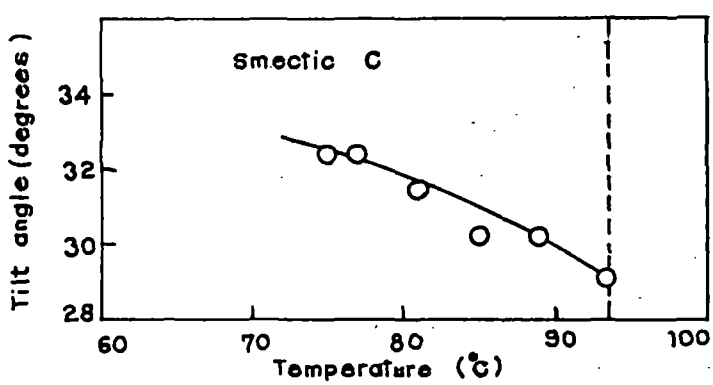

Figure 3.3 Temperature variation of tilt angle θ_t in the smectic C phase of HAB.
Line drawn is guide to the eye only.

$\cos^{-1}(d/l)$, where l is the length of the molecule in all-trans configuration and d is the smectic layer spacing. The molecular model length of the HAB molecule in all- trans configuration is 30.55Å. The tilt angles so determined vary from 40 to 42 degree. However, Leadbetter et al from direct measurements [1], have shown that in the smectic C phase of HAB the tilt angle is (32± 2) degree. This seems to conform to the view [1] that the effective molecular lengths are shorter than the most extended configuration by about 3Å, implying considerable disorder in the alkyl chains. Thus the tilt angles in the smectic C phase has been calculated using l= 27.55Å in the present work. Temperature variation of the tilt angle is small, varying from 29.2 degree at 93°C to 32.7 degree at 75°C as shown in Figure 3.3. Experimentally obtained layer spacing d = 24.38Å ± 0.22, which is in agreement with the previously reported values of Leadbetter et al [1].

The orientational distribution function $f(\theta)$ and hence the orientational order parameters $\langle P_2 \rangle$ and $\langle P_4 \rangle$ have been determined from x-ray intensity data using the method described previously [9]. The temperature variation of $\langle P_2 \rangle$ and $\langle P_4 \rangle$ are shown in Figure 3.4. The $\langle P_2 \rangle$ and $\langle P_4 \rangle$ values reported by Leadbetter et al in the nematic phase of HAB is also shown in the figure. Experimental $\langle P_2 \rangle$ and $\langle P_4 \rangle$ values in the nematic phase agree quite well with those of Leadbetter et al [1] and also with those calculated from Maier-Saupe mean field theory [14]. We have also calculated the orientational order parameters using McMillan's potential [15]

$$\varepsilon(\cos\theta, z) = -\varepsilon_o \left[\delta\alpha\tau \cos(2\pi z/d) + \left\{ \eta + \alpha\sigma\cos(2\pi z/d) \right\} P_2(\cos\theta) \right] \qquad (3.1)$$

where α and δ are two adjustable parameters, z is the

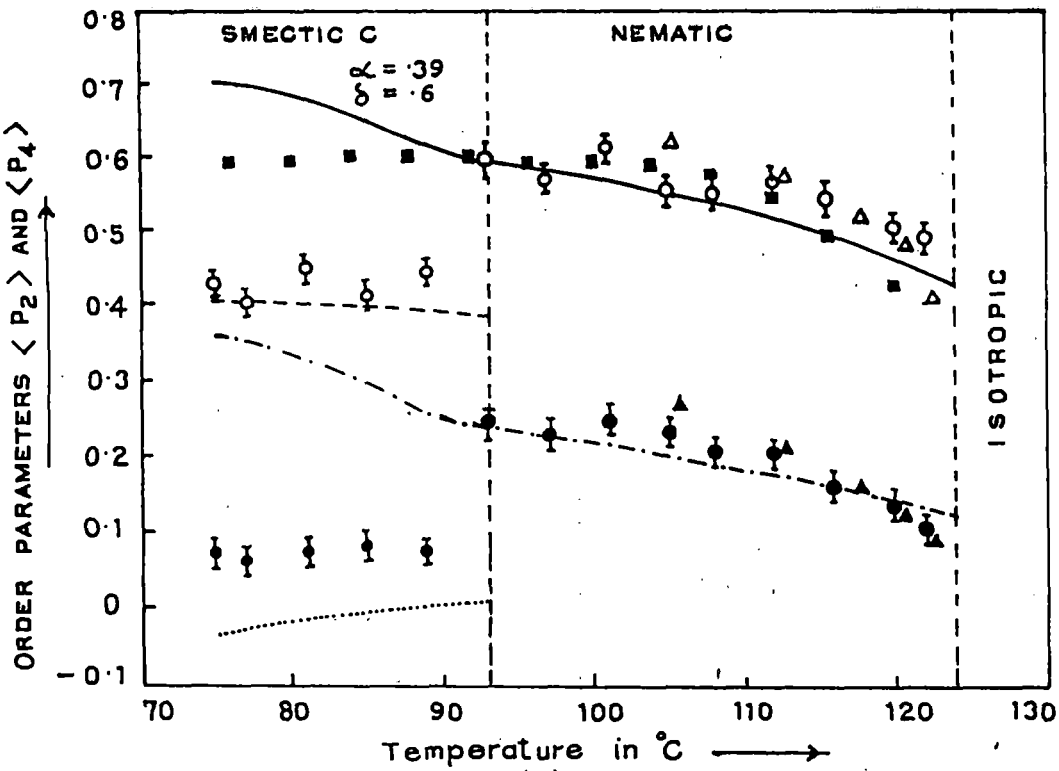

Figure 3.4 The orientational order parameters for HAB; o, x-ray data for $\langle P_2 \rangle$; ●, x-ray data for $\langle P_4 \rangle$; ■, refractive index data for $\langle P_2 \rangle$; solid line is theoretical $\langle P_2 \rangle$ from McMillan's potential; dashed line is theoretical $\langle P_4 \rangle$ from McMillan's potential In smectic C phase the experimental points o and ● correspond to apparent values of order parameters determined with respect to the layer normal. Theoretical apparent order parameters for the smectic C phase including allowance for the tilt angle are represented as follows : — — — — , apparent $\langle P_2 \rangle$; ..... apparent $\langle P_4 \rangle$; △ , x-ray data for $\langle P_2 \rangle$ from Leadbetter et al; ▲ , x-ray data for $\langle P_4 \rangle$ from Leadbetter et al (reference 1). Vertical bars show estimated errors.

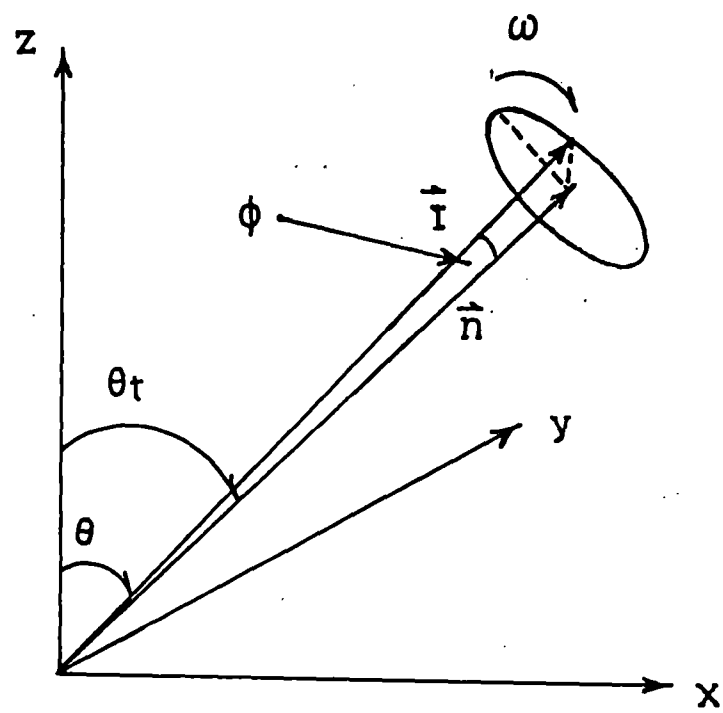

Figure 3.5 The definition of the parameters: θ_t = smectic C tilt angle, $\vec{l}$ is a unit vector along the molecular axis, $\vec{n}$ is the director and the z axis represent the smectic layer normal.

displacement along the layer normal, d is the layer thickness, η = $\langle P_2(\cos\theta)\rangle$, the orientational order parameter, while τ = $\langle\cos(2\pi z/d)\rangle$ is the translational order parameter and σ = $\langle P_2(\cos\theta)\cos(2\pi z/d)\rangle$ is the mixed translational and orientational order parameter. Though this potential is applicable to smectic A phase, it was assumed to be valid for smectic C phase as well. Using the values of δ = .6, α = .39, the experimental nematic to isotropic and smectic C to nematic transition temperatures are reproduced and a reasonably good fit to the measured orientational order parameters in the nematic phase is obtained. However, the agreement between the experimental and calculated $\langle P_2\rangle$ and $\langle P_4\rangle$ in the smectic C phase is poor, the experimental order parameters decreasing with decreasing temperature. This is due to the fact that the molecular tilt at lower temperatures causes the observed orientational distribution function with respect to the layer normal to become broader at lower temperatures. Since the layer normal is parallel to the applied magnetic field direction and normal to the x-ray beam, the diffraction pattern is caused by the apparent orientational distribution function about the layer normal and not by the real distribution function about the director. Figure 3.5 shows the relative orientations of the layer normal (z), the local director ($\hat{n}$) and the long axis of a molecule ($\hat{I}$) and it is clear from the figure that

$$\cos\theta = \cos\theta_t\cos\phi + \sin\theta_t\sin\phi\cos\omega \qquad (3.2)$$

Substituting this value of $\cos\theta$ in equation (3.1), we get for the orientational distribution function about the layer normal

$$f'(\cos\phi) = N\int\exp\,[-\varepsilon(\theta_t,\phi,\omega,z)/kT]\,dz\,d\omega \qquad (3.3)$$

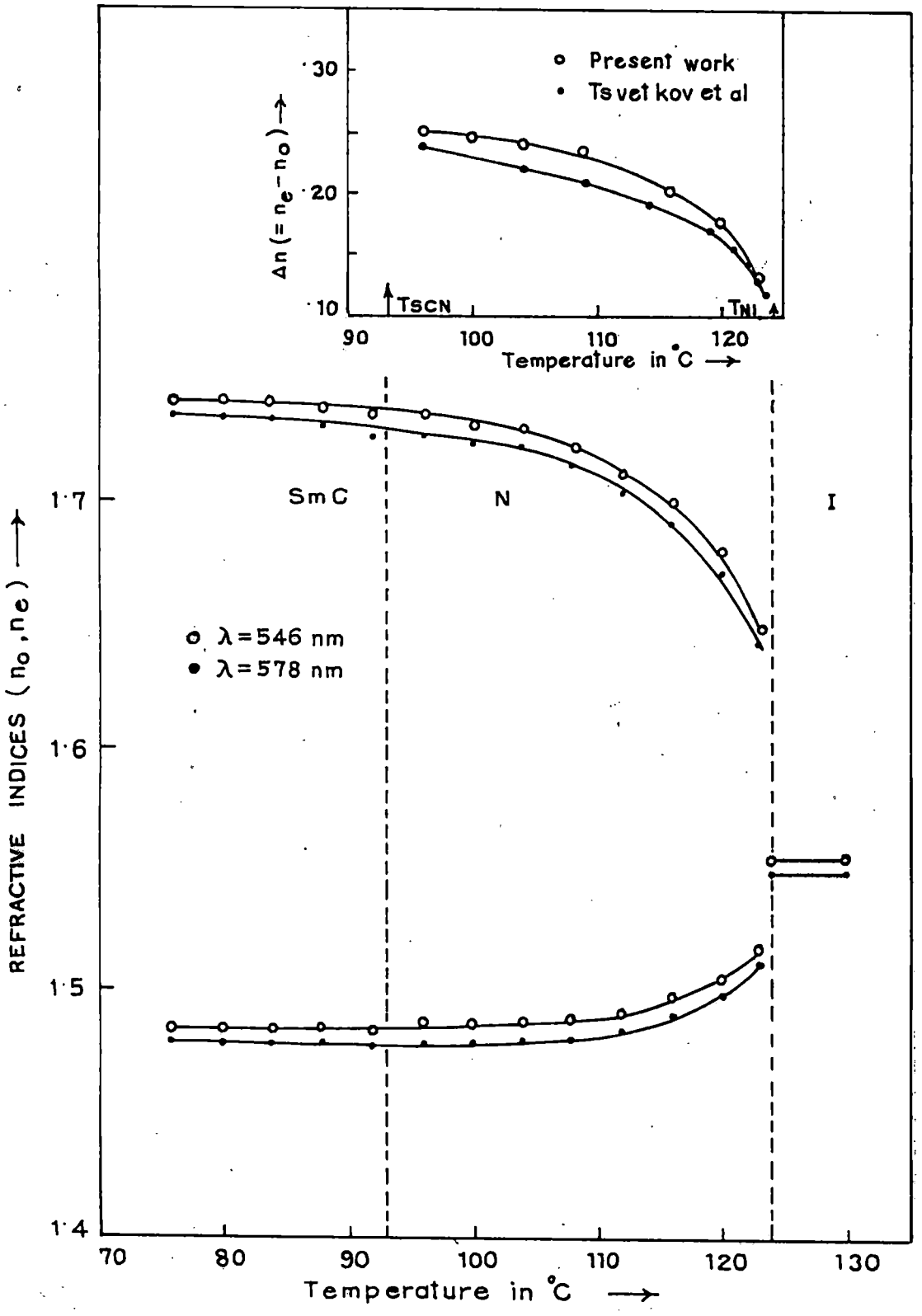

Figure 3.6 Temperature dependence of the ordinary (n_o) and extraordinary (n_e) refractive indices of HAB. Inset shows birefringence values in the nematic phase as compared with Tsvetkov et al.(reference 7).

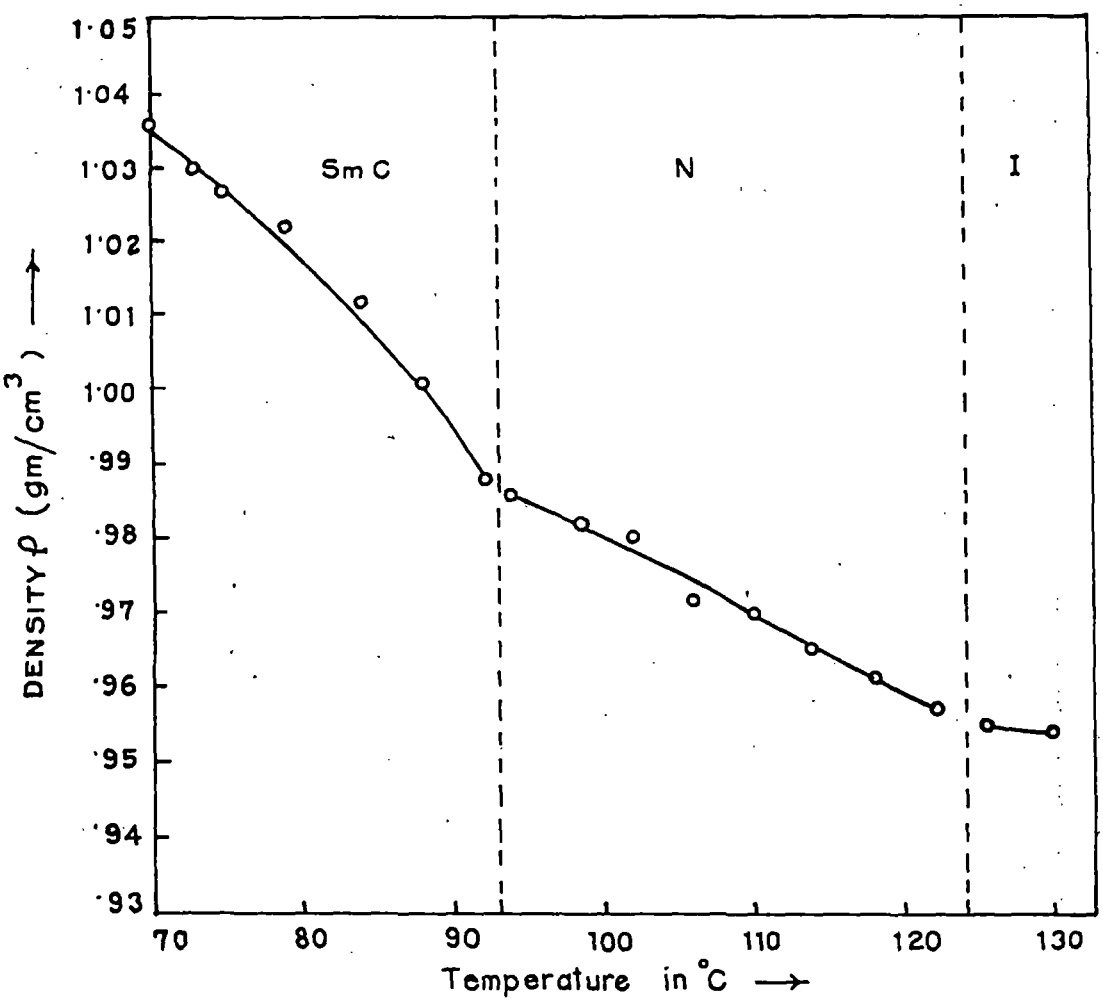

Figure 3.7 The density of HAB as a function of temperature. Solid line is guide to the eye only.

where N is a normalising constant. The distribution function $f'(\cos\phi)$ is thus obtained from the analysis of the x-ray data, and knowing the tilt angle θ_t, the expression for $f'(\cos\phi)$ can be integrated and apparent order parameters $\langle P_2(\cos\theta)\rangle_{app}$ and $\langle P_4(\cos\theta)\rangle_{app}$ calculated. Figure 3.4 also shows $\langle P_2(\cos\theta)\rangle_{app}$ and $\langle P_4(\cos\theta)\rangle_{app}$ in the smectic C phase calculated by the above method, assuming experimental tilt angles only, i.e. introducing no adjustable parameter. It is seen that the agreement between the experimental and calculated values is fairly good (see figure 3.4). The normalised distribution function $f'(\cos\phi)$ values, obtained following this procedure is given in table 3.4 and the calculated values of the apparent order parameter values $\langle P_2\rangle_{app}$ and $\langle P_4\rangle_{app}$ in the smectic C phase of HAB is given in table 3.5.

Figure 3.6 shows the temperature dependences of refractive indices, n_o,n_e at two different wavelengths λ=578nm and 546nm. On comparing the Δn (= $n_e - n_o$) values of the present work, as shown in inset of Figure 3.6, with those obtained by Tsvetkov et al [7] at λ=546nm, in nematic phase, a reasonable agreement is found.

The density variation of HAB in the temperature range 70^{o}C to 130^{o}C is shown in Figure 3.7. From the Figures 3.6 and 3.7 it appears that there is a continuous change in the refractive index and density values in going from smectic C to nematic phase, implying second order phase transition.

Orientational order parameter values obtained on analysing the refractive index and density data, as a function of temperature, using Vuks procedure, are also shown in Figure 3.4. Although there is good agreement between the OOP's determined from x-ray and refractive index methods in the nematic phase, there is a large discrepancy in the order parameters in the smectic C phase. This is due to the fact that in the refractive

index determination experiment, the director, in both the nematic and smectic C phases, is pinned along the direction of the surface alignment, whereas, in the x-ray diffraction studies we have seen that the director in the smectic C phase is randomly oriented on a cone about the layer normal. Hence the anisotropy and OOP, which depends on anisotropy, are greater in case of surface aligned samples of HAB than the magnetically aligned samples. However, the OOP values from refractive index measurements in the smectic C phase are still lower than the theoretical values, which may be due to the observed disordering in the alkyl chain [1] part of the HAB molecules in the smectic C phase, causing anisotropy of the system to be reduced.

The transverse (i.e., perpendicular to the director) correlation lengths in both nematic and smectic C phases have been determined from the x-ray diffraction intensity data after corrections for flat plate and beam width as described in chapter 2. The corrected x-ray intensity profile I(q) in the transverse q(wave vector) direction is fitted using a least-squares method to the Lorentzian form with a quadratic background:

$$I(q) = \frac{a}{b + (q - q_o)^2} + cq^2 + dq + e \qquad (3.4)$$

where a, b, q_o, c, d and e are adjusted to obtain the best fit. Convergence was good for for all the profiles (Figures 3.8(a)-3.8(j)). The value of q_o gives the position of the x-ray diffraction peak and correlation length ξ is equal to $2\pi(b)^{-1/2}$. The temperature variations of q_o and ξ are shown respectively in Figures 3.9 and 3.10. The values of ξ at different temperatures of HAB are listed in table 3.6 and the values of q_o and intermolecular distance D at different temperatures are arranged

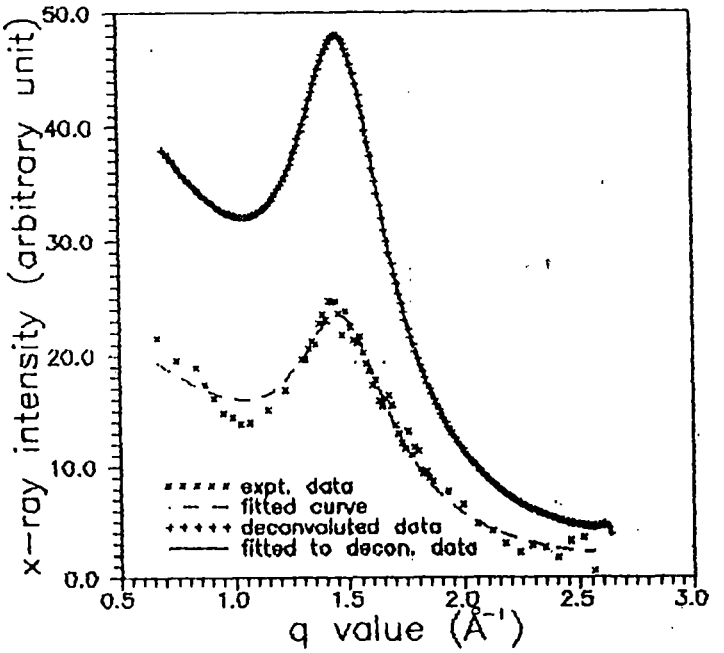

Fig.3.8a Comparison of experimental x-ray intensity data before and after deconvolution; HAB at 81 deg C.

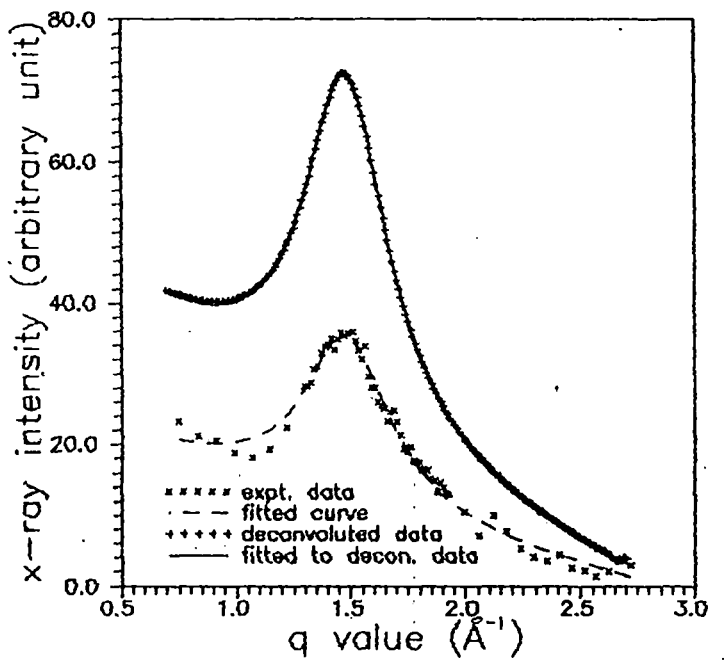

Fig.3.8b Comparison of experimental x-ray intensity data before and after deconvolution; HAB at 93 deg C.

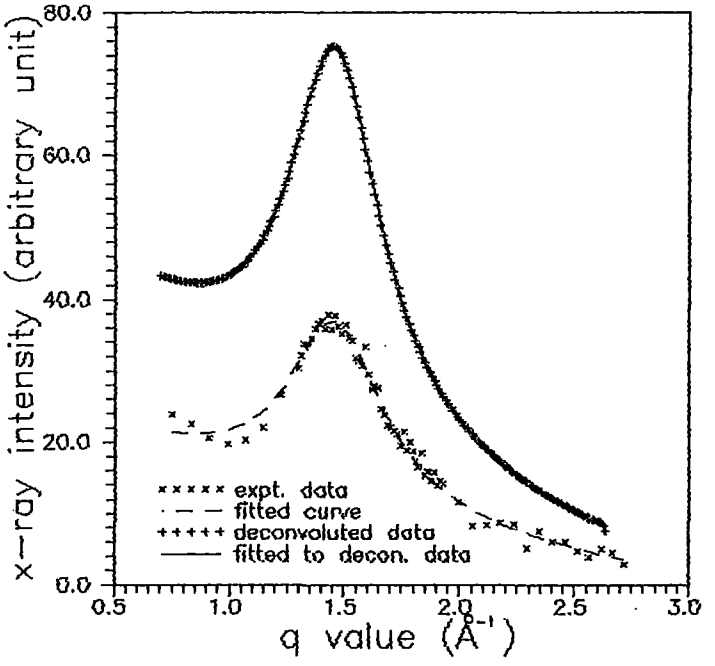

Fig.3.8c Comparison of experimental x-ray intensity data before and after deconvolution; HAB at 97 deg C.

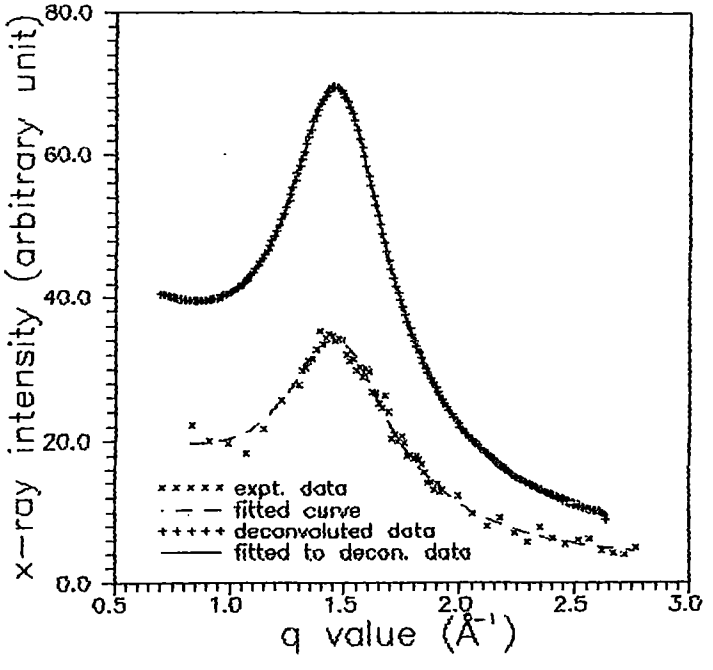

Fig.3.8d Comparison of experimental x-ray intensity data before and after deconvolution; HAB at 101 deg C.

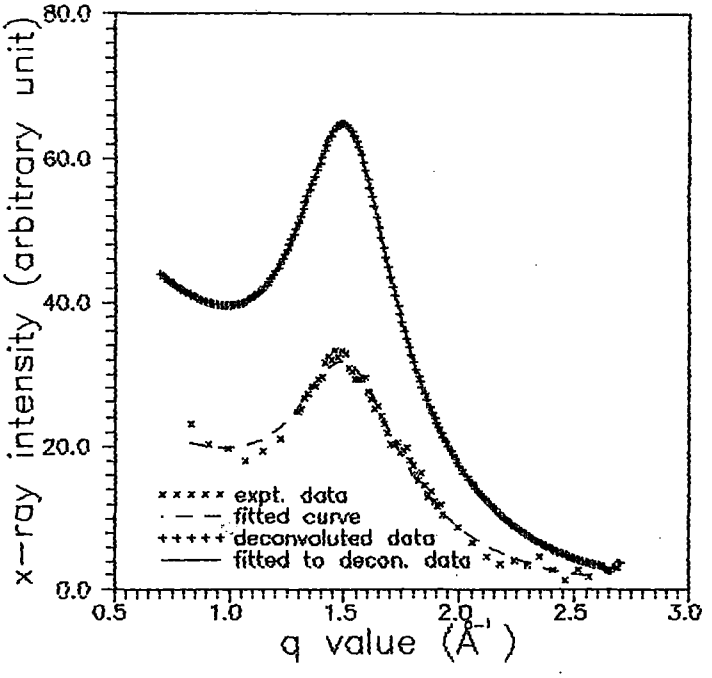

Fig.3.8e Comparison of experimental x-ray intensity data before and after deconvolution; HAB at 105 deg C.

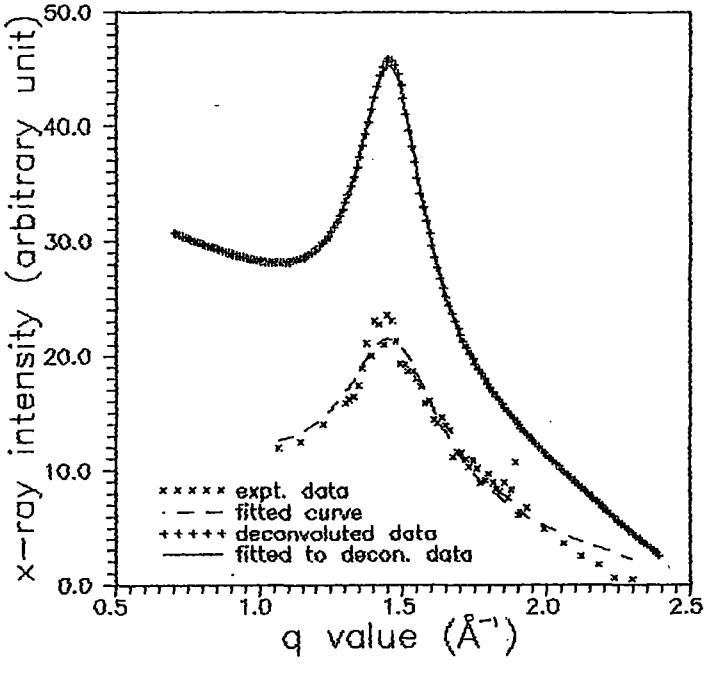

Fig.3.8f Comparison of experimental x-ray intensity data before and after deconvolution; HAB at 108 deg C.

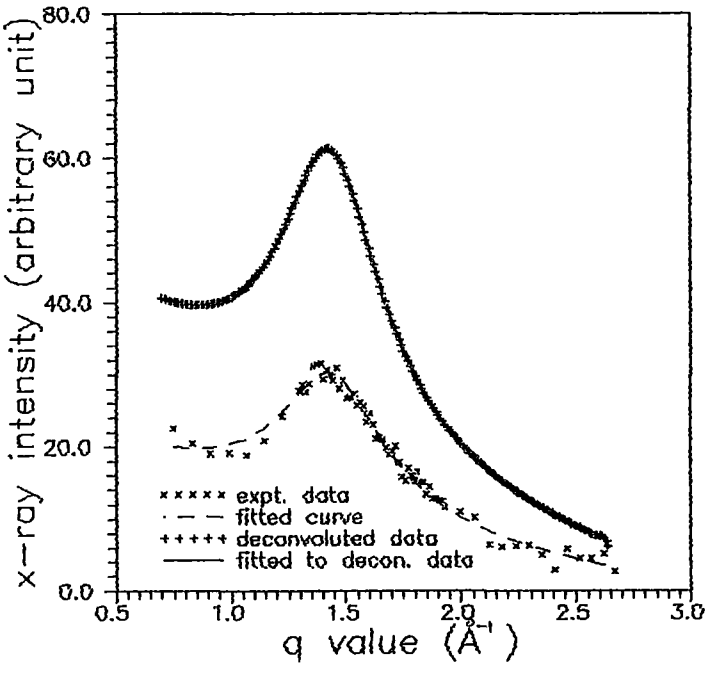

Fig.3.8g Comparison of experimental x-ray intensity data before and after deconvolution; HAB at 112 deg C.

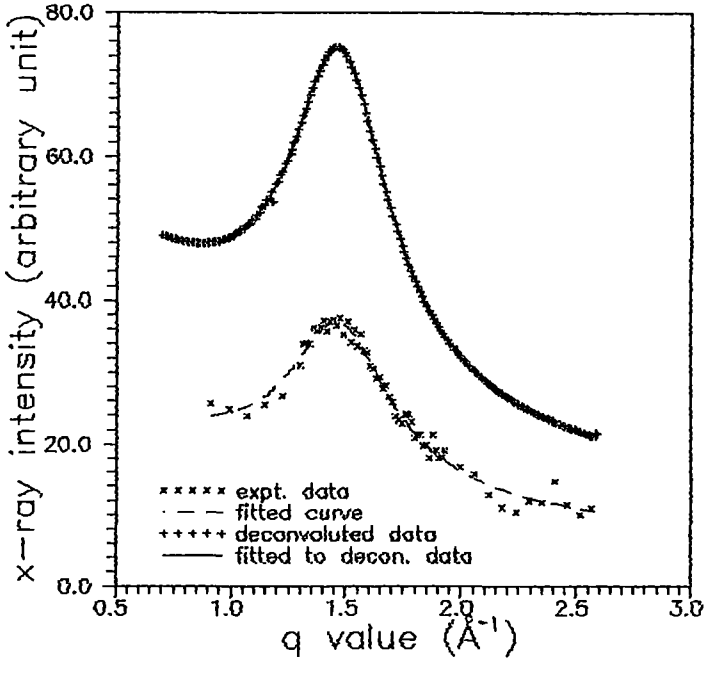

Fig.3.8h Comparison of experimental x-ray intensity data before and after deconvolution; HAB at 116 deg C.

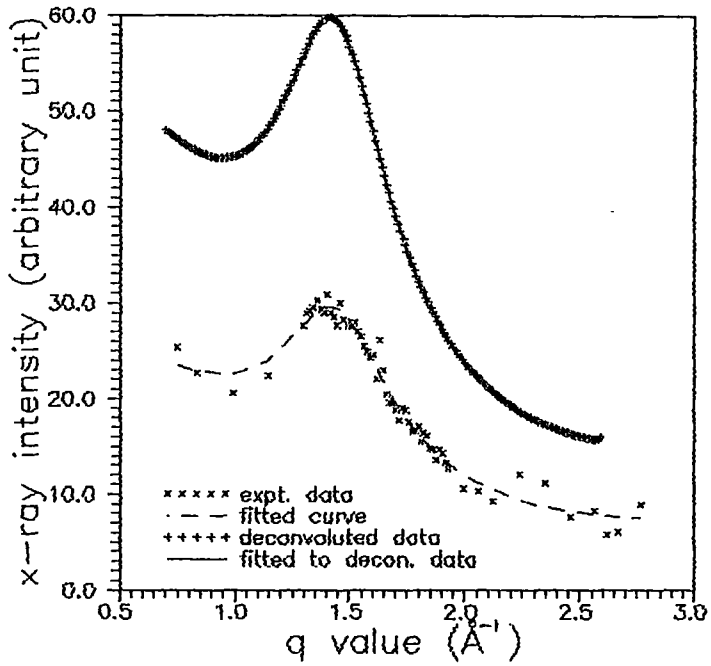

Fig.3.8i Comparison of experimental x-ray intensity data before and after deconvolution; HAB at 120 deg C.

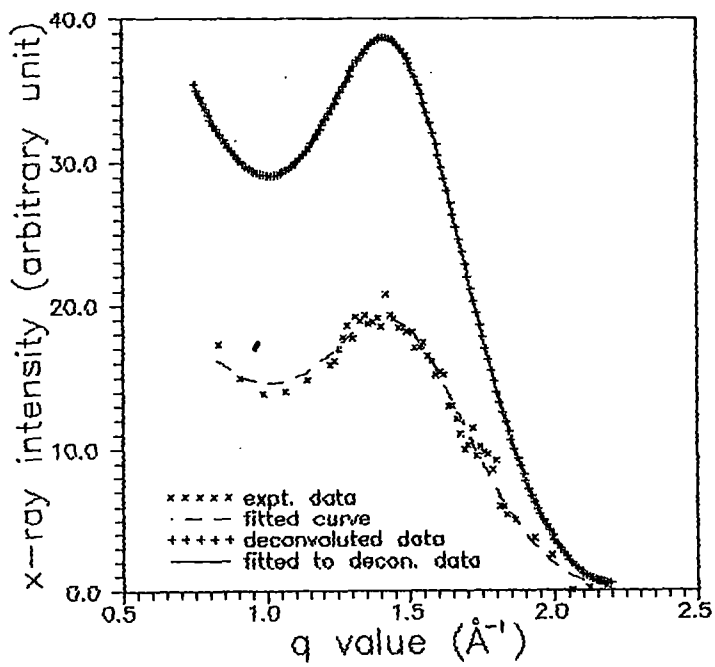

Fig.3.8j Comparison of experimental x-ray intensity data before and after deconvolution; HAB at 125 deg C (isotropic phase).

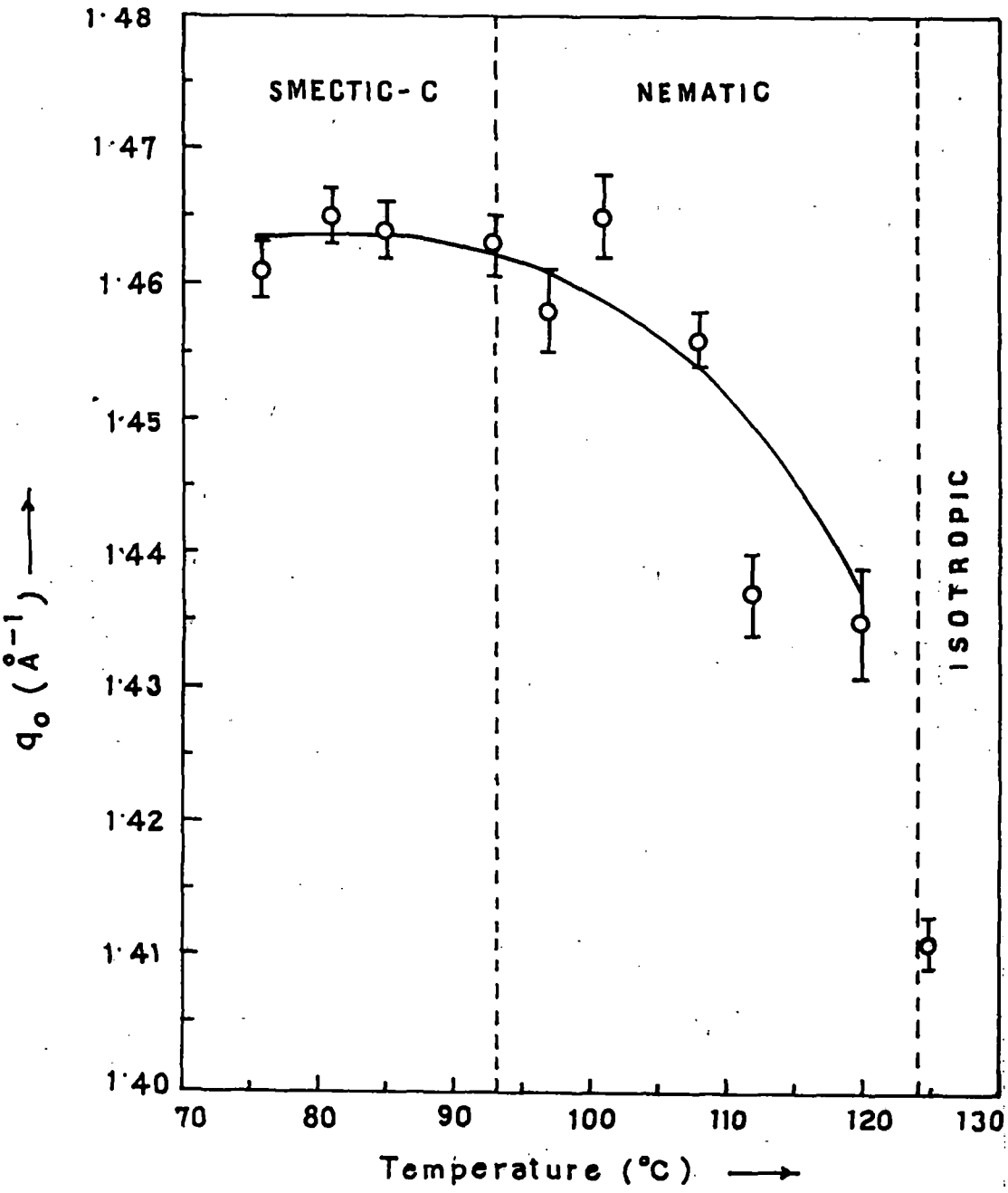

Figure 3.9 Variation of magnitude of peak scattering vector q_o ($\AA^{-1}$) with temperature of HAB. Solid line is guide to the eye only. Vertical bars show estimated errors.

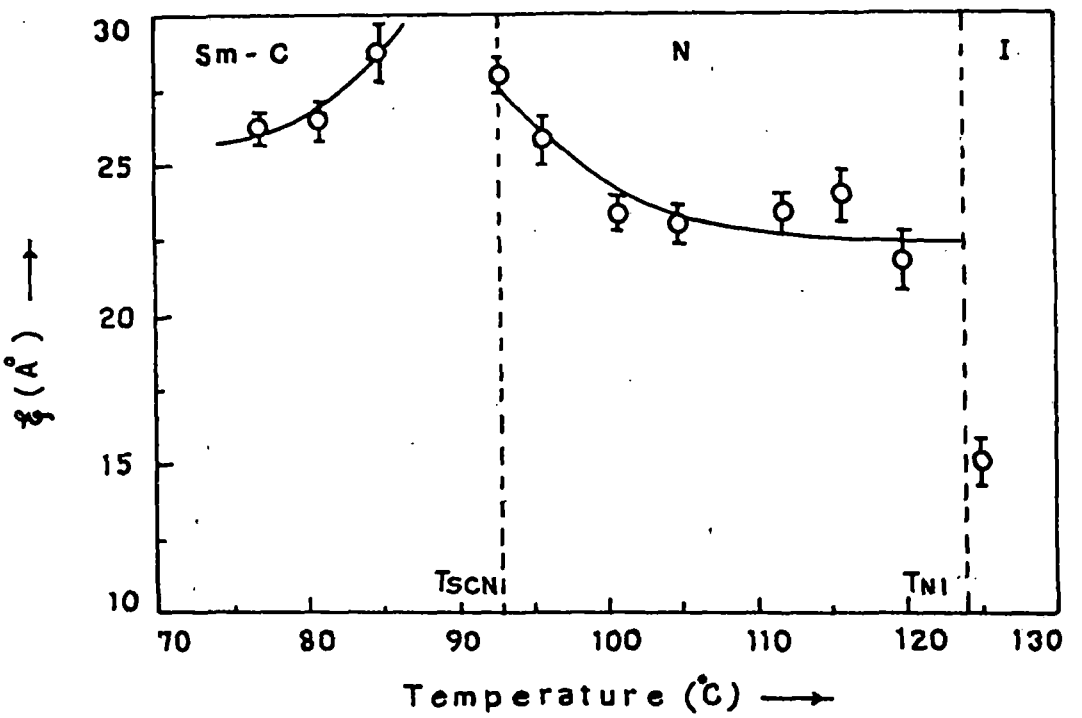

Figure 3.10 Variation of transverse correlation length ξ with temperature of HAB. Solid line is guide to the eye only. Vertical bars show estimated errors.

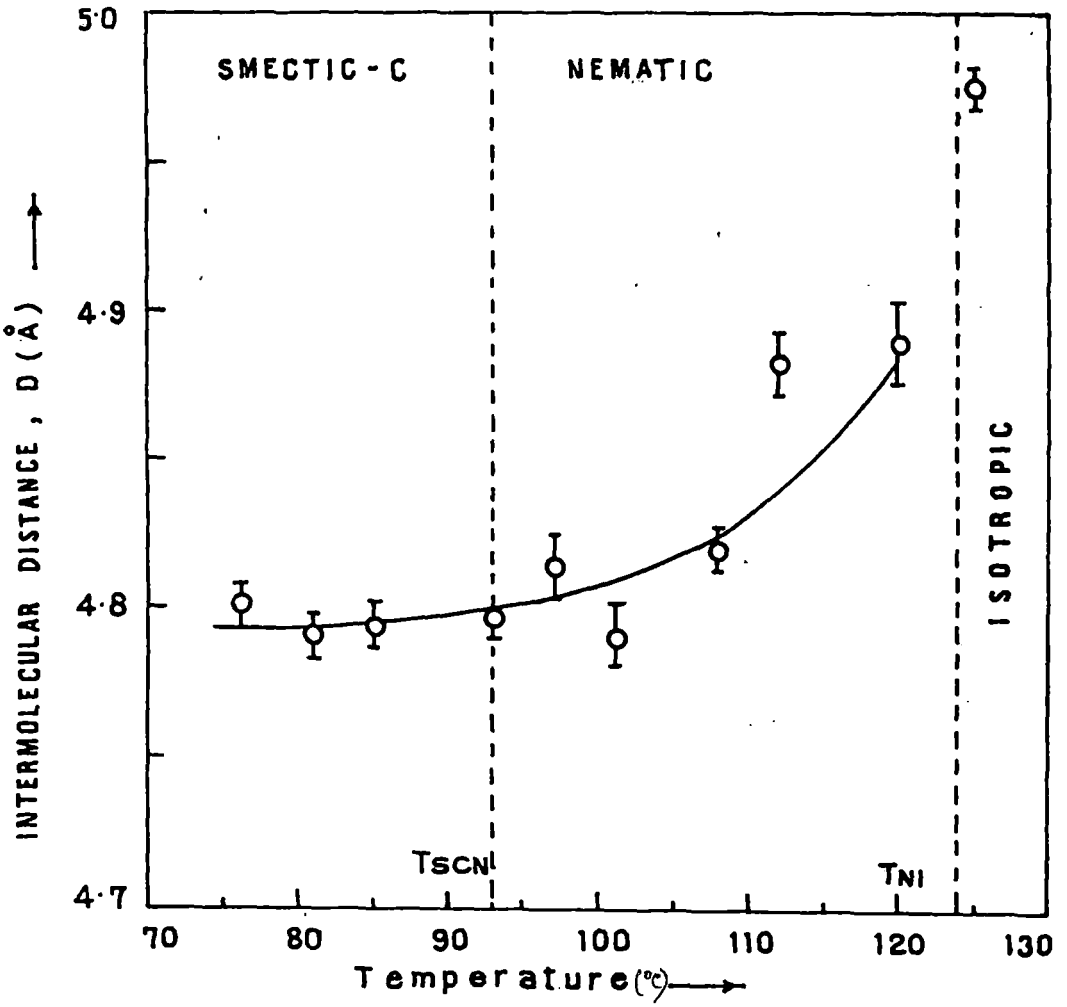

Figure 3.11 Variation of intermolecular distance, D, with temperature of HAB. Solid line is guide to the eye only. Vertical bars show estimated errors.

in table 3.7. Variation of the intermolecular distance, D (= $2.234\pi/q_o$) with temperature is shown in Figure 3.11. As expected the intermolecular distance increases quite rapidly near the nematic - isotropic tansition. Figure 3.10 shows that ξ increase near the smectic C - nematic transition, as expected for a second-order phase transition. However, the temperature uncertainty did not permit to pursue this trend very close to the transition temperature.

Table 3.1

Mean experimental intensity values $I(\psi)$, in arbitrary units, of HAB after background correction.

ψ (degree)	$I(\psi)$ values at different temperatures in ^{o}C						
	75.0	77.0	81.0	85.0	89.0	93.0	97.0
0	11.6	18.4	14.1	14.6	10.3	22.3	21.4
5	11.1	17.9	13.7	14.3	9.9	21.5	20.8
10	10.6	17.0	12.6	13.5	9.3	19.2	12.0
15	9.7	16.2	11.7	12.3	8.7	16.4	14.2
20	8.8	14.7	10.2	10.8	7.8	13.1	11.2
25	7.7	12.5	9.1	9.6	7.0	9.9	8.7
30	6.9	11.0	8.1	8.5	6.2	7.6	6.8
35	6.0	9.9	7.0	7.4	5.3	6.1	5.6
40	5.2	8.6	6.0	6.4	4.5	4.7	4.4
45	4.3	7.5	5.0	5.5	3.7	3.7	3.6
50	3.6	6.5	4.2	4.8	2.9	2.7	2.9
55	3.0	5.4	3.4	4.0	2.3	2.2	2.3
60	2.4	4.5	2.6	3.4	1.8	1.7	1.9
65	1.8	3.6	1.9	2.6	1.4	1.3	1.4
70	1.3	2.8	1.4	2.0	1.1	0.9	1.0
75	0.9	1.9	0.9	1.5	0.9	0.7	0.7
80	0.6	1.2	0.5	1.1	0.7	0.4	0.4
85	0.4	0.7	0.3	0.7	0.4	0.1	0.2
90	0.2	0.2	0.2	0.2	0.2	0.0	0.0

(continued)

Table 3.1

Mean experimental intensity values $I(\psi)$, in arbitrary units, of HAB after background correction.

ψ (degree)	$I(\psi)$ values at different temperatures in ^{o}C						
	101.0	105.0	108.0	112.0	116.0	120.0	122.0
0	18.0	18.9	8.8	13.0	17.5	11.9	14.5
5	17.0	18.4	8.5	12.6	17.1	11.6	14.1
10	15.0	17.1	7.7	11.5	16.3	10.6	13.3
15	12.5	14.5	6.3	9.6	14.3	9.6	12.1
20	10.4	11.0	5.2	7.5	12.2	8.3	10.6
25	8.2	8.7	4.3	6.1	10.3	6.9	9.1
30	6.4	6.8	3.5	4.9	8.6	5.6	7.8
35	4.6	5.2	2.8	4.0	6.7	4.8	6.6
40	3.5	4.1	2.2	3.4	5.1	4.0	5.6
45	2.7	3.5	1.7	2.7	4.0	3.2	4.6
50	2.1	3.0	1.3	2.2	3.2	2.6	3.6
55	1.6	2.5	1.0	1.6	2.4	2.0	2.8
60	1.1	2.0	0.8	1.1	2.0	1.6	2.1
65	0.8	1.6	0.6	0.8	1.4	1.3	1.6
70	0.5	1.3	0.5	0.6	0.9	0.9	0.8
75	0.3	1.0	0.4	0.4	0.6	0.6	0.4
80	0.2	0.6	0.3	0.3	0.4	0.4	0.2
85	0.1	0.3	0.2	0.2	0.2	0.3	0.1
90	0.0	0.0	0.1	0.0	0.0	0.1	0.0

Table 3.2

Normalised distribution function values f(β) of HAB.

β (degree)	f(β) values at different temperatures in ^{o}C						
	75.0	77.0	81.0	85.0	89.0	93.0	97.0
0	4.49	3.74	4.98	4.50	4.43	7.84	11.33
5	4.38	3.78	4.81	4.42	4.34	7.92	9.86
10	4.03	3.78	4.32	4.12	4.05	7.60	7.00
15	3.50	3.48	3.63	3.56	3.55	6.15	4.75
20	2.93	2.91	2.96	2.91	2.99	4.20	3.49
25	2.48	2.38	2.47	2.39	2.55	2.82	2.81
30	2.16	2.03	2.16	2.04	2.26	2.12	2.27
35	1.89	1.79	1.92	1.78	2.01	1.73	1.71
40	1.60	1.54	1.62	1.51	1.69	1.33	1.19
45	1.28	1.24	1.28	1.22	1.30	0.87	0.84
50	1.01	0.99	0.99	0.97	0.96	0.55	0.65
55	0.82	0.84	0.80	0.81	0.73	0.40	0.55
60	0.68	0.76	0.67	0.71	0.58	0.36	0.47
65	0.54	0.66	0.52	0.60	0.47	0.33	0.35
70	0.37	0.48	0.34	0.44	0.34	0.23	0.22
75	0.22	0.27	0.18	0.27	0.22	0.11	0.11
80	0.12	0.13	0.09	0.15	0.13	0.04	0.06
85	0.08	0.08	0.05	0.09	0.09	0.02	0.03
90	0.06	0.06	0.04	0.08	0.08	0.01	0.02

(continued)

Table 3.2

Normalised distribution function values $f(\beta)$ of HAB.

β (degree)	$f(\beta)$ values at different temperatures in ^{o}C						
	101.0	105.0	108.0	112.0	116.0	120.0	122.0
0	9.02	7.28	7.92	7.49	5.75	5.63	5.07
5	8.44	7.31	7.57	7.47	5.75	5.55	5.03
10	7.06	7.02	6.56	7.00	5.53	5.20	4.77
15	5.54	5.85	5.14	5.63	4.81	4.48	4.16
20	4.27	4.19	3.79	3.90	3.80	3.57	3.37
25	3.28	2.83	2.83	2.64	2.98	2.79	2.72
30	2.44	2.01	2.22	1.99	2.45	2.42	2.29
35	1.73	1.53	1.79	1.68	2.02	1.84	1.97
40	1.18	1.15	1.37	1.40	1.53	1.46	1.61
45	0.81	0.82	0.98	1.05	1.03	1.11	1.23
50	0.59	0.60	0.67	0.73	0.69	0.83	0.92
55	0.46	0.50	0.49	0.54	0.52	0.64	0.74
60	0.35	0.46	0.38	0.43	0.45	0.53	0.61
65	0.24	0.43	0.31	0.34	0.38	0.41	0.45
70	0.13	0.31	0.23	0.22	0.25	0.28	0.25
75	0.06	0.17	0.15	0.11	0.11	0.16	0.10
80	0.03	0.08	0.09	0.05	0.04	0.09	0.04
85	0.02	0.04	0.06	0.03	0.02	0.05	0.02
90	0.01	0.03	0.05	0.02	0.01	0.04	0.00

Table 3.3

Order parameter values at different temperatures of HAB.

Temp. in ^{o}C	$\langle P_2 \rangle$	$\langle P_4 \rangle$
75.0	0.429	0.066
77.0	0.400	0.057
81.0	0.446	0.075
85.0	0.412	0.074
89.0	0.443	0.073
93.0	0.598	0.242
97.0	0.571	0.226
101.0	0.617	0.245
105.0	0.559	0.228
108.0	0.557	0.204
112.0	0.564	0.203
116.0	0.544	0.158
120.0	0.503	0.137
122.0	0.497	0.100

Table 3.4

Normalised distribution function values $f'(\phi)$ of HAB, in the smectic C phase, after allowing for the tilt angle.

$\alpha = 0.39$, $\delta = 0.6$

ϕ (degree)	$f'(\phi)$ values at different temperatures in ^{o}C						
	75.0	76.8	78.6	80.4	82.2	84.0	85.8
0	1.85	1.89	2.02	2.09	2.17	2.24	2.32
5	1.90	1.94	2.07	2.14	2.21	2.28	2.35
10	2.06	2.09	2.20	2.26	2.32	2.38	2.43
15	2.27	2.29	2.38	2.43	2.47	2.51	2.53
20	2.47	2.48	2.55	2.57	2.59	2.60	2.60
25	2.60	2.59	2.62	2.62	2.62	2.61	2.59
30	2.58	2.56	2.56	2.55	2.53	2.50	2.46
35	2.40	2.37	2.35	2.33	2.30	2.26	2.23
40	2.07	2.05	2.02	1.99	1.96	1.93	1.90
45	1.67	1.66	1.62	1.60	1.58	1.56	1.53
50	1.25	1.25	1.22	1.21	1.20	1.19	1.18
55	0.89	0.89	0.87	0.87	0.86	0.86	0.86
60	0.60	0.61	0.60	0.60	0.60	0.60	0.61
65	0.39	0.40	0.40	0.40	0.41	0.42	0.43
70	0.25	0.26	0.26	0.27	0.28	0.28	0.30
75	0.17	0.17	0.18	0.18	0.19	0.20	0.21
80	0.11	0.12	0.13	0.13	0.14	0.15	0.16
85	0.09	0.10	0.10	0.11	0.11	0.12	0.13
90	0.08	0.09	0.09	0.10	0.10	0.11	0.12

(continued)

Table 3.4

Normalised distribution function values $f(\beta)$ of HAB, in the smectic C phase, after allowing for the tilt angle.

$\alpha = 0.39$, $\delta = 0.6$

ϕ (degree)	$f'(\phi)$ values at different temperatures in ^{o}C.			
	87.6	89.4	91.2	93.0
0	2.40	2.46	2.53	2.61
5	2.42	2.48	2.54	2.62
10	2.49	2.53	2.58	2.65
15	2.56	2.57	2.62	2.67
20	2.60	2.58	2.61	2.65
25	2.56	2.52	2.53	2.55
30	2.42	2.37	2.36	2.36
35	2.17	2.12	2.11	2.10
40	1.86	1.81	1.80	1.78
45	1.51	1.48	1.46	1.45
50	1.16	1.16	1.14	1.13
55	0.87	0.87	0.86	0.85
60	0.62	0.64	0.63	0.63
65	0.44	0.46	0.46	0.46
70	0.32	0.33	0.34	0.34
75	0.23	0.25	0.25	0.25
80	0.18	0.20	0.20	0.20
85	0.15	0.17	0.17	0.17
90	0.14	0.16	0.16	0.16

Table 3.5

Calculated values of the order parameter at different temperatures in the smectic C phase of HAB considering random tilt distibution of the director. The tilt angles were determined as mentioned in the text.

Temp. in ^{o}C	tilt angle θ_t(deg)	$\langle P_2 \rangle$	$\langle P_4 \rangle$
75.0	32.7	0.398	-0.031
76.8	32.6	0.395	-0.029
78.6	32.0	0.401	-0.020
80.4	31.7	0.400	-0.016
82.2	31.4	0.399	-0.011
84.0	31.1	0.397	-0.007
85.8	30.8	0.393	-0.003
87.6	30.5	0.387	0.001
89.4	30.1	0.379	0.005
91.2	29.7	0.381	0.009
93	29.2	0.384	0.014

Table 3.6

Transverse correlation length ξ at different temperatures for HAB.

Temp. in ^{o}C.	ξ ± S.D.
77.0	26.25 ± 0.5
81.0	26.62 ± 0.7
85.0	28.92 ± 0.9
93.0	28.07 ± 0.4
97.0	25.93 ± 0.7
101.0	23.30 ± 0.5
105.0	23.14 ± 0.5
112.0	23.43 ± 0.5
116.0	24.11 ± 0.8
120.0	21.80 ± 0.8
125.0 (iso)	15.09 ± 0.6

Table 3.7

Magnitudes of the peak scattering vector q_o and values of intermolecular distance D at different temperatures for HAB.

Temp. in ^oC	$q_o \pm$ S.D. ($\AA^{-1}$)	D $\pm$ S.D. ($\AA$)
77.0	1.461 ± 0.002	4.804 ± 0.007
81.0	1.465 ± 0.002	4.791 ± 0.007
85.0	1.464 ± 0.002	4.794 ± 0.007
93.0	1.463 ± 0.002	4.797 ± 0.007
97.0	1.458 ± 0.003	4.814 ± 0.010
101.0	1.465 ± 0.003	4.791 ± 0.010
108.0	1.456 ± 0.002	4.820 ± 0.007
112.0	1.437 ± 0.003	4.884 ± 0.010
120.0	1.435 ± 0.004	4.891 ± 0.014
125.0(iso)	1.411 ± 0.002	4.974 ± 0.007

Table 3.8

Density (ρ) and refractive indices (n_o,n_e) at different temperatures of HAB.

Temp. in ^oC	Density (ρ) in gms/c.c	λ = 578 nm		λ = 546 nm	
		n_o	n_e	n_o	n_e
76.0	1.026	1.479	1.734	1.485	1.740
80.0	1.018	1.479	1.734	1.485	1.740
84.0	1.009	1.478	1.733	1.485	1.740
88.0	0.999	1.478	1.732	1.485	1.738
92.0	0.988	1.479	1.730	1.485	1.738
96.0	0.984	1.479	1.728	1.485	1.735
100.0	0.980	1.480	1.725	1.486	1.733
104.0	0.976	1.480	1.723	1.488	1.730
108.0	0.972	1.480	1.715	1.488	1.723
112.0	0.968	1.483	1.704	1.490	1.712
116.0	0.963	1.490	1.693	1.498	1.700
120.0	0.959	1.495	1.670	1.505	1.680

Table 3.9

Polarizabilities (α_o, α_e) at different temperatures and for different wavelengths (λ) of HAB by Vuk's method.

Temp. in ^oC	λ = 578 nm		λ = 546 nm	
	α_o	α_e	α_o	α_e
76.0	43.90	74.15	44.36	74.64
80.0	44.22	74.70	44.69	75.19
84.0	44.49	75.28	45.09	75.86
88.0	44.94	76.00	45.57	76.34
92.0	45.61	76.54	46.08	77.19
96.0	45.85	76.61	46.32	77.26
100.0	46.13	76.56	46.63	77.21
104.0	46.35	76.59	46.97	77.19
108.0	46.66	76.04	47.26	76.65
112.0	47.20	74.98	47.83	75.59
116.0	48.36	73.90	48.93	74.44
120.0	49.51	71.29	50.11	72.19

α_o, α_e are in 10^{-24} cm^3 unit.

Table 3.10

Polarizabilities (α_o, α_e) at different temperatures and for different wavelengths (λ) of HAB by Neugebauer's method.

Temp. in ^oC	λ = 578 nm		λ = 546 nm	
	α_o	α_e	α_o	α_e
76.0	45.75	70.44	46.24	70.89
80.0	46.09	70.96	46.58	71.41
84.0	46.38	71.51	47.00	72.05
88.0	46.84	72.20	47.47	72.53
92.0	47.50	72.76	48.00	73.34
96.0	47.73	72.85	48.23	73.43
100.0	47.99	72.85	48.52	73.43
104.0	48.20	72.90	48.84	73.46
108.0	48.44	72.46	49.07	73.03
112.0	48.88	71.61	49.53	72.18
116.0	49.91	70.80	50.50	71.30
120.0	5.083	68.66	51.47	69.49

α_o, α_e are in 10^{-24} cm^3 unit.

Table 3.11

Order parameters $\langle P_2 \rangle$ of HAB at different temperatures by Vuk's method.

Temp.. in °C	λ = 578 nm $\langle P_2 \rangle$	λ = 561 nm $\langle P_2 \rangle$	Average $\langle P_2 \rangle$
76.0	0.590	0.589	0.590
80.0	0.594	0.593	0.594
84.0	0.600	0.599	0.600
88.0	0.606	0.599	0.603
92.0	0.603	0.605	0.604
96.0	0.600	0.602	0.601
100.0	0.593	0.595	0.594
104.0	0.590	0.588	0.589
108.0	0.573	0.572	0.573
112.0	0.542	0.540	0.541
116.0	0.498	0.496	0.497
120.0	0.424	0.430	0.427

Table 3.12

Order parameters $\langle P_2 \rangle$ of HAB at different temperatures by Neugebauer's method.

Temp. in ^{o}C	λ = 578 nm	λ = 561 nm	Average
	$\langle P_2 \rangle$	$\langle P_2 \rangle$	$\langle P_2 \rangle$
76.0	0.591	0.589	0.590
80.0	0.596	0.594	0.595
84.0	0.602	0.599	0.601
88.0	0.607	0.599	0.603
92.0	0.605	0.606	0.606
96.0	0.602	0.602	0.602
100.0	0.595	0.596	0.596
104.0	0.592	0.589	0.591
108.0	0.575	0.573	0.574
112.0	0.544	0.541	0.543
116.0	0.500	0.497	0.499
120.0	0.427	0.431	0.429

REFERENCES

[1]. A. J. Leadbetter and E. K. Norris, Molec. Phys., 38, 669 (1979).

[2]. G. Chistyakov and W. M. Chaikowsky, Mol.Cryst.Liq.Cryst 7 269 (1969).

[3]. A. de Vries, Acta Crystallographica, A25, S135 (1969).

[4]. W.L. McMillan, Phys. Rev. A, 18, 328 (1973).

[5]. H. Terauchi and R. Ohnishi, J. Phys. Soc. Japan, 40, 915 (1976).

[6] . W. H. de Jeu and P. Bordewijk, J. Chem. Phys., 68(1), 109 (1978)

[7]. V. N. Tsvetkov, E. I. Ryumtsev, I. P. Kolomiets, A. P. Kovshik and N. L. Gantseva, Opt. Spectrosk., 35, 511 (1973).

[8]. R. Paul, B. Jha and D. A. Dunmur, Liquid Crystals, 13, 629 (1993)

[9] . B. Bhattacharya, S. Paul and R. Paul, Molec. Phys. 44, 1391 (1981).

[10]. A. K. Zemindar, S. Paul and R. Paul, Mol. Cryst. Liq. Cryst., 61, 191 (1980).

[11]. M.F. Vuks, Optics and Spectroscopy, 20, 361 (1966).

[12]. H.E.J. Neugebauer, Canad. J. Phys., 32, 1 (1954).

[13]. I. Haller, H.A. Huggins, H.R. Lilienthal and T.R. McGuire, J. Phys. Chem., 77, 950 (1973).

[14]. W. Maier and A. Saupe, Z. Naturforsche., 15a, 287 (1960).

[15]. W.L. McMillan, Phys. Rev. A, 6, 936 (1972).

CHAPTER - 4

PHYSICAL PROPERTIES OF THREE BICYCLOHEXANE COMPOUNDS POSSESSING SMECTIC B PHASE I : X-RAY DIFFRACTION STUDY

4.1 Introduction

Liquid crystal material research has gained considerable importance due to their increased applicability in display devices. At the same time these compounds exhibit a wide variety of phase transitions study of which play an important role in the development of the modern theory of phase transitions and critical phenomena. Quantitative knowledge of orientational ordering and better understanding of the molecular structure of liquid crystals are required so that improved materials may be produced for applications. Study of pure compounds is also an important prerequisite in the preparation of mixtures better tuned to meet the specific demands of electro-optic display devices. In this chapter, I present the results of x-ray diffraction measurements on three non-polar alkenyl/alkenyloxy bicyclohexane compounds possessing smectic B phase, which is precursor of nematic phase in two of the compounds, while in case of the third compound the smectic B phase is followed directly by isotropic liquid. These compounds are of extraordinary interest since they do not contain any rigid aromatic core, common to most liquid crystalline compounds. They belong to a new class of liquid crystals, recently synthesised, exhibiting low optical anisotropy ($\Delta n < 0.1$), low rotational viscosity, low magnetic anisotropy ($\Delta\chi \approx 0$) and low viscoelastic ratios leading to faster response times in field effect liquid crystal displays [1]. Although some work on bicyclohexane compounds have been reported [1], no x-ray work has been done on these compounds.

In the present chapter x-ray diffraction measurements have been undertaken to investigate the Bond Orientational Order (BOO) in the smectic B phase of all the compounds. As suggested by Birgeneau and Litster [2], the smectic B phase is a

realisation of the stacked hexagonal phase possessing BOO found in two dimensions. In such systems with six fold symmetry the BOO is defined to be the thermal average of the quantity,

$$\Psi(\vec{r})=\langle \exp(i6\theta(\vec{r})\rangle \qquad (4.1)$$

where, $\theta(\vec{r})$ is the angle a nearest neighbour bond at the point $\vec{r}$ makes with a reference direction in the plane. Although x-ray [3] and electron diffraction [4] studies on smectic B phase have been reported, not much work has been done to determine the BOO. The experimentally determined bond orientational order values have been utilised to charecterise the smectic B phase in these compounds which is found to be of the Crystal B type.

Orientational order parameter, intermolecular distance, layer thickness and apparent molecular length throughout the mesomorphic range of all the three compounds have also been reported in this chapter. Translational order parameters (τ) have been measured for one of the compound only, where second order diffraction in the meridional direction have been observed. The experimental order parameters have been fitted to McMillan's theory [5-6] for smectic A phase and the agreement is found to be fairly good.

4.2 Experimental

4.2.1 Materials and texture study

The compounds were donated to us by M/S Hoffmann-La-Roche and Co., Basel, Switzerland. They were used without further purification, since the transition temperatures of the chemicals as seen under a polarising microscope, equipped with a Mettler FP80/82 Thermosystem, agreed with the supplied values

(Hoffmann-La-Roche Catalogue). The structural formula, chemical names and transition temperatures of the compounds are as follows :-

(I) 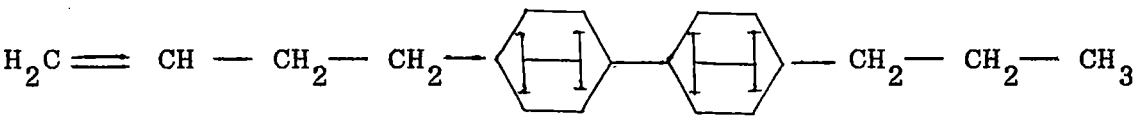

4(3″ - butenyl)4′(propyl) 1,1′ bicyclohexane (BPBCH in short)

C(18°C)Sm B(73°C)N(77°C)I

(II) 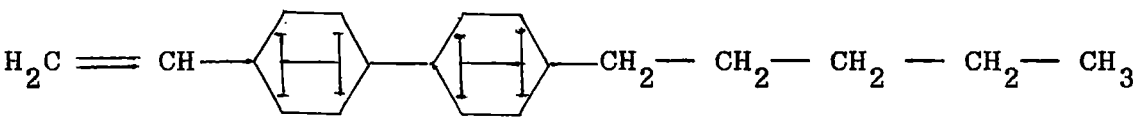

4 - Vinyl, 4′-n-pentyl bicyclohexane (VPBCH in short)

C(-8°C)Sm B(52°C)N(63°C)I

(III) 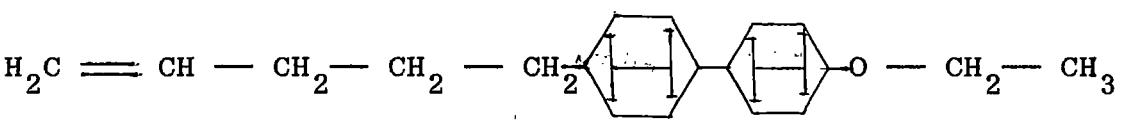

4-ethoxy,4′-Pent-4″-enyl bicyclohexane (EPEBCH in short)

C(11°C)Sm B(43°C)I

The textures of the compounds were observed under a polarising microscope. The observations were performed under crossed polarisers with magnification 150X and samples were taken between a glass slide and a coverslip. Typical marbled textures were observed in the nematic phases of BPBCH and VPBCH. The smectic B phase of BPBCH showed mosaic texture, while VPBCH and EPEBCH showed typical smectic B texture with double refracting lancets and pseudoisotropic regions.

4.2.2 X-ray diffraction study

A detailed description of the experimental set-up for x-ray diffraction has been given by Jha et al [7]. The sample was enclosed in a thin-walled lithium glass capillary of 1mm diameter. The capillary containing the sample was inserted in a thermally insulated brass block, the temperature of which was measured and regulated by a temperature controller (Indotherm model IT401D), within an accuracy of $\pm 0.5^{\circ}C$. X-ray diffraction patterns were recorded photographically on a flat plate camera using Ni filtered Cu K_{α} radiation of wavelength $\lambda=1.5418\text{Å}$. For x-ray diffraction study these compounds could not be aligned even in a magnetic field of about 0.6T. Magnetic susceptibility anisotropy, $\Delta\chi$, for these compounds being almost zero, it is not possible to obtain monodomain samples by application of magnetic field. However, aligned specimens in which the hexagonal symmetry of the smectic B phase extended throughout the bulk samples could be prepared for all these compounds by controlled cooling (0.1deg/min), of the samples kept in 1 mm diameter glass capillaries, from the isotropic state to room temperature ($\sim 20^{\circ}C$). By trial one of the monodomain samples was selected in which the capillary could be rotated in such a manner that the director (or the layer normal) coincided with the direction of the x-ray beam. At this position of the capillary x-ray diffraction photographs were recorded at regular temperature intervals from $\sim 20^{\circ}C$ upto the isotropic state. Due to lack of thermostatic arrangement with cooling facilities in our laboratory, photographs below room temperature could not be taken. Photographs for orientational order parameter measurements were taken after rotating the sample filled capillary 90 degrees with respect to the previous position such that the direction of the x-ray beam was parallel to the smectic

layer. To obtain better accuracy in the measurement of layer spacing, the film was kept at a distance of about 9cm from the samples. This procedure was followed for each compound.

The x-ray photographs were scanned both linearly and circularly by an optical densitometer (VEB Carl Zeiss Jena Model 100). Measured optical densities were converted to x-ray intensities with the help of a calibration curve following the procedure of Klug and Alexander [8] as described in detail in chapter 2.

4.3 Results and Discussions

4.3.1 Bond orientational order

Figures 4.1(a)-4.1(c) shows the x-ray diffraction photographs of the aligned sample in the smectic B phase of BPBCH, VPBCH and EPEBCH at 59°C, 30°C and 20°C respectively, with the incident x-ray beam parallel to the layer normal. The outer diffraction ring is split up into six spots, clearly showing the hexagonal molecular arrangement within the layers of the phase. Almost identical photographs have been obtained from room temperature ($\sim$ 20°C) upto the smectic B to nematic (or isotropic) transition temperature in all the three compounds under study.

The Bond Orientational Order (BOO) can be written as

$$\langle\cos(6\theta)\rangle = \int_0^{\pi/6}\cos(6\theta)f(\theta)d\theta \Big/ \int_0^{\pi/6} f(\theta)d\theta \qquad (4.2)$$

where $f(\theta)$ is the angular distribution function of centre of mass of the neighbouring molecules with respect to a central molecule and the angular distribution function has a maximum at θ = 0. However, the BOO can be approximated by the following

Figure 4.1(a) X-ray diffraction photograph of aligned sample of BPBCH recorded at 59°C (smectic B phase).

Figure 4.1(b) X-ray diffraction photograph of aligned sample of VPBCH recorded at 30°C (smectic B phase).

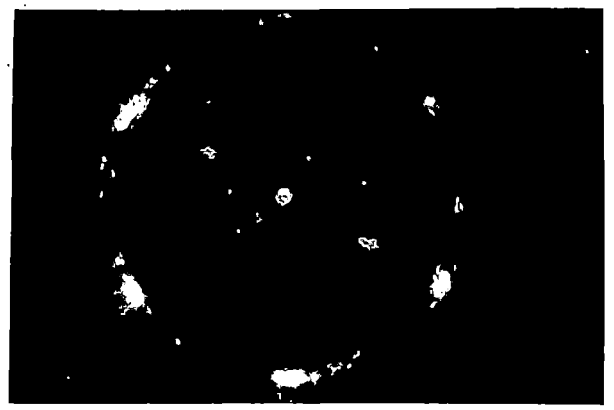

Figure 4.1(c) X-ray diffraction photograph of aligned sample of EPEBCH recorded at 20°C (smectic B phase).

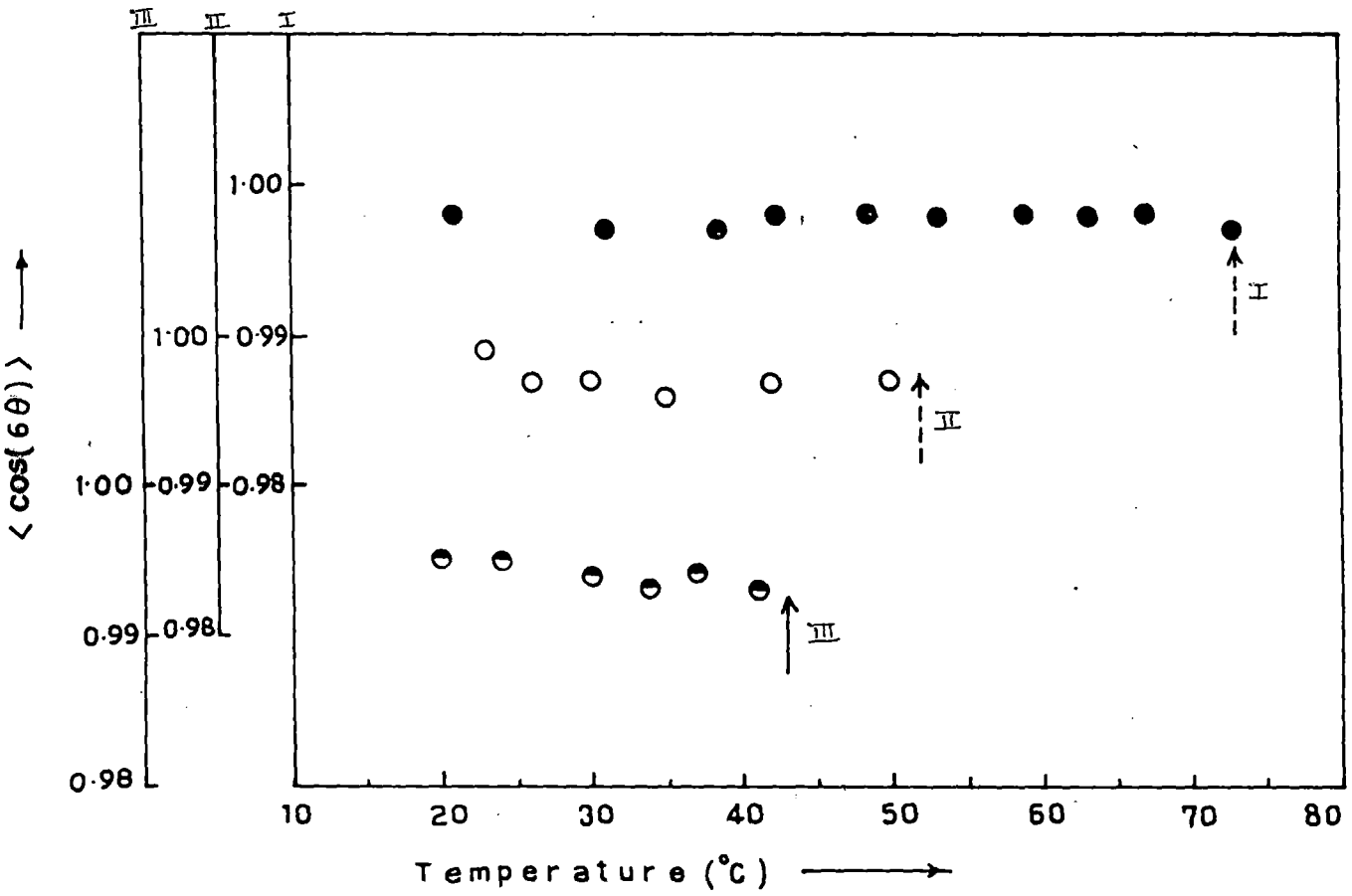

Figure 4.2 Temperature variation of bond orientatational of the three compounds. •, BOO value for BPBCH; o, BOO vaue for VPBCH; ⊖, BOO value for EPEBCH. ↑ indicates smectic B - nematic transition temperature, ↑ indicates smectic B - isotropic transition temperature.

expression, i.e.,

$$\langle\cos(6\theta)\rangle \approx \int_0^{\pi/6}\cos(6\theta)I(\theta)d\theta \Big/ \int_0^{\pi/6}I(\theta)d\theta \qquad (4.3)$$

where $I(\theta)$ is the azimuthal distribution of the x-ray diffraction intensity. Following Vainshtein [9] it has been assumed that $I(\theta)$, the intensity distribution, is proportional to $f(\theta)$ the distribution function and consequently has its maximum at $\theta = 0$ also. The experimental x-ray intensity profile for each peak has been corrected for broadening due to the width of the primary x-ray beam, using a method of deconvolution based on substitution of successive foldings [10], as described in chapter 2.

Table 4.1 shows the bond orientational order values at different temperatures in the smectic B phase of BPBCH, VPBCH and EPEBCH. The BOO's for all the three compounds are found to be almost equal to unity and independent of temperature throughout the smectic B phase (Figures 4.2(a)-4.2(c)). This result seems to indicate that the smectic B modification in these compounds are in fact of the Crystal B type in the sense that the molecular positions exhibit long range bond orientational order throughout the phase [3].

I have tried to determine the correlation length in the smectic layer plane from linear scan of the diffraction peaks. X-ray intensities were at first corrected for the use of a flat film. This corrected intensity data was then deconvoluted for finite width of the collimator. The deconvoluted intensity profile I(q) was fitted to a lorentzian form with a quadratic background, viz.

$$I(q)= \frac{a_1}{a_2+(q - q_o)^2} + a_3q^2 + a_4q + a_5, \qquad (4.4)$$

q being the magnitude of the scattering vector. The correlation length is defined as $\xi = 2\pi(a_2)^{-1/2}$. The values of the correlation lengths obtained in this way varied from 200Å to 270Å for the three compounds. However, for Crystal B phase the correlation lengths are expected to be much longer. One reason for this discrepancy may be due to the use of Ni filtered Cu K_α radiation, which contains a white background in addition to the Cu K_α peak. No correction for this white radiation, which broadens the diffraction peaks considerably, is made here. Hence, the experimental values of correlation lengths as obtained above are much shorter than the theoretically expected values.

4.3.2 Orientational order parameter and molecular parameters

The angular distribution of the x-ray diffraction intensities were utilised to obtain the orientational distribution function $f(\theta)$ [11] and hence the orientational order parameters (OOP) $\langle P_2 \rangle$ and $\langle P_4 \rangle$ following a procedure reported earlier [12]. The mean intensity values of the four quadrants are given in tables 4.2-4.4 for the three compounds. Tables 4.5-4.7 include the normalised distribution function $f(\beta)$ values for different temperatures at 5° intervals, calculated from the equation 2.15 described in chapter 2. The procedure for calculating $\langle P_2 \rangle$ and $\langle P_4 \rangle$ values has also been described in chapter 2. The values of $\langle P_2 \rangle$ and $\langle P_4 \rangle$ at different temperatures for the three compounds are arranged in tables 4.8-4.10. Figures 4.3(a)-4.3(c) show the variation of the experimentally determined OOP's with temperature for all the samples studied. The experimental $\langle P_2 \rangle$

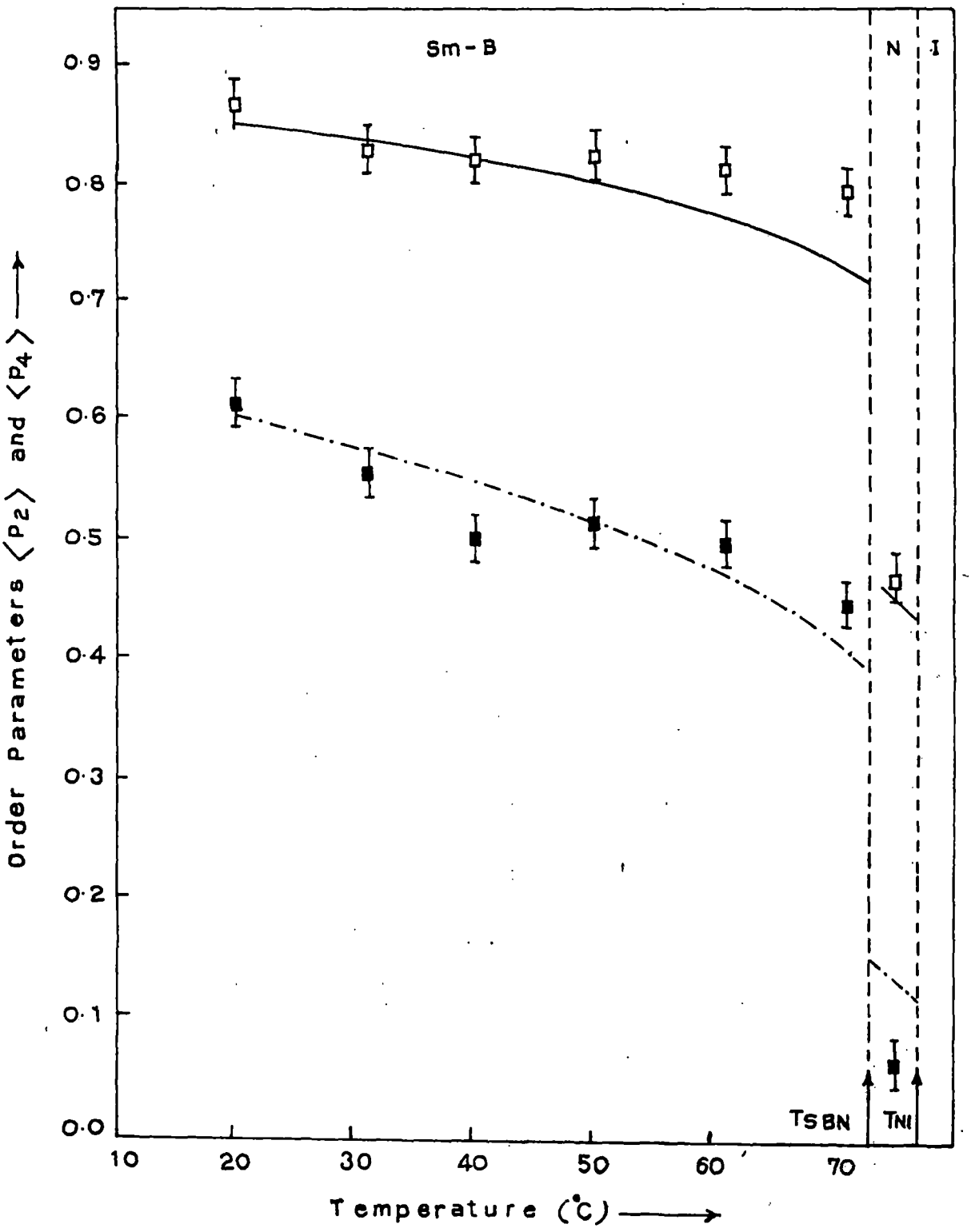

Figure 4.3(a) Temperature variation of $\langle P_2 \rangle$ and $\langle P_4 \rangle$ for BPBCH. □, $\langle P_2 \rangle$ from x-ray data; ■, $\langle P_4 \rangle$ from x-ray data; full line McMillan $\langle P_2 \rangle$ value; dashed line McMillan $\langle P_4 \rangle$ value; $\alpha=0.96$ and $\delta=0$, values of McMillan potential parameters. T_{SBN}= smectic B-nematic tansition temperature T_{NI}=nematic-isotropic transition temperature. Vertical bars show estimated errors.

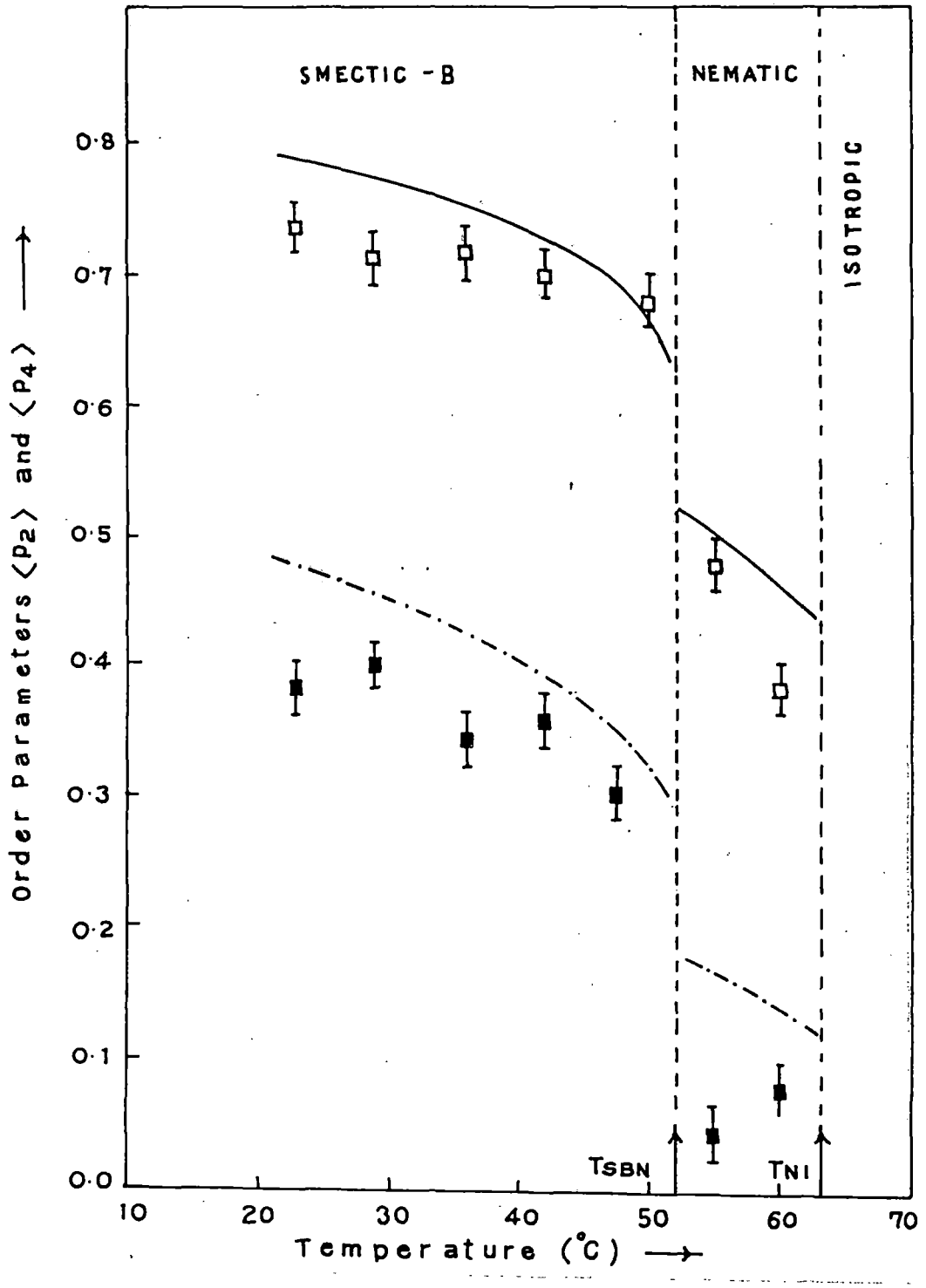

Figure 4.3(b) Temperature variation of $\langle P_2 \rangle$ and $\langle P_4 \rangle$ for VPBCH. □, $\langle P_2 \rangle$ from x-ray data; ■, $\langle P_4 \rangle$ from x-ray data; full line McMillan $\langle P_2 \rangle$ value; dashed line McMillan $\langle P_4 \rangle$ value; α=0.65 and δ=0.245, values of McMillan potential parameters. $T_{SB\ N}$= smecticB - nematic tansition temperature $T_{N\ I}$= nemati c-isotropic transition temperature. Vertical bars show estimated errors.

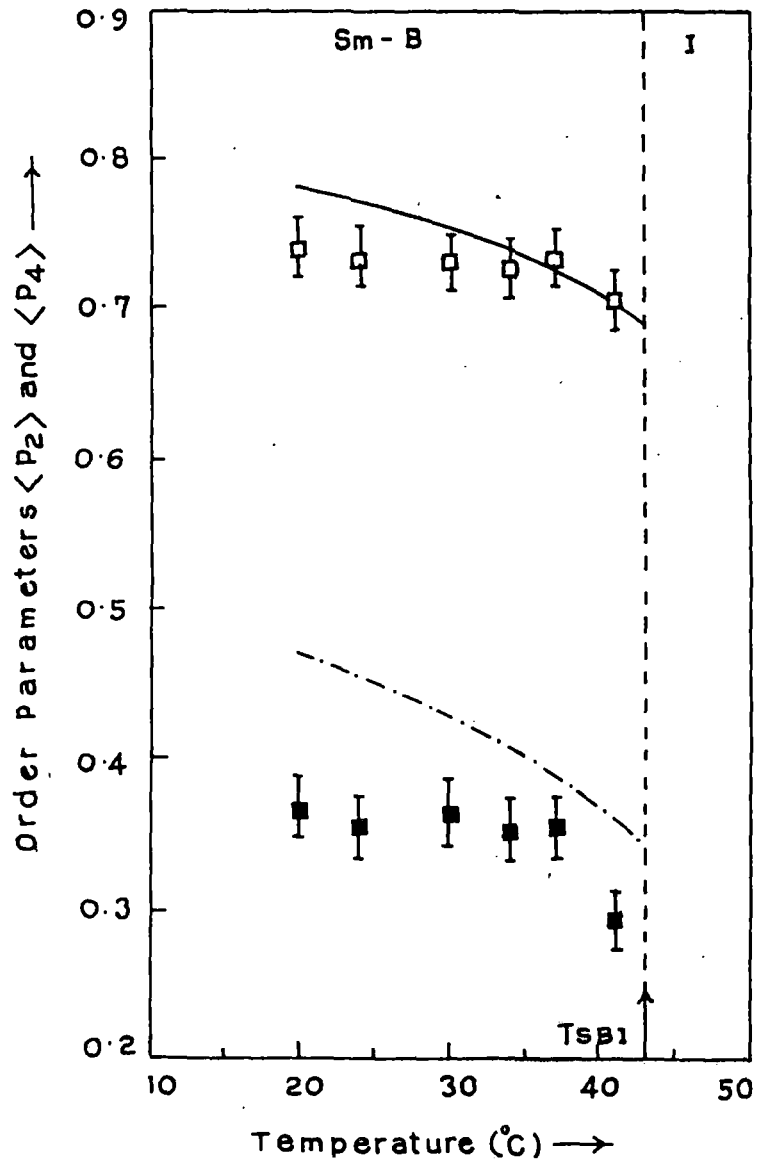

Figure 4.3(c) Temperature variation of $\langle P_2 \rangle$ and $\langle P_4 \rangle$ for EBEBCH. □, $\langle P_2 \rangle$ from x-ray data; ■, $\langle P_4 \rangle$ from x-ray data; full line McMillan $\langle P_2 \rangle$ value; dashed line McMillan $\langle P_4 \rangle$ value; α=0.714 and δ=0.251, values of McMillan potential parameters. T_{SBI}= smectic B-isotropic transition temperature. Vertical bars show estimated errors.

and $\langle P_4 \rangle$ values are found to vary very little with temperature within the smectic B phase. OOP values in the nematic phase of BPBCH and VPBCH however show marked temperature dependence. These values are also relatively high in the smectic B phase, showing the phase to be much more orientationally ordered than the neighbouring nematic phase. The smectic B to nematic phase transitions in BPBCH and VPBCH are clearly of the first order as can be seen from the abrupt jump in the order parameter values of these two compounds near the transition temperature. This again indicates that the smectic B phases of these compounds are the crystal B phases, unlike the hexatic B phase which undergoes a second order phase transition [13]. It may be mentioned that although the approximation used for calculating $\langle P_L \rangle$ (L= 2,4) is not valid for $\langle P_2 \rangle \gtrsim 0.8$ [11] (as in the case of BPBCH) I am still reporting these OOP values since at least qualitatively they show the degree of order of a liquid crystal in smectic B phase for which such values are rare.

I tried to fit the experimental order parameter values for these compounds to those calculated from McMillan's theory [5,6] for smectic A phase, using the potential parameters δ and α as adjustable constants, for the lack of other alternatives. The best fit theoretical curves are given in the respective figures (Figures 4.3(a)-4.3(c)) and the values of δ and α used for the calculations are given in the corresponding figure captions. The agreement seems to be fairly good for BPBCH and fair for other two compounds even though this theory is not strictly applicable to the smectic B phase.

I have also determined the translational order parameter τ for VPBCH (where second order reflections are present) from the experimental data using a simple procedure described by Leadbetter and Norris [11]. According to McMillan [6], the smectic layer distribution functions are directly related to the

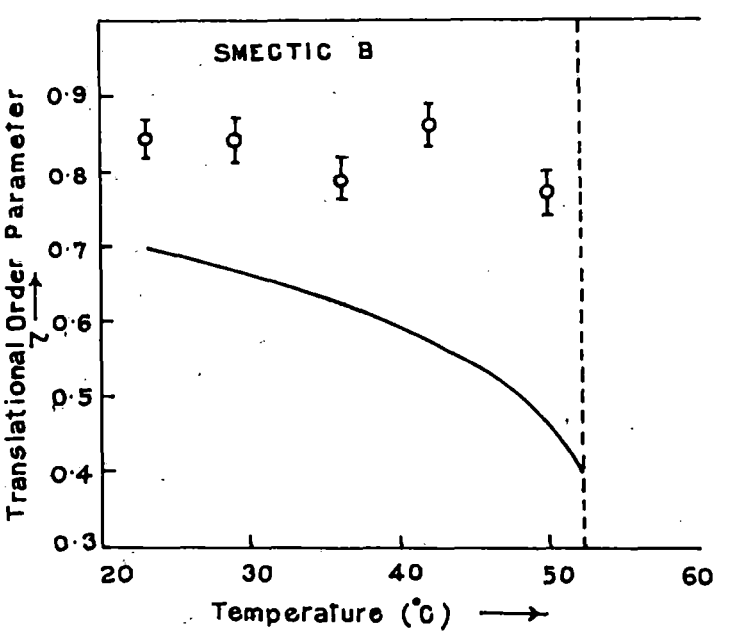

Figure 4.4 The translational order parameter τ for the smectic phase of VPBCH. o, Experimental; ———, theoretical values. Vertical bars show estimated errors.

intensity of the layer reflection. Hence the intensity of (00m) layer reflection can be expressed as

$$I(00m) = C\tau_m^2 \langle F(00m) \rangle^2 \qquad (4.5)$$

where C is a constant and F(00m) is the structure factor for a smectic layer and τ_1 is the translational order parameter. For gaussian distribution of the translational distribution function Leadbetter et al [14] derived the following relation

$$\tau_m = \tau_1^{m^2} \qquad (4.6)$$

I have measured I(002)and I(001) for VPBCH at different temperatures in the smectic B phase. The intensity values are corrected for use of flat plate camera and then assuming F(001)

$$\approx \frac{I(002)}{I(001)} = \tau_2^2 / \tau_1^2 = \tau_1^6 \qquad (4.7)$$

Using equation (4.7), the translational order parameters τ (= τ_1) have been calculated and these are compared with the values obtained from McMillan's theory as shown in figure 4.4. These τ values are much larger than those calculated from McMillan's theory. This deviation may be partly due to the assumption of gaussian distribution of molecules normal to the smectic layer in calculating τ [15]. and partly due to the fact that McMillan's theory is not applicable to smectic B phase. However it is gratifying to note that the experimental τ values are significantly larger than those calculated for smectic A phase, which is in accord with the fact that smectic B phase is more ordered phase than smectic A phase. Table 4.11 include the values of τ_1 at different temperatures in the smectic B phase of VPBCH.

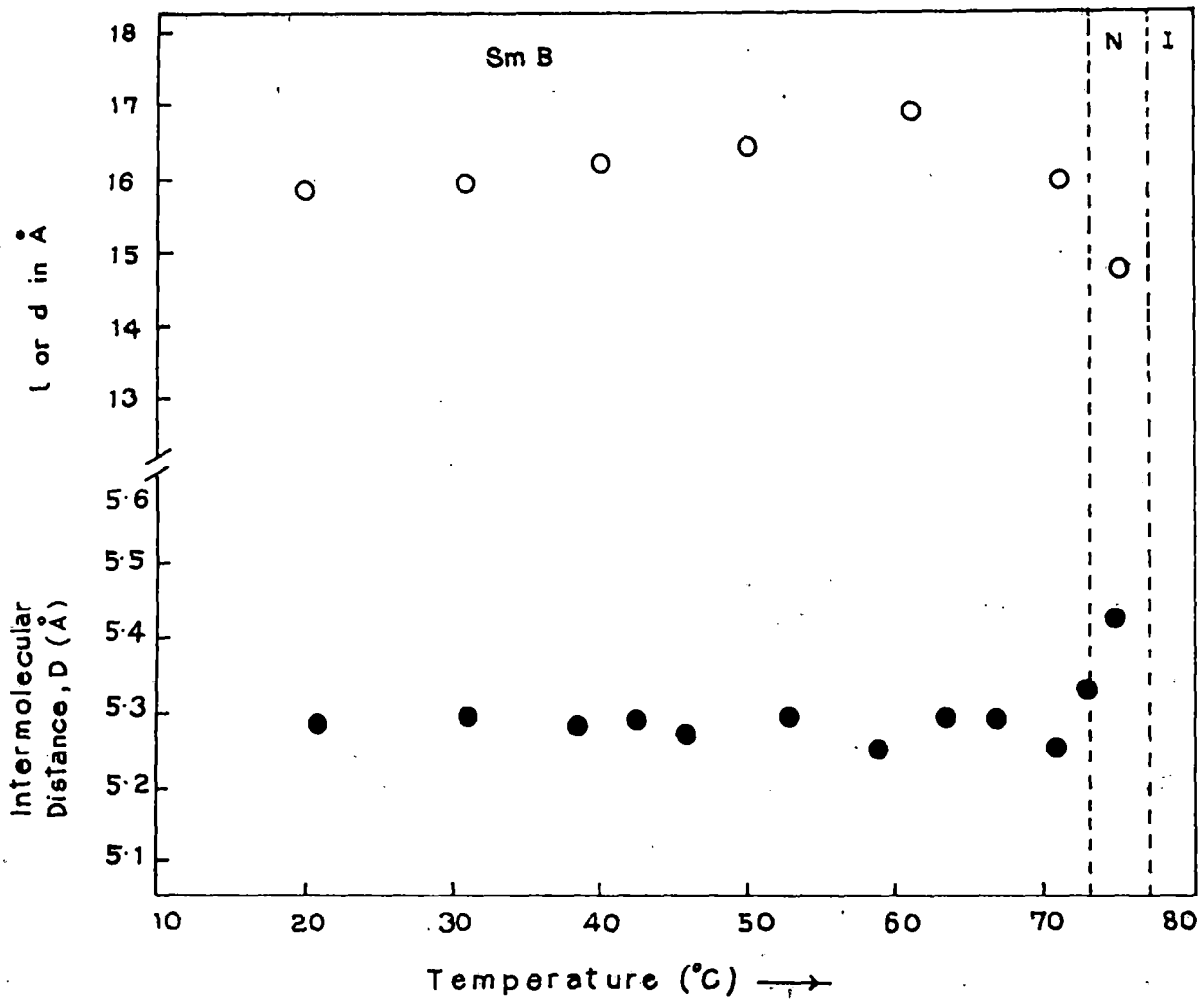

Figure 4.5(a) Variation of layer thickness,d, or apparent molecular length, l, and intermolecular distance, D with temperature for BPBCH. o, d or l value; ●, D value. Estimated errors are smaller than the size of the symbols used.

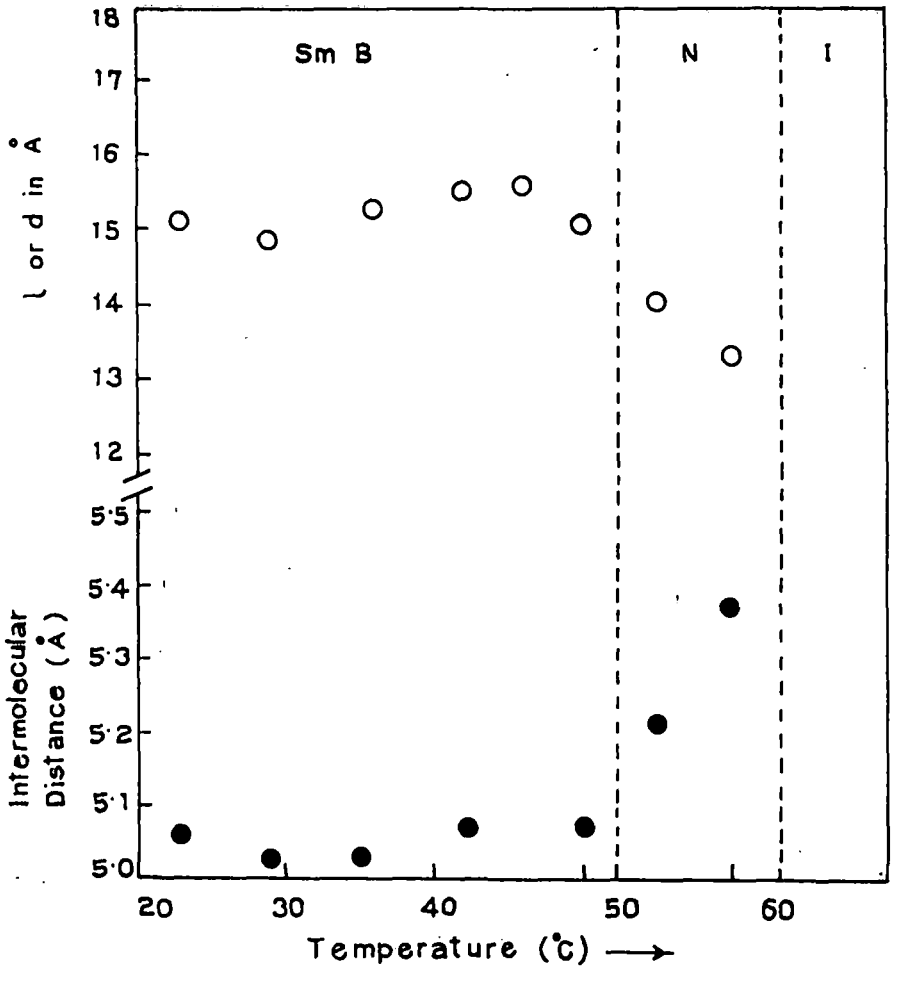

Figure 4.5(b) Variation of layer thickness,d, or apparent molecular length, l, and intermolecular distance, D with temperature for VPBCH. o, d or l value; ●, D value. Estimated errors are smaller than the size of the symbols used.

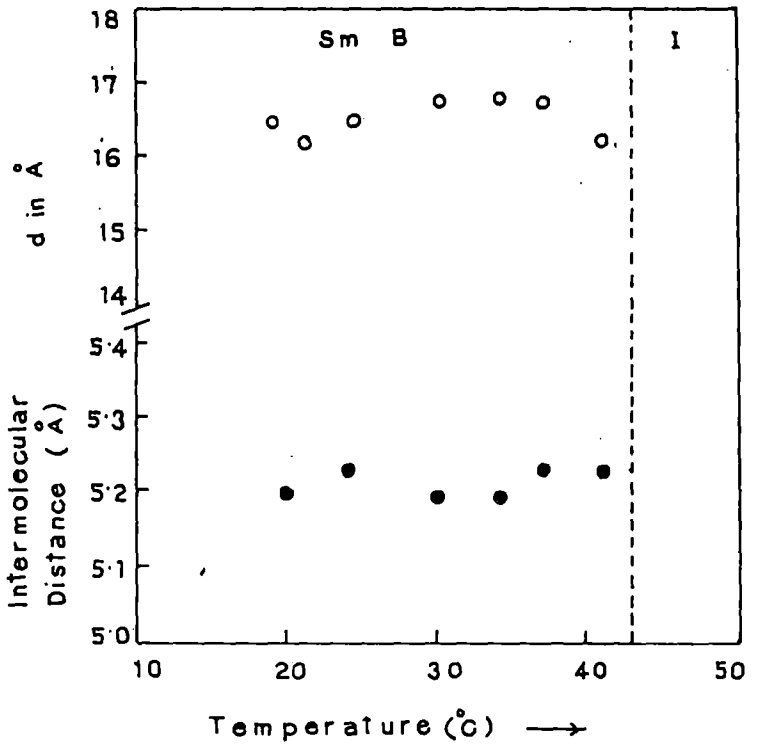

Figure 4.5(c) Variation of layer thickness, d, and intermolecular distance, D with temperature for EPEBCH. o: d value; ●: D value. Estimated errors are smaller than the size of the symbols used.

The values of the apparent molecular length (l) or layer thickness (d) and the intermolecular distance, D, at different temperatures for BPBCH, VPBCH and EPEBCH are given in tables 4.12 and 4.13 respectively. The temperature variations of d in the smectic phase and l in the nematic phase (where it is present) for the three compounds are shown in Figures 4.5(a)-4.5(c). Also shown on the same figures are the temperature dependences of the intermolecular distance, D, for these compounds. As expected the temperature variations of d and l are slight. However, for all the compounds, the layer thickness at first increases with increasing temperature but then decreases just before smectic to nematic (or isotropic) phase transition. This decrease before the phase transition is not difficult to understand, since the effective lengths of the molecules decrease due to increasing thermal vibrations of its chain part just before the transition. The low temperature variation in the layer thickness may be due to the geometry of packing in the smectic layer at these temperatures. In all the compounds the layer thicknesses are almost equal to the respective model molecular lengths (15.6 Å for BPBCH 15.25 Å for VPBCH and 16.5 Å for EPEBCH molecule) The apparent molecular lengths in nematic phase of BPBCH and VPBCH are significantly smaller than the layer thicknesses in the corresponding smectic B phases. This is not surprising considering the flexible nature of the molecules. The lateral distances of the molecules, D, in the nematic phase are significantly larger than the values observed in the case of nematics with rigid core ($\lesssim$ 5Å). Also, the temperature variations of D in the nematic phase are quite rapid, caused once again by the thermal vibrations of these flexible molecules.

Table 4.1

Bond orientational order ($\langle\cos(6\theta)\rangle$) values at different temperatures in the the smectic B phase of BPBCH, VPBCH and EPEBCH.

BPBCH		VPBCH		EPEBCH	
Temp/^{o}C	$\langle\cos(6\theta)\rangle$	Temp/^{o}C	$\langle\cos(6\theta)\rangle$	Temp/^{o}C	$\langle\cos(6\theta)\rangle$
21.0	0.998	23.0	0.999	20.0	0.995
31.0	0.997	26.0	0.997	24.0	0.995
38.5	0.997	30.0	0.997	30.0	0.994
42.5	0.998	35.0	0.996	34.0	0.993
48.5	0.998	42.0	0.997	37.0	0.994
53.0	0.998	50.0	0.997	41.0	0.993
59.0	0.998				
63.5	0.998				
67.0	0.998				
73.0	0.997				

Table 4.2

Experimental intensity values I(ψ), in arbitrary units, of BPBCH after background correction.

ψ (degree)	I(ψ) values at different temperatures in ^{o}C						
	20.0	31.0	40.0	50.0	61.0	71.0	75.0
0	9.3	11.5	11.4	9.5	7.3	6.2	9.3
5	8.7	11.2	11.3	9.1	7.1	6.0	9.1
10	7.4	10.4	10.5	8.4	6.3	5.4	8.7
15	5.7	8.9	8.8	6.8	4.9	4.5	8.1
20	3.9	6.1	6.1	4.7	3.3	3.4	7.5
25	1.9	3.0	3.8	2.6	1.7	2.4	6.7
30	0.0	1.4	1.8	1.2	1.2	1.5	5.8
35	0.0	0.5	0.6	0.6	0.7	0.6	5.0
40	0.0	0.0	0.1	0.2	0.4	0.2	4.1
45	0.0	0.0	0.0	0.0	0.0	0.0	3.5
50	0.0	0.0	0.0	0.0	0.0	0.0	2.8
55	0.0	0.0	0.0	0.0	0.0	0.0	2.0
60	0.0	0.0	0.0	0.0	0.0	0.0	1.5
65	0.0	0.0	0.0	0.0	0.0	0.0	1.0
70	0.0	0.0	0.0	0.0	0.0	0.0	0.7
75	0.0	0.0	0.0	0.0	0.0	0.0	0.4
80	0.0	0.0	0.0	0.0	0.0	0.0	0.2
85	0.0	0.0	0.0	0.0	0.0	0.0	0.2
90	0.0	0.0	0.0	0.0	0.0	0.0	0.0

Table 4.3

Experimental intensity values I(ψ), in arbitrary units, of VPBCH after background correction.

ψ (degree)	I(ψ) values at different temperatures in ^{o}C						
	23.0	29.0	36.0	42.0	50.0	55.0	60.0
0	15.1	16.9	10.0	17.6	10.3	1.4	1.2
5	15.1	16.9	9.3	17.3	10.1	1.5	1.2
10	14.0	16.2	7.9	16.7	9.4	1.5	1.1
15	10.7	14.4	5.9	14.8	8.0	1.3	1.0
20	8.0	8.6	4.5	11.6	6.3	1.2	0.9
25	5.4	5.2	3.0	7.2	4.5	1.0	0.8
30	3.7	3.3	1.8	4.4	3.2	0.9	0.7
35	2.5	2.3	1.2	2.9	2.3	0.8	0.6
40	1.5	1.7	0.8	1.8	1.7	0.7	0.5
45	0.9	1.2	0.5	1.3	1.2	0.6	0.5
50	0.7	1.0	0.4	1.0	0.8	0.5	0.4
55	0.5	0.8	0.2	0.8	0.5	0.4	0.4
60	0.3	0.6	0.1	0.6	0.3	0.3	0.3
65	0.1	0.5	0.0	0.5	0.2	0.1	0.3
70	0.0	0.4	0.0	0.4	0.1	0.0	0.2
75	0.0	0.3	0.0	0.3	0.0	0.0	0.2
80	0.0	0.2	0.0	0.2	0.0	0.0	0.2
85	0.0	0.1	0.0	0.2	0.0	0.0	0.1
90	0.0	0.0	0.0	0.1	0.0	0.0	0.1

Table 4.4

Experimental intensity values $I(\psi)$, in arbitrary units, of EPEBCH after background correction.

ψ (degree)	$I(\psi)$ values at different temperatures in ^{o}C					
	20.0	24.0	30.0	34.0	37.0	41.0
0	14.3	8.6	7.8	8.4	7.4	6.4
5	14.3	8.4	7.7	8.1	7.3	6.3
10	13.4	7.8	7.0	7.7	6.8	5.8
15	10.8	6.7	5.8	6.8	5.8	5.0
20	7.8	5.2	4.6	5.4	4.5	4.1
25	5.7	3.5	2.9	3.6	3.3	3.2
30	3.7	2.3	2.0	2.2	2.1	2.4
35	2.5	1.6	1.3	1.4	1.3	1.6
40	1.7	1.0	0.9	0.9	0.8	1.0
45	1.1	0.6	0.6	0.6	0.5	0.6
50	0.6	0.3	0.4	0.4	0.3	0.3
55	0.2	0.2	0.2	0.2	0.2	0.0
60	0.0	0.1	0.1	0.2	0.1	0.0
65	0.0	0.0	0.1	0.1	0.0	0.0
70	0.0	0.0	0.0	0.1	0.0	0.0
75	0.0	0.0	0.0	0.0	0.0	0.0
80	0.0	0.0	0.0	0.0	0.0	0.0
85	0.0	0.0	0.0	0.0	0.0	0.0
90	0.0	0.0	0.0	0.0	0.0	0.0

Table 4.5

Normalised distribution function $f(\beta)$ values of BPBCH at different temperatures.

β (degree)	$f(\beta)$ values at different temperatures in ^{o}C						
	20.0	31.0	40.0	50.0	61.0	71.0	75.0
0	15.62	11.11	11.51	12.02	13.66	10.87	4.08
5	15.11	11.15	11.24	11.82	13.10	10.53	4.01
10	13.52	10.93	10.33	11.08	11.50	9.56	3.82
15	10.86	9.83	8.64	9.50	9.10	8.11	3.54
20	7.46	7.59	6.30	7.10	6.36	6.37	3.19
25	4.07	4.70	3.80	4.39	3.84	4.56	2.82
30	1.47	2.11	1.75	2.10	1.98	2.86	2.42
35	0.07	0.51	0.52	0.69	0.92	1.47	2.04
40	-0.29	-0.05	0.06	0.15	0.46	0.53	1.67
45	-0.13	-0.01	0.02	0.09	0.28	0.05	1.35
50	0.06	0.01	0.05	0.11	0.15	-0.08	1.06
55	0.09	0.07	0.02	0.05	0.01	-0.03	0.81
60	0.02	-0.03	-0.03	-0.03	-0.08	0.03	0.59
65	-0.04	-0.07	-0.04	-0.06	-0.07	0.04	0.40
70	-0.03	-0.03	0.00	-0.02	-0.01	0.01	0.24
75	0.00	0.03	0.03	0.03	0.04	-0.02	0.13
80	0.02	0.03	0.03	0.03	0.03	-0.02	0.06
85	0.00	0.00	0.00	0.00	0.00	0.00	0.03
90	0.00	-0.02	-0.02	-0.02	-0.02	0.01	0.02

Table 4.6

Normalised distribution function $f(\beta)$ values of VPBCH at different temperatures.

β (degree)	$f(\beta)$ values at different temperatures in ^{o}C						
	20.0	29.0	36.0	42.0	50.0	55.0	60.0
0	10.74	9.03	8.91	7.33	8.27	3.77	4.21
5	10.36	9.14	8.73	7.51	8.13	3.83	4.11
10	9.28	9.12	8.13	7.76	7.64	3.91	3.84
15	7.62	8.29	7.08	7.45	6.69	3.81	3.42
20	5.66	6.39	5.64	6.22	5.31	3.39	2.93
25	3.77	3.93	4.04	4.33	3.77	2.76	2.43
30	2.30	1.81	2.60	2.44	2.42	2.15	1.99
35	1.29	0.65	1.53	1.15	1.50	1.74	1.63
40	0.77	0.40	0.88	0.56	0.99	1.57	1.35
45	0.52	0.51	0.53	0.42	0.73	1.50	1.14
50	0.36	0.52	0.35	0.37	0.54	1.36	0.97
55	0.23	0.33	0.23	0.27	0.34	1.09	0.82
60	0.11	0.11	0.13	0.15	0.18	0.72	0.69
65	0.04	0.03	0.05	0.08	0.08	0.37	0.57
70	0.02	0.09	0.02	0.08	0.04	0.12	0.46
75	0.01	0.14	0.00	0.09	0.03	0.00	0.36
80	0.01	0.11	0.00	0.07	0.02	0.00	0.27
85	0.00	0.02	0.00	0.03	0.00	0.00	0.21
90	0.00	0.00	0.00	0.01	0.00	0.00	0.19

Table 4.7

Normalised distribution function $f(\beta)$ values of EPEBCH at different temperatures.

β (degree)	$f(\beta)$ values at different temperatures in ^{o}C					
	20.0	24.0	30.0	34.0	37.0	41.0
0	9.82	9.06	9.56	7.91	8.65	8.25
5	9.59	8.91	9.36	7.96	8.55	8.00
10	8.86	8.39	8.69	7.90	8.16	7.31
15	7.54	7.34	7.47	7.35	7.29	6.29
20	5.76	5.80	5.79	6.09	5.90	5.12
25	3.89	4.06	3.96	4.35	4.23	3.96
30	2.35	2.54	2.40	2.64	2.66	2.91
35	1.38	1.48	1.36	1.39	1.50	2.02
40	0.89	0.90	0.81	0.73	0.83	1.31
45	0.64	0.59	0.56	0.46	0.50	0.76
50	0.42	0.37	0.39	0.33	0.32	0.37
55	0.18	0.17	0.23	0.21	0.19	0.13
60	0.01	0.03	0.08	0.10	0.08	0.01
65	-0.05	-0.03	0.01	0.03	0.01	-0.02
70	-0.02	-0.01	0.00	0.02	-0.01	-0.01
75	0.02	0.02	0.01	0.02	0.00	0.01
80	0.02	0.02	0.01	0.02	0.00	0.01
85	0.00	0.00	0.00	0.00	0.00	0.00
90	0.00	0.00	0.00	0.00	0.00	0.00

Table 4.8

Sample : BPBCH

Variation of $\langle P_2 \rangle$ and $\langle P_4 \rangle$ with temperature.

Temp. in ^{o}C	$\langle P_2 \rangle$	$\langle P_4 \rangle$
20.0	0.868	0.612
31.0	0.833	0.529
40.0	0.820	0.500
50.0	0.824	0.514
61.0	0.812	0.497
71.0	0.796	0.446
75.0	0.469	0.061

Table 4.9

Sample : VPBCH

Variation of $\langle P_2 \rangle$ and $\langle P_4 \rangle$ with temperature.

Temp. in ^{o}C	$\langle P_2 \rangle$	$\langle P_4 \rangle$
23.0	0.734	0.380
29.0	0.712	0.399
36.0	0.717	0.342
42.0	0.699	0.356
50.0	0.680	0.301
55.0	0.477	0.045
60.0	0.381	0.081

Table 4.10

Sample : EBEBCH

Variation of $\langle P_2 \rangle$ and $\langle P_4 \rangle$ with temperature.

Temp. in ^{o}C	$\langle P_2 \rangle$	$\langle P_4 \rangle$
20.0	0.738	0.367
24.0	0.733	0.356
30.0	0.730	0.364
34.0	0.725	0.354
37.0	0.733	0.355
41.0	0.705	0.294

Table 4.11

Translational order parameter (τ_1) at different temperatures in the smectic B phase of VPBCH.

Temp. in ^{o}C	τ_1
23.0	0.841
29.0	0.840
36.0	0.790
42.0	0.860
50.0	0.767

Table 4.12

Apparent molecular length (l) or layer spacing (d) at different temperatures of BPBCH, VPBCH AND EPEBCH.

BPBCH		VPBCH		EPEBCH	
Temp. in ^{o}C	l or d in $\mathring{A}$	Temp. in ^{o}C	l or d in $\mathring{A}$	Temp. in ^{o}C	l or d in $\mathring{A}$
20.0	15.88	23.0	15.14	19.0	16.48
31.0	15.99	29.0	14.93	21.0	16.19
40.0	16.21	36.0	15.37	24.0	16.48
50.0	16.44	42.0	15.64	30.0	16.75
61.0	16.92	46.0	15.72	34.0	16.75
71.0	15.99	50.0	15.14	37.0	16.61
75.0	14.77	55.0	14.14	41.0	16.22
		60.0	13.44		

Table 4.13

Intermolecular distance (D) at different temperatures of BPBCH, VPBCH AND EPEBCH.

BPBCH		VPBCH		EPEBCH	
Temp. in ^{o}C	D in $\mathring{A}$	Temp. in ^{o}C	D in $\mathring{A}$	Temp. in ^{o}C	D in $\mathring{A}$
21.0	5.29	23.0	5.06	20.0	5.19
31.0	5.30	29.0	5.03	24.0	5.22
38.5	5.29	35.0	5.03	30.0	5.19
42.5	5.30	42.0	5.07	34.0	5.19
48.5	5.28	50.0	5.07	37.0	5.22
53.0	5.30	55.0	5.22	41.0	5.22
59.0	5.26	60.0	5.38		
63.5	5.30				
67.0	5.30				
71.0	5.26				
73.0	5.34				
75.0	5.44				

REFERENCES

[1]. M. Schadt, R. Buchecker and K. Müller, Liq. Cryst.,5, 293 (1989).

[2]. R.J. Birgeneau and J.D. Litster, J.Phys. Letts. 39, L399, (1978).

[3]. C.C. Huang (1992), K.J. Strandburg (Ed.)Bond Orientational Order in Condensed Matter Systems, Springer - Verlag, Berlin - New York, pp. 78-136

[4]. M. Cheng, J.H. Ho, S.W. Hui and R. Pindak, Phys. Rev. Letts. 59, 1112, (1987).

[5]. W.L. McMillan, Phys. Rev., 13, 137, (1971).

[6]. W.L. McMillan, Phys. Rev., A6, 936, (1972).

[7]. B. Jha and R. Paul, Proc. Nucl. Phys. Solid State Phys.Symp., (India), 19C, 491, (1976).

[8]. H.P. Klug and L.E. Alexander,X-ray diffraction procedure for Polycrystalline and Amorphous Materials, John Wiley and Sons, New York, pp. 114-116 and pp. 473-474, (1974).

[9]. B.K. Vainshtein, X-ray diffraction by chain molecules, Elsevier Publishing Co., London, pp. 353-355 (1966).

[10]. S. Ergun, J. Appl. Cryst., 1, 19 (1968).

[11]. A.J. Leadbetter, and E.K. Norris, Mol. Phys., 38, 669, (1979).

[12]. B Bhattacharjee, S. Paul and R. Paul,Mol. Phys.,44, 1391, (1981).

[13]. R. Pindak, D.E. Moncton, S.C. Davey and J.W. Goodby, Phys. Rev. Lett., 46, 1135 (1981).

[14]. A.J. Leadbetter, R.M. Richardson, and C.N. Colling, J. Phys. (Paris), 36, C1-37 (1975).

[15]. A.J. Leadbetter and P.G. Wrighton,J. Phys. (Paris), 40, C3-234, (1979).

CHAPTER - 5

PHYSICAL PROPERTIES OF THREE BICYCLOHEXANE COMPOUNDS POSSESSING SMECTIC B PHASE II : REFRACTIVE INDEX AND DENSITY MEASUREMENTS

5.1 Introduction

In chapter 4, I have reported some physical properties of three non-polar alkenyl/alkenyloxy bicyclohexane compounds from x-ray diffraction measurements [1]. In this chapter the results of refractive index and density measurements on the same compounds, throughout their mesomorphic range is presented. The optical birefringence of liquid crystals is the visible result of their long range order and is defined only for a uniformly ordered domain. The refractive index data have been analysed to determine the molecular polarizabilities using different internal field models [2-3]. The orientational order parameter $\langle P_2 \rangle$ values at different temperatures for each compound have been calculated from these polarizability data. These order parameter values have been compared with those previously obtained by me for these mesogens from x-ray diffraction studies [1] as given in chapter 4. The temperature dependences of $\langle P_2 \rangle$ and ρ and the nature of the smectic B to nematic phase transition in these compounds have also been discussed.

5.2 Experimental

The compounds were donated to us by M/S Hoffmann-La-Roche and Co., Basel, Switzerland, and were used without further purification, since the transition temperatures of the chemicals as seen under the polarising microscope agreed with the supplied values (Hoffmann-la-Roche Catalogue). The phase transitions of these compounds as observed from texture studies have been reported earlier [1] in chapter 4.

5.2.1 Density measurements

The densities of all the three compounds were measured with the help of a dilatometer of capillary type. Temperature during the experiment was controlled to about $\pm 0.5^{\circ}C$ by a temperature controller. Experimental uncertainty of density measurements is 0.1%.

5.2.2 Refractive index measurements

Refractive indices (n_o,n_e) for three wave lengths of mercury vapour lamp were measured within ± 0.001 by thin prism method (refracting angle $< 2^{\circ}$). The prisms were made of optically flat glass plates, the inside surfaces of which were coated with thin layer of polyvinyl alcohol and then rubbed for aligning the liquid crystalline samples. The experimental details of this procedure have been reported by Zemindar *et al* [4]. Surface alignment technique was used to align the optic axis along the refracting edge of the prism. The diamagnetic anisotropy $\Delta\chi$ for these compounds being almost equal to zero [5], no magnetic field was applied to align the samples. The prism was put inside a brass thermostat heated electrically and controlled by a temperature controller (Indotherm model IT401D) to $\pm 0.5^{\circ}C$ to measure the refractive indices. Due to lack of thermostatic arrangement with cooling facilities in our laboratory measurements below room temperature ($\approx 20^{\circ}C$) was not possible.

5.3 Results and discussions

The refractive index and density values of BPBCH, VPBCH and EPEBCH are given in tables 5.1-5.3 respectively and the refractive indices (n_o, n_e) for the three compounds are plotted

in Figures 5.1(a)-5.1(c). The ordinary (n_o) as well as the extraordinary (n_e) refractive indices are found to be independent of temperature in the smectic B phase, except very near the smectic B to nematic/isotropic transition temperature for all the compounds. The n_o, n_e values are however quite sensitive to temperature in the nematic phase of these compounds (as in the case of BPBCH and VPBCH). The smectic B to nematic phase transitions in these two compounds are also marked by discontinuities in the refractive index values. From density and refractive index data the principal molecular polarizabilities (α_o,α_e) have been calculated for the three compounds using Vuks' isotropic [2] and Neugebauer's anisotropic [3] internal field models and are given in tables 5.4-5.9 for the three compounds.The orientational order parameter $\langle P_2 \rangle$ has been evaluated using the expression [6]

$$\langle P_2 \rangle = (\alpha_e - \alpha_o)/(\alpha_{||} - \alpha_{\perp}) \qquad (5.1)$$

where α_o, α_e are respectively the effective polarizabilities for ordinary and extraordinary rays respectively, and $\alpha_{||}$ and $\alpha_{\perp}$ are the polarizabilities parallel and transverse to the long axis of the molecule. I have adopted the extrapolation procedure of Haller et al [7] to calculate the polarizability anisotropy ($\alpha_{||} - \alpha_{\perp}$) as crystal data are not available.

I have calculated the optical birefringence ($\Delta n = n_e - n_o$) for wavelength λ= 5780 Å for all the three compounds which is listed in table 5.10. It is observed that Δn values for all these compounds are very low and is less than 0.1 even in the smectic B phase. This is not surprising because all the three bicyclohexane compounds have low polarisability anisotropy due to their non linear structure and absence of conjugated π-bond in the molecules. It may be mentioned here that recent efforts

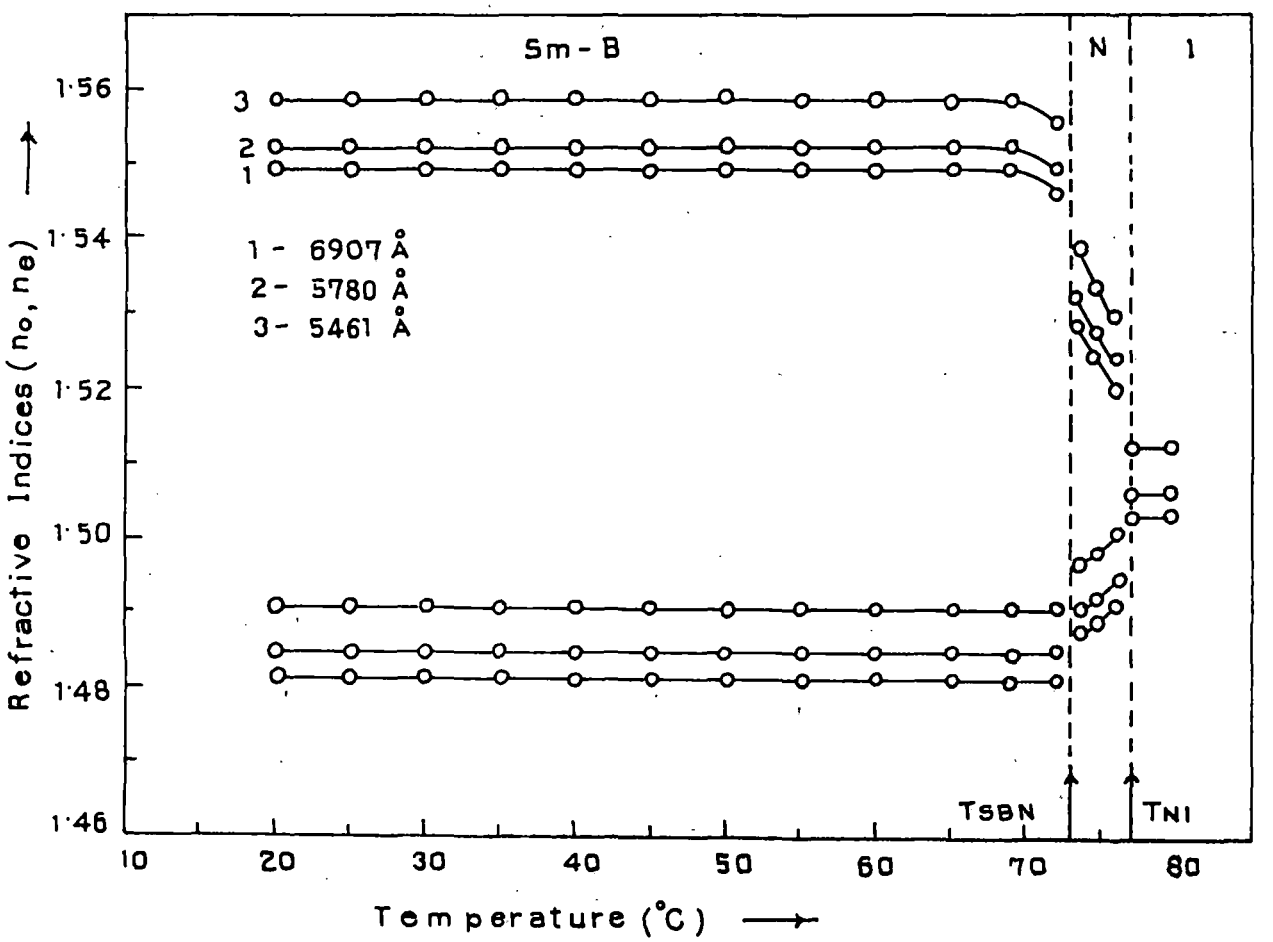

Figure 5.1(a) Variation of refractive indices (n_o,n_e) of BPBCH with temperature. T_{SBN} = smectic B to nematic transition temperature, T_{NI} = nematic to isotropic transition temperature.

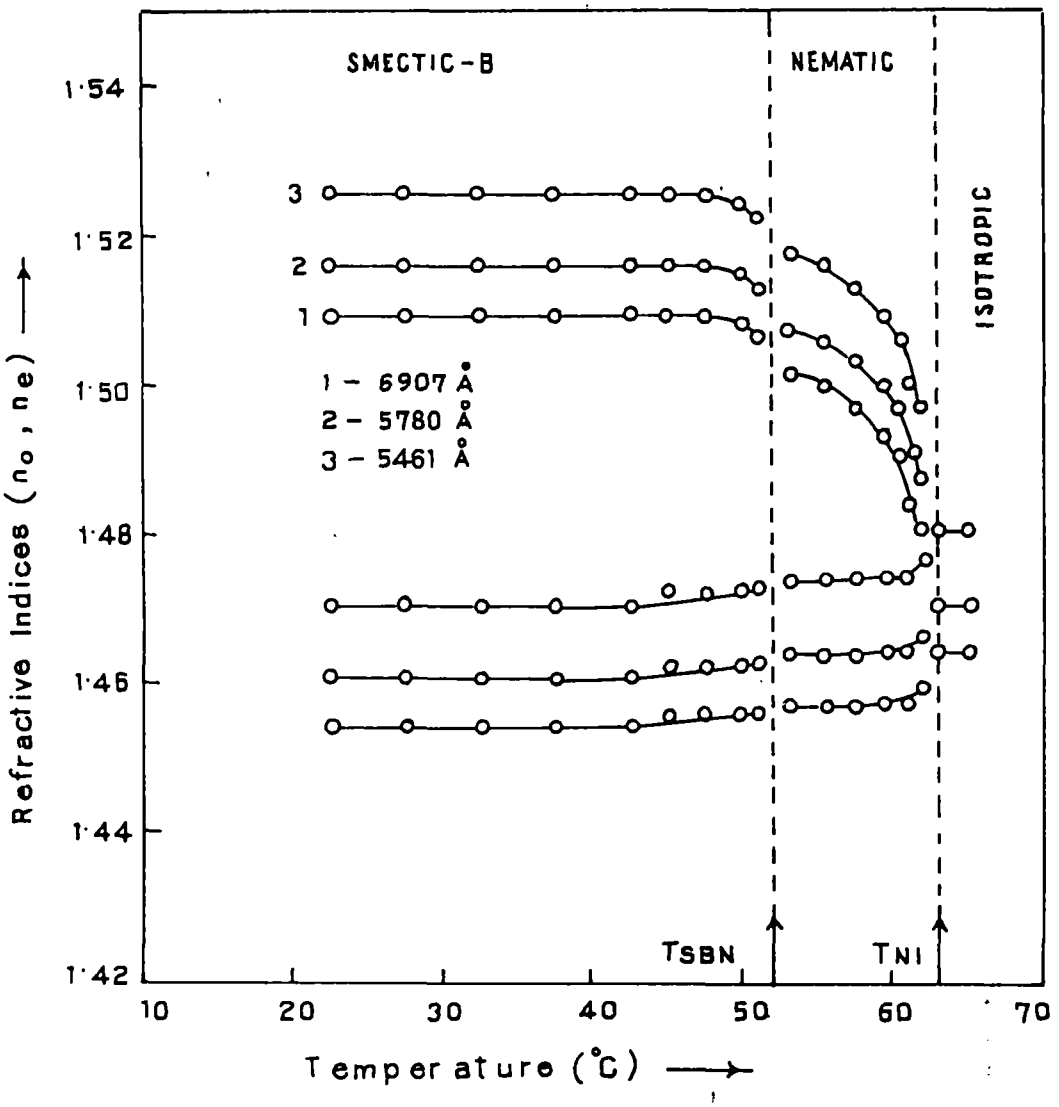

Figure 5.1(b) Variation of refractive indices (n_o,n_e) of VPBCH with temperature. T_{SBN} = smectic B to nematic transition temperature, T_{NI}= nematic to isotropic transition temperature.

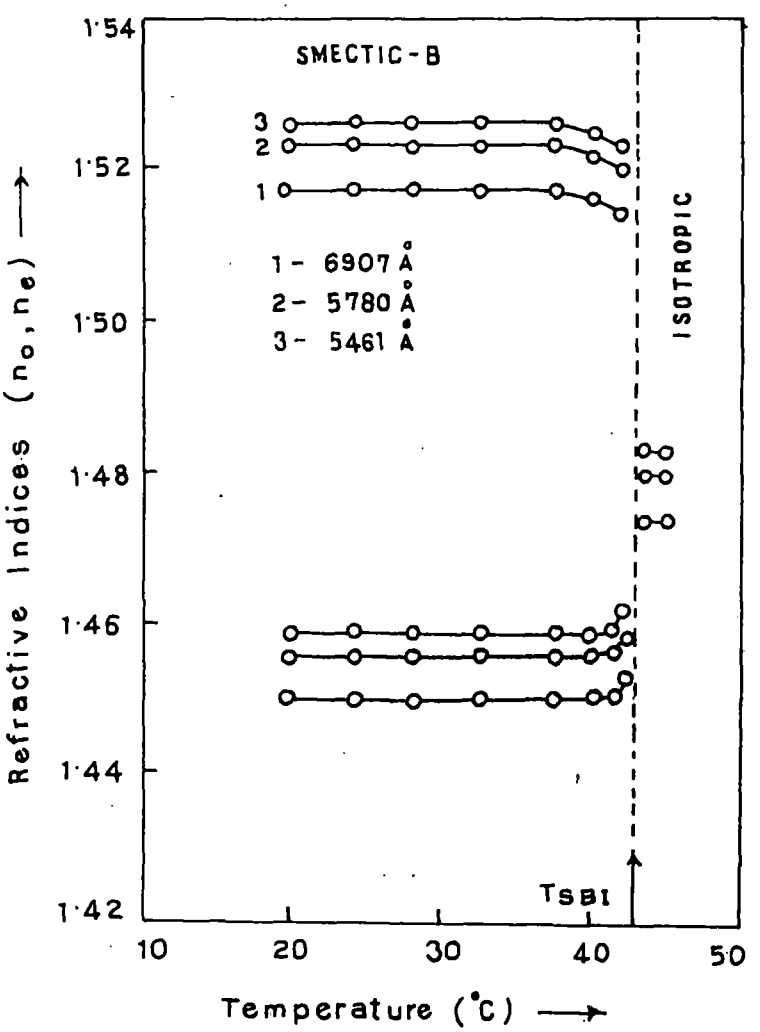

Figure 5.1(c) Variation of refractive indices (n_o,n_e) of EPEBCH with temperature. T_{SBI} = smectic B to isotropic transition temperature.

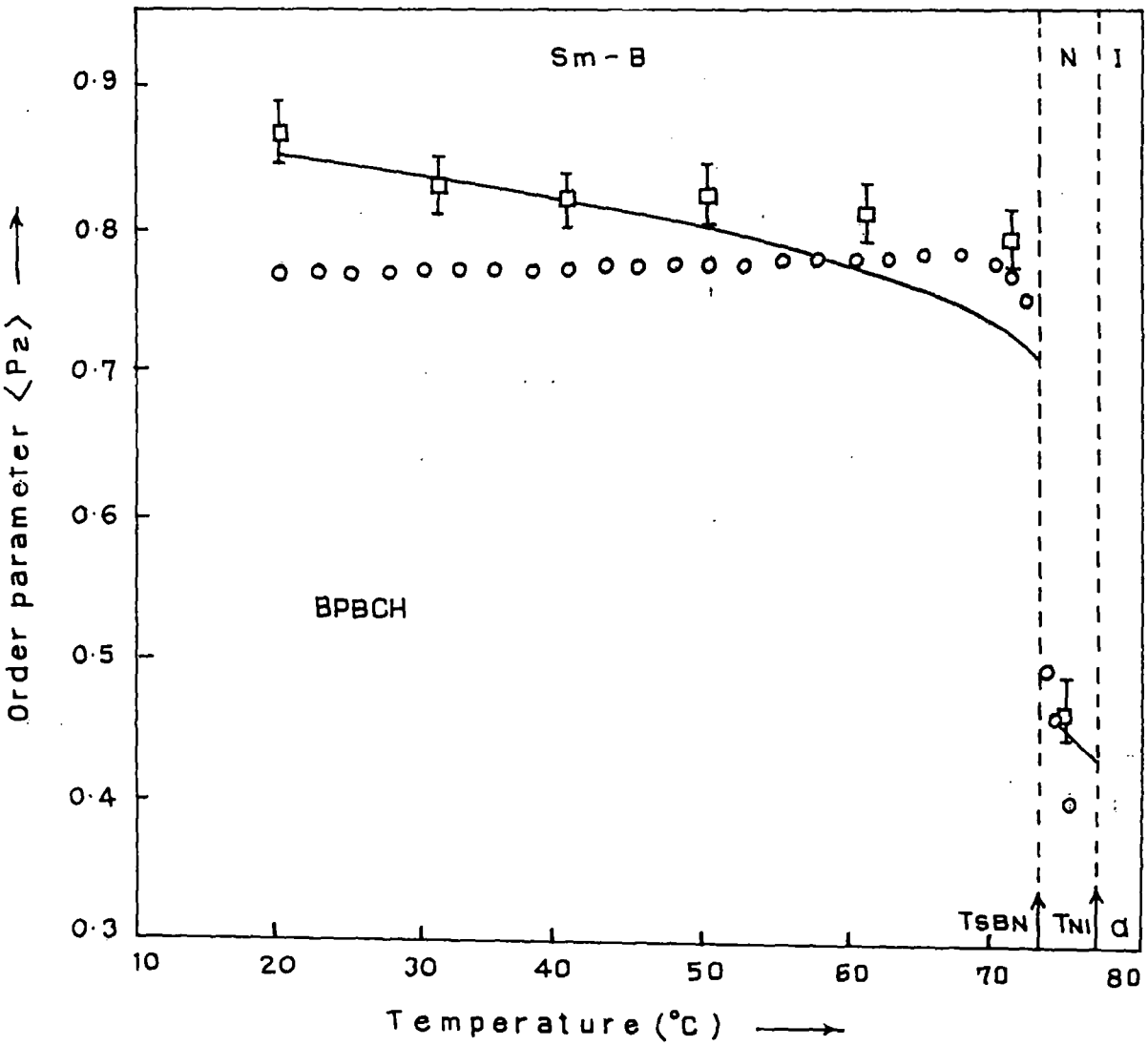

Figure 5.2(a) Plot of orientational order parameter $\langle P_2 \rangle$ with temperature for BPBCH. o, $\langle P_2 \rangle$ from refractive index data; □, $\langle P_2 \rangle$ from x-ray data. Continuous curve correspond to McMillan's theory with δ=0.0 and α=0.96

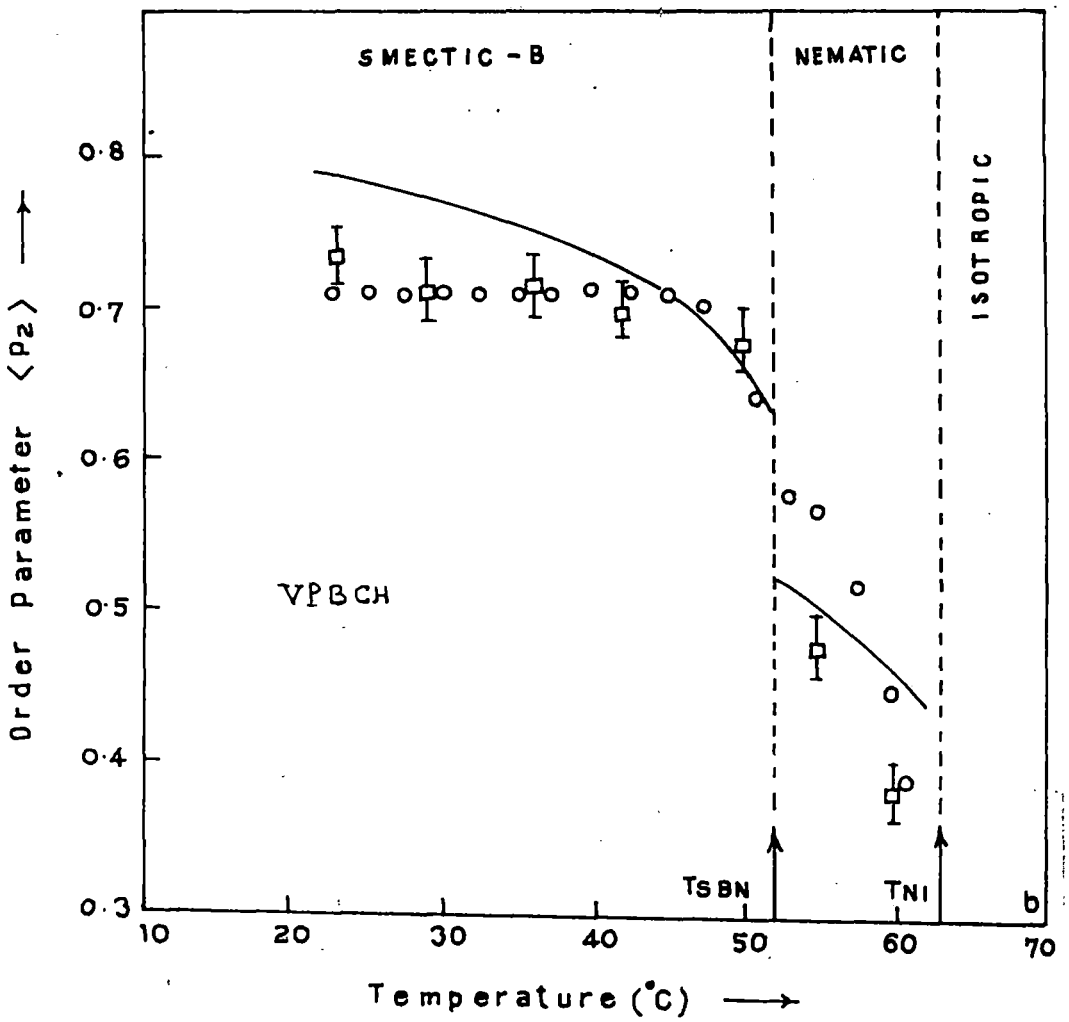

Figure 5.2(b) Plot of orientational order parameter $\langle P_2 \rangle$ with temperature for VPBCH. o, $\langle P_2 \rangle$ from refractive index data; □, $\langle P_2 \rangle$ from x-ray data. Continuous curve correspond to McMillan's theory with δ=0.245 and α=0.65

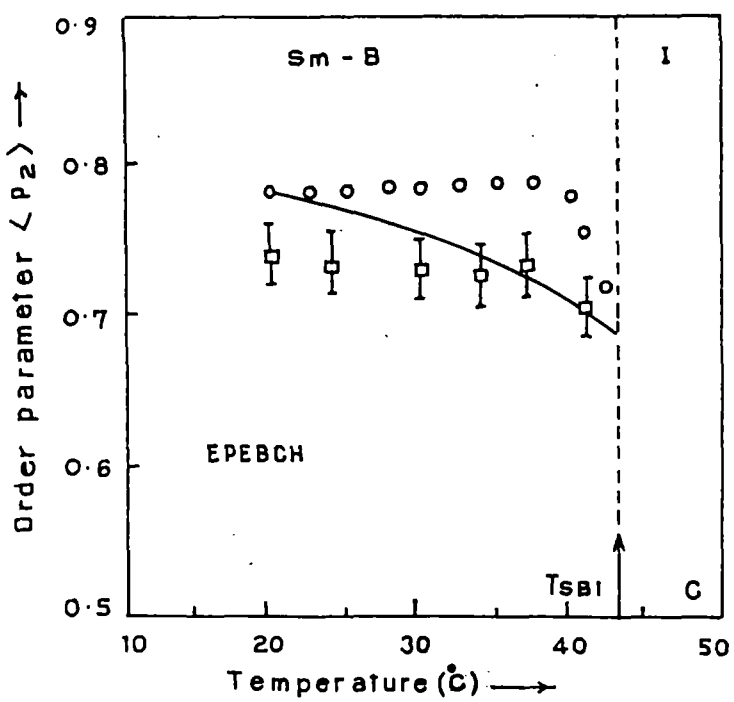

Figure 5.2(c) Plot of orientational order parameter $\langle P_2 \rangle$ with temperature for EPEBCH. o, $\langle P_2 \rangle$ from refractive index data; □, $\langle P_2 \rangle$ from x-ray data. Continuous curve correspond to McMillan's theory with δ=0.251 and α=0.714.

are being made to synthesize new liquid crystalline materials with low optical anisotropy which are especially required to develop fast and high information content liquid crystal displays [5]. It is clear from tables 5.4-5.9 that although the Vuks' and Neugebauer's models give slightly different absolute values of polarizabilities, but the order parameter values obtained from the two models maintain a good agreement.

The temperature variation of the orientational order parameter $\langle P_2 \rangle$ values obtained following Neugebauer's model is shown graphically in Figures 5.2(a)-5.2(c) for all the compounds under study. Physical considerations imply that the Neugebauer's model is more realistic than Vuks' approach for such anisotropic compounds, since the anisotropy of the local field factors have been considered in this model. The values of the order parameters $\langle P_2 \rangle$ at different temperature obtained from the three different wavelengths and their average value for the three compounds have been included in tables 5.11-5.16.

I have also compared the experimentally determined $\langle P_2 \rangle$ values with McMillan's theory [8-9] for smectic A phase. The mean field potential of McMillan's theory is given by,

$$\varepsilon(\cos\theta, z) = -\varepsilon_o \left[\delta\alpha\tau \cos(2\pi z/d) + \left\{ \eta + \alpha\sigma \cos(2\pi z/d) \right\} \right] P_2(\cos\theta) \qquad (5.2)$$

where α and δ are two adjustable parameters, z is the displacement along the layer normal, d is the layer thickness, $\eta = \langle P_2(\cos\theta) \rangle$, the orientational order parameter, while $\tau = \langle \cos(2\pi z/d) \rangle$ is the translational order parameter and $\sigma = \langle P_2(\cos\theta)\cos(2\pi z/d) \rangle$ is the mixed translational and orientational order parameter. The theoretically calculated values of the orientational order parameters are also shown in

Figures 5.2(a)-5.2(c) for the respective compounds. It is seen that the experimental $\langle P_2 \rangle$ values remain unchanged in the smectic B phase for all the three compounds, while in the nematic phases (where it is present) $\langle P_2 \rangle$ show significant temperature dependence. Similar behaviour in the temperature variation of orientational order parameter of these compounds have been obtained from x-ray diffraction studies [1] as well which are also shown in Figures 5.2(a)-5.2(c). The experimental $\langle P_2 \rangle$ values from refractive index and x-rays agree quite well for VPBCH. However, the agreement is not good in other two cases. This may be due to the fact that order parameter determined from x-ray studies depends on the electron density distribution in the sample, whereas that calculated from refractive index measurements depends on polarisability of the sample. Hence, the two techniques may give different values of the order parameter. The smectic B to nematic phase transition is marked by abrupt change in the order parameter values in both the compounds (BPBCH and VPBCH) which have such transitions. Agreement between the experimental order parameter and those calculated from McMillan's theory are poor. Haller's extrapolation procedure [7], which was adopted in evaluating $\langle P_2 \rangle$ for these compounds, may lead to somewhat arbitrary values of the order parameter rather than the absolute values. Discrepancy in temperature variation of order parameter also arises due to the fact that McMillan's theory is not strictly applicable to the smectic B phase.

Figures 5.3-5.5 show the temperature variation of density of BPBCH, VPBCH and EPEBCH respectively. Measurements have been made from room temperature ($\sim 20^{\circ}C$) to slightly above the nematic/isotropic transition temperature. It is seen from the figures that as expected the smectic B to nematic transitions in BPBCH and VPBCH are first order phase transitions. This result

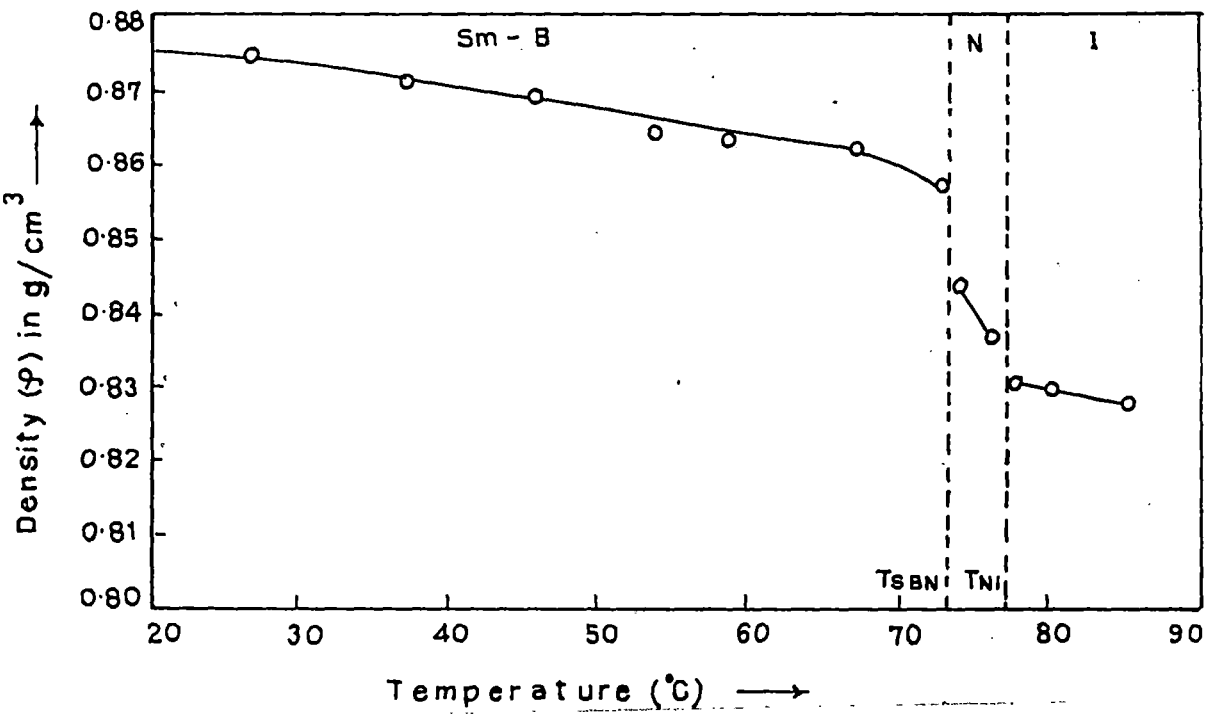

Figure 5.3 The density of BPBCH as a function of temperature. Solid line is guide to the eye only.

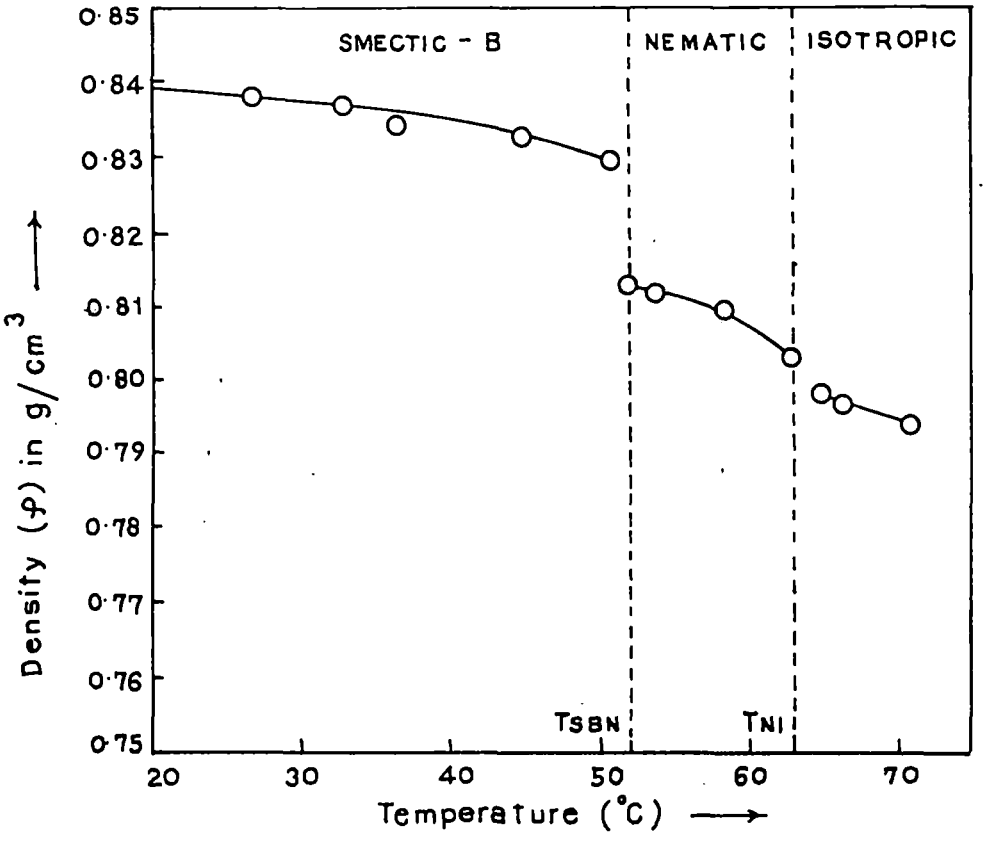

Figure 5.4 The density of VPBCH as a function of temperature. Solid line is guide to the eye only.

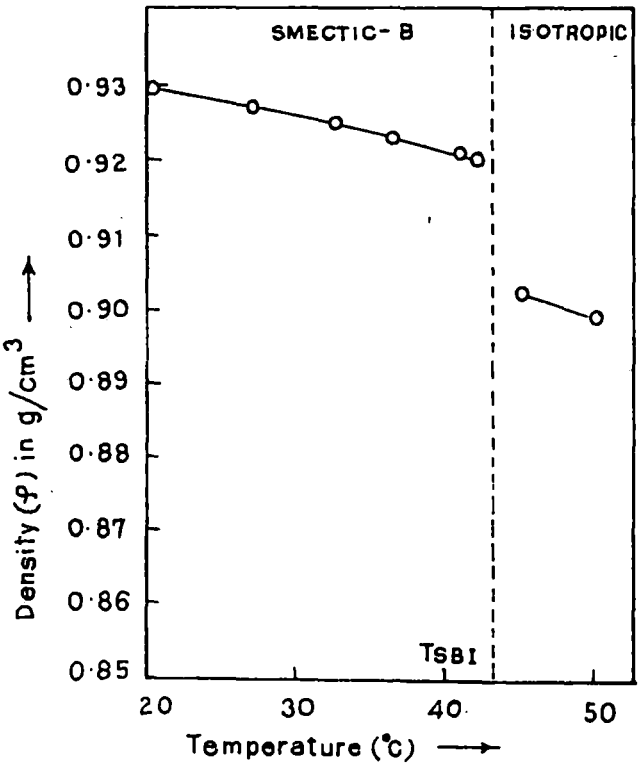

Figure 5.5 The density of EPEBCH as a function of temperature. Solid line is guide to the eye only.

is also consistent with the observations of temperature variation of order parameters as obtained from x-ray diffraction as well as refractive index measurements. Also it can be seen that the changes in density at the smectic B-nematic transitions are significantly greater than those at the nematic-isotropic transitions. This implies that the entropy change at the smectic B-nematic transition is greater than that at nematic-isotropic transition for both BPBCH and VPBCH. Unfortunately, due to unavailability of DTA/DSC in our laboratory this could not be confirmed from thermal analysis.

The higher order smectic phases often exhibit optical biaxiallity due to hindered rotation. I studied a well aligned sample in the smectic B phase of EPEBCH by varying the angle of incidence in the thin prism method with a view to observe the effect of biaxiallity in the sample. The calculations are given below.

The equation of ellipsoid in biaxial crystal can be written as [10]

$$ax^2 + by^2 + cz^2 = v^2 \qquad (5.3)$$

where v = velocity of light in vacuum and a,b and c are the velocity of light in the three principal axes directions (x, y and z), so that $\mu_1 = v/a$, $\mu_2 = v/b$ and $\mu_3 = v/c$.
Equation (5.3) can be rewritten as

$$\frac{x^2}{\mu_1^2} + \frac{y^2}{\mu_2^2} + \frac{z^2}{\mu_3^2} = 1 \qquad (5.4)$$

In any other cartesian co ordinate system (x', y', z'), equation (5.4) can be written as

$$\frac{(a_{11}x' + a_{12}y' + a_{13}z')^2}{\mu_1^2} + \frac{(a_{21}x' + a_{22}y' + a_{23}z')^2}{\mu_2^2}$$

$$+ \frac{(a_{31}x' + a_{32}y' + a_{33}z')^2}{\mu_3^2} = 1 \qquad (5.5)$$

where a_{ij} are the matrix elements of the transformation matrix A for the transformation $\vec{r} = A\,\vec{r}'$ [11]. The intersection of this ellipsoid with $y' = 0$ plane, which gives the effective refractive indices for the light beam propagating along y' direction, is given by

$$Ax'^2 + Bz'^2 + Cx'z' = 1, \qquad (5.6)$$

where
$$A = \frac{a_{11}^2}{\mu_1^2} + \frac{a_{21}^2}{\mu_2^2} + \frac{a_{31}^2}{\mu_3^2}$$

$$B = \frac{a_{13}^2}{\mu_1^2} + \frac{a_{23}^2}{\mu_2^2} + \frac{a_{33}^2}{\mu_3^2}$$

and
$$C = 2\left[\frac{a_{11}a_{13}}{\mu_1^2} + \frac{a_{21}a_{23}}{\mu_2^2} + \frac{a_{31}a_{33}}{\mu_3^2}\right]$$

Now, the (x', y', z') can be rotated about y' axis by an angle α, such that the equation (5.6) in the new system (x'', y'', z'') is given by

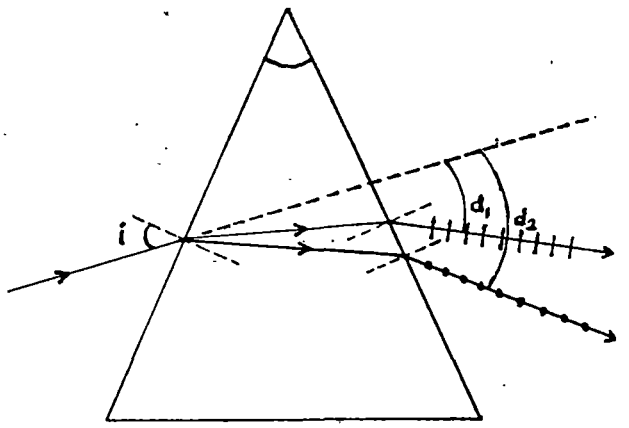

Figure 5.6 Angles i, d_1 and d_2 as measured in the experiment and shown in table 5.17. | indicates horizontal polarisation and • indicates vertical polarisation

$$\frac{x''^2}{p^2} + \frac{z''^2}{q^2} = 1 \qquad (5.7)$$

where, $$\alpha = \frac{1}{2} \tan^{-1}\left(\frac{C}{A - B}\right)$$

$$p = 2^{1/2}\left[A + B + \left\{C^2 + (A - B)^2\right\}^{1/2}\right]^{-1/2}$$

and $$q = 2^{1/2}\left[A + B - \left\{C^2 + (A - B)^2\right\}^{1/2}\right]^{-1/2}$$

The observed refractive indices for the beam along y"(= y') axis are obviously p and q.

Since the direction of pricipal axes and the values of principal refractive indices are not known initially in an experimental set up, there are six unknown parameters, viz, μ_1, μ_2, μ_3, and the three Eulerian angles θ, ϕ and ψ. In the actual experiment, the liquid crystal sample, EPEBCH, was kept in a thin prism, inner surfaces of which were rubbed in the direction of the prism edge, and a monochromatic unpolarised ray of light was incident on it at various angles from 0^o to 70^o. The deviations of refracted rays, consisting of two orthogonally plane polarised rays, were measured and their paths through the liquid crystal medium were calculated. The experimental values were used in a computer programme, written for this purpose, to determine the six unknown parameters. The computer output indicated that within the experimental uncertainty the sample (EPEBCH in the smectic B phase), can be treated as uniaxial. The angle of incidence (i) and the deviations (d_1 and d_2) as measured in the experiment are shown in Figure 5.6 and the

corresponding values at room temperature (≈ 20°C) for EPEBCH are listed in table 5.17.

Table 5.1

Density (ρ) and refractive indices (n_o,n_e) at different temperatures of BPBCH

Temp. in °C	Density (ρ) in gms/c.c	λ = 6907 Å		λ = 5780 Å		λ = 5461 Å	
		n_o	n_e	n_o	n_e	n_o	n_e
20.0	0.876	1.482	1.549	1.485	1.552	1.491	1.558
22.5	0.875	1.482	1.549	1.485	1.552	1.491	1.558
25.0	0.875	1.482	1.549	1.485	1.552	1.491	1.558
27.5	0.874	1.482	1.549	1.485	1.552	1.491	1.558
30.0	0.873	1.482	1.549	1.485	1.552	1.491	1.558
32.5	0.873	1.482	1.549	1.485	1.552	1.491	1.558
35.0	0.872	1.482	1.549	1.485	1.552	1.491	1.558
37.5	0.871	1.482	1.549	1.485	1.552	1.491	1.558
40.0	0.871	1.482	1.549	1.485	1.552	1.491	1.558
42.5	0.870	1.482	1.549	1.485	1.552	1.491	1.558
45.0	0.869	1.482	1.549	1.485	1.552	1.491	1.558
47.5	0.868	1.482	1.549	1.485	1.552	1.491	1.558
50.0	0.867	1.482	1.549	1.485	1.552	1.491	1.558
52.5	0.866	1.482	1.549	1.485	1.552	1.491	1.558
55.0	0.866	1.482	1.549	1.485	1.552	1.491	1.558
57.5	0.865	1.482	1.549	1.485	1.552	1.491	1.558
60.0	0.864	1.482	1.549	1.485	1.552	1.491	1.558
62.5	0.863	1.482	1.549	1.485	1.552	1.491	1.558
65.0	0.862	1.482	1.549	1.485	1.552	1.491	1.558
67.5	0.862	1.482	1.549	1.485	1.552	1.491	1.558
70.0	0.859	1.482	1.549	1.485	1.552	1.491	1.558
71.0	0.859	1.482	1.548	1.485	1.551	1.491	1.557
72.0	0.857	1.482	1.546	1.485	1.549	1.491	1.556
73.5	0.845	1.488	1.529	1.491	1.533	1.491	1.539
74.0	0.844	1.488	1.527	1.491	1.530	1.497	1.536
75.0	0.840	1.490	1.523	1.493	1.527	1.499	1.533
77.0(iso)	0.836	1.503	1.503	1.506	1.506	1.512	1.512

Table 5.2

Density (ρ) and refractive indices (n_o, n_e) at different temperatures of VPBCH

Temp. in °C	Density (ρ) in gms/c.c	λ = 6907 Å		λ = 5780 Å		λ = 5461 Å	
		n_o	n_e	n_o	n_e	n_o	n_e
22.5	0.839	1.455	1.510	1.461	1.516	1.471	1.526
25.0	0.838	1.455	1.510	1.461	1.516	1.471	1.526
27.5	0.838	1.455	1.510	1.461	1.516	1.471	1.526
30.0	0.838	1.455	1.510	1.461	1.516	1.471	1.526
32.5	0.837	1.455	1.510	1.461	1.516	1.471	1.526
35.0	0.836	1.455	1.510	1.461	1.516	1.471	1.526
37.5	0.836	1.455	1.510	1.461	1.516	1.471	1.526
40.0	0.835	1.455	1.510	1.461	1.516	1.471	1.526
42.5	0.834	1.455	1.510	1.461	1.516	1.471	1.526
45.0	0.833	1.455	1.510	1.462	1.516	1.471	1.526
47.5	0.832	1.456	1.510	1.462	1.516	1.472	1.526
50.0	0.830	1.456	1.508	1.463	1.516	1.472	1.524
51.0	0.830	1.457	1.506	1.464	1.513	1.473	1.523
53.0	0.813	1.458	1.502	1.464	1.508	1.474	1.518
55.0	0.812	1.458	1.501	1.464	1.507	1.474	1.517
57.5	0.811	1.458	1.497	1.465	1.503	1.474	1.513
60.0	0.808	1.458	1.492	1.465	1.498	1.474	1.508
61.0	0.807	1.459	1.487	1.465	1.494	1.475	1.505
63.0(iso)	0.804	1.464	1.464	1.471	1.471	1.481	1.481

Table 5.3

Density (ρ) and refractive indices (n_o, n_e) at different temperatures of EPEBCH

Temp. in °C	Density (ρ) in gms/c.c	λ = 6907 Å		λ = 5780 Å		λ = 5461 Å	
		n_o	n_e	n_o	n_e	n_o	n_e
20.0	0.930	1.450	1.517	1.456	1.523	1.459	1.526
22.5	0.929	1.450	1.517	1.456	1.523	1.459	1.526
25.0	0.928	1.450	1.517	1.456	1.523	1.459	1.526
27.5	0.927	1.450	1.517	1.456	1.523	1.459	1.526
30.0	0.926	1.450	1.517	1.456	1.523	1.459	1.526
32.5	0.925	1.450	1.517	1.456	1.523	1.459	1.526
35.0	0.924	1.450	1.517	1.456	1.523	1.459	1.526
37.5	0.923	1.450	1.517	1.456	1.523	1.459	1.526
40.0	0.921	1.450	1.516	1.456	1.522	1.459	1.524
41.0	0.921	1.451	1.515	1.457	1.521	1.460	1.524
42.0	0.920	1.453	1.514	1.459	1.520	1.462	1.523
44(iso)	0.905	1.474	1.474	1.480	1.480	1.483	1.483

Table 5.4

Polarizability (α_o, α_e) at different temperatures and for different wavelengths (λ) of BPBCH by Vuk's method.

Temp. in °C	λ = 6907 Å		λ = 5780 Å		λ = 5461 Å	
	α_o	α_e	α_o	α_e	α_o	α_e
20.0	33.31	39.01	33.49	39.19	33.85	39.55
22.5	33.33	39.03	33.51	39.21	33.87	39.57
25.0	33.55	39.06	33.53	39.23	33.89	39.60
27.5	33.37	39.08	33.55	39.25	33.91	39.62
30.0	33.41	39.12	33.59	39.30	33.95	39.66
32.5	33.42	39.15	33.61	39.32	33.97	39.69
35.0	33.44	39.17	33.63	39.34	33.99	39.71
37.5	33.48	39.21	33.67	39.39	34.03	39.76
40.0	33.50	39.24	33.69	39.41	34.05	39.78
42.5	33.54	39.28	33.73	39.46	34.09	39.82
45.0	33.56	39.30	33.74	39.48	34.11	39.85
47.5	33.60	39.35	33.78	39.53	34.14	39.89
50.0	33.64	39.39	33.82	39.57	34.18	39.94
52.5	33.67	39.43	33.85	39.61	34.22	39.98
55.0	33.70	39.46	33.88	39.64	34.24	40.01
57.5	33.72	39.49	33.91	39.67	34.27	40.04
60.0	33.75	39.53	33.94	39.71	34.30	40.08
62.5	33.79	39.58	33.98	39.75	34.34	40.12
65.0	33.82	39.61	34.01	39.79	34.37	40.16
67.5	33.85	39.65	34.04	39.82	34.40	40.19
70.0	33.95	39.71	34.13	39.88	34.50	40.28
71.0	33.98	39.66	34.17	39.84	34.53	40.23
72.0	34.07	39.59	34.26	39.77	34.61	40.21
73.5	35.11	38.71	35.29	38.97	35.67	39.30
74.0	35.19	38.59	35.37	38.78	35.74	39.14
75.0	35.49	38.42	35.71	38.65	36.06	39.06

α_o, α_e are in 10^{-24} cm^3 unit.

Table 5.5

Polarizability (α_o, α_e) at different temperatures and for different wavelengths (λ) of VPBCH by Vuk's method.

Temp. in °C	λ = 6907 Å		λ = 5780 Å		λ = 5461 Å	
	α_o	α_e	α_o	α_e	α_o	α_e
22.5	33.18	38.05	33.59	38.46	34.20	39.07
25.0	33.20	38.07	33.61	38.48	34.23	39.09
27.5	33.21	38.08	33.62	38.49	34.23	39.10
30.0	33.23	38.10	33.64	38.51	34.25	39.12
32.5	33.25	38.12	33.66	38.54	34.27	39.15
35.0	33.28	38.16	33.69	38.57	34.31	39.19
37.5	33.31	38.20	33.72	38.60	34.34	39.22
40.0	33.35	38.24	33.76	38.65	34.38	39.27
42.5	33.40	38.28	33.82	38.69	34.43	39.31
45.0	33.47	38.32	33.88	38.73	34.47	39.36
47.5	33.54	38.36	33.95	38.77	34.55	39.39
50.0	33.65	38.29	34.09	38.77	34.67	39.32
51.0	33.76	38.17	34.17	38.58	34.80	39.19
53.0	34.54	38.51	34.97	38.92	35.59	39.54
55.0	34.59	38.51	35.02	38.88	35.64	39.55
57.5	34.69	38.24	35.13	38.65	35.75	39.29
60.0	34.86	37.95	35.31	38.33	35.92	38.99
61.0	35.03	37.59	35.43	38.06	36.06	38.80
63.0(iso)	35.75	35.75	36.18	36.18	36.81	36.81

α_o, α_e are in 10^{-24} cm^3 unit.

Table 5.6

Polarizability (α_o, α_e) at different temperatures and for different wavelengths (λ) of EPEBCH by Vuk's method.

Temp. in ^oC	λ = 6907 Å		λ = 5780 Å		λ = 5461 Å	
	α_o	α_e	α_o	α_e	α_o	α_e
20.0	31.39	37.05	31.75	37.41	31.93	37.59
22.5	31.42	37.09	31.78	37.45	31.96	37.63
25.0	31.45	37.13	31.82	37.49	32.00	37.67
27.5	31.49	37.17	31.85	37.53	32.03	37.71
30.0	31.52	37.21	31.89	37.57	32.07	37.75
32.5	31.56	37.25	31.92	37.61	32.10	37.79
35.0	31.59	37.29	31.95	37.65	32.14	37.83
37.5	31.64	37.35	32.01	37.71	32.19	37.89
40.0	31.70	37.33	32.07	37.69	32.26	37.80
41.0	31.80	37.26	32.16	37.62	32.35	37.76
42.0	31.98	37.18	32.34	37.55	32.52	37.73
44.0(iso)	34.28	34.28	34.65	34.65	34.83	34.83

α_o, α_e are in 10^{-24} cm^3 unit.

Table 5.7

Polarizability (α_o, α_e) at different temperatures and for different wavelengths (λ) of BPBCH by Neugebauer's method.

Temp. in °C	λ = 6907 Å		λ = 5780 Å		λ = 5461 Å	
	α_o	α_e	α_o	α_e	α_o	α_e
20.0	33.62	38.39	33.81	38.56	34.17	38.92
22.5	33.64	38.41	33.83	38.58	34.19	38.94
25.0	33.66	38.43	33.85	38.60	34.21	38.96
27.5	33.68	38.45	33.86	38.63	34.23	38.98
30.0	33.72	38.50	33.90	38.67	34.27	39.03
32.5	33.74	38.52	33.92	38.69	34.29	39.05
35.0	33.76	38.54	33.94	38.72	34.31	39.07
37.5	33.80	38.59	33.98	38.76	34.35	39.12
40.0	33.82	38.61	34.00	38.78	34.36	39.14
42.5	33.85	38.65	34.04	38.83	34.40	39.19
45.0	33.87	38.68	34.06	38.85	34.42	39.21
47.5	33.91	38.72	34.10	38.89	34.46	39.25
50.0	33.95	38.77	34.14	38.94	34.50	39.30
52.5	33.98	38.80	34.17	38.97	34.54	39.34
55.0	34.01	38.83	34.20	39.01	34.56	39.37
57.5	34.04	38.86	34.23	39.04	34.59	39.40
60.0	34.07	38.90	34.26	39.07	34.62	39.44
62.5	34.11	38.94	34.30	39.12	34.66	39.48
65.0	34.14	38.98	34.33	39.16	34.70	39.52
67.5	34.17	39.01	34.36	39.19	34.72	39.55
70.0	34.26	39.08	34.45	39.25	34.82	39.64
71.0	34.29	39.04	34.48	39.21	34.85	39.60
72.0	34.38	38.99	34.56	39.17	34.92	39.59
73.5	35.30	38.32	35.49	38.57	35.87	38.90
74.0	35.37	38.23	35.55	38.41	35.92	38.77
75.0	35.65	38.10	35.87	38.33	36.22	38.73

α_o, α_e are in 10^{-24} cm^3 unit.

Table 5.8

Polarizability (α_o, α_e) at different temperatures and for different wavelengths (λ) of VPBCH by Neugebauer's method.

Temp. in °C	λ = 6907 Å		λ = 5780 Å		λ = 5461 Å	
	α_o	α_e	α_o	α_e	α_o	α_e
22.5	33.43	37.55	33.84	37.95	34.46	38.55
25.0	33.45	37.57	33.87	37.97	34.48	38.58
27.5	33.46	37.58	33.87	37.98	34.49	38.59
30.0	33.48	37.60	33.89	38.01	34.51	38.61
32.5	33.50	39.05	33.91	38.03	34.53	38.63
35.0	33.53	37.66	33.95	38.06	34.57	38.67
37.5	33.56	37.69	33.97	38.10	34.59	38.70
40.0	33.60	37.74	34.02	38.14	34.64	38.75
42.5	33.65	37.78	34.07	38.19	34.68	38.79
45.0	33.72	37.82	34.13	38.23	34.73	38.84
47.5	33.79	37.86	34.21	38.27	34.81	38.88
50.0	33.89	37.81	34.34	38.28	34.92	38.83
51.0	33.98	37.71	34.40	38.12	35.03	38.72
53.0	34.74	38.10	35.17	38.51	35.80	39.12
55.0	34.79	38.11	35.22	38.48	35.85	39.14
57.5	34.87	37.88	35.31	38.29	35.93	38.92
60.0	35.01	37.64	35.46	38.02	36.08	38.67
61.0	35.16	37.33	35.57	37.79	36.20	38.51
63.0(iso)	35.74	35.76	36.18	36.18	36.81	36.81

α_o, α_e are in 10^{-24} cm^3 unit.

Table 5.9

Polarizability (α_o, α_e) at different temperatures and for different wavelengths (λ) of EPEBCH by Neugebauer's method.

Temp. in ^oC	λ = 6907 Å		λ = 5780 Å		λ = 5461 Å	
	α_o	α_e	α_o	α_e	α_o	α_e
20.0	31.68	36.46	32.04	36.82	32.23	36.99
22.5	31.71	36.50	32.08	36.86	32.26	37.03
25.0	31.75	36.54	32.11	36.90	32.29	37.07
27.5	31.78	36.58	32.15	36.94	32.33	37.11
30.0	31.82	36.62	32.18	36.98	32.36	37.15
32.5	31.85	36.66	32.22	37.02	32.40	37.19
35.0	31.88	36.70	32.25	37.06	32.43	37.23
37.5	31.94	36.76	32.30	37.12	32.49	37.29
40.0	31.99	36.75	32.36	37.11	32.55	37.22
41.0	32.08	36.69	32.44	37.05	32.63	37.20
42.0	32.24	36.65	32.61	37.00	32.80	37.18
44.0(iso)	34.28	34.28	34.65	34.65	34.83	34.83

α_o, α_e are in 10^{-24} cm^3 unit.

Table 5.10

Birefringence (Δn) at different temperatures of BPBCH, VPBCH and EPEBCH.

BPBCH		VPBCH		EPEBCH	
Temp/^{o}C	$\Delta n = n_e - n_o$	Temp/^{o}C	$\Delta n = n_e - n_o$	Temp/^{o}C	$\Delta n = n_e - n_o$
20.0	0.067	22.5	0.055	20.0	0.067
22.5	0.067	25.0	0.055	22.5	0.067
25.0	0.067	27.5	0.055	25.0	0.067
27.5	0.067	30.0	0.055	27.5	0.067
30.0	0.067	32.5	0.055	30.0	0.067
32.5	0.067	35.0	0.055	32.5	0.067
35.0	0.067	37.5	0.055	35.0	0.067
37.5	0.067	40.0	0.055	37.5	0.067
40.0	0.067	42.5	0.055	40.0	0.066
42.5	0.067	45.0	0.055	41.0	0.064
45.0	0.067	47.5	0.054	42.0	0.061
47.5	0.067	50.0	0.053		
50.0	0.067	51.0	0.050		
52.5	0.067	53.0	0.044		
55.0	0.067	55.0	0.043		
57.5	0.067	57.5	0.039		
60.0	0.067	60.0	0.033		
62.5	0.067	61.0	0.029		
65.0	0.067				
67.5	0.067				
70.0	0.067				
71.0	0.066				
72.0	0.064				
73.5	0.042				
74.0	0.039				
75.0	0.034				

Table 5.11

Order parameter $\langle P_2 \rangle$ of BPBCH at different temperatures by Vuk's method.

Temp. in °C	λ = 6907 Å	λ = 5780 Å	λ = 5461 Å	Average
	$\langle P_2 \rangle$	$\langle P_2 \rangle$	$\langle P_2' \rangle$	$\langle P_2 \rangle$
20.0	0.756	0.770	0.787	0.771
22.5	0.756	0.771	0.787	0.771
25.0	0.757	0.771	0.788	0.772
27.5	0.757	0.771	0.788	0.772
30.0	0.759	0.773	0.790	0.774
32.5	0.759	0.773	0.790	0.774
35.0	0.759	0.774	0.790	0.774
37.5	0.760	0.774	0.791	0.775
40.0	0.760	0.776	0.791	0.776
42.5	0.761	0.776	0.793	0.777
45.0	0.761	0.776	0.793	0.777
47.5	0.763	0.777	0.794	0.778
50.0	0.764	0.778	0.795	0.779
52.5	0.764	0.780	0.795	0.780
55.0	0.765	0.780	0.797	0.781
57.5	0.765	0.781	0.797	0.781
60.0	0.767	0.781	0.798	0.782
62.5	0.767	0.781	0.798	0.782
65.0	0.768	0.782	0.799	0.783
67.5	0.768	0.782	0.799	0.783
70.0	0.764	0.778	0.798	0.780
71.0	0.753	0.767	0.787	0.769
72.0	0.732	0.747	0.773	0.751
73.5	0.479	0.498	0.501	0.493
74.0	0.452	0.462	0.471	0.462
75.0	0.387	0.398	0.414	0.400

Table 5.12

Order parameter $\langle P_2 \rangle$ of VPBCH at different temperatures by Vuk's method.

Temp. in °C	λ = 6907 Å	λ = 5780 Å	λ = 5461 Å	Average
	$\langle P_2 \rangle$	$\langle P_2 \rangle$	$\langle P_2 \rangle$	$\langle P_2 \rangle$
22.5	0.721	0.714	0.705	0.714
25.0	0.721	0.714	0.707	0.714
27.5	0.721	0.714	0.707	0.714
30.0	0.721	0.714	0.707	0.714
32.5	0.721	0.715	0.707	0.715
35.0	0.723	0.715	0.708	0.715
37.5	0.724	0.715	0.708	0.716
40.0	0.724	0.717	0.710	0.717
42.5	0.724	0.715	0.710	0.716
45.0	0.718	0.713	0.708	0.713
47.5	0.714	0.707	0.703	0.708
50.0	0.687	0.685	0.676	0.683
51.0	0.653	0.647	0.637	0.646
53.0	0.588	0.579	0.573	0.580
55.0	0.581	0.566	0.568	0.571
57.5	0.526	0.516	0.514	0.519
60.0	0.459	0.443	0.446	0.449
61.0	0.379	0.386	0.398	0.388

Table 5.13

Order parameter $\langle P_2 \rangle$ of EPEBCH at different temperatures by Vuk's method.

Temp. in °C	λ = 6907 Å	λ = 5780 Å	λ = 5461 Å	Average
	$\langle P_2 \rangle$	$\langle P_2 \rangle$	$\langle P_2 \rangle$	$\langle P_2 \rangle$
20.0	0.791	0.773	0.772	0.779
22.5	0.793	0.773	0.772	0.779
25.0	0.793	0.774	0.773	0.780
27.5	0.794	0.775	0.774	0.781
30.0	0.794	0.775	0.774	0.781
32.5	0.795	0.777	0.776	0.783
35.0	0.797	0.777	0.776	0.783
37.5	0.798	0.778	0.777	0.784
40.0	0.787	0.768	0.755	0.770
41.0	0.763	0.745	0.739	0.749
42.0	0.728	0.711	0.710	0.716

Table 5.14

Order parameter $\langle P_2 \rangle$ of BPBCH at different temperatures by Neugebaur's method

Temp. in °C	λ = 6907 Å	λ = 5780 Å	λ = 5461 Å	Average
	$\langle P_2 \rangle$	$\langle P_2 \rangle$	$\langle P_2 \rangle$	$\langle P_2 \rangle$
20.0	0.761	0.774	0.785	0.773
22.5	0.761	0.775	0.785	0.774
25.0	0.761	0.775	0.785	0.774
27.5	0.761	0.775	0.787	0.774
30.0	0.763	0.777	0.787	0.776
32.5	0.763	0.777	0.789	0.776
35.0	0.765	0.777	0.789	0.777
37.5	0.765	0.778	0.789	0.777
40.0	0.765	0.778	0.790	0.778
42.5	0.766	0.780	0.790	0.779
45.0	0.766	0.780	0.790	0.779
47.5	0.768	0.780	0.792	0.780
50.0	0.768	0.782	0.793	0.781
52.5	0.769	0.782	0.793	0.781
55.0	0.769	0.783	0.793	0.782
57.5	0.771	0.783	0.795	0.783
60.0	0.771	0.785	0.795	0.784
62.5	0.773	0.785	0.797	0.785
65.0	0.773	0.787	0.797	0.786
67.5	0.773	0.787	0.798	0.786
70.0	0.768	0.782	0.797	0.782
71.0	0.758	0.770	0.785	0.771
72.0	0.737	0.751	0.772	0.753
73.5	0.482	0.502	0.500	0.495
74.0	0.456	0.464	0.471	0.464
75.0	0.391	0.401	0.415	0.402

Table 5.15

Order parameter $\langle P_2 \rangle$ of VPBCH at different temperatures by Neugebauer's method.

Temp. in °C	λ = 6907 Å	λ = 5780 Å	λ = 5461 Å	Average
	$\langle P_2 \rangle$	$\langle P_2 \rangle$	$\langle P_2 \rangle$	$\langle P_2 \rangle$
22.5	0.716	0.711	0.704	0.710
25.0	0.716	0.711	0.704	0.710
27.5	0.716	0.711	0.704	0.710
30.0	0.716	0.711	0.705	0.711
32.5	0.716	0.711	0.705	0.711
35.0	0.718	0.712	0.705	0.712
37.5	0.718	0.712	0.707	0.712
40.0	0.719	0.714	0.707	0.714
42.5	0.718	0.712	0.707	0.712
45.0	0.713	0.709	0.707	0.711
47.5	0.709	0.704	0.700	0.704
50.0	0.681	0.681	0.673	0.678
51.0	0.648	0.643	0.635	0.642
53.0	0.584	0.578	0.571	0.578
55.0	0.577	0.564	0.566	0.569
57.5	0.523	0.515	0.513	0.517
60.0	0.455	0.443	0.444	0.447
61.0	0.377	0.386	0.397	0.387

Table 5.16

Order parameter $\langle P_2 \rangle$ of EPEBCH at different temperatures by Neugebauer's method.

Temp. in °C	λ = 6907 Å	λ = 5780 Å	λ = 5461 Å	Average
	$\langle P_2 \rangle$	$\langle P_2 \rangle$	$\langle P_2 \rangle$	$\langle P_2 \rangle$
20.0	0.793	0.781	0.775	0.783
22.5	0.794	0.782	0.775	0.777
25.0	0.796	0.782	0.777	0.785
27.5	0.796	0.784	0.777	0.786
30.0	0.797	0.784	0.778	0.786
32.5	0.797	0.786	0.778	0.787
35.0	0.799	0.786	0.780	0.788
37.5	0.799	0.787	0.782	0.789
40.0	0.789	0.774	0.759	0.774
41.0	0.766	0.754	0.743	0.754
42.0	0.730	0.718	0.713	0.720

Table 5.17

i, d_1 and d_2 values at room temperature for EPEBCH

Angle of prism = 54.5′

angle of incidence(i) (degree)	d_1 (horizontally polarised)	d_2 (vertically polarised)
0	24.83	28.50
30	31.33	36.33
40	42.33	47.33
45	46.66	53.00
50	55.00	63.00
55	68.33	75.00
60	79.66	89.33
65	106.33	120.00
70	142.33	158.33

REFERENCES

[1]. B. Adhikari and R. Paul, Physical properties of three bicyclohexane compounds possessing smectic B phase I: X-ray diffraction technique , Phase transitions, 1995. (accepted for publication).

[2]. M..F. Vuks, Optics Spectrosc., 20, 361, (1966).

[3]. H.E.J. Neugebauer, Canad. J. Phys., 32, 1 (1954).

[4]. A.K. Zemindar, S. Paul and R. Paul Mol. Cryst. Liq. Cryst., 61, 191 (1980).

[5]. M.R. Schadt, Buchecker and K. Muller, Liq. Cryst.,5, 293 (1989).

[6]. P.G. de Gennes, Mol. Cryst. Liq. Cryst., 12, 193 (1971).

[7]. I. Haller, H.A. Huggins, H.R. Lilienthal and T.R. McGuire, J. Phys. Chem., 77, 950, (1973).

[8]. W.L. McMillan, Phys. Rev., 13, 137, (1971).

[9]. W.L. McMillan, Phys. Rev., A6, 936, (1972).

[10]. See for example "Light" by R.W. Ditchburn. ELBS, 1963.

[11]. H. Goldstein, Classical Mechanics, Addison - Wesley Publishing Co.

CHAPTER - 6

PHYSICAL PROPERTIES OF THE MESOPHASES OF 4 - n - HEPTYLOXY BENZYLIDINE - 4' - AMINOAZOBENZENE (HBAAB)

6.1 Introduction

Study of the mesomorphic properties of liquid crystals is important both from the point of view of applicability of the liquid crystalline compound in display devices and in the study of the nature of phase transitions in condensed matter systems. In this regard x-ray diffraction studies provide a powerful tool to deduce structural informations. In the present work I have undertaken small angle x-ray diffraction study of the richly polymorphic mesogen 4-n- heptyloxybenzylidene - 4'-aminoazobenzene (HBAAB) [1], having the following structural formula,

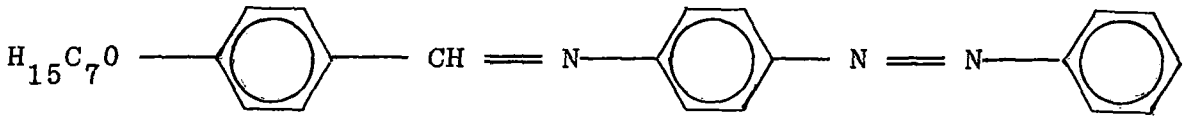

HBAAB has nematic, smectic A, smectic B and several crystalline phases. Results of the x-ray diffraction experiment on magnetically aligned samples of HBAAB have been analysed to determine the structural and orientational order parameters (OOP) throughout the mesomorphic range. Translational order parameter (τ) in the smectic phases of this compound has been determined from second order reflections in the meridional direction. Refractive index measurements for HBAAB have also been carried out by me in the nematic phase only and the OOP values determined therefrom have been compared with those obtained from x-ray diffraction studies. The experimentally determined order parameters have been fitted to McMillan's theory for the smectic A phase [2,3]. Density and DSC studies of isotropic - nematic (NI), nematic-smectic A (NA) and smectic A - smectic B (AB) phase transitions have also been carried out and results discussed.

6.2 Experimental

The synthesis and DSC study of HBAAB took place at the Department of Applied Chemistry, M.S. University of Baroda and all other experimental work was conducted at the Department of Physics, University of North Bengal. An examination of this compound by optical microscopy and differential scanning calorimetry has led to the following phase behaviour :

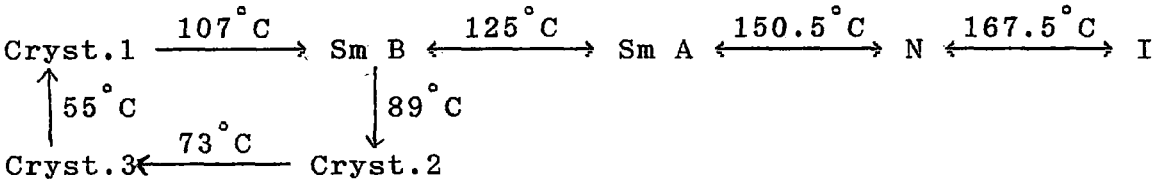

Texture study of this compound were done under a polarising microscope equipped with Mettler FP80/82 Thermosystem. The compound on cooling from the isotropic phase showed a marbled texture, often found in the nematic phase. Below the nematic phase a simple fan - shaped texture, typical of the smectic A phase was observed. On further cooling smectic A to smectic B phase transition took place, marked by the occurrence of small transition bars which gradually gave way to the smectic B mosaic texture with strong paramorphic boundaries [4]. On further cooling no flow could be observed in the sample, indicating that the compound has gone to the crystalline phase. From x-ray diffraction studies three different types of solid phases could be identified in the low temperature range. However, I have not tried to characterise the solid phases in the present chapter.

The experimental set up and the procedure for order parameter determination from x-ray diffraction [5] and refractive index [6] studies have been described in detail in chapter 2. The x-ray diffraction patterns were recorded photographically on a flat plate camera using nickel filtered Cu K_{α} radiation of mean

wavelength λ = 1.5418 Å. Samples were aligned using a magnetic field of about 3 Kilogauss for x-ray diffraction experiment. To obtain better accuracy in the measurement of layer thickness, x-ray diffraction photographs of inner spots were taken with sample to film distance increased to about 9cm. The x-ray films were scanned linearly and circularly by using a Zeiss micro - densitometer (model MD 100) and the optical density values were converted to x-ray intensity data following a standard procedure[7], as described in chapter 2. The details of analysis of data are also given in chapter 2, where the procedure for obtaining orientational distribution function, order parameters, layer thickness and intermolecular distance are mentioned.

The outer rings of the x-ray diffraction photographs in the smectic B phase being very sharp, I scanned the film linearly at first and from these readings the values of x-ray intensities along the circular arc were calculated. Refractive indices were measured by a thin hollow prism method, sample being surface aligned by rubbing. Due to absorption of the extraordinary beam in the smectic phases of this compound, it has not been possible to measure the extraordinary refractive index (n_e) in those phases. The ordinary refractive index (n_o) could be measured throughout the mesomorphic range. The experimental uncertainty of refractive index measurements are $\pm$ 0.001.

6.3 Results and Discussion

X-ray diffraction photographs of magnetically aligned sample of HBAAB in the nematic (T =155^{o}C), smectic A (T =147^{o}C) and smectic B (T = 123^{o}C) phases are shown in Figures 6.1(a)-6.1(c) respectively. The angular variation of intensities I(ψ) at different temperature are given in table 6.1. From intensity values of the outer rings at different temperatures, I

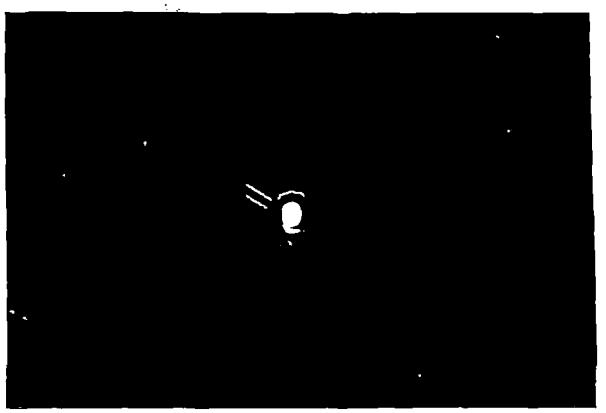

Figure 6.1(a). X-ray diffraction photograph of the oriented sample of HBAAB in the nematic phase at 155°C.

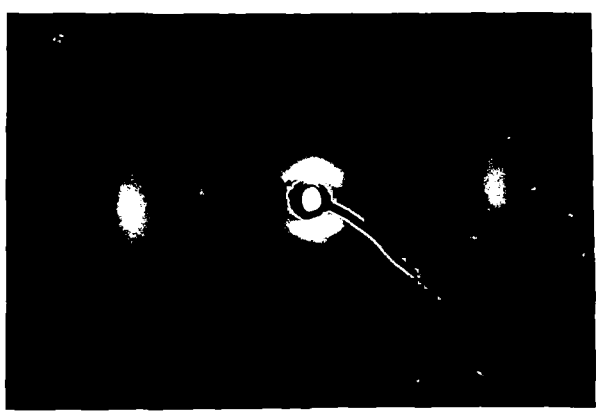

Figure 6.1(b). X-ray diffraction photograph of the oriented sample of HBAAB in the smectic A phase at 147°C.

Figure 6.1(c). X-ray diffraction photograph of the oriented sample of HBAAB in the smectic B phase at 123°C.

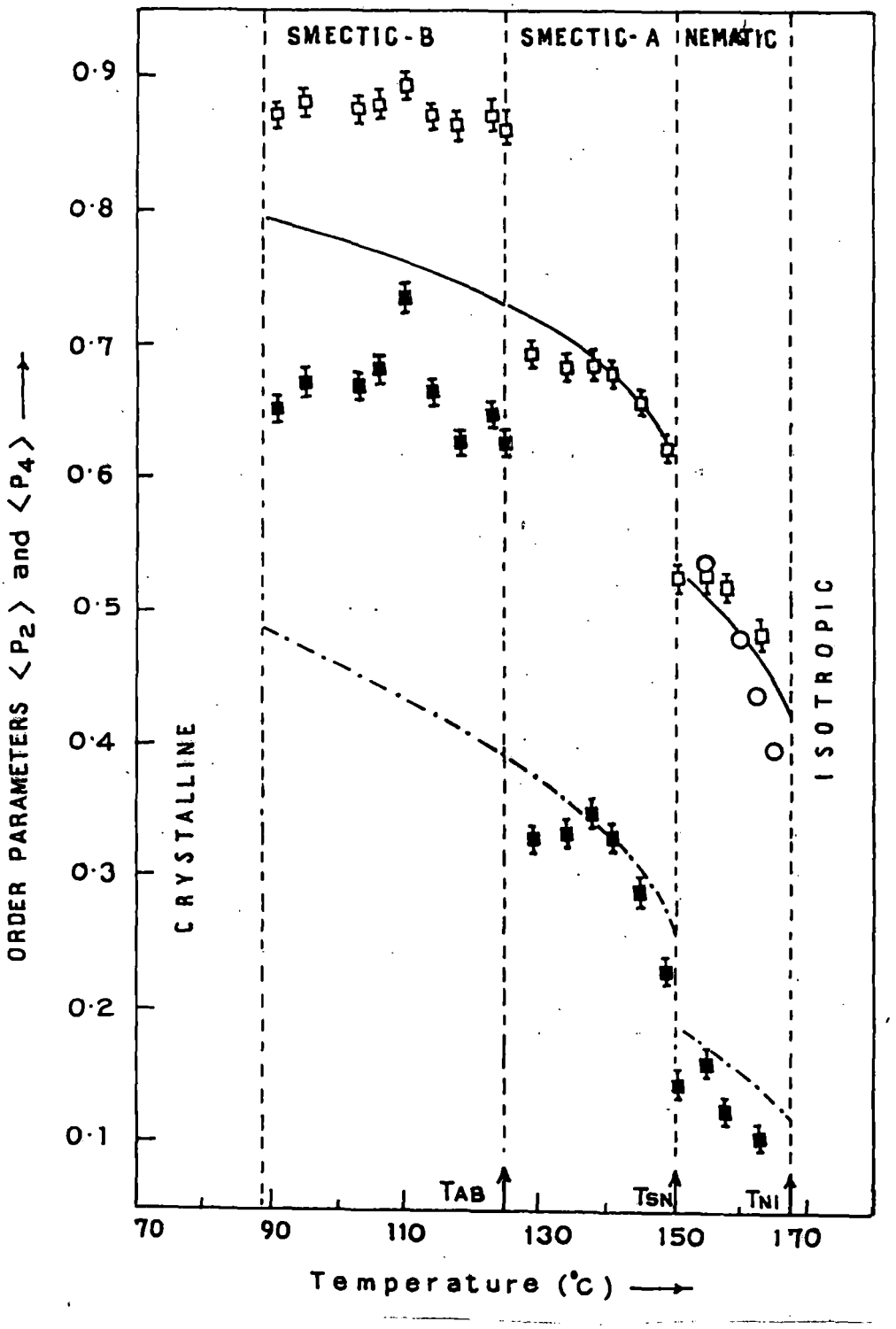

Figure 6.2. Temperature dependences of $\langle P_2 \rangle$ and $\langle P_4 \rangle$ for HBAAB. Key to symbols : (□) x-ray data for $\langle P_2 \rangle$; (■) x-ray data for $\langle P_4 \rangle$; (o) refractive index data for $\langle P_2 \rangle$; Solid line is theoretical $\langle P_2 \rangle$ from McMillan's potential with α = o.45, δ = 0.595; dashed line is theoretical $\langle P_4 \rangle$ from McMillan's potential. T_{NI} = nematic - isotropic transition temperature ; T_{SN} = smectic A - nematic transition temperature; T_{AB} = smectic A - smectic B transition temperature.Vertical bars show estimated errors.

calculated $f(\beta)$, the orientational distribution function following the procedure described in chapter 2, which is given in table 6.2. The orientational order parameters (OOP) $\langle P_2 \rangle$ and $\langle P_4 \rangle$, as obtained from the x-ray data, have been plotted as function of temperature for HBAAB in Figure 6.2. It is seen from Figure 6.2 that the nematic - smectic A phase transition is of the first order, since the values of $\langle P_2 \rangle$ and $\langle P_4 \rangle$ change abruptly in passing from the nematic to the smectic A phase. Values of $\langle P_2 \rangle$ and $\langle P_4 \rangle$ at different temperatures are shown in table 6.3. Figure 6.1(c) shows the x-ray diffraction photograph of a monodomain sample in the smectic B phase at 123°C, with the incident x-ray beam parallel to the smectic layers. The resultant x-ray diffraction photograph shows the presence of elongated bars of relatively intense diffuse scattering on both sides of the equatorial maxima. The widths of these bars are quite sharp. The smectic A - smectic B transition is also marked by sharp discontinuities in the order parameter values indicating first order phase transition. The OOP values in the nematic and smectic A phase of HBAAB show significant temperature dependence, while the order parameter values in the smectic B phase of this compound are found to be almost independent of temperature. The $\langle P_2 \rangle$ and $\langle P_4 \rangle$ values within the smectic B phase are also relatively higher than the neighbouring smectic A phase. This seems to indicate that the smectic B phase of this compound is of the crystal B type [8] unlike the hexatic B phase which undergoes a second order hexatic-B to smectic A phase transition [9]. It may be mentioned that although the approximation [10] used for calculating $\langle P_2 \rangle$ and $\langle P_4 \rangle$ is not valid for $\langle P_2 \rangle \gtrsim 0.8$, I are still reporting these order parameter values due to scarcity of available data on smectic B phase in the literature. These values at least give an estimation of the degree of order of a liquid crystal within the

smectic B phase.

I tried to fit the experimental order parameter values for HBAAB to those calculated from McMillan's theory for smectic A phase [2,3], using the potential parameters α (= 0.45) and δ (= 0.595) as adjustable constants and the theoretical curves are shown in Figure 6.2. The agreement of the experimental $\langle P_2 \rangle$ and $\langle P_4 \rangle$ values with the theoretical values is fairly good in the nematic and smectic A phases of HBAAB. The order of the nematic - smectic A phase transition as obtained experimentally is also reproduced from the theoretical calculations. However, agreement between the experimental order parameter values and those calculated from McMillan's theory in the smectic B phase is poor for the obvious reason that McMillan's theory is not applicable to smectic B phase.

I have also determined the translational order parameter (τ) for HBAAB, in the smectic phases from the experimental data where the second order meridional reflections were present, using a procedure described by Leadbetter and Norris [10]. These are compared with the values obtained from McMillan's theory in Figure 6.3. The agreement however is poor, which may be partly due to the crudeness of the model used for calculating τ from x-ray data. The experimentally determined τ values are very high in the smectic B phase which is as expected. The values of τ at different temperatures in smectic B phase and at one temperature in the smectic A phase of HBAAB is given in table 6.4.

The transverse correlation length, ξ, has been determined from linear scan of the diffraction peaks along the equatorial direction in the nematic and the smectic A phase of HBAAB. The x-ray intensity profile, which was first corrected for the use of a flat film, was next deconvoluted for finite width of the collimator based on a method of substitution of successive foldings [11]. The deconvoluted intensity profile I(q) was

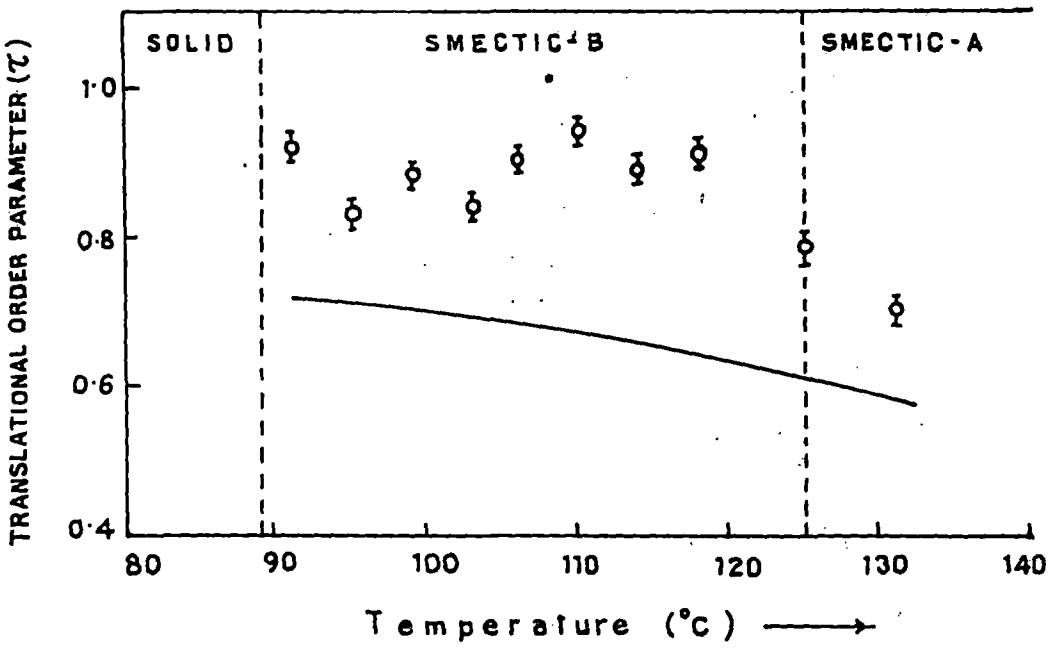

Figure 6.3. The translational order parameter (τ) for the smectic phases of HBAAB. o, experimental; ——— , theoretical values. Vertical bars show estimated errors.

fitted to a lorentzian form with a quadratic background viz,

$$I(q) = \frac{a_1}{a_2 + (q - q_o)^2} + a_3 q^2 + a_4 q + a_5 , \qquad 6.1$$

q being the magnitude of the scattering vector. a_1, a_2, a_3, a_4, a_5 and q_o are the fitting parameters. The correlation length is defined as $\xi = 2\pi(a_2)^{-1/2}$. Figure 6.4 shows the temperature variation of ξ in the smectic A and nematic phase of HBAAB, and the values of ξ at different temperatures is listed in table 6.5. The same procedure in the smectic B phase could not be carried out since the corrected intensity profile almost exactly matched the primary beam profile, implying very large value of ξ. It seems from Figure 6.4 that the correlation length varies continuously across the nematic - smectic A transition and does not diverge as in a second order phase transition. The rapid increase in ξ in the nematic phase near the smectic A - nematic transition is due to smectic fluctuations.

Figure 6.5 shows the density variation of HBAAB in the temperature range 90°C to 174°C. Also shown in the same figure is the birefringence Δn (= $n_e - n_o$) at wavelength λ = 5780 Å, in the nematic phase only of HBAAB. The refractive indices (n_o, n_e) and density of HBAAB at different temperatures is arranged in table 6.6. The principal polarizabilities (α_o, α_e) of the compound have been calculated using Neugebauer's [12] and Vuk's [13] method and are given in tables 6.7 and 6.8 respectively. The orientational order parameter $\langle P_2 \rangle$ values, which was calculated using the relation given in chapter 2, are also listed in tables 6.7 and 6.8 for the two methods. From the temperature variation of density it is seen that there are discontiniuties in the density values at the nematic - smectic A and smectic A - smectic B transition temperatures implying first

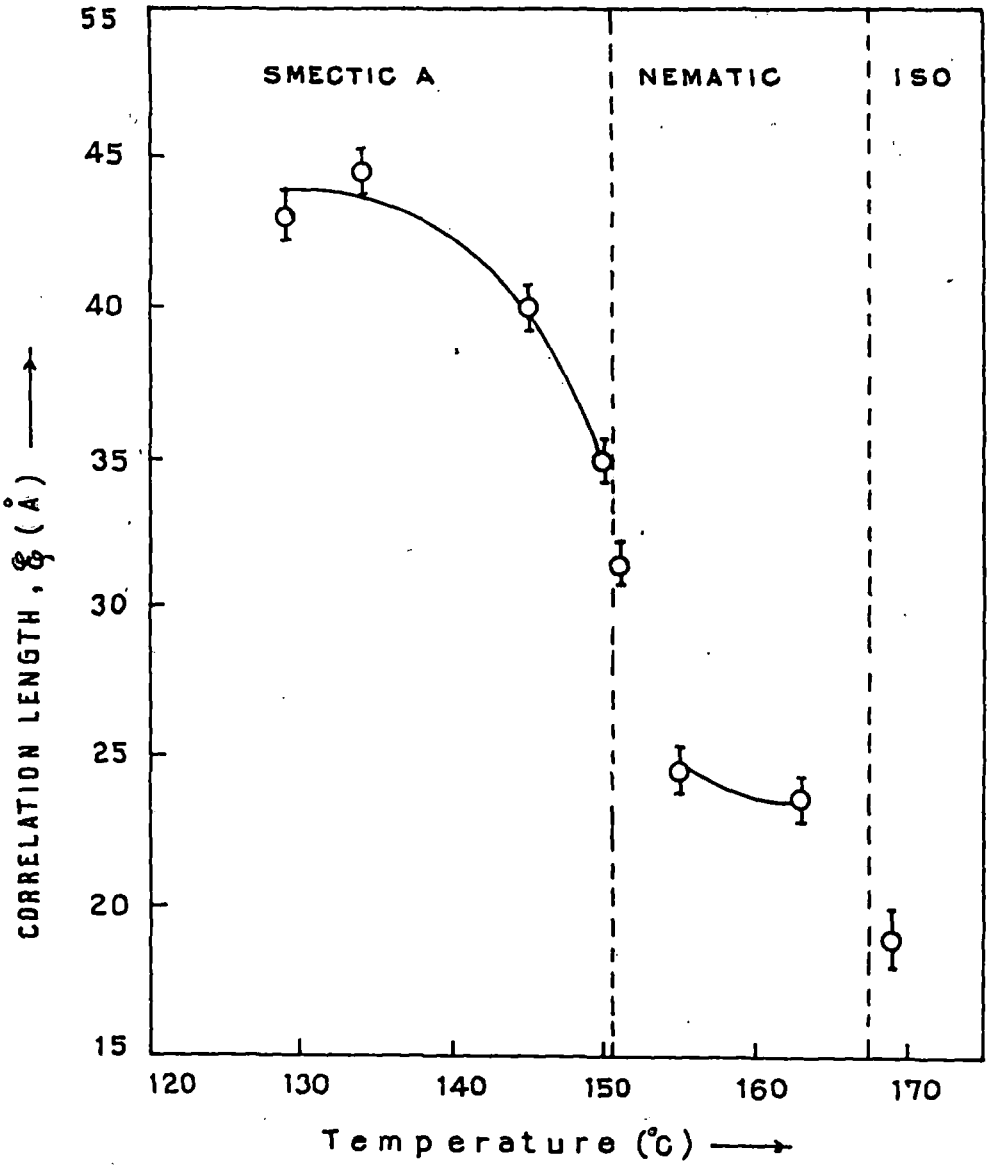

Figure 6.4. Variation of transverse correlation length ξ with temperature in the nematic and smectic A phases of HBAAB. Vertical bars show estimated errors. Solid line is guide to the eye only.

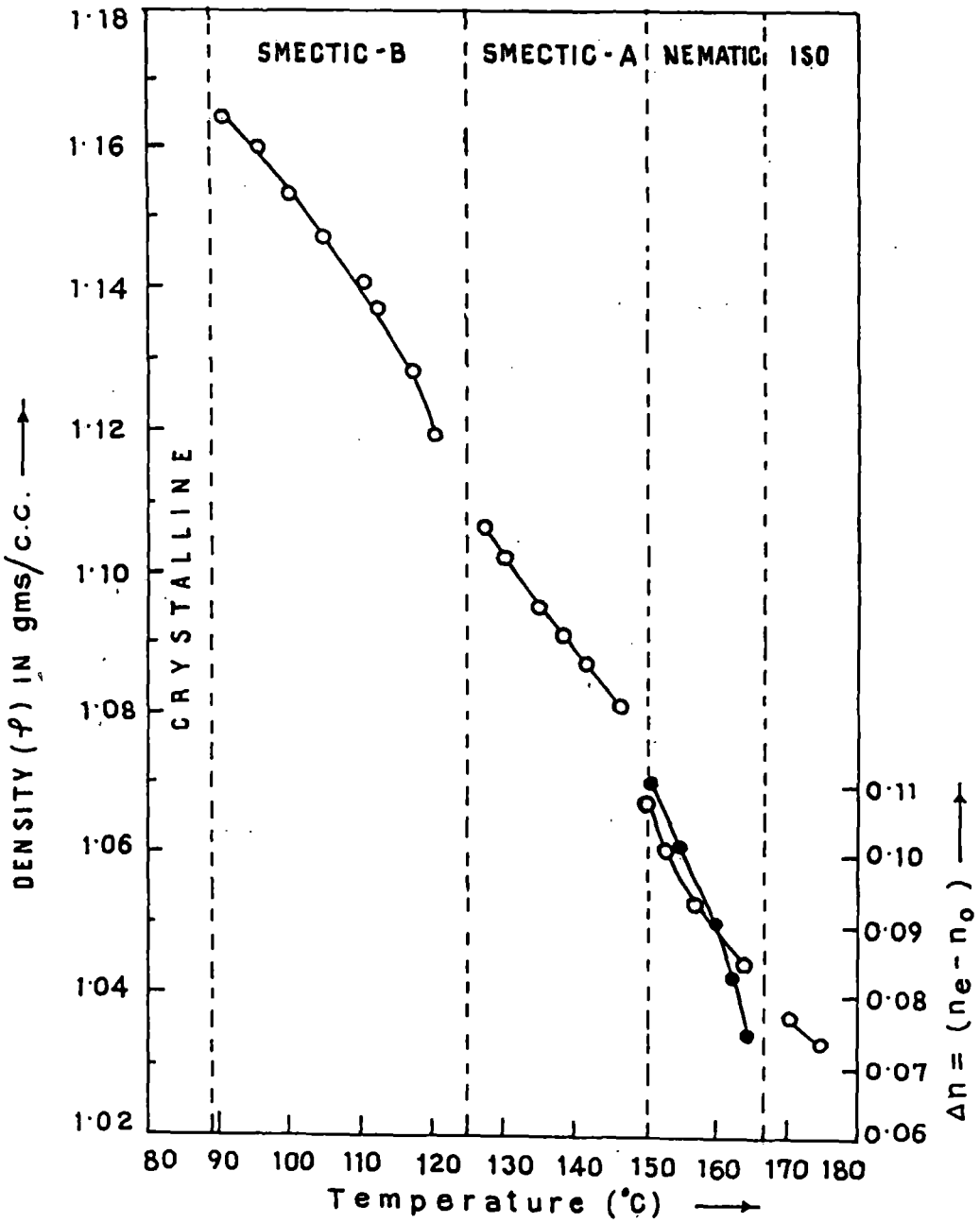

Figure 6.5. The density and birefringence (Δn, in the nematic phase) values of HBAAB as functions of temperature; o density values; • birefringence values. Lines drawn are guide to the eye only.

order phase transitions in both the cases.

Orientational order parameter values obtained on analysing the refractive index and density data, as a function of temperature (in the nematic phase) using Neugebauer's procedure [12] are also shown in Figure 6.2. It is seen from Figure 6.2 that there is a rapid decrease in the order parameter values obtained from refractive index measurements close to the nematic - isotropic transition temperature T_c. This may be due to the fluctuation of the director, which is more pronounced near the transition temperature [14]. The order parameter values obtained from x-ray diffraction and refractive index studies agree quite well within experimental uncertainties.

Results for the temperature dependence of the apparent molecular length i.e., density wave parallel to the director in nematic phase (l) and layer thickness in smectic phase (d) are given in Figure 6.6. It is seen that the layer thickness in the smectic phases and the apparent molecular length in the nematic phase are almost equal and temperature independent. The mean value of d or l is (26.15 ± 0.12) Å which is in close agreement with the molecular model length of 26.45 Å, (in the completely extended form), indicating absence of molecular associations throughout the mesomorphic range of HBAAB. This also implies that the molecules are in completely extended form in the mesophases inspite of the presence of rather long and flexible heptyl chain. In Figure 6.7 I have plotted the variation of the intermolecular distance, D, with temperature for HBAAB. The D values are found to increase with increasing temperatures, accompanied by abrupt jumps at the smectic B - smectic A and smectic A - nematic transition temperatures again indicating the order of the transition in these to be first order. The D values in the nematic phase are found to increase with increasing temperatures which is probably due to increased thermal

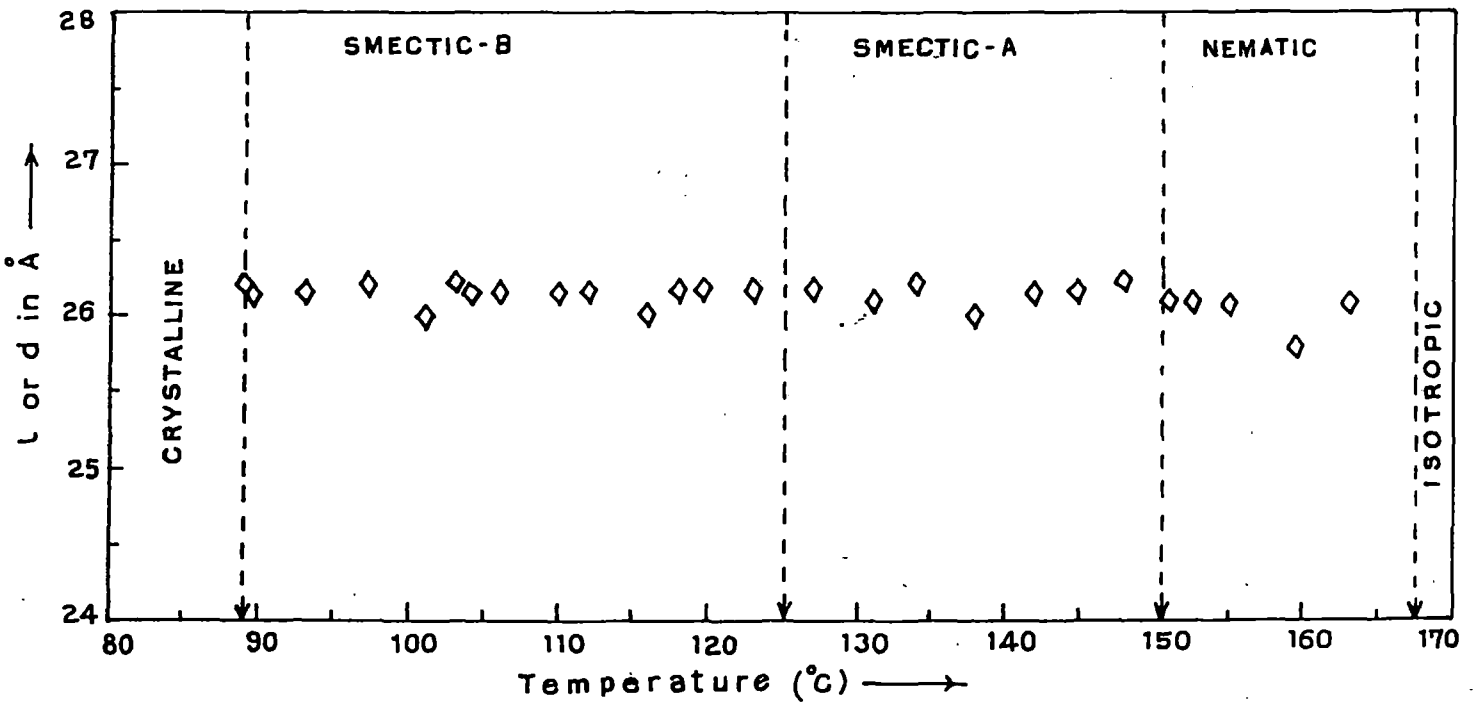

Figure 6.6. Variation of layer spacing (d) or apparent molecular length (l) with temperature. Estimated error is ± 0.15Å throughout the measured range.

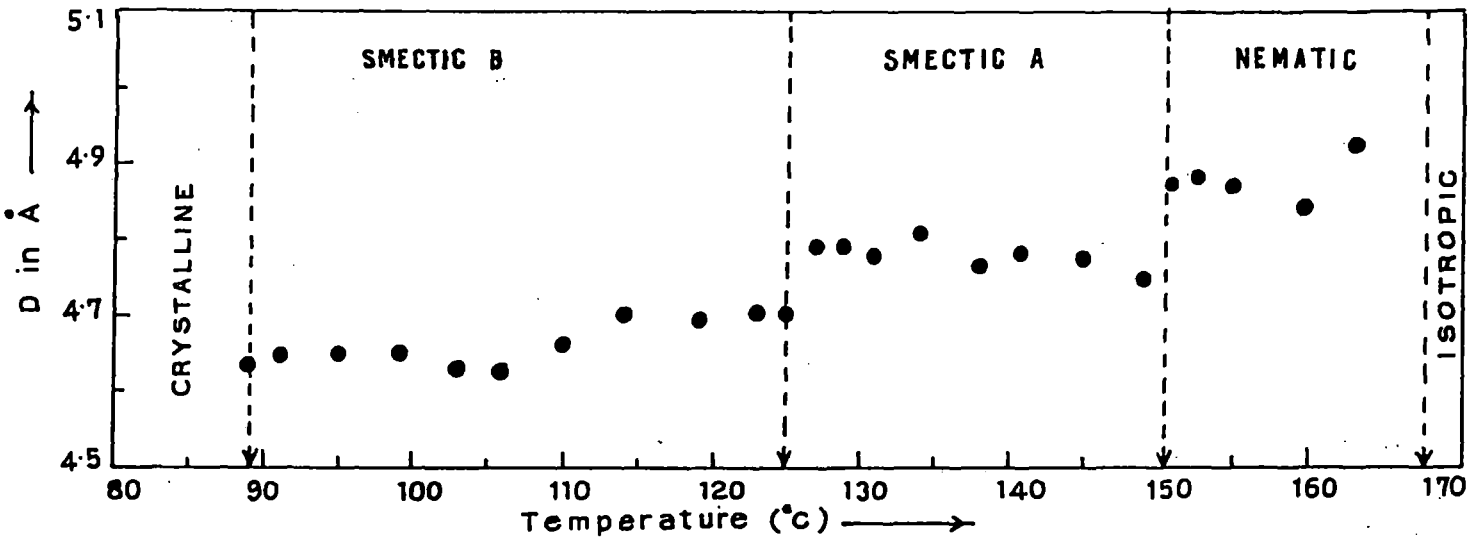

Figure 6.7. Variation of intermolecular distance D with temperature. Estimated errors are smaller than the size of the symbols used.

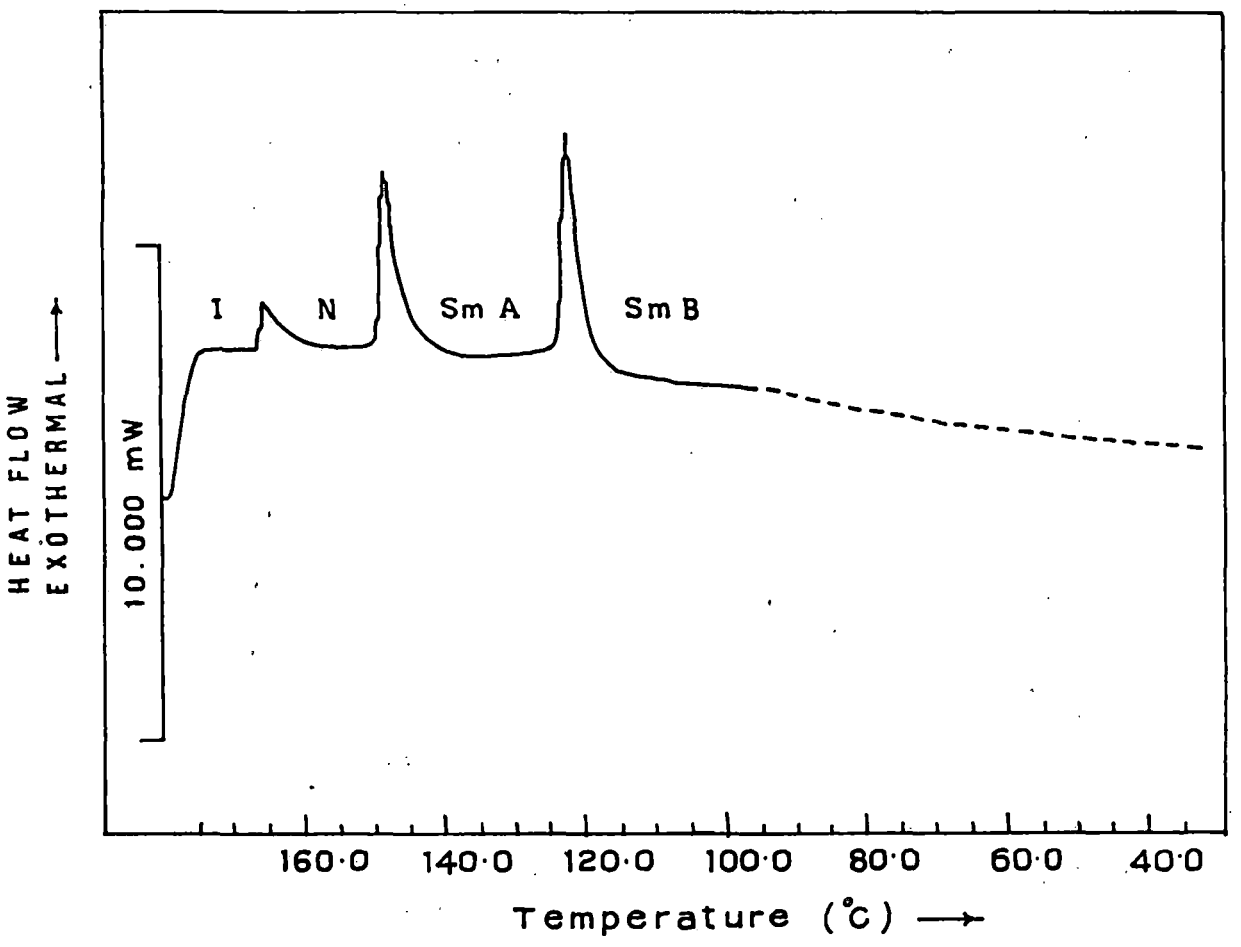

Figure 6.8. The DSC scan of HBAAB during cooling. I denotes isotropic phase, N denotes nematic phase, Sm A denotes smectic A phase and Sm B denotes smecic B phase.

vibrations. The values of l or d and the intermolecular distance D at different temperatures is given in table 6.9.

Figure 6.8 shows the DSC curve for HBAAB during cooling, and the enthalpy changes at the isotropic - nematic, nematic - smectic A and smectic A - smectic B phase transitions are listed in table 6.10. I have calculated ΔH_{SN}, the enthalpy change at the smectic A - nematic transition temperature (T_{SN}), from McMillan's theory taking the values of α and δ from the best fit theoretical curve to the experimental x-ray $\langle P_2 \rangle$ data (refer Figure 6.2). ΔH_{SN} is calculated from the following expression

$$\Delta H_{SN} = \frac{1}{2T^*_{SN}} [(\eta_S^2 - \eta_N^2) + \alpha\delta\tau^2 + \alpha\sigma^2)] NKT_{SN} \qquad 6.2$$

where $T^*_{SN} = kT_{SN}/v$. τ, σ and η_S, the order parameter in the smectic A phase, is calculated at a temperature just below the smectic A - nematic transition temperature; while η_N, the order parameter in the nematic phase, is calculated at a temperature just above the transition temperature. It is clear from table 6.10, that the behaviour of ΔH_{SN} at the NA transition is reproduced by the theory quite well. Following similar procedure I have calculated the enthalpy change at the nematic -isotropic phase transition as well. The experimental enthalpy change for nematic - isotropic phase transition is much smaller than the calculated value as seen in table 6.10. It seems that entropy change at the smectic A - nematic transition is much greater than that at the nematic - isotropic transition. This is also evident from Figure 6.5 which shows that the density change at nematic - isotropic transition is very small making the transition weakly first order. Such behaviour regarding smectic A - nematic and nematic - isotropic phase changes in a liquid crystalline mixture has also been reported [15]. No calculations of smectic B to smectic A enthalpy change is possible due to

unavailability of suitable model theory for this phase transition.

Table 6.1

Experimental intensity values I(ψ), in arbitrary units, of HBAAB after background correction.

ψ (degree)	I(ψ) values at different temperatures in ^{o}C						
	91.0	95.0	103.0	106.0	110.0	114.0	118.0
0	8.6	11.8	8.6	8.6	16.0	9.5	8.9
5	8.1	11.2	8.2	8.2	13.7	8.8	8.3
10	5.2	6.8	4.9	5.2	5.2	5.8	5.8
15	2.6	3.0	2.1	1.9	2.0	2.6	3.8
20	1.6	1.8	1.2	1.0	1.1	1.3	2.2
25	1.0	1.1	0.8	0.6	0.8	0.7	1.1
30	0.5	0.7	0.5	0.4	0.6	0.5	0.4
35	0.3	0.4	0.3	0.3	0.4	0.4	0.3
40	0.2	0.2	0.2	0.2	0.3	0.3	0.2
45	0.1	0.1	0.1	0.2	0.2	0.2	0.1
50	0.1	0.1	0.1	0.1	0.1	0.1	0.1
55	0.0	0.0	0.0	0.0	0.1	0.0	0.0
60	0.0	0.0	0.0	0.0	0.0	0.0	0.0
65	0.0	0.0	0.0	0.0	0.0	0.0	0.0
70	0.0	0.0	0.0	0.0	0.0	0.0	0.0
75	0.0	0.0	0.0	0.0	0.0	0.0	0.4
80	0.0	0.0	0.0	0.0	0.0	0.0	0.0
85	0.0	0.0	0.0	0.0	0.0	0.0	0.0
90	0.0	0.0	0.0	0.0	0.0	0.0	0.0

(continued)

Table 6.1

Experimental intensity values I(ψ), in arbitrary units, of HBAAB after background correction.

ψ (degree)	I(ψ) values at different temperatures in °C						
	123.0	125.0	129.0	134.0	138.0	141.0	145.0
0	11.8	8.6	25.4	24.0	29.7	28.7	31.6
5	11.2	8.1	25.0	23.4	28.8	27.3	31.0
10	6.4	5.4	24.1	21.2	25.6	23.5	29.3
15	3.7	3.3	21.3	17.8	19.9	18.6	24.1
20	2.2	1.9	16.8	13.0	14.8	15.1	18.4
25	1.1	1.0	12.2	9.1	10.7	11.7	15.2
30	0.8	0.6	7.7	6.2	6.9	8.2	11.0
35	0.4	0.3	4.6	4.5	5.3	5.2	6.9
40	0.2	0.2	2.9	3.4	3.8	3.4	5.2
45	0.1	0.1	2.1	2.5	2.7	2.4	3.5
50	0.0	0.1	1.6	1.8	2.0	1.9	2.5
55	0.0	0.0	1.1	1.3	1.6	1.4	2.0
60	0.0	0.0	0.8	0.8	1.2	1.1	1.4
65	0.0	0.0	0.6	0.6	0.9	0.8	1.0
70	0.0	0.0	0.5	0.3	0.6	0.6	0.7
75	0.0	0.0	0.3	0.3	0.3	0.4	0.4
80	0.0	0.0	0.2	0.1	0.2	0.2	0.3
85	0.0	0.0	0.1	0.0	0.1	0.0	0.1
90	0.0	0.0	0.0	0.0	0.0	0.0	0.0

(continued)

Table 6.1

Experimental intensity values $I(\psi)$, in arbitrary units, of HBAAB after background correction.

ψ (degree)	$I(\psi)$ values at different temperatures in ^{o}C				
	149.0	151.0	155.0	158.0	163.0
0	17.6	15.1	17.0	12.5	12.6
5	16.7	15.0	16.4	12.3	12.2
10	14.8	14.1	14.9	11.4	11.1
15	12.8	13.1	12.8	10.1	10.0
20	10.0	11.6	11.2	9.0	8.9
25	8.4	9.4	8.8	7.8	7.8
30	6.7	7.4	7.4	6.4	6.6
35	5.2	6.1	5.9	5.2	5.7
40	4.0	4.9	5.0	4.3	4.6
45	2.7	3.9	4.2	3.4	3.8
50	1.9	3.1	3.4	2.7	3.0
55	1.2	2.3	2.8	2.1	2.4
60	0.8	1.7	2.2	1.6	2.0
65	0.5	1.4	1.6	1.1	1.4
70	0.3	1.1	1.0	0.6	0.9
75	0.2	0.7	0.6	0.4	0.6
80	0.1	0.4	0.3	0.2	0.4
85	0.0	0.2	0.1	0.1	0.2
90	0.0	0.0	0.0	0.0	0.0

Table 6.2

Normalised distribution function $f(\beta)$ values of HBAAB at different temperatures.

β (degree)	$f(\beta)$ values at different temperatures in ^{o}C						
	91.0	95.0	103.0	106.0	110.0	114.0	118.0
0	29.62	32.20	33.08	44.78	13.66	31.37	23.93
5	26.47	28.59	29.32	38.84	13.10	28.00	21.86
10	18.67	19.71	20.06	24.49	11.50	19.64	16.60
15	10.00	9.98	9.95	9.51	9.10	10.27	10.34
20	3.80	3.24	3.02	0.36	6.36	3.52	5.20
25	1.10	0.60	0.39	-1.71	3.84	0.57	2.15
30	0.73	0.56	0.47	0.06	1.98	0.29	0.89
35	0.91	1.00	1.01	1.64	0.92	0.74	0.53
40	0.69	0.81	0.84	1.36	0.46	0.76	0.36
45	0.16	0.18	0.20	0.12	0.28	0.34	0.16
50	-0.17	-0.22	-0.21	-0.59	0.15	-0.04	0.01
55	-0.13	-0.17	-0.15	-0.32	0.01	-0.10	-0.02
60	-0.07	0.08	0.11	0.26	-0.08	0.03	0.02
65	0.15	0.18	0.20	0.44	-0.07	0.11	0.04
70	0.05	0.07	0.07	0.14	-0.01	0.05	0.02
75	-0.06	-0.07	-0.08	-0.19	0.04	-0.03	-0.02
80	-0.07	-0.09	-0.10	-0.21	0.03	-0.05	-0.02
85	0.00	0.00	0.00	-0.00	0.00	0.00	0.00
90	0.04	0.05	0.05	-0.02	0.13	0.03	0.05

(continued)

Table 6.2

Normalised distribution function $f(\beta)$ values of HBAAB at different temperatures.

β (degree)	$f(\beta)$ values at different temperatures in ^{o}C						
	123.0	125.0	129.0	134.0	138.0	141.0	145.0
0	29.93	25.82	6.84	9.55	10.70	11.40	8.12
5	26.67	23.35	7.14	9.28	10.46	10.35	8.12
10	18.63	17.17	7.63	8.46	9.43	8.13	7.75
15	9.80	10.06	7.33	7.09	7.36	6.14	6.54
20	3.62	4.60	5.87	5.34	4.97	4.78	4.85
25	1.08	1.75	4.02	3.56	3.15	3.72	3.43
30	0.87	0.87	2.53	2.14	2.04	2.64	2.48
35	1.08	0.74	1.51	1.27	1.37	1.61	1.77
40	0.76	0.55	0.86	0.86	0.92	0.88	1.15
45	0.12	0.20	0.48	0.68	0.60	0.50	0.67
50	-0.25	-0.04	0.29	0.53	0.40	0.34	0.40
55	-0.17	-0.07	0.21	0.35	0.29	0.27	0.28
60	0.08	0.03	0.18	0.19	0.23	0.23	0.23
65	0.17	0.08	0.14	0.10	0.20	0.18	0.19
70	0.06	0.03	0.09	0.07	0.12	0.10	0.13
75	-0.07	-0.03	0.05	0.06	0.06	0.05	0.06
80	-0.08	-0.04	0.02	0.04	0.03	0.02	0.02
85	0.00	0.00	0.01	0.01	0.01	0.01	0.01
90	0.05	0.00	0.00	0.00	0.00	0.01	0.00

(continued)

Table 6.2

Normalised distribution function $f(\beta)$ values of HBAAB at different temperatures.

β (degree)	$f(\beta)$ values at different temperatures in ^{o}C				
	149.0	151.0	155.0	158.0	163.0
0	8.61	4.68	6.51	5.62	5.54
5	8.35	4.87	6.43	5.47	5.37
10	7.38	5.11	5.97	5.01	4.83
15	5.67	4.80	4.91	4.30	4.01
20	3.99	3.89	3.65	3.54	3.20
25	2.92	2.97	2.70	2.92	2.63
30	2.41	2.37	2.15	2.44	2.29
35	2.07	1.97	1.78	2.00	2.01
40	1.57	1.54	1.41	1.53	1.62
45	0.98	1.07	1.03	1.12	1.19
50	0.57	0.72	0.76	0.83	0.86
55	0.36	0.54	0.63	0.66	0.68
60	0.27	0.47	0.58	0.54	0.59
65	0.19	0.40	0.49	0.40	0.48
70	0.10	0.28	0.30	0.23	0.31
75	0.04	0.14	0.12	0.10	0.15
80	0.01	0.06	0.04	0.04	0.06
85	0.00	0.03	0.02	0.02	0.03
90	0.00	0.02	0.01	0.01	0.02

Table 6.3

Sample : HBAAB

Variation of $\langle P_2 \rangle$ and $\langle P_4 \rangle$ with temperature.

Temp. in ^{o}C	$\langle P_2 \rangle$	$\langle P_4 \rangle$
91.0	0.873	0.652
95.0	0.882	0.673
103.0	0.876	0.670
106.0	0.879	0.684
110.0	0.899	0.735
114.0	0.872	0.666
118.0	0.864	0.628
123.0	0.873	0.649
125.0	0.862	0.626
129.0	0.693	0.327
134.0	0.684	0.331
138.0	0.685	0.348
141.0	0.681	0.329
145.0	0.658	0.289
149.0	0.624	0.229
151.0	0.526	0.144
155.0	0.526	0.160
158.0	0.519	0.125
163.0	0.485	0.105

Table 6.4

Translational order parameter (τ) at different temperatures in the smectic B phase of HBAAB.

Temp. in ^{o}C	τ_1
91.0	0.920
95.0	0.830
99.0	0.875
103.0	0.843
106.0	0.900
110.0	0.940
114.0	0.887
118.0	0.903
125.0	0.776
131.0(smectic A)	0.702

Table 6.5

Transverse correlation length ξ at different temperatures for HBAAB.

Temp. in ^{o}C	$\xi \pm 0.75$
129.0	43.05
134.0	44.65
145.0	40.14
149.0	35.07
151.0	31.46
155.0	24.61
163.0	23.58
169.0(iso)	18.87

Table 6.6

Density (ρ) and refractive indices (n_o, n_e) at different temperatures of HBAAB for λ = 5780 Å.

Temp. in °C	Density (ρ) in gms/c.c.	n_o	n_e
90.0	1.165	1.542	——
95.0	1.160	1.543	——
100.0	1.154	1.544	——
105.0	1.147	1.545	——
110.0	1.140	1.546	——
115.0	1.131	1.548	——
120.0	1.222	1.550	——
128.0	1.106	1.554	——
130.0	1.103	1.555	——
135.0	1.095	1.556	——
140.0	1.089	1.558	——
145.0	1.083	1.564	——
151.0	1.067	1.596	1.706
155.0	1.057	1.602	1.703
160.0	1.049	1.610	1.700
162.5	1.046	1.615	1.697
165.0	1.043	1.620	1.694
167.5(iso)	1.040	1.640	1.640
174.0(iso)	1.025	1.637	1.637

Table 6.7

Polarizabilities (α_o, α_e) and order parameters at different temperatures in the nematic phase of HBAAB by Neugebauer's method.

Temp. in ^oC	α_o	α_e	$\langle P_2 \rangle$
155.0	50.83	59.34	0.537
160.0	51.81	59.44	0.481
162.5	52.34	59.30	0.439
165.0	52.88	59.16	0.396

(α_o, α_e) are in 10^{24} cm^3 unit

Table 6.8

Polarizabilities (α_o, α_e) and order parameters at different temperatures in the nematic phase of HBAAB by Vuk's method.

Temp. in ^oC	α_o	α_e	$\langle P_2 \rangle$
155.0	50.10	60.78	0.548
160.0	51.16	60.74	0.491
162.5	51.75	60.49	0.448
165.0	52.34	60.24	0.407

(α_o, α_e) are in 10^{24} cm^3 unit

Table 6.9

Temperature variation of apparent molecular length (l) or layer spacing (d) and intermolecular distance, D , of HBAAB.

Temp. in ^{o}C	l or d in $\AA$	Temp. in ^{o}C	D in $\AA$
89.0	26.24	89.0	4.63
90.5	26.18	91.0	4.65
93.0	26.18	95.0	4.65
97.0	26.24	99.0	4.65
101.0	26.01	103.0	4.63
103.0	26.24	106.0	4.63
104.0	26.18	110.0	4.66
106.0	26.18	114.0	4.70
112.0	26.18	118.0	4.69
116.0	26.01	123.0	4.70
118.0	26.18	125.0	4.70
119.0	26.18	127.0	4.79
123.0	26.18	129.0	4.79
127.0	26.18	131.0	4.78
131.0	26.18	134.0	4.81
134.0	26.24	138.0	4.76
138.0	26.01	141.0	4.78
142.0	26.18	145.0	4.78
145.0	26.18	149.0	4.75
148.0	26.24	151.0	4.75
151.0	26.10	152.25	4.87
152.25	26.10	155.0	4.89
155.0	26.10	158.0	4.87
159.5	25.81	159.5	4.84
163.0	26.10	163.0	4.92

Table 6.10

Enthalpy change associated with different phase transition of HBAAB.

Temp. in ^{0}C.	ΔH(J/G) Experimental	ΔH(J/G) Calculated
125.0	2.233	——
150.5	3.557	3.040
167.5	0.857	3.912

REFERENCES

[1]. G. Fishel and R. Patel, *Mol.Cryst. Liq. Cryst.*, 17, 139(1972).

[2]. W.L. McMillan, *Phys. Rev.*, A6, 936 (1972).

[3]. W.L. McMillan, *Phys. Rev.*, A8, 328 (1973).

[4]. D. Demus and L. Richter, *Textures of Liquid Crystals*, Verlag Chemie p. 158-159 (1978).

[5]. B. Bhattacharya, S. Paul and R. Paul, *Molec. Phys*, 44, 1391 (1981).

[6]. A.K. Zemindar, S Paul and R. Paul, *Mol. Cryst. Liq. Cryst.*, 61, 191 (1980).

[7]. H.P. Klug and L.E. Alexander, *X-ray Diffraction Procedure for Polycrystalline and Amorphous Materials*, John Wiley and Sons, New York, pp. 114 - 116 and pp. 473 - 474.

[8]. C.C. Huang, In K.J. Strandburg (Ed.) *Bond Orientational Order in Condensed Matter Systems*, Springer - Verlag, Berlin - New York , pp. 78-136.

[9]. R. Pindak, D.E. Moncton, S.C. Davey and J.W. Goodby *Phys. Rev. Lett.*, 46, 1135 (1981).

[10]. A.J. Leadbetter and E. K. Norris, *Molec. Phys.*, 38, 669 (1979).

[11]. S. Ergun, *J. Appl. Cryst.*, 1, 19 (1968).

[12]. H.E. J. Neugebauer, *Canad. J. Phys.*, 32, 1 (1954).

[13]. M.F. Vuks, Optics and Spectroscopy, 20, 361 (1966).

[14]. M. Mitra, S. Paul and R. Paul, *Pramana - J. Phys.*, 29,409 (1987).

[15]. M.K. Das, R. Paul and D.A. Dunmur, *Mol. Cryst. Liq. Cryst.*, 258, 239 (1995).

CHAPTER - 7

COMPARISON OF EXPERIMENTAL ORDER PARAMETERS OF NEMATOGENS WITH FABER'S THEORY

An alternative to Maier-Saupe mean field theory [1] for nematics has been suggested by Faber [2]. This theory is analogous to the spin-wave theory of ferromagnetism. According to Faber, the nematic medium is treated as a continuum with a perfectly aligned ground state, in which a spectrum of distortion modes involving splay, twist and bend are thermally excited with amplitudes determined by the Frank stiffness constants K_1, K_2 and K_3. It is argued that there cannot be more than 2N independent modes, where N is the number of molecules, and a cut-off is applied to the spectrum, resembling the cut-off used in the Debye theory of solids. The theory is used to predict values for the order parameter $\langle P_2 \rangle$ in terms of K_1, K_2 and K_3. Moreover, the theory predicts a very simple relationship between different orientational order parameters, $\langle P_n \rangle$s, which is easy to verify.

X-ray diffraction studies on a large number of different liquid crystalline samples have been reported from our laboratory [3-14]. Experimental orientational order parameters (OOP), $\langle P_2 \rangle$ and $\langle P_4 \rangle$ obtained from magnetically aligned nematic samples, have been compared earlier with Faber's Continuum theory (earlier) [15]. In continuation of this work, I have compared higher OOP's $\langle P_4 \rangle$, $\langle P_6 \rangle$ and $\langle P_8 \rangle$ of all the different liquid crystalline materials in their nematic range with the predictions of Faber's Continuum and Maier-Saupe mean field theories. In contradiction to previous finding regarding $\langle P_2 \rangle$ and $\langle P_4 \rangle$ [15], the agreement with Faber's theory is not good.

I have calculated the orientational distribution function $f(\beta)$ from the X-ray diffraction intensity distribution $I(\psi)$, using the expression derived by Leadbetter and Norris [16]:

$$I(\psi) = C \int_{\beta=\psi}^{\pi/2} f(\beta) \sec^2 \psi \, [\tan^2 \beta - \tan^2 \psi \,]^{-1/2} \sin\beta \, d\beta. \qquad (7.1)$$

The derivation of this equation and meaning of the symbols are given in the original paper of Leadbetter and Norris [16]. A method of calculating $f(\beta)$ as a polynomial of $\cos^2\beta$ is given by Bhattacharjee et al [3] and also discussed in detail in chapter 2. I have reanalysed all the previous measurements of $I(\psi)$ to calculate normalised $f(\beta)$ upto $\cos^{14}\beta$ term. Since the coefficients of $\cos^n\beta$ in the expression for $f(\beta)$ at first increase but later decrease with increasing n, not much error is incurred by truncating the series after the term containing $\cos^{14}\beta$. Then, integrating $P_{2n}f(\beta)$ over all possible orientations, $\langle P_{2n}\rangle$ (n = 1 to 5) can be obtained easily.

I have also tried an alternative method of calculating $\langle P_n\rangle$. Using the relation,

$$f(\beta)=\sum_{n=1}^{5}\frac{4n+1}{2}\langle P_{2n}\rangle P_{2n}(\cos\beta), \qquad (7.2)$$

one can write P_{2n}s as polynomials in $\cos^2\beta$ and hence equate the coefficients of $\cos^2\beta$, $\cos^4\beta$,.....,$\cos^{10}\beta$ on either side of equation (1). The coefficients on the right hand side of the equation contain $\langle P_2\rangle$, $\langle P_4\rangle$,....,$\langle P_{10}\rangle$. By solving the five simultaneous equations, the values of $\langle P_2\rangle$ etc. were determined. However, these values are quite different from those obtained from the previous method. Sometimes the calculated value of $\langle P_2\rangle$ was even greater than 1. The reason for this is not difficult to understand. The coefficient of $\cos^{10}\beta$ contains only $\langle P_{10}\rangle$ and its value is determined by the coefficient of $\cos^{10}\beta$ in $f(\beta)$ expansion. However, the higher coefficients are more likely to have larger relative errors, hence not only $\langle P_{10}\rangle$ calculated in this manner is subject to large error, this error is added to the value of $\langle P_8\rangle$, when it is calculated from the coefficient of $\cos^8\beta$ and so on. Hence, all errors accumulate in the value of

$\langle P_2 \rangle$, which becomes often unrealistic. Hence this method was not used to calculate order parameters in this chapter.

Faber's continuum theory [2] predicts that $\ln\langle P_n \rangle / \ln\langle P_m \rangle = n(n+1)/m(m+1)$, which is independent of both the nature of the compound and the experimental temperature. In this chapter I have analysed data for 22 nematogens. including two recently obtained compounds, viz, ethyl and heptyl members of the 5-(4-alkylcyclohexyl)- 2-(4 cyanophenyl)- pyrimidine series [17]. It has been already shown that this relation holds surprisingly well for the ratio of the logarithms of $\langle P_2 \rangle$ and $\langle P_4 \rangle$ [15]. In table 7.1, I have compared the ratios containing higher order parameters, as obtained from our experimental data, with those predicted from Faber's theory. It can be seen from table 7.1 that the ratios with higher OOP's deviate progressively more from Faber's theory. There is also more scatter in the experimental data, which is reflected in the rather large values of standard deviation of these ratios in table 7.1.

In Figure 7.1, I have plotted experimental $\ln\langle P_6 \rangle$ values against $\ln\langle P_4 \rangle$ together with the best fitted straight line through the experimental points and the curves according to Faber's and Maier-Saupe theories. The best fitted straight line has the following form:

$$\ln \langle P_6 \rangle = 0.4721 + 1.5203 \ln \langle P_4 \rangle \qquad (7.3)$$

I had to neglect one experimental point from our calculations, since $\langle P_6 \rangle$ value for this point was negative.

In Figure 7.2, the same procedure is followed for $\langle P_6 \rangle$ and $\langle P_8 \rangle$. Here I had to discard 18 experimental points because of negative $\langle P_8 \rangle$ values. It may not be out of place to mention that in no case negative $\langle P_2 \rangle$ or $\langle P_4 \rangle$ values was obtained from the experimental data. The best fitted straight line for this case is:

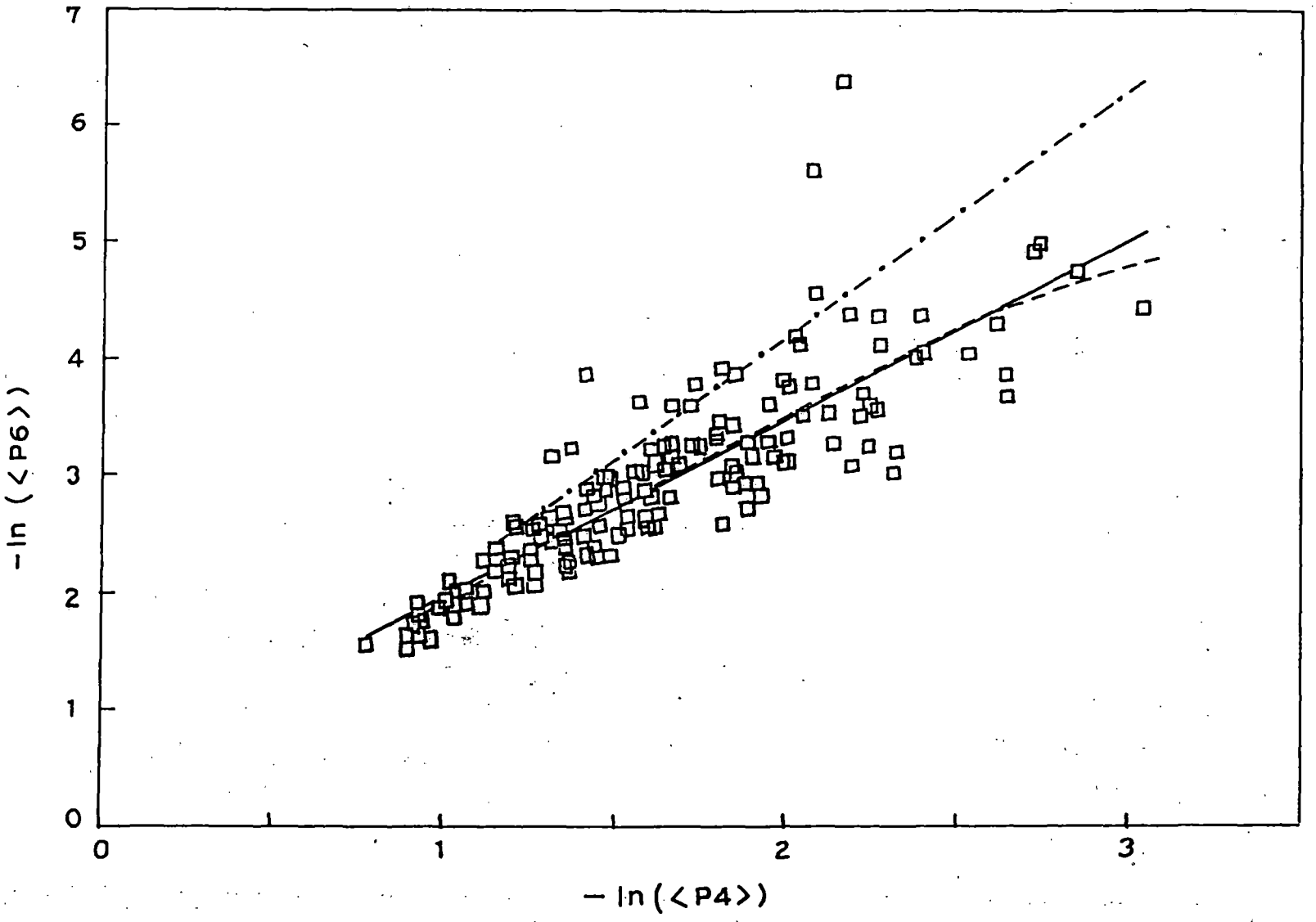

Figure 7.1. Comparison of experimental $\langle P_4 \rangle$ and $\langle P_6 \rangle$ values with different theories, □ , experimental values; ——·——·—,Maier - Saupe mean field theory;-·-·-·-·-·-·-·-, Faber's theory; ———, linear least square fit (equation (7.3)).

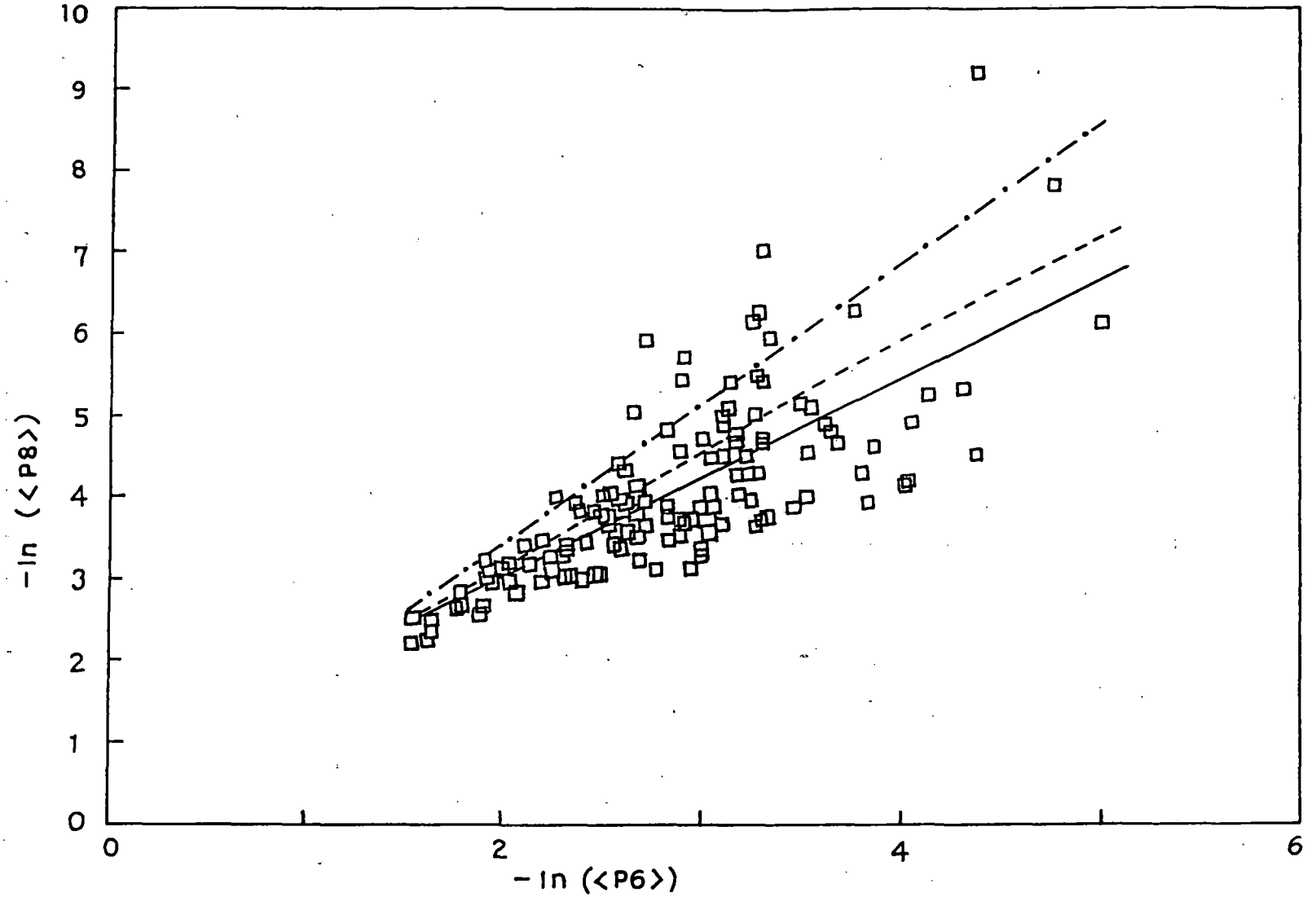

Figure 7.2. Comparison of experimental $\langle P_6 \rangle$ and $\langle P_8 \rangle$ values with different theories, □ , experimental values; ——·——·——, Maier - Saupe mean field theory;-·-·-·-·-·-·-·-·-·-, Faber's theory; ———, linear least square fit (equation (7.4)).

$$\ln \langle P_8 \rangle = 0.5937 + 1.2151 \ln \langle P_6 \rangle \qquad (7.4)$$

Both these figures show that the experimental lines are closer to Maier - Saupe curve than to the Faber's. However, no great significance may be given to this since experimental uncertainties and truncation errors due to series termination make the experimental values of $\langle P_6 \rangle$ and $\langle P_8 \rangle$ certainly more unreliable than $\langle P_2 \rangle$ or $\langle P_4 \rangle$. Estimated errors in the calculated $\langle P_2 \rangle$ and $\langle P_4 \rangle$ values are $\pm$ 0.02. Although error estimation have not been done for the calculated $\langle P_6 \rangle$ and $\langle P_8 \rangle$ values, however, these may be somewhat larger than 0.02.

It has been found before [15] that the ratio R1 (= $\ln\langle P_2 \rangle / \ln\langle P_4 \rangle$) is significantly larger for compounds having long rigid core. However, in the present work we do not find such variation in the ratios R2 and R3 for these molecules. We think more accurate experimental data are needed before any definite conclusion in this regard may be made.

Table 7.1

Comparison of theoretical with experimental values.

Ratio	Continuum theory	Mean Expt.values ($\pm$ s.d.)
R1 $=\ln\langle P_2\rangle/\ln\langle P_4\rangle$	0.300	0.308 $\pm$ 0.018
R2$=\ln\langle P_4\rangle/\ln\langle P_6\rangle$	0.476	0.530 $\pm$ 0.053
R3$=\ln\langle P_6\rangle/\ln\langle P_8\rangle$	0.583	0.739 $\pm$ 0.075

REFERENCES

[1]. W. Maier and A. Saupe Z. Natureforsch, 14a. 882 (1959) and 15a, 287 (1960).

[2]. T.E. Faber, Proc. R. Soc. A, 35, 247 (1977).

[3]. B. Bhattacharjee, S. Paul and R. Paul, Molec.Phys.,44, 1391, (1981).

[4]. B. Bhattacharjee, S. Paul and R. Paul, Mol. Cryst. Liq. Cryst. 89, 181 (1982).

[5]. B. Jha, B. Bhattacharjee, S. Paul and R. Paul, Phys.,Stat. Sol. (a), 72, 461 (1983).

[6]. B. Jha, A. Nandi, S. Paul and R. Paul, Mol. Cryst. and Liq. Cryst., 104, 289 (1984).

[7]. B. Jha, P. Mandal, S. Paul and R. Paul, Phase Transitions, 15, 39 (1989).

[8]. P. Mandal, R. Paul and S. Paul, Mol. Cryst. and Liq. Cryst. 131, 299 (1985).

[9]. P. Mandal, M. Mitra, B. Bhattacharjee, S. Paul and R. Paul, Mol. Cryst. and Liq. Cryst., 149, 203 (1987).

[10]. M. Mitra, R. Paul and S. Paul Mol. Cryst. and Liq. Cryst., 177, 71 (1989).

[11]. P. Mandal, M. Mitra, S. Paul and R. Paul, Liq. Cryst. 2, 183 (1987).

[12]. M. Mitra, B. Mazumdar, R. Paul and S. Paul Mol. Cryst. Liq Cryst., 180, 187 (1990).

[13]. B. Jha, A. Zeminder, S. Paul and R. Paul, North Bengal University Rev.,, 1, 123 (1980).

[14]. B. Mazumdar, Ph.D. Thesis, University of North Bengal (Unpublished data), 1988.

[15]. R. Paul, Liq. Cryst. 9, 239 (1991).

[16]. A.J. Leadbetter and E.K. Norris, Molec. Phys., 38, 669 (1979).

[17] S. Gupta, B. Mazumdar, P. Mandal, S. Paul and R. Paul,

Phase Transitions, 40, 73 (1992).

CHAPTER - 8

DETERMINATION OF ELASTIC CONSTANTS OF A POLAR - NONPOLAR MIXTURE SHOWING INJECTED SMECTIC PHASE

8.1 Introduction

Measurements of Frank elastic constants play an important role in characterising liquid crystal display devices. Especially, the ratio of the bend to splay elastic constants (K_3/K_1) is one of the controlling parameters affecting the sharpness of electro - optic response of display devices. Since, generally, no pure compound has the required nematic range, mixtures of mesomorphic compounds are used in nematic displays. One of the unusual aspects of binary liquid crystal mixtures of strongly dipolar and weakly dipolar mesogens is the formation of smectic phases, called injected smectic phases, from components which do not show smectic properties in their pure state [1-4]. Though the formation of injected smectic phase is undesirable in liquid crystal display (LCD) materials, its presence at a lower temperature than the working temperature of the LCD may be helpful under certain conditions [5]. With this view in mind I have measured the bend to splay elastic constant (K_3/K_1) ratios of a binary liquid crystalline mixture comprising of 4-n-pentyl -4′- cyanobiphenyl (5CB) and 4-n- pentyl phenyl - 4-n′- hexyloxy benzoate (ME6O.5) at different compositions. This mixture shows the presence of an injected smectic phase, some of the physical properties of which have been studied earlier in our laboratory by Das et al [6-8]. They have measured the refractive indices and density [6], as well as calculated orientation order parameters [7] and layer thickness [8] from x-ray diffraction studies [7,8] at different compositions of this mixture over their mesomorphic range.

One of the most convenient methods of determining elastic constants is from Freedericksz transition, where an electric or magnetic field is applied to deform a thin layer of surface

aligned nematogenic sample. Depending on the geometry of the arrangement, splay, twist or bend elastic constant can be determined from Freedericksz transition [9]. Measurements of the bend to splay elastic constant ratios have been carried out at different compositions of this mixture in their nematic phase only. Temperature dependence of (K_3/K_1) values for different compositions of the mixtures has been studied. The splay and bend elastic constants of n- pentyl cyanobiphenyl (5CB) have been widely reported by several authors [10-13]. In this chapter I have taken the (K_3/K_1) values of 5CB reported from our laboratory [13] by Das et al. Since no magnetic susceptibility anisotropy data on these mixtures have been reported so far it has not been possible to determine the individual values of the bend (K_3) and splay (K_1) elastic constants.

8.2 Experimental

The liquid crystal samples were donated by E. Merck, U.K. and were used without further purification. The chemical names, molecular structure and transition temperatures of the two components are given below:

Component 1: 4-n-pentyl -4'- cyanobiphenyl (5CB)

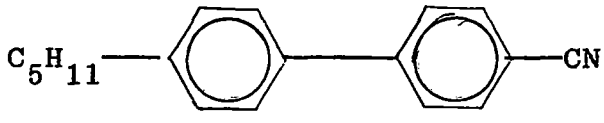

Solid $\xleftrightarrow{22.5^{\circ}C}$ Nematic $\xleftrightarrow{35.3^{\circ}C}$ Isotropic

Component 2: 4-n- pentyl phenyl - 4-n'- hexyloxy benzoate (ME6O.5)

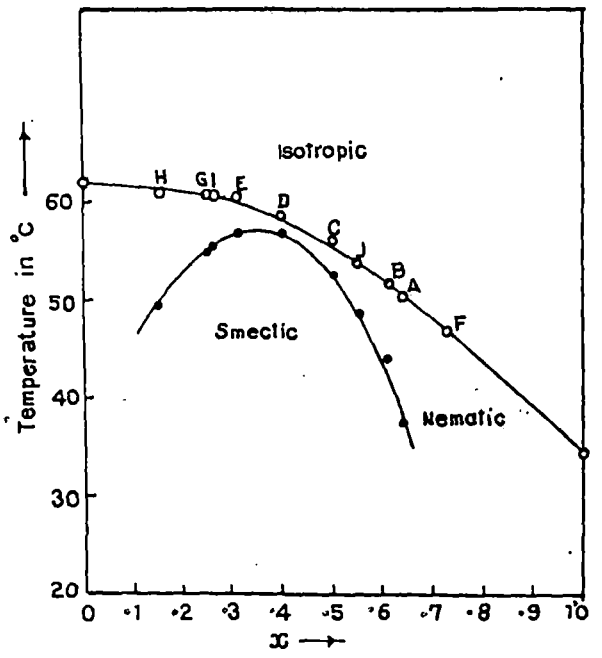

Figure 8.1 Temperature—concentration phase diagram for the binary system of 4-*n*-pentyl-4′-cyanobiphenyl (5CB) and 4-*n*-pentyl phenyl-4-*n*′-hexyloxy benzoate (ME6O.5). x is the mole fraction of 5CB. o nematic-isotropic transition temperature. • smectic-nematic transition temperature (reference 6).

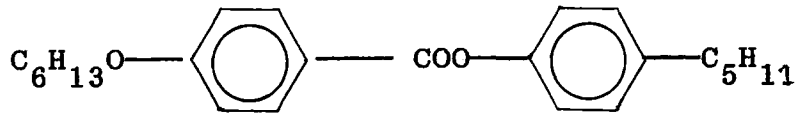

Solid $\underset{35.4^{\circ}C}{\overset{49.5^{\circ}C}{\rightleftharpoons}}$ Nematic $\overset{62.2^{\circ}C}{\rightleftharpoons}$ Isotropic

The phase diagram of this system as obtained by Das and Paul [6] is shown in Figure 8.1. The nematic-isotropic and induced smectic A-nematic phase transition temperatures are plotted against mole fraction of 5CB (x) in Figure 8.1 and the corresponding transition temperatures of different compositions of this mixture are shown in table 8.1. Mixtures for the same concentration (as given in Figure 8.1) were prepared by me, by weighing materials into a small glass bottle and mixing thoroughly by agitating the heated mixture in its isotropic state and keeping at that temperature for about twenty four hours to ensure the formation of a homogeneous mixture. The transition temperatures of the mixtures thus prepared were checked under a polarising microscope equipped with a Mettler FP-80/82 Thermo system, and were found to agree with the literature values [6].

The experimental set up for the determination of elastic constants has been described in chapter 2. The liquid crystal samples were filled in a specially surface treated glass cell of thickness of about 50μm. Depending upon the surface treatment, either planar or homeotropic alignment were produced. The cells were examined under a polarising microscope to check the uniformity of alignment before using in the experiment. The cells were placed in a brass thermostat with glass windows. The temperature of the thermostat was kept constant within $\pm$ 0.5°C during the experiment using a temperature controller (Indotherm-457). The sample cell with the thermostat was placed in a magnetic field with relevant

geometry [7] for the measurement of splay or bend elastic constant. A polarized light beam from sodium vapour lamp was passed through the cell and a crossed analyser was placed before a photomultiplier tube (RAC 931) used for measuring the transmitted light intensity. The current output from the photomultiplier tube was amplified and measured. The magnetic field was measured with the help of a calibration hall probe. The critical magnetic field for the Freedericksz transition could be observed quite accurately (within 0.5%) from the sudden change in the current from the photomultiplier tube. The relevant elastic constant K_i (i = 1,3) was calculated from the well known equation

$$K_i = H_c^2 \, d^2 \, \Delta\chi \, / \pi^2$$

where H_c is the critical field with geometry relevant for the particular elastic constant measurement, d the thickness of the sample and $\Delta\chi$ the magnetic susceptibility anisotropy. However, since no magnetic susceptibility data is available for this mixture, the value of the ratio K_3/K_1 is only given in this thesis.

8.3 Results and Discussions

The bend to splay elastic constant ratios (K_3/K_1) for different compositions of the binary mixture (ME60.5 + 5CB) was measured by me in the nematic phase only, since the bend elastic constant tends to infinity in smectic liquid crystals. The results are plotted in Figures 8.2 and 8.3. As mentioned in the introduction, the bend and splay elastic constants and their ratio (K_3/K_1) for 5CB have been reported earlier [13] from our laboratory. From Figure 8.2 it is seen that in the

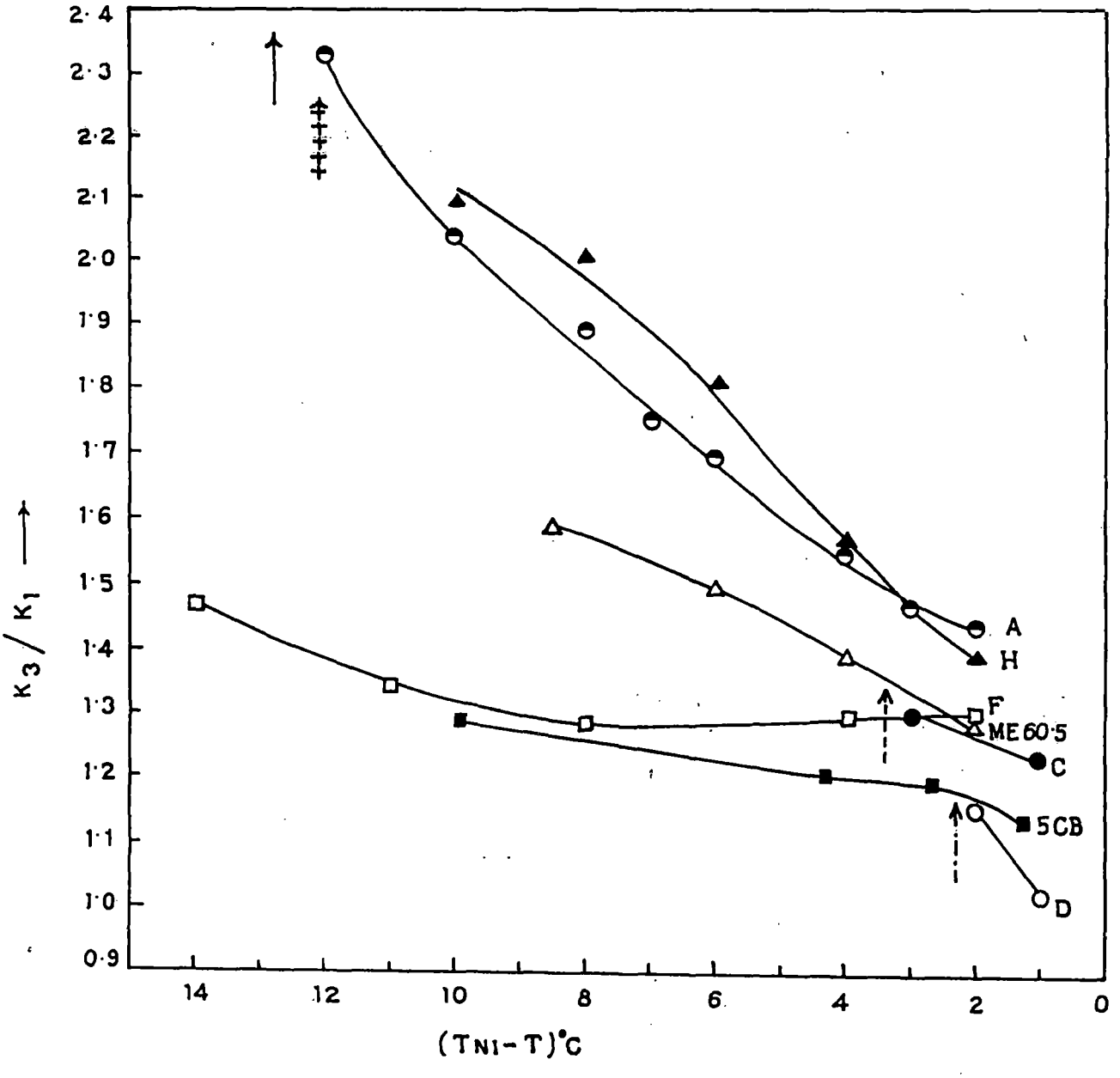

Figure 8.2 Ratio of the bend to splay elastic constants K_3/K_1 as function of relative temperature $(T_{NI}-T)^{\circ}C$ for the different mixtures and the pure compounds. Key to symbols : ◓ , mixture A, ↑ indicates smectic A - nematic transition temperature (T_{AN}) for mixture A; ● , mixture C, ↑ indicates T_{AN} for mixture C; ○ , mixture D, ↑ indicates T_{AN} for mixture D; □ , mixture F; ▲ , mixture H, ↑ indicates T_{AN} for mixture H; △ , ME60.5; ■ 5CB [13]. Lines drawn are guide to the eye only.

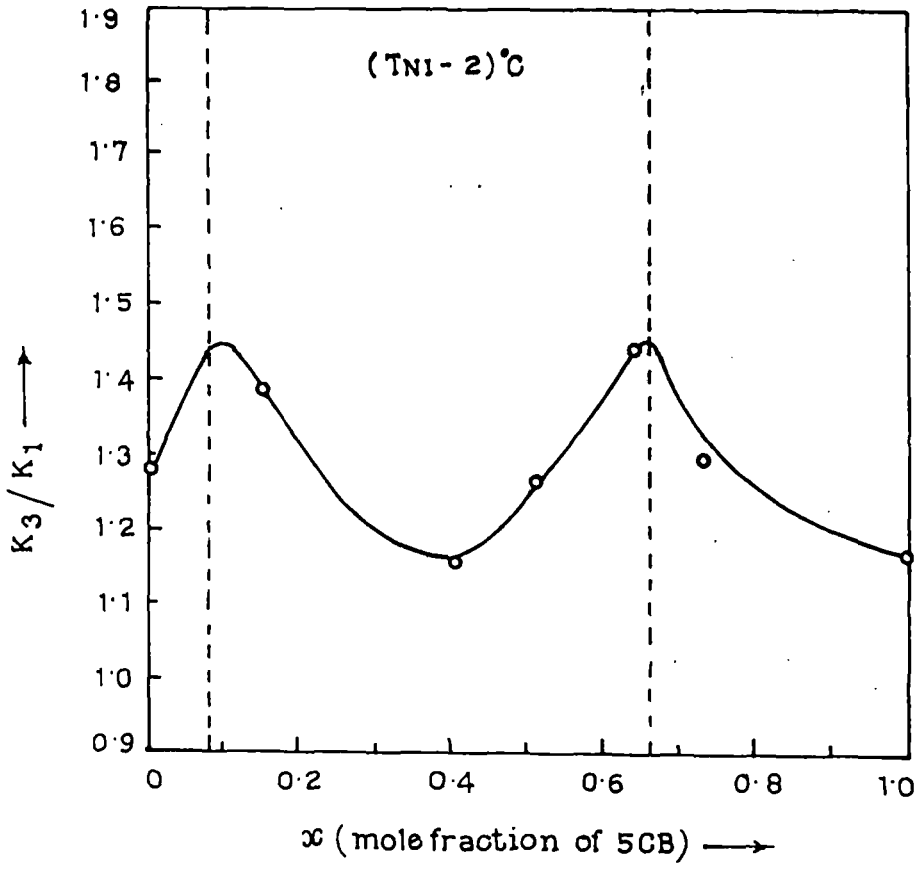

Figure 8.3 The bend to splay elastic constant ratios plotted against mole fraction of 5CB at a fixed relative temperature $(T_{NI} - 2)^{\circ}C$. Lines drawn are guide to the eye only. The dotted vertical lines indicate the extent of the injected smectic phase. x is the mole fraction of 5CB.

region of the phase diagram (Figure 8.1) where the mixtures show injected smectic phase, (Mixtures A,C,D and H) there is a sharp increase in the K_3/K_1 values particularly near the smectic A - nematic transition temperatures. This divergence of the bend to splay ratios has also been reported by Bradshaw et al in hybrid mixtures containing phenyl benzoate esters [14]. Possible reason for this may be formation of smectic clusters as pre-transitional effect. Since for smectics K_3/K_1 is almost infinity, the presence of these smectic clusters enhances the value of K_3/K_1. In mixture F, however, such rapid increase in K_3/K_1 values is not found, possibly because this mixture was studied in the temperature range which is far away from the injected smectic phase region. The K_3/K_1 values of ME60.5 are higher than that of 5CB. Temperature variation of K_3/K_1 ratio for ME60.5 is also greater than that for 5CB. The Frank elastic constant ratio's for different composition of this mixture, together with those of the pure compounds is included in table 8.2.

In Figure 8.3, I have plotted the K_3/K_1 values at $(T_{NI}-2)^{o}C$ against mole fraction of 5CB. It is clear from the figure that K_3/K_1 values, near the clearing temperature, show a minimum near equimolar concentration. Previous workers [6-8] have also observed a similar trend in the variation of birefringence [6], density [6],orientational order parameters $\langle P_2 \rangle$ and $\langle P_4 \rangle$ [7] and layer thickness [8] of this mixture. Similar behaviour have also been reported by Dunmur et al in a related mixture (ME50.5 + 5CB) [4]. Further analysis of the elastic constants data is not possible due to the absence of magnetic susceptibility data for the mixture (ME60.5 + 5CB) reported in this thesis. Magnetic susceptibility measurements on this mixtures are currently being done in our laboratory which will help in providing better physical understanding of this system.

Table 8.1

Mole fraction and transition temperatures of different mixtures [6].

Name of the mixtures	Mole fraction of 5CB	T_{AN} (^{o}C)	T_{NI} (^{o}C)
A	0.6455	37.8	50.6
C	0.5001	53.3	56.7
D	0.4017	56.7	59.0
F	0.7316	——	47.1
H	0.1504	49.5	61.6

Table 8.2

Sample : ME6O.5, 5CB and mixture F.

Temperature dependence of Frank elastic constant ratio's K_3/K_1.

ME6O.5		5CB*		mixture F	
$(T_{NI}-T)^{o}C$	K_3/K_1	$(T_{NI}-T)^{o}C$	K_3/K_1	$(T_{NI}-T)^{o}C$	K_3/K_1
2.0	1.28	1.3	1.14	2.0	1.31
4.0	1.39	2.7	1.20	4.0	1.30
6.0	1.50	4.3	1.21	8.0	1.28
8.5	1.59	10.0	1.29	11.0	1.33
				14.0	1.47

(continued)

* K_3/K_1 values taken from reference [13].

Table 8.2

Sample : mixture A, mixture C, mixture D and mixture H.

Temperature dependence of Frank elastic constant ratio's K_3/K_1.

mixture A		mixture C		mixture D		mixture H	
$(T_{NI}-T)^{\circ}C$	K_3/K_1	$(T_{NI}-T)^{\circ}C$	K_3/K_1	$(T_{NI}-T)^{\circ}C$	K_3/K_1	$(T_{NI}-T)^{\circ}C$	K_3/K_1
2.0	1.44	1.0	1 24	1.0	1.03	2.0	1.39
3.0	1.48	3.0	1.31	2.0	1.16	4.0	1.58
4.0	1.56					6.0	1.81
6.0	1.70					8.0	2.01
7.0	1.75					10.0	2.09
8.0	1.89						
10.0	2.04						
12.0	2.34						

REFERENCES

[1]. J. S. Dave, P. R. Patel and K.L.Vasant, Mol. Cryst. Liq.Cryst., 8, 93 (1969).

[2]. B. Engelen and F. Schneider, Z. Naturforsch.,33a, 1077 (1978).

[3]. C.S. Oh Mol. Cryst. Liq. Cryst., 42, 1 (1977).

[4]. D.A. Dunmur, R.G. Walker and P. Palffy-Muhoray, Mol.Cryst. Liq. Cryst. 122, 321 (1985)

[5]. N. V. Madhusudana, Liquid Crystals, Applications and uses, (Ed. B. Bahadur), World Scientific, Vol. 1, 1991.

[6]. M.K. Das and R. Paul, Phase Transitions, 46, 185 (1994).

[7]. M.K. Das and R. Paul, Phase Transitions, 48, 255 (1994).

[8]. M. K. Das and R. Paul, Mol. Cryst. Liq. Cryst., 260, 477 (1995)

[9]. W.H. de Jeu, Physical Properties of Liquid Crystalline Materials, Chapter 6, Gordon and Breach Science Publisher, New York, 1980.

[10]. P. Karat and N. V. Madhusudana, Mol. Cryst. Liq. Cryst., 40, 239 (1977).

[11]. H. Hakemi, E. F. Jagodzinski and D. B. Dupre, J. Chem. Phys., 78, 1513 (1983).

[12]. M. Hara, J. Hirakata, T. Tayooka, H. Takazoe and A. Fukuda, Mol. Cryst. Liq. Cryst., 122, 161 (1985).

[13]. M. K. Das and R. Paul, Mol. Cryst. Liq. Cryst. (in press).

[14]. M.J. Bradshaw and E.P. Raynes, Mol. Cryst. Liq. Cryst. 138, 307 (1986).

CHAPTER - 9

SUMMARY AND CONCLUSION

Liquid crystals are being increasingly used in display devices due to their extremely low power consumption. The knowledge of physical properties of a liquid crystal is essential for its application in a device. In the present dissertation I have reported the physical properties of different liquid crystalline samples as observed from x-ray diffraction, optical birefringence and elastic constant measurements. I am giving below, in a nutshell, the salient features of the different works undertaken by me.

A short review on the different types of liquid crystals especially, thermotropic liquid crystals, has been presented in chapter 1. Interest in liquid crystals in recent years has increased markedly leading to the discovery of more and more of exotic liquid crystalline mesophases in systems ranging from polymers to biological complexes. Since, it is impossible to cover all the mesophases and their peculiarities, I have concentrated only on those studied by me, namely the nematic, smectic A, smectic C and smectic B phases, and referred a few works which cover other aspects of liquid crystal research.

In chapter 2, I have descibed briefly the different theories of liquid crystals that have been tested in this dissertation. Detailed description of the x-ray diffraction technique and the analysis of the x-ray data leading to the values of orientational, translational and bond orientational order parameters, correlation length, layer thickness etc. has been given. A method to correct the experimental x-ray intensity data for finite width of the x-ray collimator and to analyse the corrected x-ray intensity profiles for correlation length determination has been given. Experimental procedure for the refractive index measurements by a thin prism method, as well as the method for calculation of the orientational order parameters

from this data have been outlined in this chapter. The bend and splay elastic constant measurements, the data analysis and the technique of preparing aligned samples have been treated.

In chapter 3, the orientational order parameters (OOP) in the smectic C and nematic phases of heptyloxyazoxybenzene (HAB) have been determined from x-ray diffraction and refractive index studies. Order parameters determined from x-ray studies have been corrected for the random orientation of the director in a cone in the smectic C phase of HAB. The orientational order parameters $\langle P_2 \rangle$ and $\langle P_4 \rangle$ as determined from x-ray diffraction studies are found to differ significantly from those calculated from refractive index measurements. Reason for this has been attributed to the different modes of alignment of the sample in the two methods. The transverse correlation length ξ was found to diverge near the smectic C - nematic transition temperature indicating that the transition is of second order. This trend has also been supported by density and refractive index measurements.

In chapter 4, results of small angle x-ray diffraction data from aligned samples of three bicyclohexane compounds (BPBCH, VPBCH and EPEBCH) in smectic B and nematic phase have been analysed to determine the Bond Orientational Order (BOO), Orientational order parameters (OOP), translational order parameter (TOP), layer thickness (in smectic B phase), apparent molecular length (in nematic phase) and lateral molecular distance as function of temperature. Bond orientational orders in the smectic B phase of these compounds are found to be nearly perfect and almost temperature independent throughout the phase. The smectic B phase of these compounds has been charecterised to be of the crystal B type. Correlation lengths in the smectic layer plane have also been estimated. The experimental OOP and

TOP values have been compared with McMillan's theory. From the temperature dependences of the orientational order parameters, layer thickness (d) in the smectic B phase or apparent molecular length (l) in the nematic phase and inter molecular distance (D) the order of the smectic B - nematic/isotropic and nematic/smectic B - isotropic phase transition has been found to be of the first order.

I have measured the refractive indices and densities of the three bicyclohexane alkenyl/alkenyloxy compounds, studied in chapter 4, in smectic B and nematic phases, results of which have been presented in chapter 5. These values of refractive indices and densities have been used to the calculate orientational order parameters in both smectic B and nematic phases. These order parameter values have been compared with those previously obtained by me for these mesogens from x-ray diffraction studies (Chapter 4). Reasons for discrepancy between the two sets of order parameter data have been discussed. For two of these compounds, the density change at smectic B-nematic transition is significantly greater than that at the nematic-isotropic transition. This implies greater entropy change at the smectic B-nematic transition than nematic-isotropic transition for these mesogens.

I have undertaken small angle x-ray diffraction study of 4-n-HeptyloxyBenzylidene - 4' - AminoAzoBenzene (HBAAB) in chapter 6. HBAAB has nematic, smectic A, smectic B and three crystalline phases. From x-ray diffraction studies of the aligned mesomorphic phases, the orientational order parameters ($\langle P_2 \rangle$ and $\langle P_4 \rangle$), transverse correlation length (ξ), translational order parameter (τ) and layer thickness in the smectic phases or apparent molecular length in the nematic phase and intermolecular distance have been calculated as function of

temperature. Both nematic - smectic A (NA) and smectic A - smectic B (AB) phase transitions are found to be of the first order. The HBAAB molecules remain in the fully extended form throughout the mesomorphic range and the smectic layers are mono molecular. Orientational order parameter values in the nematic and smectic A phases have been fitted satisfactorily with the calculated values from McMillan's theory with $\alpha = 0.45$ and $\delta = 0.595$. Refractive indices (n_o and n_e) have been measured in the nematic phase and $\langle P_2 \rangle$ calculated using both Neugebauer's and Vuk's formulae. These $\langle P_2 \rangle$ values agree within experimental uncertainties with those obtained from x-ray studies. Experimental enthalpy changes, obtained from DSC studies, have been compared with those calculted from McMillan's theory. While agreement between experimental and calculated enthalpy change at Sm A-N transition is quite good, the experimental enthalpy change at N-I transition is much smaller than the theoretical value. The density measurements also show a very small density change at the N-I transition, making it weakly first order.

Orientational order parameters $\langle P_4 \rangle$, $\langle P_6 \rangle$ and $\langle P_8 \rangle$, as calculated from the x-ray diffraction studies done in our laboratory, with aligned samples of nematogens, have been compared with the predictions of Faber's continuum and Maier - Saupe mean - field theories in chapter 7. In contradiction with previous findings regarding $\langle P_2 \rangle$ and $\langle P_4 \rangle$, the agreement with Faber's theory is not good. However, experimental inaccuracies and truncation errors during calculations preclude any definite conclusion in this matter.

The ratio of the bend to splay elastic constants of a binary liquid crystalline mixture (5CB/ME60.5) which show injected smectic phase, has been determined by Freedericksz transition in nematic phase, results of which have been reported in the last

chapter (chapter 8). It has been found that K_3/K_1 values show a divergence as the injected smectic phase is approached. The K_3/K_1 values also show a minimum near equimolar concentration, which is similar to the minimum in other physical properties of this mixture at this concentration found by previous workers. Magnetic susceptibility data at different compositions of this mixture will help in further understanding of this system.

LIST OF PUBLICATIONS

1. Comparison of Experimental Order Parameters of Nematogens with Faber's Theory - Banani Adhikari, Gurupada Chaudhuri and Ranjit Paul - Liquid Crystals 14, No.4, 1217, 1993
2. Orientational order parameters in the Smectic C and Nematic phase of Heptyloxy Azoxy Benzene (HAB), Banani Adhikari and Ranjit Paul, Mol. Cryst. Liq. Cryst., 261, 241, 1995.
3. Physical properties of three bicyclohexane compounds possessing smectic B phase I: X-ray diffraction technique, B. Adhikari and R. Paul, Phase Transitions, accepted for publication.
4. Physical properties of three bicyclohexane compounds possessing smectic B phase II: Refractive index and density measurements, B. Adhikari and R. Paul, Phase Transitions, accepted for publication.
5. Physical properties of the mesophases of 4-n-HeptyloxyBenzylidene - 4′ - AminoAzoBenzene (HBAAB), B. Adhikari, R.A. Vora and R. Paul, communicated to Mol. Cryst. Liq. Cryst.

The following has been presented at national seminars/ symposiums and international conferences :

1. An Experimental test of Continuum Theory, Banani Adhikari, Gurupada Chaudhuri and Ranjit Paul-Proceedings of the Solid State Physics Symposium, Banaras Hindu University, (India) Dec. 1991. Page No.351.
2. Comparison of Experimental order Parameters of Nematogens with Faber's Theory - Banani Adhikari, Gurupada Chaudhuri and Ranjit Paul -Proceedings of the 14th International Liquid

Crystal Conference PISA. Italy (1992), Page No 627, Abstract-H-P24.

3. X-ray diffraction study of the Smectic B phase of 4(4" - butenyl) 4' (propyl) 1,1' bicylohexane (BPBCH), Banani Adhikari and Ranjit Paul. Proceedings of the Winter Workshop on Liquid Crystals, Department of Physics, North Bengal University, Dec. 1992 - Jan. 1993.

4. Bond Orientational Order of the Sm B phase of BPBCH from x-ray diffraction study. Banani Adhikari and Ranjit Paul. Presented at the first Indian Liquid Crystal Society Seminar held at the University of Mysore, Department of Physics, from 18-20 October, 1993.

5. Orientational order parameters in the Smectic C and Nematic phase of Heptyloxy Azoxy Benzene (HAB), Banani Adhikari and Ranjit Paul. Proceedings of the 15th International Liquid Crystal Conference Budapest, Hungary (1994), Abstract No - C - P 41. page no. 303, Vol 1.

6. Study of a bicyclohexane compound with Crystal-B-Nematic phase sequence. B. Adhikari and R.Paul, Proceedings of the Solid State Physics Symposium, University of Rajasthan, Jaipur, December, 1994, page 26.

7. Studies on the mesophases of HBAAB by x-ray diffraction and refractive index technique, B. Adhikari, R. A. Vora and R. Paul. Accepted for presentation at the Solid State Physics Symposium to be held at the Indian Association for the Cultivation of Science, Calcutta, December 1995.